The · Calibration · of · the · ERS-1 · Radar ·Altimeter

The Venice Calibration Campaign

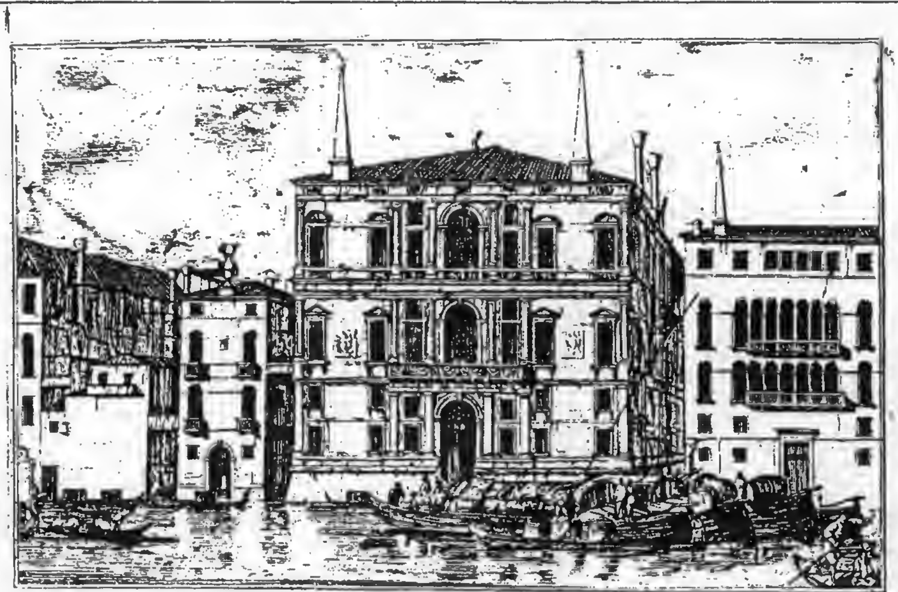

PALAZZO CVCINA SOPRA IL CANAL GRANDE
Architettura d' Andrea Palladio

Report: ER-RP-ESA-RA-0257
Issue: 2.0
Date: 1 March 1993

ESA/ESTEC
Noordwijk
The Netherlands

The · Calibration · of · the · ERS-1 · Radar · Altimeter

The Venice Calibration Campaign

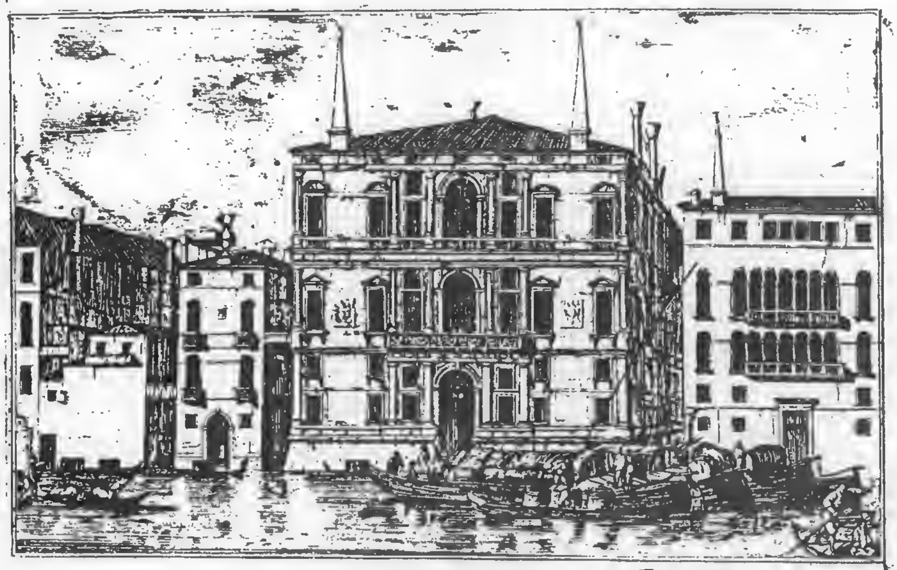

PALAZZO CUCINA SOPRA IL CANAL GRANDE
Architettura d' Andrea Palladio

Report: ER-RP-ESA-RA-0257
Issue: 2.0
Date: 1 March 1993

ESA/ESTEC
Noordwijk
The Netherlands

Cover Illustration:

PALAZZO COCCINA TIEPOLO (XVI CENTURY), in a woodcut by L. Carlevrijs (c. 1703). This palace is now the home of the *Istituto per lo Studio della Dinamica della Grandi Masse* (ISDGM), of the Italian *Consiglio Nazionale della Richerche* (CNR).

The work described in this report has been performed by a large and varied team over a period of several years. Many groups and individuals made contributions or measurements before the launch of the satellite and finished their part before the launch. Others joined the team quite late to provide skills needed in the final analysis phase.

It is invidious to try to name all participants because in this there is a real risk of omitting some. Despite this risk, the institutes and participants are given in alphabetical order respectively.

Agenzia Spaziale Italiana (ASI)
- Giuseppe "Pippo" Bianco
- Giovanni Sylos-Labini

Centre d'Etudes et de Recherches Géodynamiques et Astronomiques (CERGA)
- François Barlier

Centre Nationale d'Etudes Spatiale (CNES)
- Philippe Escudier
- Nicolas Picot

Delft University of Technology/Kootwijk Observatory for Satellite Geodesy (DUT/KOSG)
- Wiard Beek
- Carolus van Es
- Danny van Loon
- Niek Rodenburg
- Dave Samson
- Erik Vermaat
- Ruud van Wuyckhuise

Delft University of Technology/Section Orbital Mechanics (DUT/SOM)
- Boudewijn Ambrosius
- Wim van Gaalen
- Gert-Jan Mets
- Ron Noomen
- Bart Overgaauw
- Remko Scharroo
- Karel Wakker

Deutsches Geodätisches Forschungsinstitut (DGFI)
- Franz Heiner Massmann
- Wolfgang Bosch

European Space Agency (ESA)
- Berthyl Duesmann
- Richard Francis
- Bruno Greco
- Wolfgang Schumann
- Jan van Essen

ETH Zürich
- Beat Bürki

Institut für Angewandte Geodäsie (IfAG)
- Georg Weber

Institut für Navigation Stuttgart (INS)
- Wolfgang Schaeffer

Istituto Geografico Militare Italiano
- Renzo Maseroli
- Marco Pierozzi

Istituto di Ricerca sulle Onde Elettromagnetiche
- Luigi Ciraolo
- Paolo Spalla

Istituto Studio Dinamica Grandi Masse (ISDGM)
- Luigi Cavaleri
- Silvestro Curiotto
- Gianfranco Dallaporta
- Roberto Frassetto

James Rennel Centre for Physical Oceanography
- Peter Challenor
- Trevor Guymer

Telespazio SpA
- Tommaso dell'Acqua
- Franco Ambrico
- Alberto Cenci
- Emanuele di Cuia
- di Giannantonio
- Eustachio Lunalbi
- Michele Poggi
- Ezio Rainis
- Domenico del Rosso
- Franco Schiavone

Università di Padova
- Moreno de Angelis
- Alessandro Caporali
- Antonio Galgaro

Università di Roma "*La Sapienza*"
- Piero Ciotti
- Nazzareno Pierdicca

Universität Bern
- Werner Gurtner
- Thomas Schildknecht
- Urs Wild

Universität Graz
- Georg Kirchner

Substantial financial support was provided by ASI, in the general framework of support for the Italian Principle Investigators.

In addition to the efforts of the calibration team, the overall campaign depended on the excellent support by ISDGM for the activities on the research tower "*Acqua Alta*", which included significant extensions to it, by the Italian Air Force for the permission and enthusiastic cooperation in using a site within the Monte Venda facility, by the Kootwijk laser observatory for making MTLRS2 available both before and during the campaign, by IfAG for the loan of spare parts, by ASI, by Telespazio who actually installed the laser pad at Monte Venda, and by many other institutes.

Editing Author:
C. R. Francis

Contributing Authors:
A. Caporali
L. Cavaleri
A. Cenci
P. Ciotti
L. Ciraolo
W. Gurtner
F. H. Massman
D. del Rosso
R. Scharroo
P. Spalla
E. Vermaat

ESA Report: ER-RP-ESA-RA-0257, Issue 2.0, 1 March 1993

Document Change Record

Issue	Date	Page	Description of Change
1.0	23 Oct 1992	all	Initial Issue
2.0	1 Mar 1993	22, 145, 146	change in estimated error of "zero" tide gauge level, and associated bias error
		23, 147	change in "zero" tide level *wrt* WM90 and consequent table entries
		24, 148, 149	change in final bias value and error estimate, and intermediate values
		25, 148	modified plot reflecting changed results
		71–73	description of new results of the tide gauge "zero"
		213, 214	improved definition of reference marks

Table of Contents

Executive Summary

Introduction

ERS-1 was launched by an Ariane 40 launcher at 01:46:31 UTC on 17 July 1991, from Kourou in French Guiana. Following the initial switch-on of the Radar Altimeter on 25 July 1991, and early orbital operations, continuous operation of the instrument started on 28 July 1991, eleven days after launch.

The Commissioning Phase orbit was a sun-synchronous near-polar orbit (as are all the possible ERS-1 orbits) in which the ground-track was retraced after 3 days, corresponding to 43 orbits. It was acquired on 26 July 1991, 9.7 days after the launch, and maintained until 13 December 1991. The Commissioning Phase orbit is also called the "Venice Orbit", as it overflew the "*Acqua Alta*" Oceanographic Research Platform, off the coast of Venice, once every 3 days for the purpose of calibrating the ERS–1 Radar Altimeter.

Requirements for Calibration

The height measurements made by the ERS-1 Radar Altimeter have a long and short-term stability at the millimetre level thanks to the design and operation of the instrument. The ultimate noise level is about 2.5 cm. However determination of the bias in the height measurements to an equivalent accuracy was not possible prior to the launch, the residual error being estimated at about half a metre. Consequently it was necessary to determine the height bias error after launch, by means of a dedicated measurement campaign. It was known that maintaining control of all the measurements contributing to this determination would be a delicate task, but it had been achieved before *(Kolenkiewicz and Martin*, 1982).

Calibration has many interpretations. In this case the requirements were clearly identified, being stated by *Francis and Duesmann* (1988) as follows:

1 *The objective is engineering calibration. Geophysical effects shall be minimised or eliminated wherever possible. The requirement is to calibrate the instrument rather than any particular data-product.*

2 *Both the accuracy and the precision shall be maximised, with an overall goal of 5 cm for the combined error.*

3 *The calibration shall avoid potential single-point failures, and be resistant to the effects of single errors.*

4 *The calibration shall be performed during the Commissioning Phase, ie the first 3 months of the mission.*

5 *The orbit to be used shall also fulfil the calibration requirements of other ERS-1 sensors, specifically the Wind Scatterometer and the SAR.*

6 *The calibration shall be carried out within Europe.*

Overall Description

The calibration concept, which evolved some years prior to the launch, made maximum use of existing European facilities, particularly the uniquely high density of satellite laser ranging (SLR) stations. The key elements of the method are:

1. Arranging that the satellite overflies a well-defined, instrumented point in the open sea;
2. Measuring the sea-level (tide) at this point, together with all relevant environmental properties (tropospheric and ionospheric content, winds, waves *etc*) from a small fixed installation;
3. Using several SLR sites surrounding the comparison site, including one close to the satellite track. Slew-rate limitations do not prevent continuous tracking by any of the systems;
4. Dedicated campaigns to measure the three-dimensional positions of all reference points, and the local geoid;
5. Having a high degree of redundancy in the system to aid error resistance.

The ground-track of the northbound pass over the northern Adriatic Sea and the "*Acqua Alta*" tower is shown in Figure 1. This pass was over the sea for about 25sec before the tower overpass, which was known to be sufficient for the altimeter to acquire the sea-surface.

The satellite was tracked simultaneously by several SLR sites. In addition to the fixed sites Grasse, Graz, Herstmonceux, Matera, and Zimmerwald a new mobile laser site was required and this was installed at Baiamonte on Monte Venda, in the hills south of Padova. This site is

FIGURE 1

The ECN laser sites and the ERS–1 ground-tracks over Europe. The tick marks along the calibration pass over the Venice Tower are drawn at 20-second intervals. The time of overflight is given in UTC.

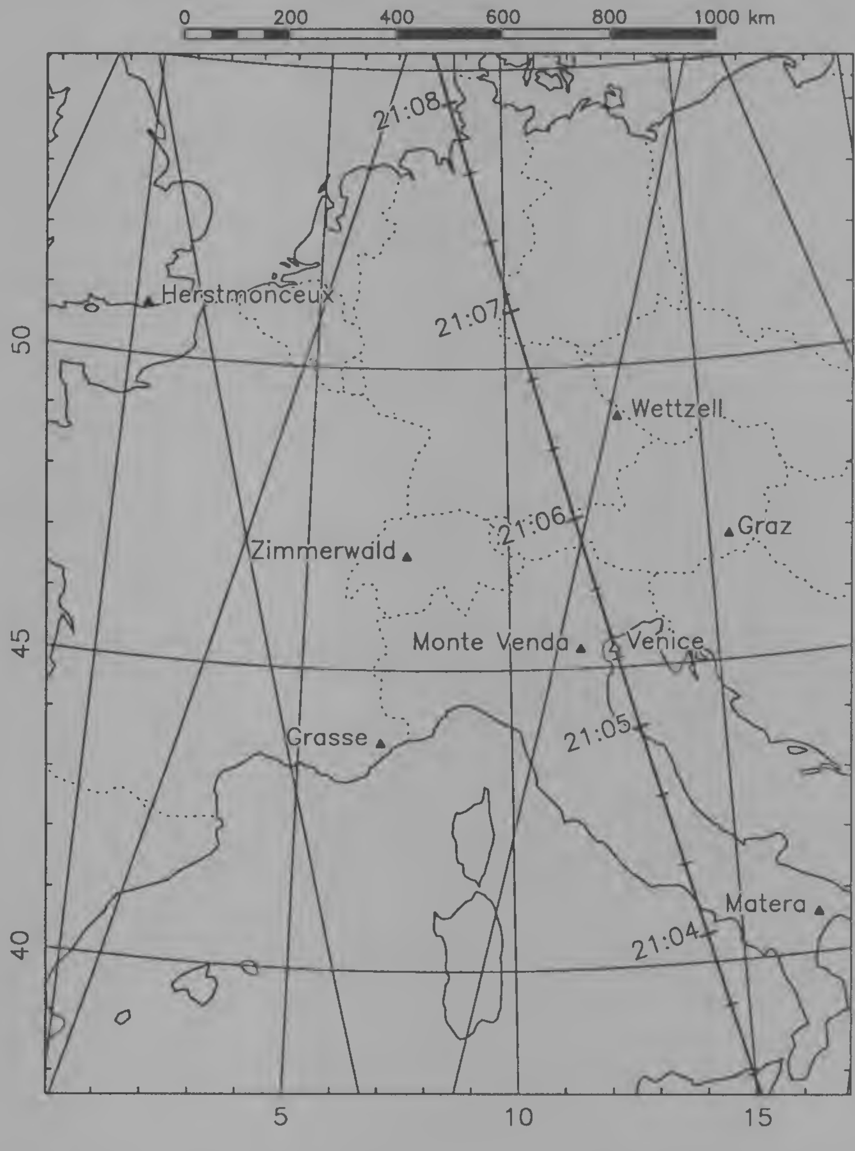

about 60km to the west of the tower. The area proved to be a good choice during the campaign itself. The six lasers provided a network surrounding the calibration site, with a favourable topology; this network had considerable redundancy. Analysis had shown (*Francis and Duesmann*, 1988; *Scharroo* et al, 1990) that useful results would be obtained with various subsets of the lasers, and this was a major contributor to the reliability of the system.

The tower was localised in the same network as the laser sites by a series of measurement campaigns using the GPS system. This enabled a direct *in-situ* measurement of the position of the ocean surface at the calibration point in the same local frame of reference as the lasers.

Figure 2 summarises the general data flow and processing steps involved in the calibration activity. Four separate elements can be identified:

1. Tracking of ERS-1 by satellite laser ranging (SLR) systems provides the possibility to accurately determine the satellite's location and

FIGURE 2 The ERS–1 radar altimeter processing diagram

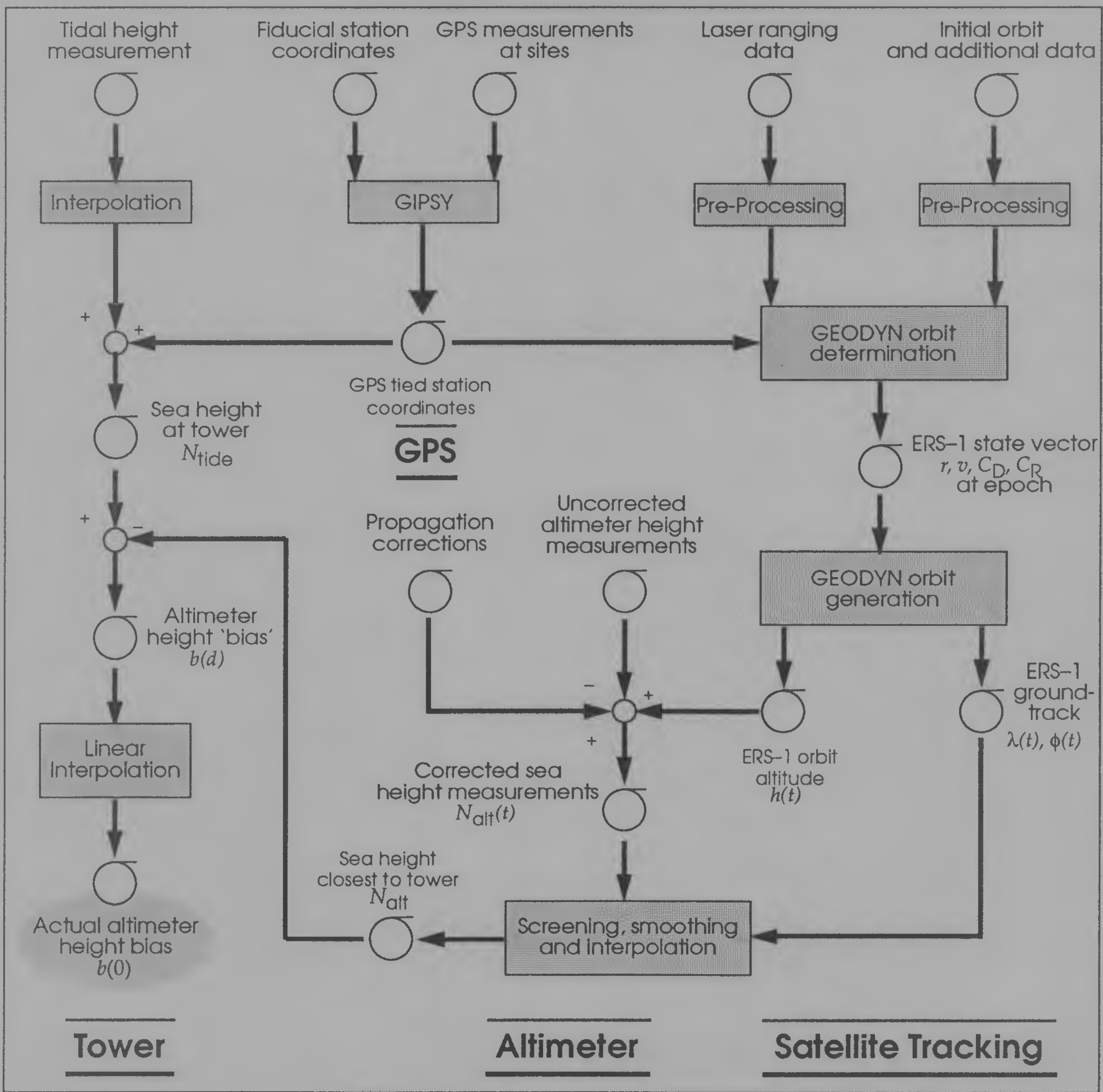

altitude. The details of the orbit determination are given in CHAPTER 5, "The Trajectory".

2. The altimeter measurements are corrected for internal and external delays, and thereafter are subtracted from the orbital height to form samples of the sea surface height along the satellite's track in the vicinity of the *Acqua Alta* tower. The corrections applied are instrumental (such as the internal delay of the radar pulse and the centre-of-mass offset), environmental (tropospheric and ionospheric delays, measured by equipment on board the tower), or physical (Doppler effect and EM-bias). A smoothing and interpolation technique (based on collocation) is used to determine the altimetric sea height closest to this tower. The processing of the altimeter measurements is described in CHAPTER 6, "The Satellite and its Measurements".
3. The tide gauge at the *Acqua Alta* tower produces an independent assessment of the sea surface height (See CHAPTER 4, "Local Measurements"). Comparison with the measured altimetric sea level, corrected for the sea surface slope along the shortest line between the tower and the ERS-1 ground track, gives the altimeter measurement bias. This comparison is fully described in CHAPTER 7, "The Results".
4. The Global Positioning System (GPS) has been used to tie the *Acqua Alta* tide gauge to the reference frame of the tracking systems. Additionally, local surveys have been conducted to refer the GPS markers to the origins of the laser ranging systems and the tide gauge. In that way both the sea height measured by the altimeter and by the tide gauge are brought into the same reference frame, and can be compared. For more details, see CHAPTER 3, "The Three-Dimensional Network".

Although the interpolation provides the sea surface height at the point along the track closest to the *Acqua Alta* Tower, it does not provide the altimetric height exactly at the tide gauge itself, due to deviations in the ground track from the ideal. As ERS-1 always passed *Acqua Alta* within 600 m, a correction may be computed from the local deflection of the vertical. In this approach it is assumed that the local sea surface slope equals the geoid slope, which is a realistic assumption since there are no strong currents expected in this specific region. Alternatively, a linear interpolation between a number of bias estimates, determined along various tracks and at varying distances from the tower, provides an independent assessment of the local mean sea surface slope.

Additionally, the height of the zero-level has to be corrected for Earth tides. This is necessary because such a correction is always included in the establishment of high accuracy terrestrial reference frames, and in using arrays of tracking systems located in these reference frames for precision orbit determination.

Finally, a local survey at the Venice Tower was needed to refer the zero sea level height to the GPS marker on the Tower. Thus the actual height of the water column in the well had to be known when the tide gauge was reading a certain value. This proved to be a rather troublesome activity.

The relative magnitudes of the measurements and effects contributing to the calibration are shown in Table 1.

TABLE 1 Approximate magnitudes of the contributions to the overall calibration.

Contribution	*Magnitude (cm)*
Altimeter measurement	78500000
Trajectory determination	78500000
Tower Position	6300000
Tide Gauge — GPS Reference	1000
Tropospheric Delay	250
Tide Gauge Measurement	100
Satellite Centre of Mass Offset	100
Solid Earth Tide	10
Ionospheric Delay	5
Cross-Track Slope	2
Sea State Bias	1
Doppler Effect	1

The GPS Networks

The determination of the exact location of the sea level during the calibration passes of ERS–1 was possible because the sea-level recorded by the tide gauge on-board could be referred to a geodetic reference point on the *Acqua Alta* tower. This reference point is a node of a regional network, in the sense that a number of measured baselines connect this point to other geodetic reference points on land. The origin of the network is the laser site at Baiamonte, on the Monte Venda. The coordinates of this point have been determined in two independent ways: one by direct LAGEOS laser ranging, the other by means of GPS surveys (the "Large" GPS Campaigns of October 1990 and September 1991) involving other European laser/GPS stations These involved, besides Monte Venda, also the tower itself. Therefore the origin, azimuth and scale of the local network are completely defined by the coordinates of the tower and Monte Venda. The vector associated to this baseline is 64 km long and is completely included in the network.

The GPS measurements from the Large Campaign of October 1990 were analysed both by the Delft University of Technology, Section

Orbital Mechanics (DUT/SOM) using the GPS Inferred Positioning SYs-tem software (*GIPSY*), and by the Astronomical Institute of the University of Berne (AUIB) with the *Bernese* GPS Software. This dual approach was adopted to enhance the reliability of the analysis.

A second campaign in September 1991, organized by the Institute of Space Research Graz for the purpose of transponder positioning was used as a further determination of the Mount Venda—*Acqua Alta* platform baseline. This campaign has been processed by AIUB only.

Table 2 shows a summary of the GPS solutions performed at AIUB (1990/1991) and DUT (1990), as well as the SLR-derived coordinates of Monte Venda 7542 in the system ERS90B[1].

TABLE 2 GPS solutions processed at AIUB and DUT; SLR solution processed at DUT (ERS90B System).

Year	*Obs*	*Proc*	*Station*	*x* (m)	*y* (m)	*z* (m)	*h* (m)
1990	GPS	AIUB	MV 7542	4399363.527	910506.391	4512940.815	523.186
1990	GPS	DUT	MV 7542	4399363.582	910506.368	4512940.800	523.210
1991	GPS	AIUB	MV 7542	4399363.564	910506.408	4512940.772	523.183
1991	SLR	DUT	MV 7542	4399363.543	910506.419	4512940.880	523.248
1990	GPS	AIUB	VT WM90	4386229.603	973073.288	4512012.437	55.634
1990	GPS	DUT	VT WM90	4386229.670	973073.271	4512012.435	55.677
1991	GPS	AIUB	VT WM90	4386229.651	973073.347	4512012.393	55.645

The results show that the coordinates of the GPS markers at Monte Venda (WM90) and *Acqua Alta* (WM90), and therefore the coordinates of the SLR marker at Monte Venda, have been determined very accurately. The processing of the LAGEOS quick-look Monte Venda SLR data has yielded coordinates that agree to within 8 cm with the GPS-computed SLR marker coordinates (after accounting for the known local eccentricity).

The results also compare favorably among those derived independently by the two groups at DUT and AIUB. Table 3 shows the baseline components of the individual solutions. Differences in the baseline components between the solution are on the centimeter level. Somewhat larger are the differences in the absolute positions of the two baseline endpoints.

Very interesting are the comparisons between the results of the two campaigns of 1990 and 1991, using different instruments: The agree-

1. ERS90B is a reference frame developed during the course of the calibration analysis, which includes all of the participating SLR stations as well as the GPS stations occupied during the Large Campaign of 1990. See page 16.

TABLE 3

Baseline components

Year	*Proc*	*dx* (m)	*dy* (m)	*dz* (m)	*dh* (m)
1990	AIUB	13133.924	-62566.897	928.378	467.552
1990	DUT	13133.912	-62566.903	928.365	467.533
1991	AIUB	13133.913	-62566.939	928.379	467.538
Average		13133.916	-62566.913	928.374	467.541

ment is within 6 centimeters in the absolute position and 4 centimeters in the baseline components. The height differences agree within the centimeter.

Formal errors, repeatabilities, and comparisons between the 1990 and 1991 suggest an accuracy of the height difference between Monte Venda and Venice tower of the order of 2 centimeters, therefore easily meeting the requirements for the calibration of the radar altimeter.

The Local Geoid

The geoid may be described as a surface coinciding with mean sea-level in the oceans, and lying under land at the level to which the sea would reach if admitted by small frictionless channels. Mathematically, the geoid is an equipotential surface of the earth's gravitational and centrifugal potential and coincides with the mean sea level in the open ocean. The undulation of the geoid (geoidal heights) are referred to a spheroidal surface (reference ellipsoid) of semi major axis and flattening such that the undulations have a mean value closest to zero. The deflection of the vertical is the angle of the vertical (direction of gravity) reckoned from the normal to the reference spheroid, and is usually given in terms of N-S and E-W components.The deflection of the vertical thus gives the slope of the geoid to the ellipsoid.

Francis and Duesmann (1988) showed that, along the ERS-1 ground track, both the geoid-ellipsoid separation and the slope of the geoid relative to the reference ellipsoid enter into the equation yielding the calibration bias. The geoid-ellipsoid separation, or geoidal height, defines a "mean sea level" surface with respect to the ellipsoid. The scale origin of the tide gauge on the tower and the scale origin of the tide gauges on shore must be points on such a smooth surface. The geoidal slope, or deflection of the vertical, enters the error budget (their eq. 3.5) as a multiplier of the position of the subsatellite point relative to the tower, bearing in mind that this varied over a range of one kilometre during the campaign.

In order to determine the desired geoidal heights and deflections of the vertical along the ground track of ERS-1 direct measurements of these quantities have been made on land. The area in which the observations have been made has an extension of approximately 100×100 km; comparable to the resolution of the most detailed global models of geoid, such as the OSU91A model of the Ohio State University complete to degree and order 360. Then, using a suitable interpolation algorithm the measured values have been interpolated to the desired zone, *ie* the calibration ground track.

Further details may be found in ANNEX C, "Regional Geoid Determination".

Sea Level Measurement

Two tide gauges are present on the oceanographic platform, "*Acqua Alta*", referred to as 1 and 2 respectively. Gauge 1 is run by the *Istituto Studio Dinamica Grandi Masse* (ISDGM) (*see Cavaleri and Curiotto*, 1979, for a full description of the instrument). It is of the conventional type, consisting of a vertical well solidly connected to the tower structure which penetrates into the sea for about 3 metres. A suitable filter avoids any appreciable influence of wind waves (frequency range above 0.05 Hz and mostly above 0.12 Hz) on its inner water level. A float follows the vertical movements of the water level inside the well; its movements are transmitted via an intermediate metal ribbon, tensioned by a suitable counterweight, to the external wheel of a graphic recorder

The motivation to build tide gauge 1 was originally to know the actual sea level with an accuracy better than 1 cm. Because under rapid tidal variation differences of up to 30 cm in one hour can be experienced, a time constant of less than a minute was required. In the 16 metres of depth this clashes with the necessity of filtering the relatively high frequency wind waves. The overall requirement was achieved by filtering the wind waves in three different ways:

1. picking up the signal as deeply as possible, namely at the bottom;
2. splitting the gauge pipe at the bottom into six pipes extending horizontally for 40 m in six radial directions at 60° intervals so achieving also a filtering in space;
3. making the pipes large enough (50 mm diameter) to allow an immediate flow for the tidal variations, but allowing the damping of wind wave oscillations by friction and inertia of the water into the pipes.

Gauge 2, run by the *Servizio Previsione Maree* of the *Comune di Venezia* (Tidal Forecasting Centre of the Venice town authorities), has the same basic structure, but the water level is digitally recorded at 5-minute intervals and with a 1 cm resolution, and radio-transmitted in real time to the Forecasting Centre in Venice. A full description of these tidal measurements is given by the *Comune di Venezia* (1989).

The hydraulic filter is a conventional one, *ie* the bottom of the well, at 3 metres depth, is connected to the sea by a very small metal pipe (inner diameter 20 mm). While this is highly effective in filtering out the wind waves, it introduces an appreciable delay between a variation of the outer sea level and the consequent response inside the well. The actual time constant is close to 10 minutes.

In summary the basic differences between the two gauges are the following: gauge number 1 records on paper and gauge number 2 in digital memory. Both are very effective in filtering out the wind waves, but, while gauge number 1 offers an immediate response to tidal variations, number 2 has a delay of more than 10 minutes. The last point becomes particularly important when short level oscillations, with periods between 10 and 20 minutes, are superimposed on the main tidal variation. These oscillations, with a horizontal scale of 10–20 km, are important for the signal picked up by the radar altimeter. They are usually connected to shelf waves, and are virtually filtered out by gauge 2.

Tropospheric Effects

The altitude measurements of the Radar Altimeter are affected by the time delay due to the atmospheric refraction and need a suitable correction. In the troposphere the refractivity can be separated into a dry (and predictable) component and a highly variable wet component, which depends mainly on the water vapour. The tropospheric effect produces an altitude overestimate of the order of 2.5m with the predominant part of the error coming from the dry component; however, due to variability in the atmospheric water vapour content, there may be changes in the wet tropospheric correction of 10-20 cm with length scale on the order of 150–500 km.

Assuming that the atmosphere follows the perfect gas law and that it is in hydrostatic equilibrium, the dry component can be directly related to the surface atmospheric pressure alone and does not require assumptions on temperature or pressure profiles (*Saastamoinen*, 1972). This is not so for the wet term, as the high variability and non uniform mixing with the dry air of water vapour makes it very difficult to predict the altitude distribution of water vapour from a simple ground measurement of humidity. The correction could be made very accurately only if the value of the atmospheric parameters and thus the refractivity were known along the whole path. In addition the wet term should be also expressed as the sum of two contributions, due to water vapour and cloud liquid water .

The wet refractive range error can be inferred from microwave radiometric observations of brightness temperature at suitable frequencies. In the microwave region and in non-precipitating conditions, the tropospheric attenuation is mainly due to the spectral absorption produced by oxygen, water vapour and cloud borne liquid water. The integrated precipitable water vapour, the integrated liquid water content and their contribution to the tropospheric refractivity can be estimated by using a dual-channel ground-based microwave radiometer (with a water vapour and a window channel).

In the case of a ground based radiometer the measured temperature is simply due to the downward atmospheric brightness temperature plus the free space radiation attenuated by the atmosphere itself. In this case, considering that the dry term is simply proportional to the surface pressure, P_s, the total (dry plus wet) excess path length can be expressed as a linear combination of the opacities at the two frequencies (τ_1 and τ_2) and of the atmospheric pressure at the surface:

$$\delta H = a_0 + a_1\tau_1 + a_2\tau_2 + a_3P_s$$

The coefficients which appear in the equation retain all the inaccuracies of the assumed models and the uncertainties due to other geophysical variables or parameters not explicitly included and therefore assumed constant on a climatological basis.

The coefficients for retrieving δH have not been calculated from models, having instead been computed by a multivariate analysis of a large set of meteorological data from the Adriatic basin in the period from July to September over five years, including data acquired during the ERS-1 campaign. The independent variables of the regression analysis were obtained from radiosondes either directly (the meteorological parameters) or through a deterministic model (the radiative model which allows computation of the opacity of the atmosphere for each of the radiosonde observations, RAOB's). The quantity to be estimated can be also computed from RAOB's by simply integrating the atmospheric refractivity. This method overcomes the absence of a suitable data set including both radiometric and meteorological observations.

The accuracy of the final estimate can be based on the regression itself. The computed RMS errors were 0.98 cm for clear conditions and 1.3 cm for cloudy conditions (a total of about 2500 RAOB's have been processed).

A microwave radiometer system was based on the "*Acqua Alta*" tower in order to make the necessary measurements, supported by meteorological measurements (air pressure, air temperature and relative humidity) at the radiometer site. The instrument consisted mainly of a dual-channel microwave radiometer operating at the frequencies, 20.6 and 36.0 GHz respectively.

One of most critical problems was the absolute calibration of the radiometer, which operated in a very uncontrolled environmental condition. Therefore it was necessary to continuously monitor and update the calibration curve. The final results showed a quite stable behaviour of the instrument in AGC mode while the Dicke mode was affected by instabilities which could be related to having switched off the instrument during the campaign.

The excess path length was also estimated from meteorological data. The comparison with the radiometric estimate shows a RMS difference of 3.3 cm and a bias of 0.9 cm. The results are shown in Table 4 for each ERS-1 pass.

TABLE 4 Final results of tropospheric measurements

Date	Day	Total Meteo (cm)	Wet Meteo (cm)	Total MWR (cm)	Wet MWR (cm)	Meteo Conditions	P_s(mb)	T_s (C)	R_h (%)	Total Tropo (cm)	Estimated Error (cm)
31 Jul	211	246.4	17.2			cloudy	1010.3	20.8	77	246.4	
3 Aug	214	249.0	18.4			clear	1016.3	25.7	62	249.0	
6 Aug	217	252.2	21.9	252.1	21.7	clear	1014.9	26.7	71	252.1	1.0
9 Aug	220	258.4	27.7	250.3	19.7	partly	1016.4	27.3	82	252.7	7.0
12 Aug	223	254.5	24.7	254.1	24.3	clear	1012.7	27	80	254.2	1.0
15 Aug	226	253.1	22.8	249.8	19.5	partly	1014.7	26.2	71	250.8	2.0
18 Aug	229	254.6	25.5	249.3	20.2	partly	1009.8	27.3	75	250.9	4.0
21 Aug	232	247.9	17.4	245.4	14.9	clear	1015.7	24.7	62	246.1	1.0
24 Aug	235	254.7	23.6	255.5	24.4	clear	1018.6	26.2	79	255.3	1.0
27 Aug	238	249.6	18.2	253.0	21.6	partly	1019.7	26.3	55	252.0	2.0
30 Aug	241	245.9	13.8	245.6	13.6	clear	1022.6	23	53	245.7	1.0
2 Sep	244	251.4	18.9	251.3	18.8	clear	1024.4	23.9	71	251.3	1.0
5 Sep	247	251.4	20.2	249.8	18.5	clear	1018.9	24	76	250.2	1.0
8 Sep	250	243.7	12	250	18.9	clear	1021.1	22.2	47	248.1	2.0
11 Sep	253	252.1	21.5	256.5	25.9	clear	1016.2	23.7	83	255.1	2.0
14 Sep	256	rain (no data)								247.0[1]	
17 Sep	259	252.3	21.6	257.1	26.4	clear	1016.6	23.4	85	255.6	2.0

1. Based on measurement of shore-based barometer

Ionospheric Effects

The effects of electrons of the ionospheric plasma on an electromagnetic signal travelling from a satellite to ground include:

- Phase and group delays;
- Rotation of the polarization ellipse (Faraday Rotation);

The ionospheric effect on group delay is an error source for the altimeter measurement. In both cases, the ionospheric parameter which directly affects delay and Faraday Rotation is the total number of electrons in an unit cross section column along the ray path from the satellite to the observer or to the target. This parameter is known as Total Electron Content (TEC). Measurements of TEC can be made by satellite measurements, making use of these two effects.

- GPS provides accurate relative measurements by differential phase, and less accurate absolute measurements by differential group delay, provided delays at the satellite are known. The time coverage is quasi-continuous. The column extends up to the GPS satellite height (20000 km) and reaches the plasmasphere;
- geostationary beacons provide accurate relative measurements and continuous time coverage. Although the column extends also to the plasmasphere, Faraday Rotation measurements provide information only up to about 2000 km, as the effect is weighted by the magnetic field of the Earth.
- DORIS measures the Doppler shift, counting over 10 seconds, at two frequencies (2 GHz and 400 MHz) from a global network of about 50 beacons. The orbital height of SPOT 2 is the same as for ERS-1, and it is also sun-synchronous at about the same local time.

Faraday Rotation Measurements

At *Istituto di Ricerca sulle Onde Elettromagnetiche* (IROE) determinations of TEC are carried out continuously using Faraday Rotation. This method provides vertical TEC geographically above the subionospheric point. During the campaign the Meteosat 2 beacon has been used; for this satellite and this period, the subionospheric point is located at 40.2° North and 8.5° East. For the extrapolation of the determination of TEC from this point to Venice, account was taken of the following points:

- The displacement in longitude is equivalent to about fifteen minutes in time. Therefore it is sufficient to use observations taken at 21:20 (Faraday Observations are taken each minute).
- The displacement of 5° at middle latitudes introduces errors, believed to be comparable to the overall errors involved in the observations and data reduction. This is supported by tests with simultaneous Faraday observations taken with the same type of instruments in Firenze and Trieste, in which no influence due to the difference in latitude (≈2.5°) was noticeable. However since some indication of the ionospheric density gradient is available from the GPS and DORIS results, these have been taken into account in generating the final values.

GPS

The GPS phase observations L1 and L2 may also be used to compute a model of the Total Electron Content of the ionosphere above the GPS receiver station. In this case the GPS measurements were performed on the *Acqua Alta* tower for 2 hours centred on each calibration pass. The measurements were processed by AUIB, using a facility of the *Bernese* GPS software.

DORIS

DORIS measurements from August 1991 were processed at CNES.

The model used to represent TEC was defined by a latitude–longitude grid and an interpolation method. The TEC values at each grid point was given by a 3rd order polynomial interpolation over the 16 surrounding grid points. The latitude parameter of the grid represents latitude plus local-time variations, while the longitude parameter represents longitude plus absolute time variations.

The unknown parameters were estimated using a least squares fit over the whole set of measurements during two days. Measurements were weighted for measurement noise characteristics. The grid was regular to avoid divergence in areas where there are few DORIS beacons, and a constraint on slope variations is applied.

Results

In Table 5 are reported all the final results for TEC at 21:05 of given days over Venice, the corresponding delay in cm, and the relative errors. The results from the Faraday Rotation technique have been propagated to the location of the *Acqua Alta* tower using the longitudinal and latitudinal profiles derived from the GPS technique. For the conversion from TEC to delay, the classical formula (*Davies* 1990) has been used.

$$l = \frac{40.3}{cf^2}\mathrm{TEC} \times 100$$

Trajectory

The precise orbit for the calibration pass was computed in two steps, both using the DUT/SOM version of the NASA GEODYN II orbit determination software. First, a 4-day long arc solution was generated using ERS–1 so-called quick-look normal points from a global network of satellite laser ranging systems. Secondly, this orbit served as *a priori* information for the determination of a short-arc orbit over the Venice Tower and a European Calibration Network (ECN) of fixed laser stations. This procedure maximises the orbit accuracy over the *Acqua Alta* Tower and minimises the possibility of obtaining an unrealistic or non-converging orbit solution. Once they became available the short-arc orbits were based on high-quality full-rate SLR data.

TABLE 5

Summary of the ionospheric measurements and results using the different techniques. The asterisk attached to Fraraday Rotation measurements means that a modified processing was used in these cases.

Date	Da y	Faraday Rotation		GPS			DORI S	Total	
		cm	RMS	Instrument	cm	RM S	cm	cm	erro r
31 Jul	211	3.91	0.6					3.9	1.0
3 Aug	214	1.35	0.6	WM102	2.05	0.1	3.1	2.1	1.0
6 Aug	217			WM102	2.83	0.1	2.2	2.5	0.5
9 Aug	220	3.25	0.5	WM102	4.43	0.1	3.2	3.6	0.8
12 Aug	223	2.08	0.5	WM102	4.29	0.1	1.5	2.6	1.5
15 Aug	226	2.61	0.5	WM102	2.48	0.2	2.6	2.6	0.4
18 Aug	229	4.62	0.5	WM102	3.03	0.1	3.9	3.9	0.8
21 Aug	232	2.50	3.0*	WM102	6.43	0.2	3.3	4.1	2.0
24 Aug	235	4.91	3.0*	WM102	5.36	0.1	4.9	5.0	0.2
27 Aug	238	4.22	3.0*	WM102	7.22	0.2	5.1	5.5	1.5
30 Aug	241	1.89	1.3*	WM102	2.65	0.1	2.5	2.3	0.4
2 Sep	244	2.94	1.3*					2.9	0.2
5 Sep	247	3.30	1.3*					3.3	0.2
8 Sep	250	3.95	2.8*	TRIMBLE ST	3.68	0.1		3.8	0.2
11 Sep	253	2.60	2.8*	TRIMBLE ST	3.40	0.1		3.0	0.4
14 Sep	256	4.37	1.3*	TRIMBLE ST	4.55	0.1		4.5	0.2
17 Sep	259	5.38	1.3*	TRIMBLE ST	4.30	0.1		4.8	0.4

To accurately track the satellite during its pass over the *Acqua Alta* Tower the Dutch Modular Transportable Laser Ranging System (MTLRS–2), which is operated by DUT's Kootwijk Observatory for Satellite Geodesy, arrived on 17 April 1991 at Monte Venda. Between its arrival and the launch of ERS–1 the MTLRS–2 system had already tracked 48 passes of the geodetic satellite LAGEOS from this site. From 17 July until 18 September, when the system returned to The Netherlands, it tracked another 23 LAGEOS passes in between the first-priority ERS–1 passes.

Although, in contrast to the Bermuda approach, none of the tracking systems is vertically beneath the calibration pass, the network of tracking systems is sufficient to ensure an accurate determination of the satellite's height. Many pre-launch simulation studies were performed by ESTEC and DUT/SOM to investigate the radial orbit accuracy achievable with different tracking stations configurations and applying realistic measurement and dynamic error models. Table 6 summarises part of the results for 6 possible laser tracking configurations. It shows that the tracking by the Monte Venda laser, which is closest to the pass over the *Acqua Alta* Tower, is essential for achieving a high radial orbit accuracy, especially when some of the fixed laser systems are not able to track ERS–1. Since for this short-arc analysis no dynamic model errors propagate into the radial orbit error budget, it is clear that the dynamical determination of the orbit height is virtually equivalent to any geometrical solution. The results show that if sufficient laser tracking is available a radial orbit accuracy of better than 10 cm may be realised.

TABLE 6

Contribution of errors in the measurements and dynamic models to the error in the ERS-1 computed altitude near Venice for different tracking system configurations. Values are listed in centimetres.

Configuration	*A*	*B*	*C*	*D*	*E*	*F*
Monte Venda	•		•		•	
3 fixed sites West of the track	•	•	•	•		
3 fixed sites East of the track	•	•			•	•
Error sources						
Dynamics	0	0	0	0	0	0
Coordinates	2	5	6	15	4	15
Measurements	3	3	7	11	5	11
Refraction	4	4	9	13	6	13
RSS error	5	7	13	24	9	24

To obtain the most accurate orbit determination, high-quality station coordinates are imperative. During the ERS-1 Radar Altimeter Calibration Campaign two alternative sets of coordinates were used.

- ETRF-89: the 1989 set of SLR coordinates published by IERS. Since this set does not include the Monte Venda or *Acqua Alta* tower coordinates, these are obtained from the "Large" 1990 GPS Campaign and the Local GPS Campaign.
- ERS90B: coordinates of the ECN SLR systems converted from the DUT/SOM ERS90 coordinates solution. The SLR marker coordinates of Grasse, Graz, Herstmonceux, Matera and Wettzell are computed from LAGEOS full-rate Release A normal points SLR data, covering the period September to December 1990. The SLR coordinates of Zimmerwald and Monte Venda are computed from quick-look LAGEOS SLR data, acquired until 25 June 1991. All solutions are converted to the epoch 1 September 1991. The position of the *Acqua Alta* tower is determined by adding the baseline between the *Acqua Alta* tower and Baiamonte obtained from the "Large" 1990 GPS Campaign to the SLR-based coordinates for Baiamonte.

Long-Arc Orbits

On 17 July 20:29 UTC, only about 18.7 hours after launch, the Grasse laser system acquired the first laser tracking data on ERS–1. The next day both the Grasse and the Zimmerwald lasers tracked the satellite. Then the other lasers stations followed and within 2 weeks a total of 13 stations in Australia, Austria, England, France, Germany, Hawaii, Italy, Japan, Peru, Switzerland, and the USSR had tracked ERS–1. At that time, 30 July, the ERS–1 orbit computation experiments by DUT/SOM started.

To get a better insight in the accuracy of the computed orbits a series of overlapping arc analyses were performed. To allow this kind of analysis most of the 4-day orbital arcs were selected such that successive arcs have a 1-day overlap. The RMS orbit differences for that 1-day period were generally found to be about 0.6–1.0 m, 0.6–2.1 m and 1.5–6 m in the radial, cross-track and along-track directions, respectively. The values obtained for the RMS laser range residuals and the RMS orbit differences indicate that the ERS–1 4-day arc orbits computed by DUT/SOM generally have an accuracy of about 0.8 m, 1.5 m and 3 m in the radial, cross-track and along-track directions. This accuracy level is sufficient to use these orbits as *a priori* estimates for the short-arc orbit determination process.

Short-Arc Orbits

For the computation of precise short-arc orbits over the *Acqua Alta* the tracking coverage of the ECN lasers during the ERS–1 zenith pass over the tower is, of course, extremely important. The tracking was, in general, rather sparse. The altimeter passes of 3 and 6 August were tracked by only one ECN laser, while in many cases only 2 to 3 out of the 7 lasers have acquired tracking data. The Monte Venda laser, which plays a crucial role in the computation of the precise radial position of ERS–1 over the *Acqua Alta* Tower, tracked the satellite during all zenith passes after 3 August, except for the passes on 24 August, and 8 and 14 September. Since it is known that the orbit accuracy degrades rapidly as less stations track the satellite, it was decided to use only those passes during which the satellite was tracked by the Monte Venda laser and at least one of the other ECN lasers.

The short-arc orbit computations referred to here are all based on the high-quality full-rate laser ranging data available from all ECN SLR sites. These observations are corrected for all known internal and external delays of the laser pulse, which include

- Corrections for tropospheric refraction using the Marini-Murray model;
- Measured system biases;

- Distance from the ERS–1 optical centre of the laser retro-reflector (LRR) to its geometrical centre.

For the ten passes used the weighted full-rate normal points were processed using the DUT/SOM version of the GEODYN II orbit determination software and a force model. In addition to the observation corrections mentioned above, the fact that they refer to the LRR geometrical centre and not to the satellite's centre-of-mass (CM) is taken into account by adding the distance between the two points in the direction of each observation to the SLR range.

In order to make a quantitative assessment of the radial orbit accuracy, the orbit determination was also run with the ETRF-89 coordinate set. This solution gave slightly worse residual statistics than in the former solution, from which one can conclude that the ERS90B solution is a bit more accurate. The level of accuracy can be quantified by comparing the radial position of the satellite over the *Acqua Alta* Tower (which is of the most importance) for all ten passes, listed in Table 7.

TABLE 7

Height of the ERS-1 centre of mass (h) above the WGS84 reference ellipsoid at the time of the closest approach (TCA) to the *Acqua Alta* tower and the altitude difference (Δh) between the ETRF-89 and ERS90B solutions.

Date	TCA (UTC)	h (m)	Δh (m)
12 August	21:05:21.9106	784271.287	0.048
15 August	21:05:22.8837	784337.916	0.012
18 August	21:05:23.6536	784297.798	0.027
21 August	21:05:22.9073	784244.115	0.039
27 August	21:05:22.2837	784332.734	0.058
30 August	21:05:22.8475	784310.336	0.032
2 September	21:05:22.1491	784293.975	0.045
5 September	21:05:20.5341	784279.589	0.038
11 September	21:05:21.1293	784329.496	0.022
17 September	21:05:20.8605	784294.757	0.101
Total		Mean	0.042
		RMS about mean	0.023
Total (except 17 Sep)		Mean	0.036
		RMS about mean	0.013

The average difference between the satellite altitude solutions in either frame is 3.6 cm[1], which corresponds to a similar difference in the height solution of the Venice Tower GPS marker in the two frames

1. Except 17 September, where the ETRF89 solution is suspect.

(3.1 cm). Hence, this does not affect the altimeter bias determination. However, the RMS of the radial orbit difference about this mean, being 1.3 cm, is a clear indication of the orbit uncertainty caused by uncertainties in the station coordinates. Since the ETRF-89 and ERS90B sets are independent, we may assume the uncertainty in either solution to be √2 of this, or roughly 1.0 cm. ERS90B, being slightly better that ETRF-89, produces less than 1 cm radial orbit error.

The Altimeter Data

The RA data used in the calibration processing have been processed at ESTEC, in a reference RA processor developed for the calibration task. Neither the Fast Delivery nor the Off-line products were used. This is because a retracking scheme was introduced to avoid potential tracking problems over this short stretch of often-calm water, which proved to be a wise precaution. Furthermore detailed control of the relevant characterisation parameters was thereby possible.

Amongst the tasks performed in this processor were the following:

1. Compensation of the measured waveform for the IF transfer function of the instrument;
2. Application of the internal and pre-launch calibration measurements (*ie* the internal delay), and conversion to "calibrated engineering units", according to the algorithms given by *Francis* (1991);
3. Estimation of the offset between the centre of the measured waveform (*ie* the RA tracking point, corresponding to the onboard height measurement) and the estimated mean sea level in the measured waveform. This is done by performing a least-squares fit of the Brown model (*Brown*, 1977) to the measured waveform. The least squares fit is an iterative process performed in three stages. In the first stage uniform weighting is applied to the waveform samples. This stage is intended to find a first estimate of the mean sea level. Based on the results of this stage a "zoned" weighting is applied, in which little weight is given to the echo before the leading edge, maximum weighting is applied to the leading edge itself, and an intermediate weighting is given to the echo plateau. The parameters estimated are Browns quantities τ, σ_s and $\sigma°$. Finally a third stage of estimation is performed in which only Browns parameter ξ, the antenna mispointing, is estimated, with high weighting applied to the plateau of the waveform. In each stage a maximum of 40 iterations is allowed.

The reprocessed altimeter data from the ten passes which had a reasonable ECN laser tracking geometry, and good-quality altimeter measurements, have been processed to determine the ERS-1 altimeter bias. Firstly all the reprocessed altimeter height observations were corrected for:

- offset of the altimeter reference point (the centre of the antenna aperture plane) with respect to the nominal centre-of-mass of the satellite. This distance is 851.9 mm;
- tropospheric and ionospheric propagation delay of the altimeter signal. Although the corrections should only apply to altimeter measurements taken vertically above the tower, the same correction is applied to all measurements over the Adriatic sea;
- Electro-Magnetic (EM) bias, determined by using a correction of 2% of the waveheight measured by in-situ instrumentation;
- Doppler shift due to the vertical velocity of the satellite with respect to the sea surface;

Then, the sea surface height profile N_{alt} along the track over the Adriatic Sea was determined by subtracting all 20-per-second fully-corrected altimeter measurements h_{alt} from the orbital height h_{orb}.

Since none of the "full-rate" sea surface heights, which are separated by about 340 m, were actually made precisely over the tower, and their noise is about 8 cm (compared with the 2 cm obtained with the 1-per-second averages), a smoothing and interpolation has to be performed. The smoothing and interpolation scheme implemented was based on the technique of collocation, also known as objective analysis, which makes optimal use of *a priori* information of the expected 'shape' of the altimeter profile. The spatial covariance function was taken to be an isotropic one, based on the expected deviations of the sea level from the 360×360 Ohio State University geoid model OSU91A (*Rapp et al*, 1991). For longer wavelengths (above the spatial resolution of the geoid model) the covariance function was determined by the calibrated degree standard deviation of this model, and for short wavelengths (until 20 km) by Kaula's rule of thumb.

The altimetric sea height profiles from two of these passes are shown in Figure 3. These two passes, on 27 August and 30 August, show respectively "good" and "bad" passes. The latter is significantly disturbed due to the presence of specular echoes from the smooth sea surface which exists in some areas on this day. In order to remove the major slopes in the sea height profiles, they are plotted with respect to the OSU91A geoid model. The markers in these plots represent the reprocessed samples. Circles indicate samples used to form the smoothed sea surface profile (curved full line). Triangles and crosses indicate erroneous measurements. The time is measured relative to the time of closest approach to the *Acqua Alta* tower. The shaded areas show when the satellite is over land, while the sea in-between is the *Laguna Veneta.*

Although the altimeter measurements have a noise of about 8 cm, the interpolation of the sea level can be performed to an accuracy of about 2 cm, in general. The interpolated value can be found from the right hand axis.

FIGURE 3

Smoothing and interpolation of the relative sea surface height derived from the 20-per-second altimeter samples of 27 August 1991 and 30 August 1991. The upper panel of each pair shows the smoothed altimetric sea surface height, and the lower panel the estimated error.

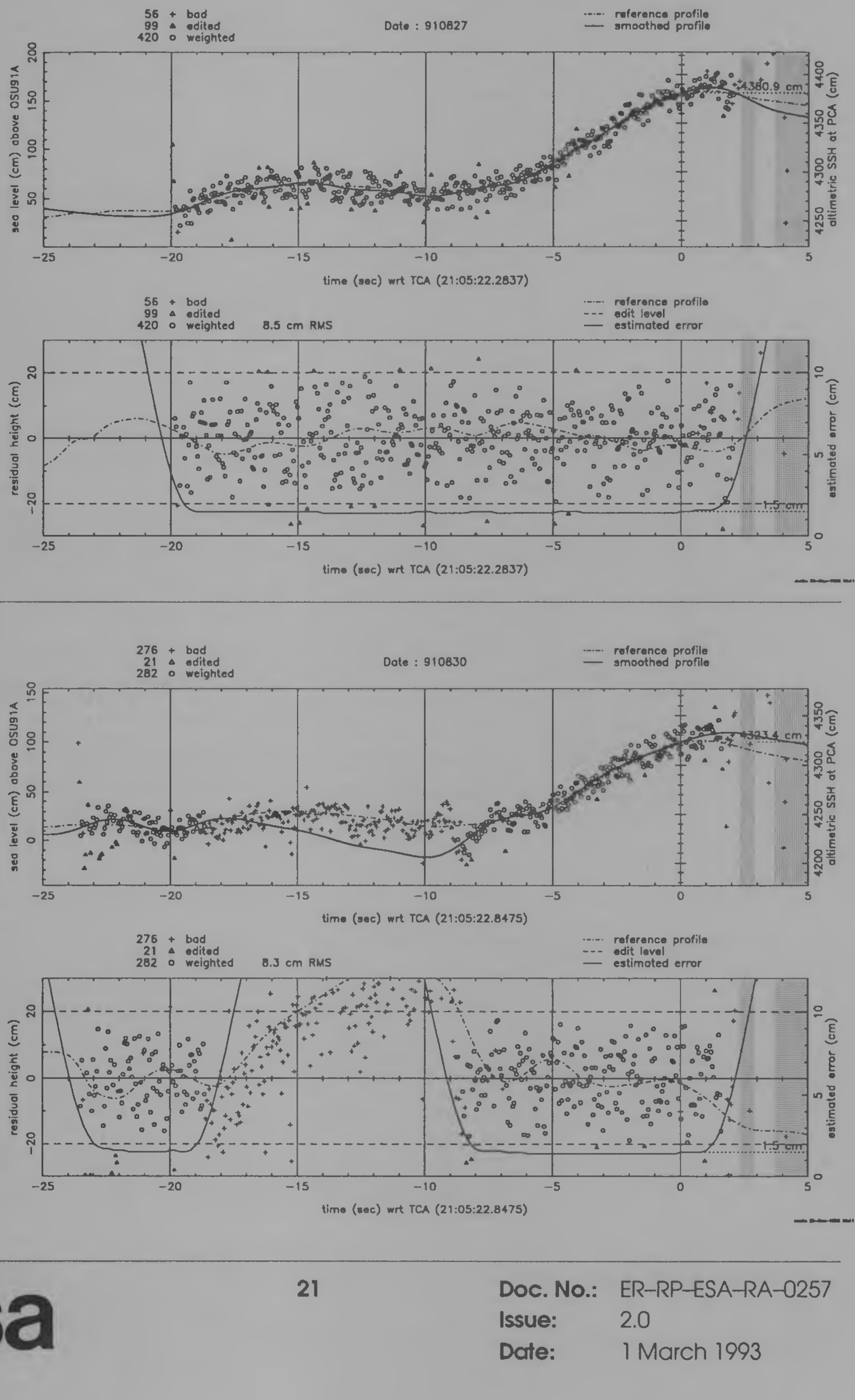

The Results

Errors

The errors which will occur in the final value of the bias calibration are of two types. Static errors (also called systematic or bias errors) are errors which are always present, for every pass. They are, for example, caused by wrong measurements of static position or by errors in models. The other type of error is the non-static (or random, or noise) error. These are different from pass to pass, are uncorrelated and can be reduced by increasing the number of calibration passes.

The contribution of errors in the measurements and models is given in Table 8. This Table is subdivided into the errors affecting the orbit determination, those affecting the altimeter measurement, and those affecting the tidal sea surface height measurement. The static errors are then combined by Root Sum of Squares (RSS) to generate an estimate of the uncertainty which will remain in the final bias value, after taking into accout all of the non-static errors, when processing the final multi-pass result.

TABLE 8 Estimated errors of the various entities building up the bias estimates per pass, in centimeters.

Entity	*Method*	*Static Error*
Recorded sea level	Analogue tide gauge	0.0
Height of the zero tide level wrt GPS marker WM90	Local survey	2.0
Height of the GPS marker WM90	GPS	2.0
Local solid Earth tide	Love Model	1.0
Station coordinates	ERS90B coordinate set	1.0
CM correction	Geometry	0.1
Bias estimate per pass	RSS	3.2

This overall uncertainty is ±3.2 cm.

The Final Result

The summary of all of the relevant values leading to the ten independent bias estimates which have been derived during the calibration campaign are given in Table 9. The following remarks should be noted:

- The sea level recorded by the tide gauge on the *Acqua Alta* tower is added to the zero reference height of the gauge, which is a fictitious marker on the *Acqua Alta* tower that indicates where the sea level is when the gauge is indicating "0". This level was

TABLE 9 Summary of the calibration measurements and results for each of the passes used in the final analysis.

	12 Aug	15 Aug	18 Aug	21 Aug	27 Aug	30 Aug	2 Sep	5 Sep	11 Sep	17 Sep
Time of PCA (sec past 21:05 UTC)	21.9106	22.8837	23.6536	22.9073	22.2837	22.8475	22.1491	20.5341	21.1293	20.8605
Location PCA wrt tower (m East)	314	44	-275	-106	187	27	134	520	362	211
Laser Tracking										
7542 Monte Venda	•	•	•	•	•	•	•	•	•	•
7835 Grasse		•	•	•					•	•
7839 Graz					•		•	•	•	•
7939 Matera	•									
7810 Zimmerwald	•	•		•				•		•
7840 Herstmonceux	•	•	•	•	•	•		•		•
Tide gauge										
Recorded sea level	1.040	0.703	0.774	0.924	1.180	0.718	0.634	0.958	1.075	0.749
Height of zero tide *wrt* WM90	-13.457									
Height of the GPS marker WM90	55.708									
Local solid Earth tide	–0.091	–0.111	–0.099	–0.061	–0.043	–0.104	–0.121	–0.038	–0.038	–0.068
Tidal SSH at tower	43.199	42.841	42.925	43.112	43.386	42.863	42.762	43.170	43.287	42.930
Altimeter										
No. of altimeter measurements	579	559	566	559	575	579	579	559	607	579
idem (weighted)	499	85	469	366	420	282	228	487	510	466
RMS of Residuals	0.079	0.081	0.077	0.081	0.085	0.083	0.071	0.074	0.078	0.079
Orbital altitude (784000+)	271.287	337.917	297.801	244.115	332.734	310.366	293.975	279.579	329.496	294.751
Raw altimeter height (784000+)	229.369	296.538	256.267	202.246	290.655	268.768	252.470	237.618	287.490	253.106
Ionospheric delay	0.026	0 .025	0.038	0.040	0.055	0.023	0.029	0.033	0.030	0.048
Tropospheric delay (dry+wet)	2.542	2.508	2.509	2.461	2.520	2.457	2.513	2.502	2.551	2.556
Doppler range error	–0.010	–0.010	–0.010	–0.010	–0.010	–0.010	–0.010	–0.010	–0.010	–0.010
C.M. Correction	0.852									
EM bias	–0.009	–0.002	–0.011	–0.003	–0.017	–0.016	–0.010	–0.005	–0.007	–0.004
Altimetric SSH at PCA	43.633	43.052	43.230	43.511	43.809	43.234	43.195	43.639	43.732	43.391
Error estimates (1σ)										
Orbital altitude	0.020	0.020	0.030	0.015	0.030	0.030	0.030	0.020	0.025	0.020
RA Noise at PCA	0.014	0.182	0.015	0.050	0.015	0.015	0.015	0.015	0.015	0.016
Sea Level	0.005	0.004	0.004	0.007	0.005	0.006	0.003	0.009	0.005	0.005
Ionosphere	0.015	0.004	0.008	0.020	0.015	0.004	0.002	0.002	0.004	0.004
Troposphere	0.010	0.020	0.040	0.010	0.020	0.010	0.010	0.010	0.020	0.020
Datation	0.001	0.001	0.001	0.001	0.001	0.001	0.001	0.001	0.001	0.001
Total σ	0.031	0.184	0.053	0.057	0.042	0.036	0.036	0.029	0.036	0.033
ERS–1 altimeter bias estimate										
From single pass	–0.434	–0.211	–0.325	–0.399	–0.423	–0.371	–0.431	–0.469	–0.445	–0.461
From multi pass	–0.420	–0.416	–0.410	–0.413	–0.418	–0.415	–0.417	–0.423	–0.421	–0.418
Difference	–0.014	0.205	0.105	0.014	–0.005	0.044	–0.016	–0.046	–0.024	–0.043
Fit: bias (m)	–0.415									
Fit: tilt (m/km)	–0.016									

determined to be 13.457m below the GPS marker WM90, which is at 55.707 m above the reference ellipsoid. Finally, since the sea level rides together with the tower and its tide gauge on the solid Earth tides, the tidal sea level is corrected for the solid Earth tidal elevation computed according to the Love model, including the permanent and frequency-dependent tides.

- The altimetric sea surface height (SSH) come from the smoothed and interpolated sea surface profiles. The Table indicates which corrections have been applied and which was the orbital altitude at the time of closest approach, as well as the "raw" (though smoothed and interpolated) altimeter measurement.
- The orbit altitude error, RSS correction error and sea surface height interpolation error are Root-Sum-Squared to form the total error of the single-pass bias estimate.
- A comparison of the altimetric and tidal sea surface height at PCA gives the single-pass bias estimate. The bias estimates per pass so obtained range from –46.9 cm to –21.1 cm.

Figure 4 shows the estimated biases per pass (and their 1σ error bars) as a function of the distance of the PCA to the *Acqua Alta* tower as derived in Table 9. The slope of the full line represents the measured slope of the geoid around the tower; the error on this measurement was estimated as ±0.5 arcsec. The origin of the line is determined by the weighted average of the single-pass bias estimates.

The combined bias estimate from this weighted fit is –41.5 ±2.0 cm.

The uncertainty in this fit represents the combination of the non-static errors, which vary pass-to-pass. This must be combined with the estimated magnitude of the static errors, as derived in Section 7.1, "Error Estimation". The method used to combine these error estimates is Root Sum of Squares.

> This results in a final bias estimation, and total uncertainty, of –41.5 ±5.2 cm.

FIGURE 4

Results of the bias determination, shown as a function of cross-track distance during the campaign. The fitted line has a slope of 1.6" as measured locally, and intercepts the poistion of the platform, at the zero line, at –41.5 cm.

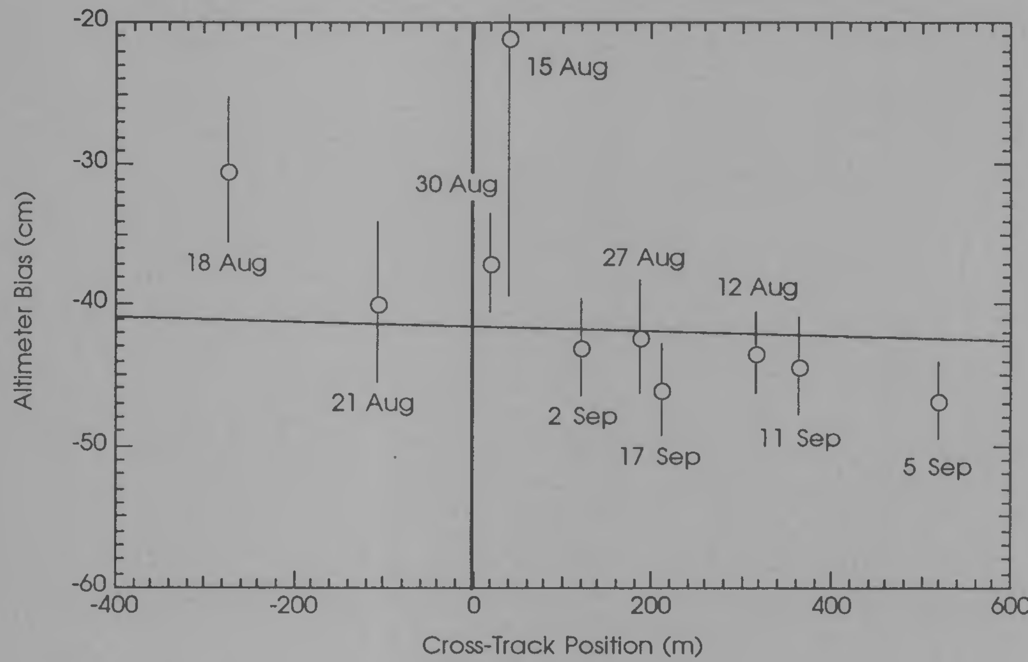

CHAPTER 1

ERS-1 and the Radar Altimeter

This chapter provides the introduction and background to the overall problem of the calibration of the ERS-1 Radar Altimeter. It briefly describes the satellite and its mission, the instrument and how it works. The functioning of the on-board calibration is described so that its relationship to the external height calibration may be understood. Complementary information is provided in CHAPTER 6, "The Satellite and its Measurements"

1.1 ERS-1 and its Orbit

1.1.1 Mission and Payload

ERS-1 was launched by an Ariane 40 launcher at 01:46:31 UTC on 17 July 1991, from Kourou in French Guiana. Following initial switch-on and early orbital operations the Commissioning Phase orbit was acquired on 26 July 1991. Continuous operation of the radar altimeter started on 28 July 1991, eleven days after launch.

The mission of the satellite is primarily environmental, and to this end it carries a small number of powerful sensors, as follows:

- The Radar Altimeter (RA);
- A Synthetic Aperture Radar (SAR) which produces high resolution radar images;
- A Scatterometer, which is used to determine wind speed and direction at sea;
- An Along-Track Scanning Radiometer (ATSR) which measures sea surface temperature;
- A nadir-viewing Microwave Radiometer, which can be used to determine the atmospheric water vapour content;

- The Precise Range and Range-rate Equipment (PRARE), which failed soon after launch—it would have enabled precise tracking of the satellite;
- A Laser Retroreflector array (LRR), which enables tracking by ground-based Satellite Laser Ranging (SLR) stations.

A photograph of the satellite in launch configuration is shown in Figure 1–1; the elements related to altimeter calibration are marked A close-up view of the LRR is shown in Figure 1–2.

1.1.2 Commissioning Phase Orbit

The Commissioning Phase orbit was a sun-synchronous near-polar orbit (as are all the possible ERS-1 orbits) in which the ground-track was retraced after 3 days, corresponding to 43 orbits. It was acquired on 26 July 1991, 9.7 days after the launch, and maintained until 13 December 1991. The characteristics of the orbit are given in Table 1–1.

The Commissioning Phase orbit is also called the "Venice Orbit", as it overflew the "*Acqua Alta*" Oceanographic Research Platform, off the coast of

FIGURE 1–2 A close-up view of the ERS–1 Laser Retroreflector. This small device has 9 optical corner cubes each about 23mm deep, arranged to provide coverage to the horizon. During near-overhead passes, such as during the calibration, the nadir-facing cube (on the top in this view) is the most important.

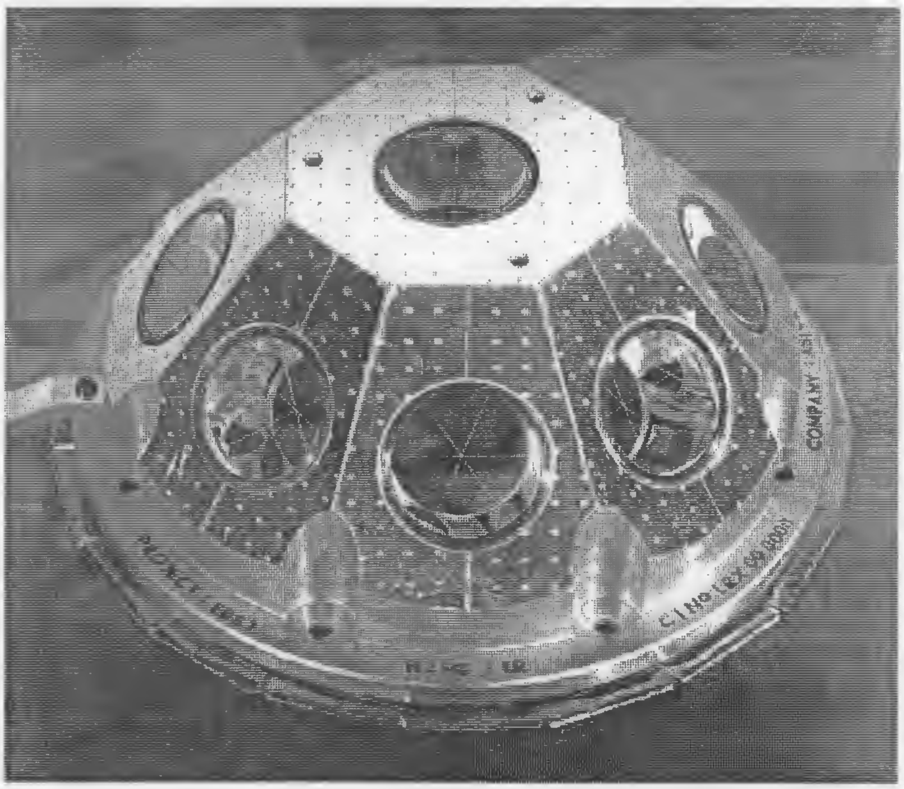

FIGURE 1–1

The ERS-1 satellite in launch configuration, viewed from the earth-facing side. The 1.2m diameter Radar Altimeter antenna is near the top, the small Laser Retroreflector is on the right hand side of the earth facing panel, and the PRARE is at the bottom.

Radar Altimeter Antenna

Laser Retroreflector

PRARE Antenna

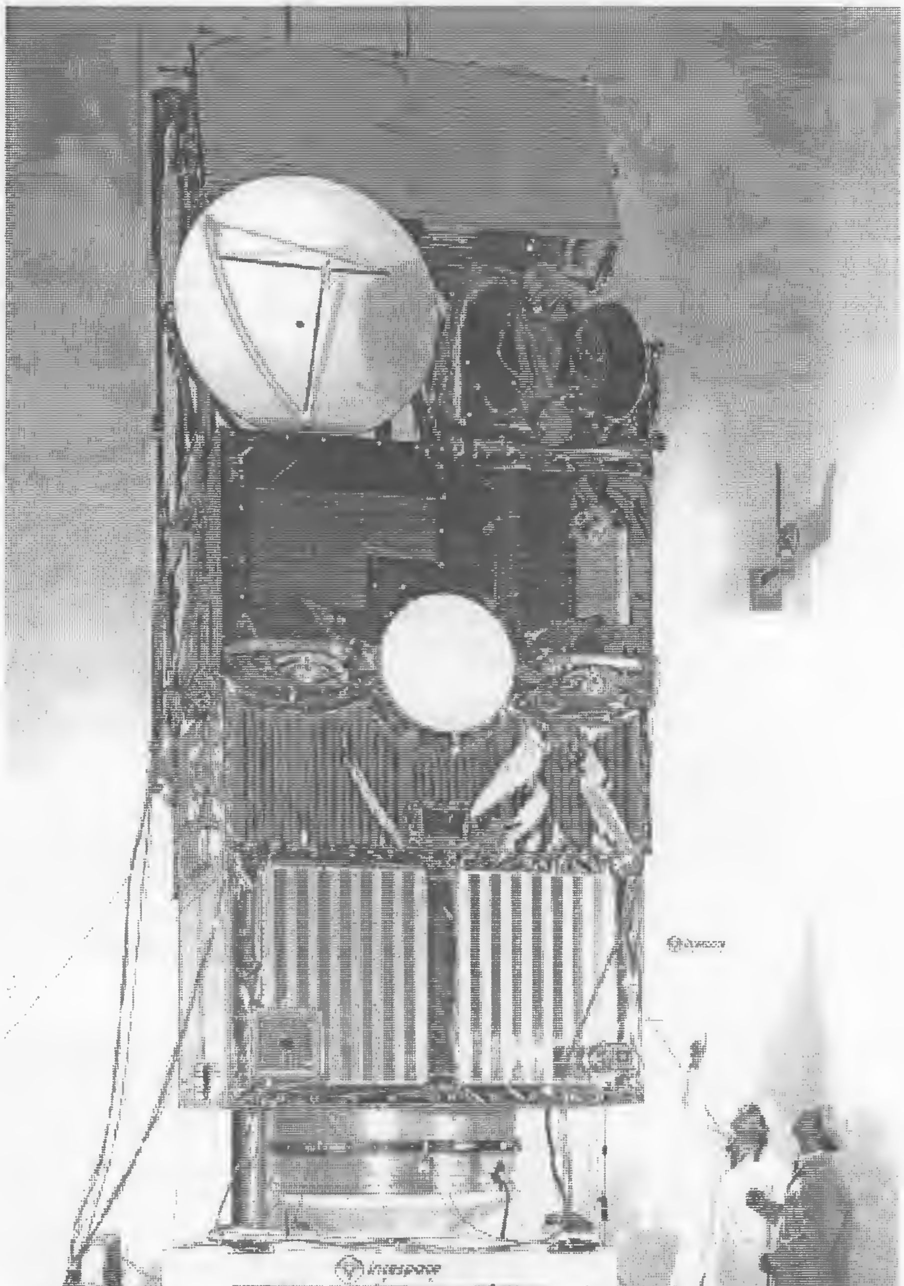

TABLE 1–1 Characteristics of the Commissioning Phase and MultiDisiplinary Phase Orbits. An additional 3-day repeat orbit with different phasing occurred between these two orbits.

Orbits	43	501
Repeat	3 days	35 days
Inclination	98.5162°	98.5429°
Semi-major Axis	7153.138 km	7159.495 km
Eccentricity	0.001165	0.001165
Phase	24.360° E	20.960° E
Start	26 July 1991	15 April 1992
End	11 December 1991	15 December 1993

Venice, once every 3 days. The repeatability of this overflight was generally within 1km and was within 500m throughout the calibration campaign.

1.2 The Radar Altimeter: Performance and Characteristics

The following description of the operation of the RA is restricted to the ocean tracking mode and the operation of internal calibration. Other modes are possible, but are not relevant.

1.2.1 How it Works

1.2.1.1 Generation of the echo

The radar altimeter is a pulse width limited radar. This means that the limiting factor on the illumination of the target is the radar pulse width, rather than the beamwidth, which is a more common mode of operation in radars. The radar signal is a narrow pulse (3ns[1], equivalent to about 90cm in thickness) which is transmitted in a narrow beam vertically down towards the ocean.

When this thin shell of microwave radiation illuminates the flat surface of the ocean the illuminated area is, at first, a rapidly expanding disc. This is shown in Figure 1–3. The received echo power increases quickly, as the surface is assumed to be diffuse so that the power scattered back to the receiver is proportional to the area. Soon the illuminated area becomes annular and from this point the illuminated area (and thus echo power) remains constant. As the annulus expands the incident and received scattered power become attenuated by the antenna pattern. Furthermore the leading edge is

1. Actually a 20μs pulse is used, but a pulse compression system reduces the equivalent pulsewidth to 3ns, with a corresponding increase in effective power.

FIGURE 1–3

Generation of the pulsewidth-limited RA echo. Note that the microwave radiation does not penetrate the water surface as shown; this is an attempt to clarify the diagram.

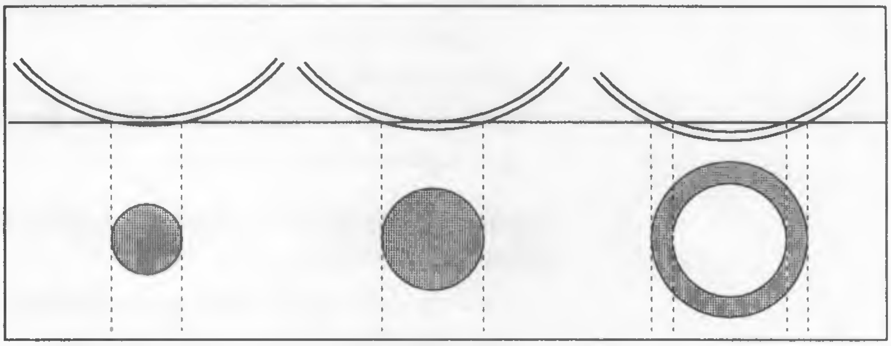

also modified by the real vertical distribution of scattering surfaces (*ie* horizontal surfaces), which over ocean surfaces is related to the waveheight.

This behaviour has been described by *Brown*, 1977, as the convolution of three functions:

- the flat-surface impulse response (which includes the antenna pattern);
- the impulse response;
- the vertical distribution of surface scatterers

The formulation of this has become known as the "*Brown Model*", and is described by the following expressions:

$$P_{fs}(\tau) = \frac{G_0^2\lambda^2 c\sigma^\circ(\psi_0)}{4(4\pi)^2 L_p h^3}\exp\left[-\frac{4}{\gamma}\sin^2\xi - \frac{4c}{\gamma h}\tau\cos 2\xi\right] \bullet I_0\left(\frac{4}{\gamma}\sqrt{\frac{c\tau}{h}}\sin 2\xi\right)$$

$$P_r(\tau) = \begin{cases} \eta P_t P_{fs}(0)\sqrt{2\pi}\sigma_p\left[1+\mathrm{erf}\left(\frac{\tau}{\sqrt{2}\sigma_c}\right)\right]/2 & \tau < 0 \\ \eta P_t P_{fs}(\tau)\sqrt{2\pi}\sigma_p\left[1+\mathrm{erf}\left(\frac{\tau}{\sqrt{2}\sigma_c}\right)\right]/2 & \tau \geq 0 \end{cases}$$

where:

P_r is the average return echo power;
τ is the two-way incremental ranging time $(\tau = t - 2\frac{h}{c})$;
η is the pulse compression ratio;
P_t is the transmitted power;
P_{fs} is the flat-surface impulse response;
σ_p is related to the width of the radars point target response;
σ_c is largely the scale-size of the distribution of surface scatterers;

G_0 is the antenna gain (on-axis);
λ is the radar wavelength;
c is the velocity of light;
$\sigma°(\psi_0)$ is the surface backscatter coefficient at incidence ψ_0;
L_p is the propagation loss;
h is the satellite height;
γ is a parameter related to the antenna beamwidth, and
ξ is the antenna mispointing.

Evidently there are several different ways to define the footprint of such a system. These include:

- the area illuminated before the illumination becomes annular;
- the area defined by the range window;
- the area defined by the antenna pattern.

When the surface is not flat (such as close to land) there is a chance that energy is echoed into the range window even when it lies outside these footprints, so long as the slant range is appropriate and the antenna pattern allows it. This case did not occur during the calibration passes.

1.2.1.2 The Instrument

The RA antenna, as already implied, has a narrow nadir-pointing beam, which is parallel to the z-axis of the spacecraft. The details of the coordinate systems and locations of reference points are given in CHAPTER 6, "The Satellite and its Measurements". Note that all measurements of height are referred to the RA reference point, which is the centre of the antenna aperture plane.

The functional block diagram for the RA in Ocean Tracking mode is shown in Figure 1–4. The radar echo consists of an ensemble of replicas of the transmitted signal, which is a pulse whose frequency changes linearly (by about 2.4%) during the pulse. For historical reasons such a signal is called a chirp. The average power envelope of the echo, over many returns, is given by the Brown model, but individual echoes have an uneven power envelope due to interference effects, sometimes called "fading noise". When the echo is expected to return, corresponding to the time delay of the two-way propagation path, a second chirp is generated, identical to the transmitted chirp, but offset in frequency (by a value which is later used for the down-conversion of the received echo signal). The difference frequency between these two chirps is constant during the pulse duration, causing the generation of a tone for each discrete chirp in the echo. The power envelope of the returns, in the time domain, is converted to a frequency spectrum, where the conversion factor is the chirp slope.

The spectrum analyser is a hardware digital signal processor. It extracts the 64 spectral components of the signal by a FFT. The spacing of these spectral components is 50kHz which, when converted to the time domain using the chirp slope, is equivalent to 3.03ns separation. A squared modulus extrac-

FIGURE 1–4 Block diagram of the Radar Altimeter

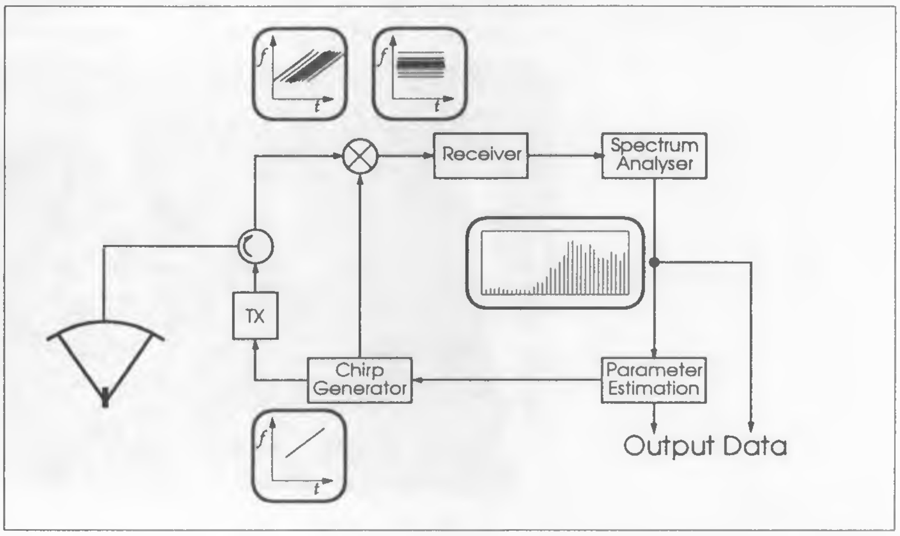

tion of the complex components is performed and these power values are averaged over 50 consecutive pulses. Before the FFT, a Hamming window is applied.

For the fine shifting of the spectrum, the phase of the video signal can be rotated by weighting the complex samples. The RX-trigger resolution is limited to 12.5ns, so this technique of fine shifting increases the overall systems delay resolution. The implementation of this 2-stage closure of the Height Tracking Loop (HTL) is as follows: the output of tracker is a 32-bit value, of which the most significant 16 bits are used to control the RX-trigger in 12.5ns increments (*ie* the time at which the deramp chirp is generated, synchronised with the 80MHz clock). The next 8 bits are used to access a look-up table containing the phase-rotation and Hamming coefficients, in order to implement the fine-shift. The least significant 8 bits are not used.

The fine shift has a dynamic range of about 4.125 filters (*ie* 12.5ns), in Ocean Mode. The fine-shifting of the spectrum is done in one direction only (moving the filter-bank 'rightwards'), due to the design of the DSP. If the spectrum were correctly centred when the fine-shift is zero there would be no aliased energy in the 'left' part of the spectrum (assuming a rectangular anti-alias IF filter). As the fine-shift increased to maximum the aliased energy would grow in the 'left' part, to a maximum of 4.125 filters. In order to reduce the impact of this error the position of the spectrum in the unshifted case is offset by 2 filters (achieved by a renumbering of the filters) so that the fine-shift effectively becomes bi-directional about the mid point. The filter-bank is thus centred on filter number 34 — this accounts for the different numbering of the ocean mode filters compared to the other cases (where this mechanism is not applied). The offset is compensated by subtracting a corresponding factor from the fine height word before recording it in the telemetry.

FIGURE 1–5

The electronic units of the Radar Altimeter. Two complete sets of units can be seen here as the instrument is fully redundant. The digital units are on the left hand side of the panel, while the microwave units are on the left. The waveguide feed to the antenna emerges at the lower right edge.

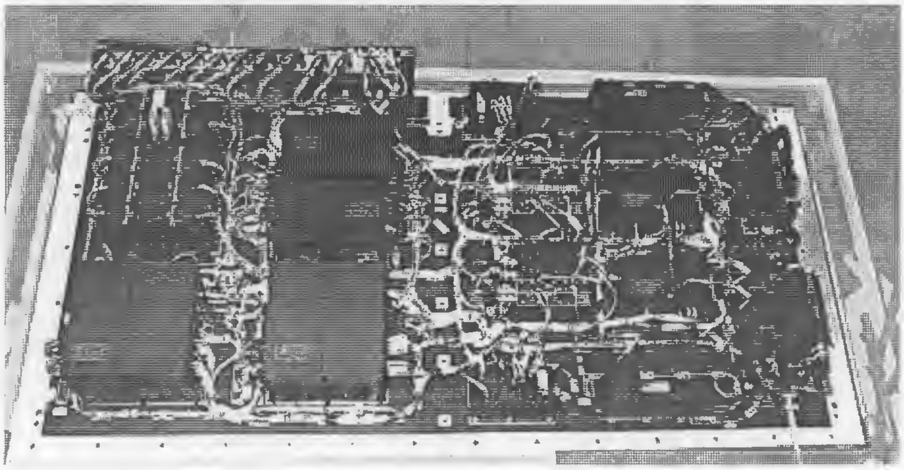

The Parameter Estimation Processor is a microcomputer (built around a 5MHz 8086) which implements 3 tracking loops in Ocean Mode: the HTL; Slope Tracking Loop (STL) which tracks the leading-edge slope, and an Automatic Gain Control (AGC) loop. Each tracking loop is composed of a discriminator, which produces an error signal, and a low-pass filter (implemented as an integrator) which produces the currently estimated parameter value, used to control the hardware. All the loop filters are of second order low pass-type, called $\alpha\beta$-filters, due to the use of two coefficients α and β in their implementation. The discriminators determine the relevant errors in the currently available average echo waveform parameters, with respect to an ideal echo, which is based on the Brown model. The algorithm is based on a Maximum Likelihood Estimator, but uses rectangular windows to represent the required partial derivative functions, for computational reasons. Thus the algorithm is a Sub-optimal Maximum Likelihood Estimator (SMLE).

A photograph of the hardware of the RA appears in Figure 1–5. The antenna is not shown in this picture, but is visible in Figure 1–1.

1.2.2 Internal Calibration

The internal calibration technique is used in-flight, and also during the prelaunch measurements at instrument level. It is not an end-to-end absolute calibration, but makes a relative calibration of the harmonic variations in the instrument measurements caused by thermal effects.

The calibration is based on a specialised form of waveform, in which the echo generated is a single point-target response (SPTR) instead of an ocean echo. The time delay associated with the centre of this SPTR can be evaluated accurately, by modelling the shape of the point target response and

FIGURE 1–6 The main elements of the internal calibration loop.

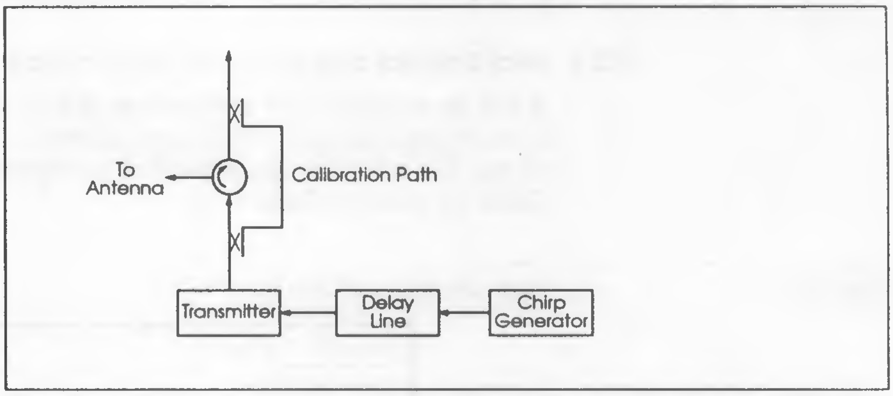

performing a fit to the FFT samples. This technique offers a robust calibration technique which does not depend on the linearity of the discriminators.

Figure 1–6 shows the essential elements of the block diagram of the internal calibration. The transmit signal (either the ice or ocean chirp) is delayed by the delay line (25μs), which is longer than the transmit (TX) signal duration (20μs), and after amplification in the transmitter is directly injected into the receiver chain through the calibration coupler. Deramping with the local oscillator (LO) chirp generates a tone whose frequency depends on the time delay between the TX and LO chirp as follows:

$$\Delta f = \Delta t \frac{B}{T}$$

where Δt is the time delay, B is the chirp bandwidth and T the chirp duration (20μs). The time delay quantum is the period of the 80MHz clock which is used for the RX trigger timing; *ie* 12.5ns. The chirp bandwidths are 82.5Mhz and 330MHz for ice and ocean respectively. Thus the smallest real interval between possible tones is 51.56kHz and 206.25kHz respectively.

The FFT samples have a Hamming weighting function applied, in order to reduce the sidelobe amplitude (in theory to –40dB, with a 30% main lobe widening). This weighting function, for t in the range $-T/2 \le t \le T/2$, and with $\alpha = 0.04$, is:

$$W(t) = \alpha + (1-\alpha)\cos^2\left(\pi\frac{t}{T}\right)$$

The open-loop calibration if performed by building up a single point target (SPTR) echo as described above. The activity takes place at a regular interval, which is programmed by macrocommand. Throughout the commissioning phase the interval has been every 30 seconds. The SPTR echoes are made alternately using ice and ocean chirps. The SPTR waveforms may be used to find a "model-independent" time-delay calibration, and they also provide the amplitude of the SPTR and the pulse-width.

1.2.3 Vital Statistics and Measured Performance

A full description of the performance of the RA will not be given here; this is described by *Francis* (1992) in a dedicated document. Instead a summary of the key technical characteristics and performances will be provided. These are shown in Table 1–2.

TABLE 1–2 Main characteristics of the ERS-1 RA

Transmit frequency	13.8 GHz
Transmit power	55W
Pulse repetition frequency	1020Hz
Chirp duration	20μs
Chirp bandwidth	330MHz
Pulsewidth	3.03ns
Antenna diameter	1.2m
Beamwidth	1.3°
Mass	96kg
Power consumption	130W
Height noise (from tracker)	4.2cm[1]
Height noise (precision processing)	2cm[2]
Height Stability	<0.1cm

1. Alenia Spazio estimate.
2. see CHAPTER 6, "The Satellite and its Measurements".

CHAPTER 2

The Problem

This chapter will define the background and objectives of the RA calibration. It will also set the scene for what follows by describing the overall concept and scenario.

2.1 Objectives and Criteria for Calibration

The height measurements made by the ERS-1 radar altimeter have a long-term stability at the millimetre level thanks to the design and operation of the instrument. The ultimate noise level is about 2.5 cm (see CHAPTER 6, "The Satellite and its Measurements"). However determination of the bias in the height measurements to an equivalent accuracy was not possible prior to the launch, the residual error being estimated at about half a metre. Consequently it was necessary to determine the height bias error after launch, by means of a dedicated measurement campaign. It was known that maintaining control of all the measurements contributing to this determination would be a delicate task, but it had been achieved before (*Kolenkiewicz and Martin*, 1982).

Calibration has many interpretations. In this case the requirements were clearly identified, being stated by *Francis and Duesmann* (1988) as:

1. *The objective is engineering calibration. Geophysical effects shall be minimised or eliminated wherever possible. The requirement is to calibrate the instrument rather than any particular data-product.*
2. *Both the accuracy and the precision shall be maximised, with an overall goal of 5 cm for the combined error.*
3. *The calibration shall avoid potential single-point failures, and be resistant to the effects of single errors.*
4. *The calibration shall be performed during the Commissioning Phase, ie the first 3 months of the mission.*
5. *The orbit to be used shall also fulfil the calibration requirements of other ERS-1 sensors, specifically the Wind Scatterometer and the SAR.*

6. *The calibration shall be carried out within Europe.*

2.2 Overall Description and Scenario

The calibration concept, which evolved some years prior to the launch, made maximum use of existing European facilities, particularly the uniquely high density of satellite laser ranging (SLR) stations. The key elements of the approach are:

1. Arranging that the satellite overflies a well-defined, instrumented point in the open sea;
2. Measuring the sea-level (tide) at this point, together with all relevant environmental properties (tropospheric and ionospheric content, winds, waves *etc*) from a small fixed installation;
3. Using several SLR sites surrounding the comparison site, including one close to the satellite track. Slew-rate limitations do not prevent continuous tracking by any of the systems;
4. Dedicated campaigns to measure the three-dimensional positions of all reference points, and the local geoid;
5. Having a high degree of redundancy in the system to aid error resistance.

A schematic illustration of the overall scenario is shown in Figure 2–1. The satellite made northward passes directly over a small research platform located about 14km offshore from Venice. This platform, called *"Acqua Alta"*, is owned and operated by the *Istituto Studio Dinamica Grandi Masse* (ISDGM) of the *Consiglio Nazionale della Ricerche* (CNR). It is a tower fixed to the sea-bed in about 16m of water, at a position 45°18.78'N, 12°30.55'E (45.3130°N, 12.5092°E). An illustration of the *"Acqua Alta"* tower during the campaign is shown in Figure 2–2.

The satellite was tracked simultaneously by several SLR sites, which have become known as the European Calibration Network, or ECN. In addition to the fixed sites Grasse, Graz, Herstmonceux, Matera, and Zimmerwald a new mobile laser site was required and this was installed at Baiamonte on Monte Venda, in the hills south of Padova (see ANNEX E, "Site Selection and Preparation"). This site is about 60km to the west of the tower. This area is suitable for a number of reasons, including superior weather conditions due to its altitude above the coastal plain. A full description of the history of the selection of this site is given in ANNEX E, "Site Selection and Preparation". The six lasers provided a network surrounding the calibration site, with a favourable topology; this network had considerable redundancy. Analysis had shown (*Francis and Duesmann*, 1988; *Scharroo et al*, 1990) that useful results would be obtained with various subsets of the lasers, and this was a major contributor to the reliability of the system.

The tower was localised in the same network as the laser sites by a series of measurement campaigns using the GPS system. This enabled a direct *in-situ*

FIGURE 2–1

An overall view of the calibration scenario.

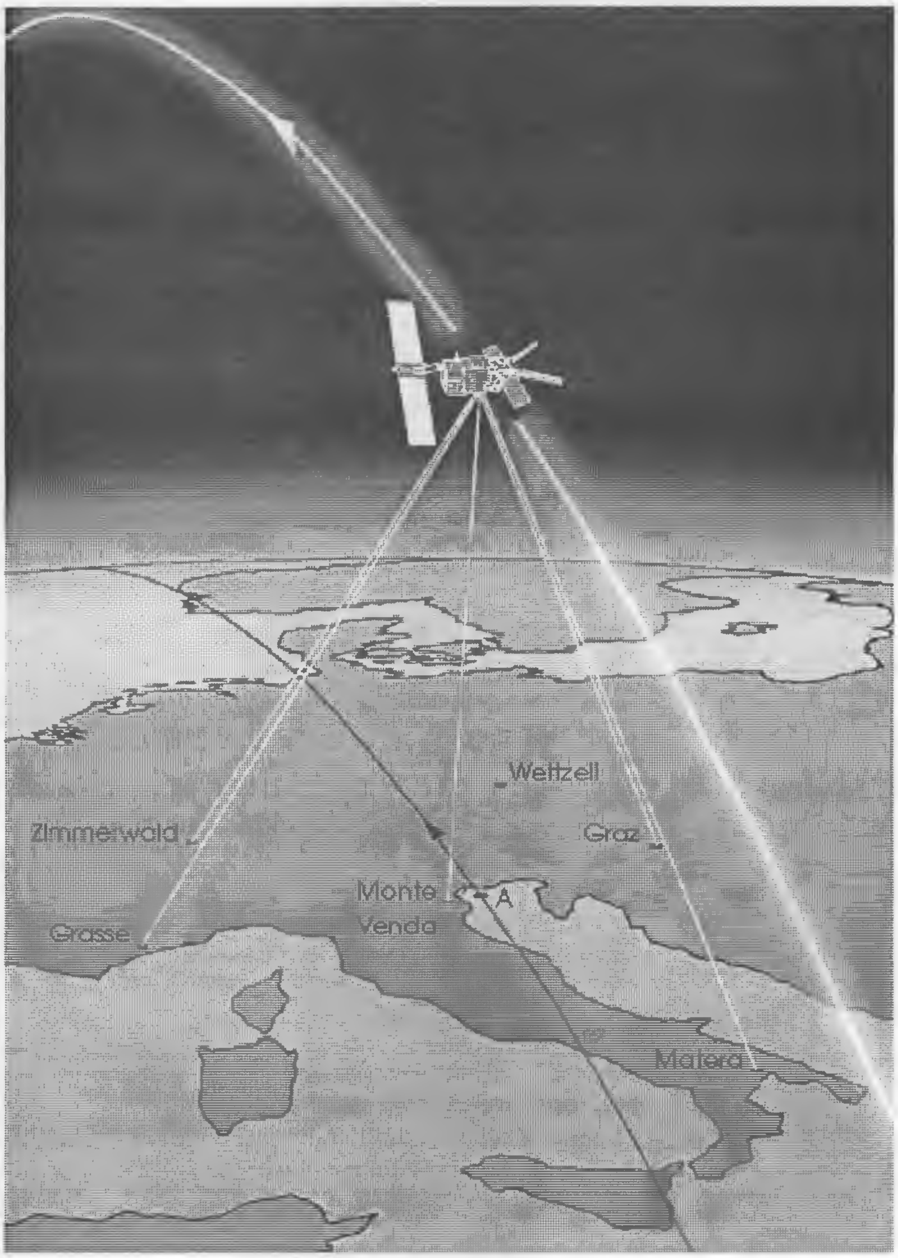

measurement of the position of the ocean surface at the calibration point in the same local frame of reference as the lasers.

The ground-track of the northbound pass over the northern Adriatic Sea and the "*Acqua Alta*" tower is shown in Figure 2–3. This pass was over the sea for about 25sec before the tower overpass, which was known to be sufficient for the altimeter to acquire the sea-surface and for the tracking loops to settle. In fact the "line" representing the pass in Figure 2–3 is the super-

FIGURE 2–2

The CNR Tower "*Acqua Alta*" during the calibration campaign. The microwave radiometer is visible on the upper platform, undergoing tip-curve calibration. The wells of the two tide gauges may be seen on either side of the access ladder.

position of the locations of all of the individual altimeter measurements actually obtained. It can clearly be seen that the altimeter is producing useful measurements very close to the coast, as the acquisition is very fast (about 1 second) and the data have been retracked, so that the transient behaviour of the tracking loops immediately after acquisition is eliminated.

It is also apparent from this figure that the ground track did not always pass directly over the tower; there was an overall cross-track spread of about one kilometre.

These northward passes of ERS-1 were night-time passes, overflying the tower at approximately 22:05 local solar time (as summer time was in use this became 23:05 local time). This was particularly favourable for the SLR systems[1] and also reduced the effect of the ionospheric delay as the ionosphere is less dense at night.

2.3 Details of the Technique

The most straightforward formulation of the altimeter calibration procedure is the following: measure the altimetric height of the satellite above the sea surface, determine the satellite's altitude from an orbit computation based on tracking data, and simultaneously measure the sea level height by a tide gauge, of which the position is known accurately. The comparison of the difference between the first two values with the latter yields the altimeter bias. This scheme is illustrated schematically in Figure 2–4. From this figure it may be concluded that, at the time of overflight of the tide gauge, the following relation holds:

$$b = N_{tide} - N_{alt} = N_{tide} - h_{orb} + h_{alt} \qquad \text{(EQ 5)}$$

where:

- b = altimeter height bias;
- h_{alt} = measured altimeter height above the sea surface around the tide gauge, corrected for instrumental and propagation effects and centre-of-mass offset;
- h_{orb} = satellite altitude above a reference ellipsoid (WGS 84);
- N_{alt} = altimetric sea surface height (SSH) with respect to the reference ellipsoid, at the position of the tide gauge;
- N_{tide} = sea surface height above the reference ellipsoid, as measured by the tide gauge.

The altimeters of GEOS 3 (*Martin and Kolenkiewicz*, 1981) and Seasat (*Kolenkiewicz and Martin*, 1982) were calibrated in a similar way, in 1976 and 1978 respectively, using overflights of Bermuda supported by a laser on Bermuda. Since these passes were almost overhead, the laser ranging data from this single site could be used for a highly accurate determination of the orbit height. A drawback in this Bermuda scenario is that no altimeter data were available when the satellite was at the zenith of the laser, because

1. This proved to be particularly important for ERS-1. The large air-drag effect rapidly degraded the orbital predictions used by the lasers; the fact that ERS-1 was very bright optically often helped in finding it. Fortunately the campaign occurred at the right time of year for ERS-1 to be visible in the European evenings.

FIGURE 2–3 The positions of the altimeter measurements made during eight of the calibration passes of ERS–1 over the Adriatic. Each of the 20Hz measurement data points are represented by a small dot. As the data have been retracked measurements are available very close to the coastline at the southern end of the track, indicating that acquisition has occurred very rapidly. The loss of track in the marshes north of the Venice lagoon is also evident.

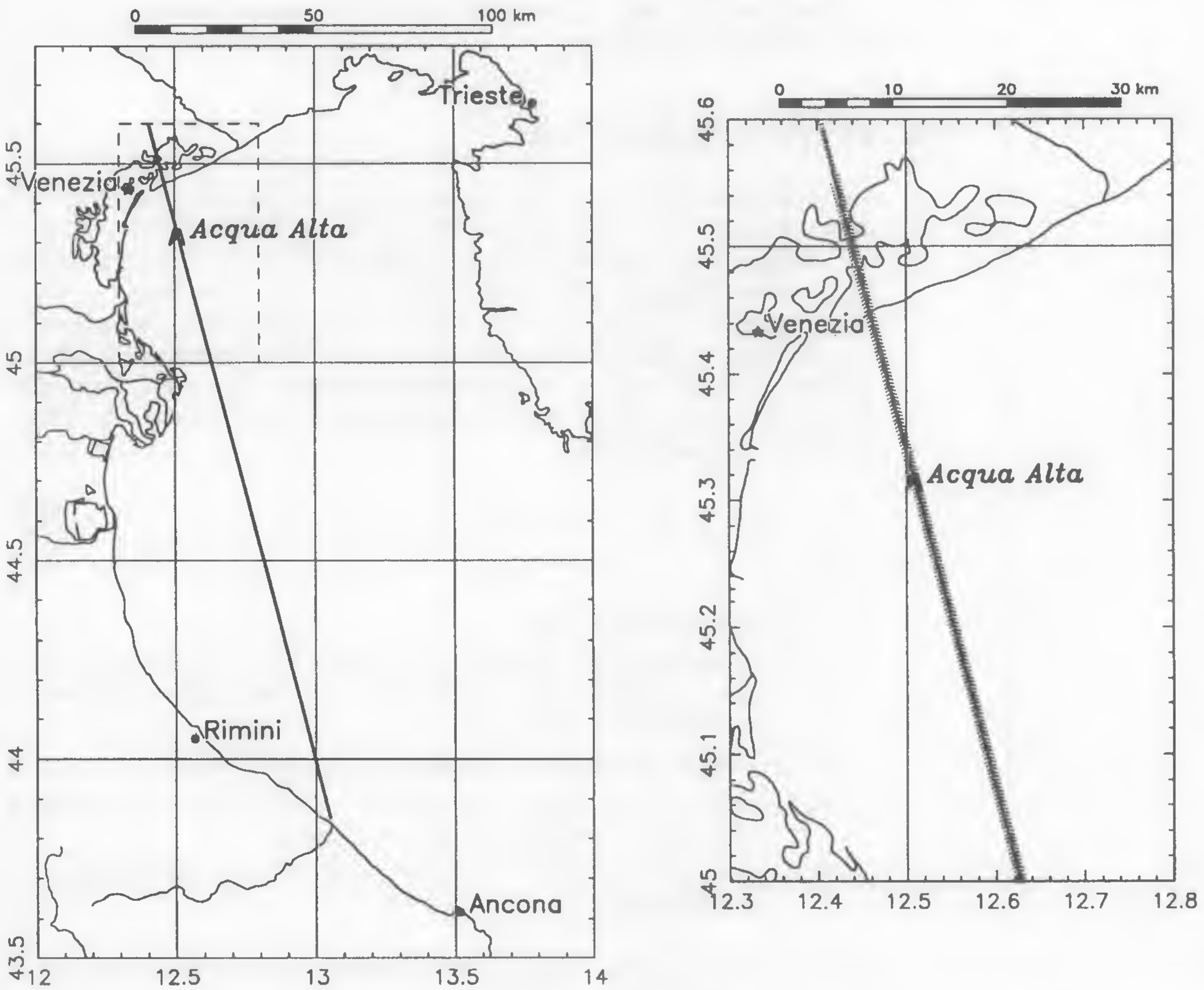

of land in the altimeter footprint. This poses a problem since the resulting altimeter data gap occurs just at the moment when the satellite's computed radial position component has maximum accuracy. Moreover, the tide gauge was not located vertically beneath the satellite's pass, which may have introduced additional problems. Though the calibration procedure for ERS-1 is quite similar to this previous scenario it differs in just these two points.

Figure 2–4 summarises the general data flow and processing steps involved in the calibration activity. Four separate elements can be identified:

1. Tracking of ERS-1 by satellite laser ranging (SLR) systems provides the possibility to accurately determine the satellite's location and altitude. Unfortunately the Precise Range And Range-rate Equipment (PRARE) failed soon after launch and was thus not able to contribute to the orbit determination. The details of the orbit determination are given in CHAPTER 5, "The Trajectory".
2. The altimeter measurements are corrected for internal and external delays, and thereafter are subtracted from the orbital height to form samples of the sea surface height along the satellite's track in the vicinity of the *Acqua Alta* tower. The corrections applied are instrumental (such as the internal delay of the radar pulse and the centre-of-mass offset), environmental (tropospheric and ionospheric delays, measured by equipment on board of the tower), or physical (Doppler effect and EM-

FIGURE 2–4 Schematic illustration of the calibration technique

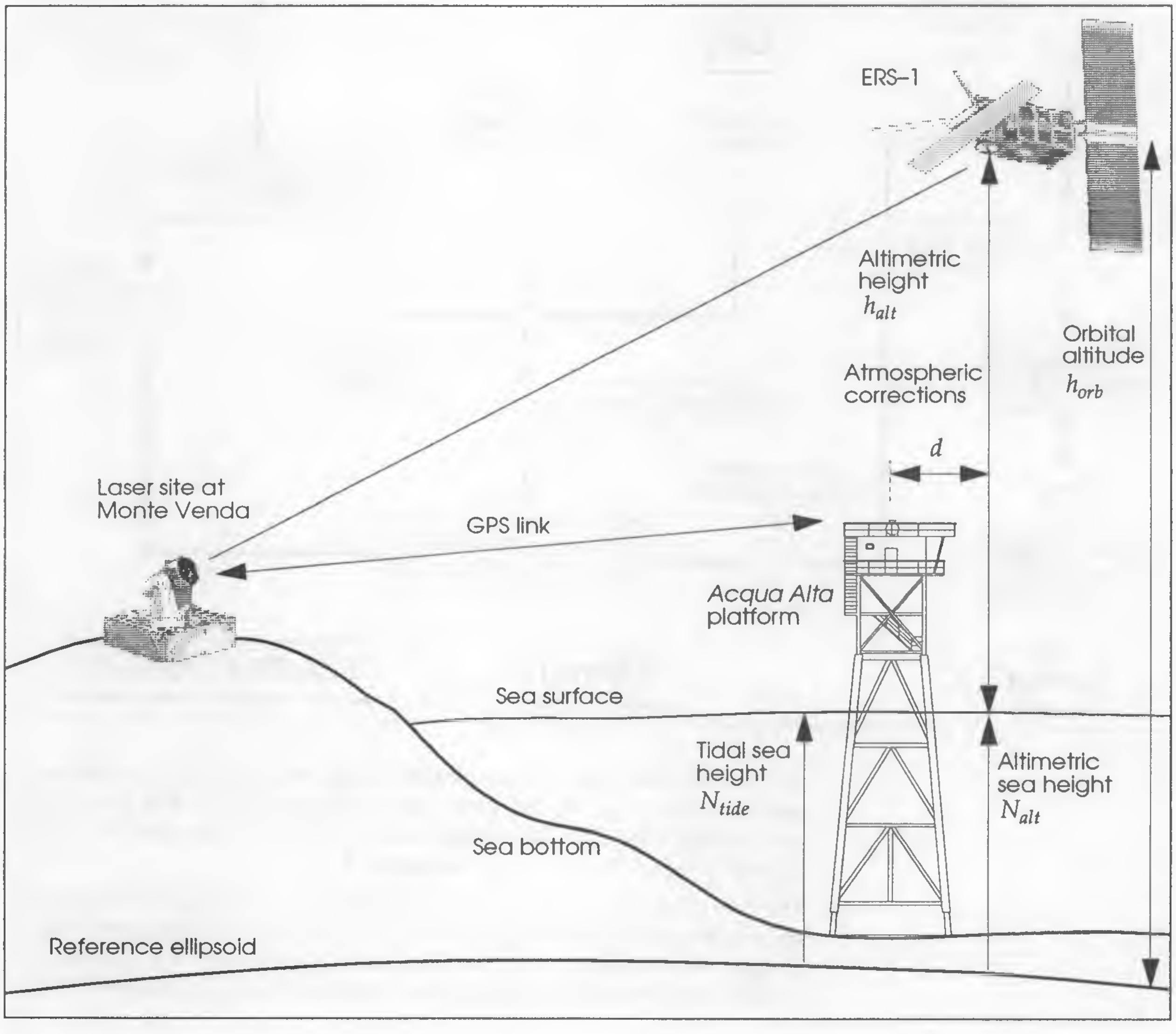

FIGURE 2–5 The ERS–1 radar altimeter processing diagram

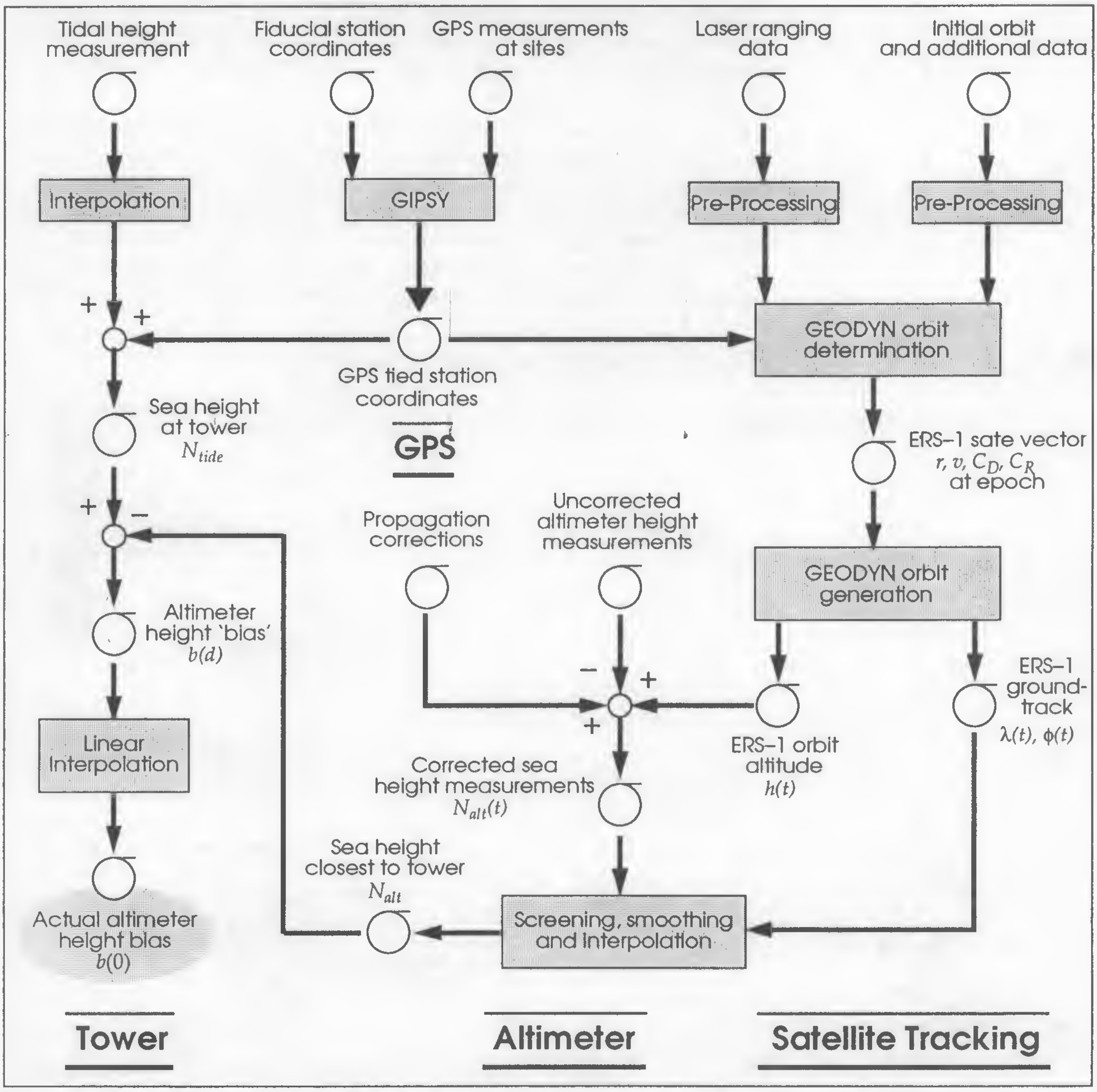

bias). A smoothing and interpolation technique (based on collocation) is used to determine the altimetric sea height closest to this tower. The processing of the altimeter measurements is further described in CHAPTER 6, "The Satellite and its Measurements".

3. The tide gauge at the *Acqua Alta* tower produces an independent assessment of the sea surface height (See CHAPTER 4, "Local Measurements"). Comparison with the measured altimetric sea level, corrected for the sea surface slope along the shortest line between the tower and the ERS-1

ground track, gives the altimeter measurement bias. This comparison is fully described in CHAPTER 7, "The Results".

4. The Global Positioning System (GPS) has been used to tie the *Acqua Alta* tide gauge to the reference frame of the tracking systems. Additionally, local surveys have been conducted to refer the GPS markers to the origins of the laser ranging systems and the tide gauge. In that way both the sea height measured by the altimeter and by the tide gauge are brought into the same reference frame, and can be compared. For more details, see CHAPTER 3, "The Three-Dimensional Network".

Although the interpolation provides the sea surface height at the point along the track closest to the *Acqua Alta* Tower, it does not provide the altimetric height exactly at the tide gauge itself, due to deviations in the ground track from the ideal. As ERS-1 always passed *Acqua Alta* within 600 m, a correction may be computed from the local deflection of the vertical. In this approach it is assumed that the local sea surface slope equals the geoid slope, which is a realistic assumption since there are no strong currents expected in this specific region. Alternatively, a linear interpolation between a number of bias estimates, determined along various tracks and at varying distances from the tower, provides an independent assessment of the local mean sea surface slope.

Additionally, the height of the zero-level has to be corrected for Earth tides.

Furthermore, a local survey at the Venice Tower was needed to refer the zero sea level height to the GPS marker on the Tower. Thus the actual height of the water column in the well had to be known when the tide gauge was reading a certain value. This proved to be a rather troublesome activity.

CHAPTER 3

The Three-Dimensional Network

This Chapter will concentrate on the invariant part of the network. It is concerned with locating in three dimensions all of the fixed elements of the calibration system. In earlier analysis of the calibration of the ERS-1 RA (Francis and Duesmann, 1988) it had been shown that locating the exact position of the Acqua Alta platform, and thus providing the means to locate the sea level in the laser frame of reference, was one of he most critical elements of the entire campaign. Consequently a significant effort was devoted to this over several years. Additionally it was evident that a determination of the local geoid in the cross-track direction was necessary. In the 1988 work Francis and Duesmann had also briefly considered the problem of determining the relative positions of the reference points on the Acqua Alta tower itself. This turned out to be a significant task.

3.1 The Regional and "Large" Networks

The determination of the exact location of the sea level during the calibration passes of ERS–1 was possible because the sea-level recorded by the tide gauge on-board could be referred to a geodetic reference point on the *Acqua Alta* tower. This reference point which is a node of a regional network (see Figure 3–1), in the sense that a number of measured baselines connect this point to other geodetic reference points on land. The boundary of the network has an approximately rectangular shape, the longest side being in the N-S direction (about 100 km), while the E-W side is approximately 80 km. The origin of the network is the laser site at Baiamonte, on the Monte Venda. The coordinates of this point have been determined in two independent ways: one by direct LAGEOS laser ranging, the other by means of GPS surveys (the "Large" GPS Campaigns of October 1990 and September 1991) involving other European laser/GPS stations.

The "Large" GPS Campaigns involved, besides Monte Venda, also the tower itself. Therefore the origin, azimuth and scale of the local network are completely defined by the coordinates of the tower and Monte Venda. The vector associated to this baseline is 64 km long and thus of the same order of magnitude as the size of the network. The baseline is completely included in the network.

Figure 3–1 shows the surveyed baselines and some of the most important points of this regional network. Note that only some of these points were eventually used for the local geoid computation, as discussed later. The original triangulation network of 1988 was complemented in 1990 by longer

FIGURE 3–1 Key vertices and baselines of the network

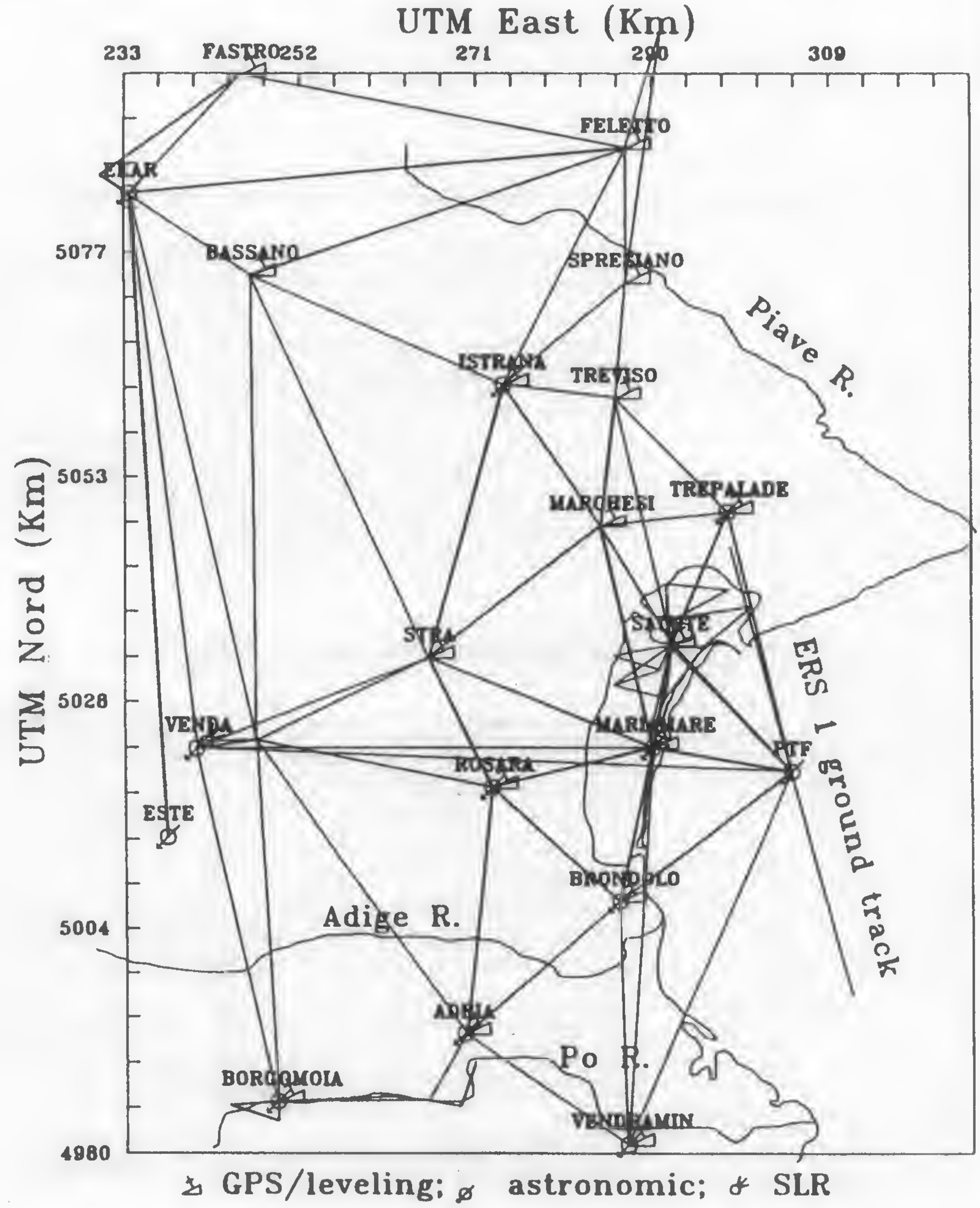

baselines made possible by the advent of dual frequency GPS receivers, which do provide more control but also tend to destroy the structure of the original triangulation. All the recorded data were processed with the standard program *PoPS* (Post Processing Software) and converted to baseline vectors. Eventually, the individual vectors and variance covariance matrices, also provided by PoPS, were adjusted as a network using the program *Geolab*.

The GPS measurements from the "Large" GPS Campaign of October 1990 have been analysed both by the Delft University of Technology, Section Orbital Mechanics (DUT/SOM) using the GPS Inferred Positioning SYstem software (*GIPSY*), as well as by the Astronomical Institute of the University of Berne (AUIB) with the *Bernese* GPS Software. This dual approach was adopted to enhance the reliability of the analysis.

A second campaign in September 1991, organized by the Institute of Space Research Graz for the purpose of transponder positioning was used as a further determination of the Mount Venda—*Acqua Alta* platform baseline. This campaign has been processed by AIUB only.

Section 3.3 presents the results of the analyses of the GPS measurements by both AIUB and DUT/SOM. The SLR marker coordinates of Monte Venda and the GPS marker coordinates of the Venice Tower are presented in both DUT/SOM's ERS90B and the ETRF89 reference frame. Formal errors and repeatability indicate an accuracy of the height component of the *Acqua Alta* platform of better than 4 cm. The results compare favourably between the independent computations and the two independent campaigns.

3.2 Fixing the Regional Network

The individual stations and their UTM coordinates are listed in Table A–1 in ANNEX A, "Network Adjustment". Their selection was primarily dictated by a) the existence of accurate levelled heights and b) the suitability for occupation by GPS receivers. The density of the points is larger near the coast than inland, because of the need to collect data on the geoid–ellipsoid separation as closely as possible to the calibration area. The mean interstation distance is approximately 15 km, which justifies the use, in the 1987 and 1988 campaigns, of single frequency GPS receivers. The astrogeodetic deflection of the vertical was determined at those few points (Ekar, Este, Tower (*Acqua Alta*) and Venda) where the levelled height was not available, and at other selected points. All occupied points have an accurate description and monumentation. They should be easily retrievable for future use with a few exceptions mentioned below.

At the Asiago Observatory (Cima Ekar) the site called Ekar is the axis of the new telescope. This was under construction, and thus accessible, in March 1990. This was no longer the case in July 1990, so the astrogeodetic station had to be made elsewhere, near the main building. To obtain the corresponding geodetic coordinates of the new site, it was surveyed by GPS in

July 1991 and called Ekar0691. Papozze was occupied in 1987. The marker was on the stony step (the first step from below) of a stairway on the left bank of the Po river. By 1990 the marker was no longer there. Therefore a new station, Papozz90, was introduced on the same step. Finally, on the *Acqua Alta* tower, the mast which was used to fix the marker for the 1988 campaigns had, by 1990, been taken away and then re-installed, presumably on a slightly different place. Therefore the new site PTF0390 was introduced in place of PTF_88 during the March 1990 campaign. PTF0390 was occupied during the "Large" GPS Campaign of October 1990. Then, due to new civil engineering works on the platform, the marker was moved to a new place, but this time an accurate determination of the relative position was made by Telespazio personnel. We remark that in the analysis each site in the pairs (Ekar, Ekar0691), (Papozze, Papozz90), (PTF_88, PTF0390) has been treated independently of its companion, since no relative positional data were available.

The vertices in Figure 3–1 were occupied during campaigns in 1987, 1988, 1990 and 1991. In 1987 and 1988 single frequency receivers, of type Wild Magnavox WM101, were used. The 1990 measurement were made with the dual frequency WM102's. In 1991, once the selection of the Baiamonte site became firm, the connection of an earlier temporary site (the Helipad) on the Monte Venda, called VENDA in these tables, to Baiamonte was made with the dual frequency WM102 GPS receiver. Table A–2 in ANNEX A, "Network Adjustment" summarizes the surveyed baselines and polygons which were used in the adjustment.

Table 3–1 summarizes the breakdown of observations, parameters and constraints of the network adjustment, while Table 3–2 summarises the statistics of the adjustment.

The adjustment provided coordinates of the vertices which minimize, in a least square sense, the vector misclosures under the constraint that two points (*Acqua Alta* and Monte Venda) are given fixed coordinates. The presence of two fixed points gives the adjustment enough control to estimate a scale constant. The adjustment is done in three dimensions in the sense that it uses cartesian components of the baseline vectors. Therefore the least squares minimisation of the vector misclosures is done in the three dimensional Euclidean space. The cartesian coordinates of the free stations, after the adjustment, are listed in Table A–3 in ANNEX A, "Network Adjustment"

The cartesian coordinates were projected onto the WGS84 ellipsoid and converted to geodetic coordinates, in order to be used as reference for the astronomic latitudes and longitudes, and for the levelled heights. The geodetic coordinates are listed in Table A–4 in ANNEX A, "Network Adjustment". Figure 3–1 shows the network geometry and the measured baselines while Table A–5 in ANNEX A, "Network Adjustment" gives the corresponding error ellipses.

TABLE 3–1 Breakdown of parameter types, data and constraints in the adjustment

Parameters		Observations	
Description	Numbe r	Description	Numbe r
All Stations	45	Directions	0
Fixed Stations	2	Distances	0
Free 3-D Stations	43	Azimuths	0
Free 2-D Stations	0	Vertical Angles	0
Free 1-D Stations	0	Zenithal Angles	0
Coord. Parameters	129	Angles	0
Astro. Latitudes	0	Heights	0
Astro. Longitudes	0	Height Differences	0
Geoid Records	0	Auxiliary Params.	0
All Aux. Pars.	1	2-D Coordinates.	0
Direction Pars.	0	2-D Coord. Diffs.	0
Scale Parameters	1	3-D Coordinates.	0
Constant Pars.	0	3-D Coord. Diffs.	294
Rotation Pars.	0		
Translation Pars.	0		
Total Parameters	**130**	**Total Observations**	**294**
Degrees of Freedom = 164			

TABLE 3–2 Summary of the statistics of the adjustment

Residual Critical Value Type	Tau Max
Residual Critical Value	3.8558
Convergence Criterion	0.001000
Confidence Level Used	95.0000
Number of Flagged Residuals	25
Estimated Variance Factor	10.1673
Number of Degrees of Freedom	164

Figure 3–2 gives the histogram of the normalised misclosures and the superimposed gaussian of width computed on the basis of the adopted statistical criterion (Tau max).

FIGURE 3–2 Histogram of 3-D Coordinate Differences (291) standardised residuals, in the sense metric residual/standard deviation

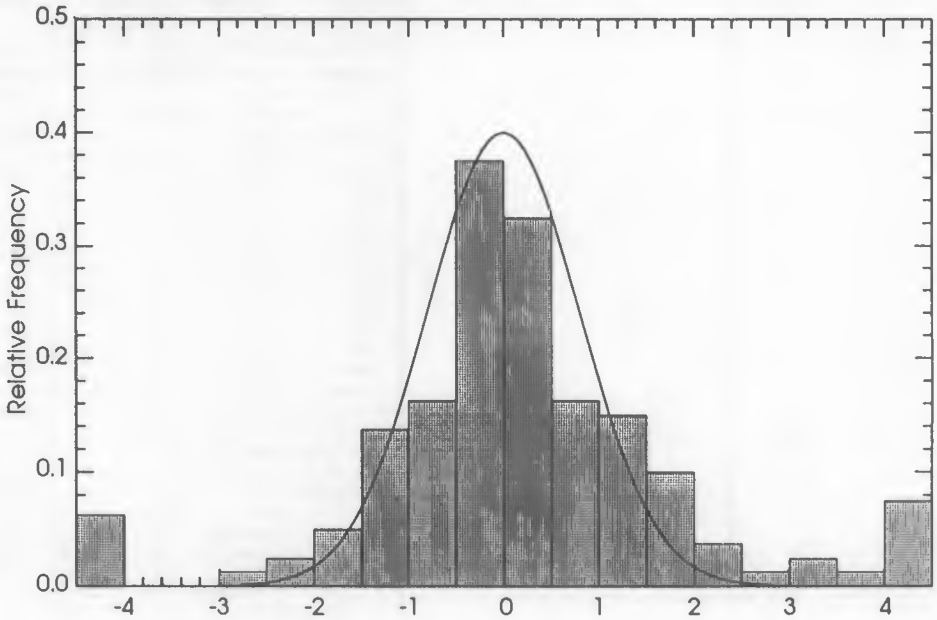

3.3 Fixing the "Large" Network

3.3.1 The October 1990 Campaign

As described above, a large GPS campaign was organized by AIUB and the University of Padova. From 14–19 October 1990, GPS data were collected in daily 8-hour sessions at 6 well established SLR sites: Grasse (France), Graz (Austria), Kootwijk (The Netherlands), Wettzell (Germany), Matera (Italy) and Zimmerwald (Switzerland), near the mobile SLR site at Monte Venda (Italy), and at the *Acqua Alta* platform (Italy). This network is shown in Figure 3–3. This was one of the two major techniques (the other being LAGEOS tracking) used to determine the location of the key points of the regional network in the same frame as the European Calibration Network (ECN) of SLR sites.

The following institutions performed the GPS measurements:

Graz	Institut für Weltraumforschung, Graz (instrument owned by Geodätisches Institut, Universität Wien)	WM-102
Grasse	Institut de Geodesie, EPFL Lausanne (2 instruments)	WM-102
Kootwijk	Kootwjik Observatory	Rogue
Matera	Telespazio, Matera	WM-102

FIGURE 3-3

Sites occupied by GPS receivers for the "Large" Campaign in 1990. The straight line indicates the 'Calibration Orbit' of ERS-1 overhead the *Acqua Alta* Tower.

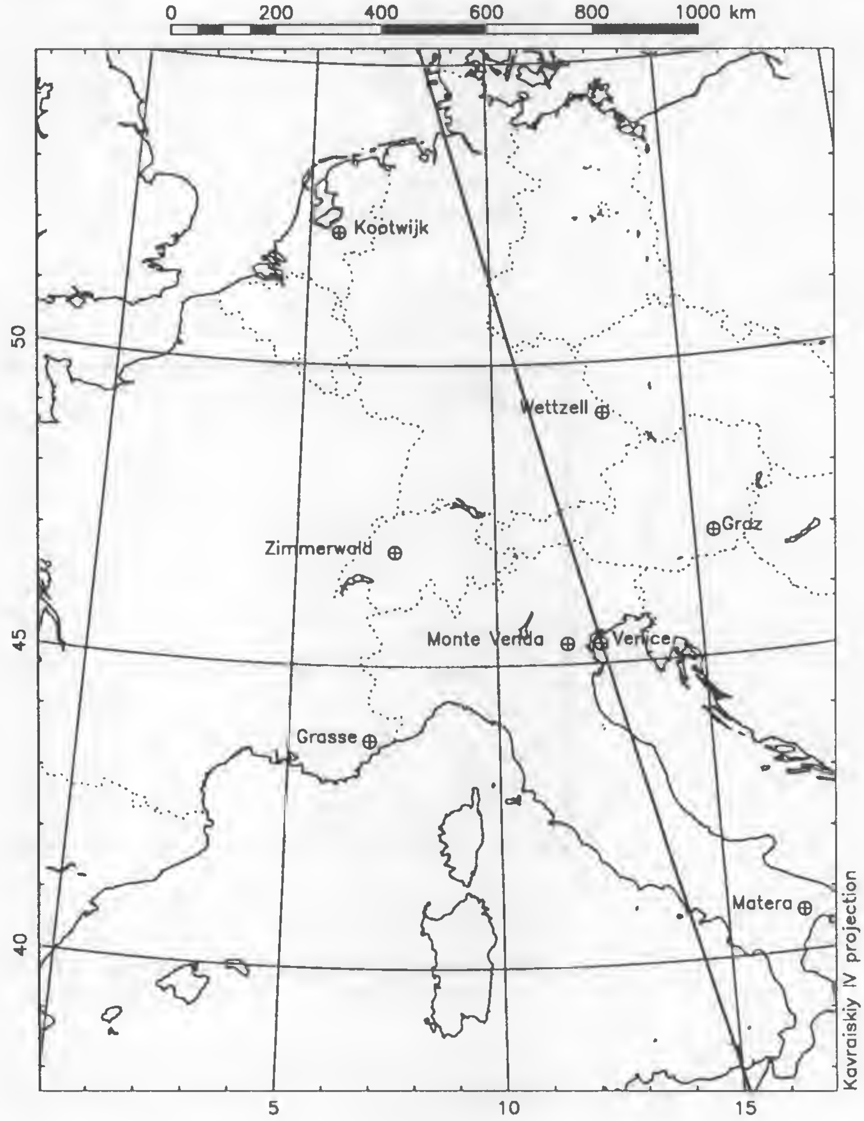

Wettzell	Institut für Angewandte Geodäsie, Wettzell	Minimac
Zimmerwald	Astronomisches Institut, Universität Bern (instrument owned by Institut für Geodesie und Photogrammetrie, ETH Zürich)	WM-102
Monte Venda	Dipartimento di Fisica, Università di Padova	WM-102
	Kootwijk Observatory	Trimble

Acqua Alta	Dipartimento di Fisica, Università di Padova	WM-102
	Kootwijk Observatory	Trimble

The primary instrument was the Wild-Magnavox WM-102 receiver, which was used at most sites. At Grasse even two WM-102 receivers were operating in parallel. The data from Wettzell were taken by a continuously operating Mini-Mac 2816 AT receiver. At Kootwijk a SNR-8 Rogue receiver was operating. Finally, two additional Trimble 4000 SST receivers were deployed at Monte Venda and the platform respectively. Table 3–3 summarizes the operation of the various receivers.

TABLE 3–3 Available GPS Calibration Campaign data (hr:min) per station- receiver pair, and per day, during the period 14–19 October 1990.

Station	Receiver	14	15	16	17	18	19
Graz	WM-102	–	8:00	8:16	7:20	8:11	7:44
Grasse (1)	WM-102	6:54	7:05	7:02	7:02	7:03	6:57
Grasse (4)	WM-102	6:53	7:07	7:02	7:02	7:02	6:58
Kootwijk	Rogue	1:20	0:33	1:38	2:05	2:04	–
Matera	WM-102	1:51	6:41	6:37	6:48	6:45	–
Monte Venda	WM-102	5:19	6:30	6:44	6:25	6:45	–
Monte Venda	Trimble 4000 SST	6:59	6:59	6:59	6:59	–	–
Acqua Alta	WM-102	5:07	3:51	5:05	6:57	7:04	–
Acqua Alta	Trimble 4000 SST	–	5:46	5:59	6:21	6:01	–
Wettzell	Mini-Mac	7:30	7:30	7:30	7:30	7:30	7:30
Zimmerwald	WM-102	–	7:14	7:47	7:52	7:51	7:49

Because the Rogue receiver at Kootwijk collected very few data, these data have not been analysed. GPS data from GPS 11 also have not been analysed, because GPS 11 experienced an orbital manoeuvre from 19:17 on 15 October until 19:17 on 16 October 1990 (*GPS Bulletin*, 1990).

GPS site coordinates often refer to an actual monument near the antenna. At tracking sites where a local tie is not available, the GPS site coordinates refer to a physical reference mark on the structure upon which the antenna is mounted. Local ties include:

- A vector between the reference monument and the monument over which the antenna is located.
- A vector from the monument to a physical reference mark on the antenna.
- A vector from the reference mark on the antenna to the antenna phase centre.

Table B–1 in ANNEX B, "The "Large" GPS Campaign" presents the local survey information between the fixed SLR marker and the GPS marker at the various SLR sites, and the eccentricity vector between the SLR marker and the GPS marker at Monte Venda. Table B–1 in ANNEX B, "The "Large" GPS Campaign", and subsequent Tables, also contain the local survey between the WM-102 GPS markers and the Trimble GPS markers at Monte Venda and *Acqua Alta*, and the antenna height and phase centre information.

The SLR marker coordinates of the European Calibration Network (ECN) SLR systems are recovered from the DUT/SOM ERS90B coordinates solution (*Noomen*, 1991). The coordinates of Grasse, Graz, Matera, and Wettzell are computed from LAGEOS full-rate Release A normal points SLR data, covering the period September to December 1990. The SLR coordinates of Zimmerwald and Monte Venda are computed from quick-look LAGEOS SLR data, acquired until 25 June 1991. All solutions are converted to the epoch 1 September 1991 (Table 3–4). The SLR-solution of the SLR marker coordinates of Monte Venda will be compared with the GPS-solution presented in this report.

TABLE 3–4 SLR marker coordinates (DUT/SOM ERS90B solution)

Station Name	x	y	z
GRASSE 7835	4581691.739	556159.335	4389359.308
GRAZ 7839	4194426.656	1162693.803	4647246.503
MATERA 7939	4641964.998	1393069.874	4133262.231
WETTZELL 7834	4075530.002	931781.248	4801618.192
ZIMMERWALD 7810	4331283.550	567549.550	4633139.925
MONTE VENDA 7542	4399363.543	910506.420	4512940.880

The coordinates of the fixed SLR sites are also given by IERS in the European Terrestrial Reference Frame 1989 (*C. Boucher*, personal communication):

TABLE 3–5 SLR marker coordinates (ETRF-89)

Station Name	x	y	z
GRASSE 7835	4581691.810	556159.420	4389359.400
GRAZ 7839	4194426.720	1162693.899	4647246.558
MATERA 7939	4641965.093	1393069.975	4133262.234
WETTZELL 7834	4075530.074	931781.339	4801618.189
ZIMMERWALD 7810	4331283.617	567549.563	4633139.956

3.3.2 The September 1991 Campaign

The Institute for Space Research, Graz, Austria (*P. Pesec*) organized a GPS campaign (called COMPASS II/GPS) from 2–4 September 1991 for the positioning of radar transponders to be used for an independent altimeter experiment. The campaign has been kindly extended to include Monte

Venda and *Acqua Alta* tower, too. The following fixed SLR sites have been observed:

- Grasse M004;
- Zimmerwald LT88;
- Wettzell 7597;
- Graz (special marker).

All of these sites were equipped with Ashtech Dual Frequency receivers. Additionally data from the permanently operating Rogue receiver at Kootwijk Observatory (KOSG) could be included into the processing. Table 3–6 shows the available data from the individual station, together with the respective sampling rate. Again the local tie and antenna data are given in Table B–4 in ANNEX B, "The "Large" GPS Campaign", and subsequent Tables.

TABLE 3–6 Available GPS data during the period September 2–4 1991

Station	2-3 Sep	3 Sep	3-4 Sep	Sampling (sec)
	Days 245-246	Day 246	Days 246-247	
Graz	16:54-06:31	11:28-19:00		20
Kootwijk	16:14-09:40	10:14-19:00	19:02-05:30	120
Wettzell	16:14-07:32	16:16-19:00	19:01-05:30	20
Zimmerwald	16:34-09:40	10:13-19:08	19:25-04:32	20
Grasse	16:57-08:05	11:26-19:00	19:01-05:43	20
Venice Tower	16:57-07:30	11:21-18:59		20
Monte Venda	17:12-07:44	11:28-19:00		20

3.3.3 Processing of the Campaigns

3.3.3.1 Processing at DUT Using the GIPSY Software

The GPS measurements were analysed with the GPS Inferred Positioning SYstem software (*GIPSY*), described by *Blewitt* (1989) and *Lichten* (1990), and developed at the Jet Propulsion Laboratory (JPL). An important feature of this software is that it processes carrier phase measurements as biased ranges. As a consequence, the behaviour of the various clocks must be modelled in the analyses of the measurements. This is usually accomplished by treating them as unknowns with stochastic properties.

The *GIPSY* software consists of various modules, which together perform the following primary tasks:

- Pre-processing: In this task, the raw observations are transformed into an uniform database which serves as the input for all subsequent modules. The data are (automatically) edited, which involves identification of bad observations and flagging of bias breaks if the phase data can not be reconnected. Subsequently, linear ionosphere-free combinations are formed to which tropospheric corrections may be added before data compression into normal points, or data decimation, takes place.

- Modelling: In this task, a separate database is created which contains, for instance, a tabulated result of model orbits. The initial GPS epoch states are numerically integrated with a multi-step Adams method (*Krough*, 1973) in the J2000 inertial reference frame (*Melbourne et al.*, 1983). Variational partial derivatives are computed relating the change in satellite position and velocity with respect to changes in the initial epoch states and with respect to force parameters. The Earth's gravity field is expressed in terms of a spherical harmonic expansion (12×12), and the gravitational effects of the sun, moon, and other planets are represented as due to point masses. The *GIPSY* software includes the Rock4 and Rock42 (*Kerr*, 1982) GPS solar radiation pressure models, allows for estimation of arbitrary unmodelled accelerations on the spacecraft, and includes impulsive motor burns when needed to model GPS manoeuvres. Precise earth models are used to model the measurements and to compute partials for measurements with respect to model parameters as a function of time (*Sovers et al.*, 1990). The models include UT1-UTC, polar motion, nutation, precession, solid earth tides, ocean tidal loading, general relativistic clock corrections, and the Lanyi tropospheric delay mapping function (*Lanyi*, 1984), which relates the tropospheric delay at various elevations to its value at the zenith. The algorithms used are based on ones developed for Very Long Baseline Interferometry (VLBI).
- Filtering: In this task, it is decided which parameters will be estimated from the observations and how their stochastic behaviour will be modelled, including the *a priori* information. Subsequently, a Kalman filter is used to estimate corrections to the parameters. The results are written to a new database which contains information about the estimated parameters at every time step.

During data pre-processing, raw GPS data were automatically edited, cycle slips were detected and, when necessary, bias breaks were flagged. Subsequently, ionosphere-free linear combinations were formed, and data were decimated into 2 minute intervals. During pre-processing it was found that Wettzell data of 16 and 18 October were contaminated with C/A- code outliers, whereas AIUB detected unexplainable systematic errors (*Gurtner*, 1991). Therefore, Wettzell data of these days were not processed.

The GPS satellite transmissions are one-way transmissions originating at the spacecraft. A carrier signal modulated by a pseudo-random noise code is broadcast (*Spilker*, 1978). Both the ionosphere-free linear combinations of the pseudorange and of the carrier phase observables were processed with a data noise of 2.5 m and 1.0 cm, respectively.

The satellite's state vector and solar radiation pressure parameters were estimated for each satellite, per day, and with loose constraints. As nominal GPS orbits, numerically integrated orbits, best fitting in the least-squares sense through all transmitted broadcast elements within the period 14–20 October 1990, were used.

Tropospheric delays were estimated per station, and per day. Therefore, the zenith wet delay was set to 10 cm, and the zenith dry delay was estimated using a Random Walk stochastic noise process with an *a priori* delay of 2 m, and a rate of change of the parameter's variance of 20 cm per day. The analytic mapping function developed by Lanyi (*Lanyi*, 1984) was used for mapping the zenith values to the observed elevation angles.

The GPS marker coordinates of the five fixed SLR sites at Grasse, Graz, Wettzell, Matera, and Zimmerwald, were tied to the marker coordinates of the SLR systems by means of local surveying, and were held fixed (fiducial stations). The GPS and SLR marker coordinates of Monte Venda (WM90, TR90, and 7542) and the GPS marker coordinates of the *Acqua Alta* Tower (WM90, and TR90) were estimated using single-day arcs. The single-day arc computations were combined into a multi-day arc computation, by combining the information matrices and observable vectors optimally, through applying a sequence of elementary Householder orthogonal transformations (*Bierman*, 1977). The *a priori* covariance of the parameters was automatically removed from all single-day arcs, except for the first one, before combining the covariances and estimates by using measurement down-dating (*Muellerschoen*, 1988).

Fixed parameters in the analyses included the fiducial station positions, but also a reference clock at Wettzell (14, 15 and 17 October) or Grasse (16 and 18 October), and parameters necessary to define the Earth's orientation in space at the time of satellite observation. The station and satellite clocks (except the reference clock) were modelled as stochastic white noise processes. Cycle ambiguities were estimated along with the parameters such as satellite state, clocks, and the geodetic parameters of interest, but were not integer resolved.

3.3.3.2 Results

After data pre-processing, GPS data from 14–18 October 1990, were analysed resulting in daily solutions for the coordinates of Monte Venda and the *Acqua Alta* tower in the ERS90B reference frame. Data from 19 October 1990, were not processed, because on that day GPS data were hardly available (see Table 3–3).

Figure 3–4 shows the scatter of the five daily delta estimates (delta with respect to the *a priori* coordinates) of the components of the baseline Monte Venda (WM90) – *Acqua Alta* (WM90). For each day the daily solution is indicated together with the 1σ formal error bar. The detailed figures are given in Table B–7 in ANNEX B, "The “Large” GPS Campaign".

On 14 October data from Graz and Zimmerwald were not available. On 16 and 18 October data from Wettzell were not processed. Therefore, the delta estimate uncertainties of the components of the baseline Monte Venda (WM90) – *Acqua Alta* (WM90) are larger for those days.

Figure 3–5 shows the scatter of the five daily GPS solutions of the height of the SLR marker at Monte Venda (7542), and of the height of the GPS marker

FIGURE 3–4

Scatter of the daily delta estimates of the baseline components of the baseline Monte Venda (WM90) - *Acqua Alta* (WM90), and 1σ formal error bars, when all fixed SLR marker coordinates were held fixed in the ERS90B reference frame. The numbers 1-5 correspond with 14 October – 18 October respectively. The '+' indicates the weighted mean delta estimate of each baseline component

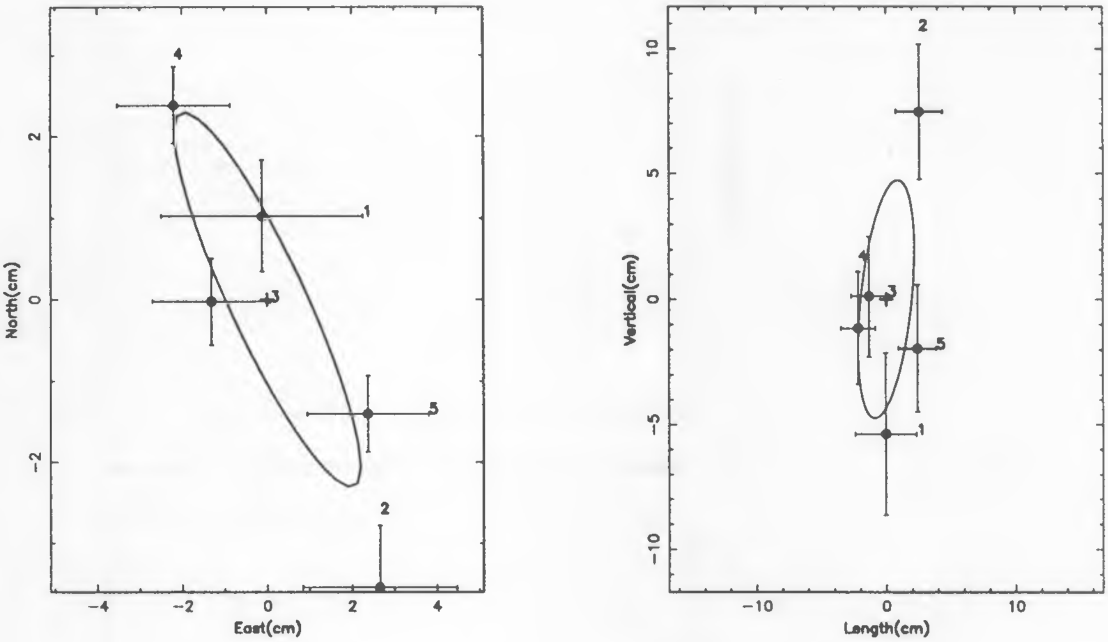

at *Acqua Alta* (WM90), which is of the highest importance for the altimeter calibration analyses. For each day the daily solution is indicated together with the 1σ formal error bar. The dashed lines indicate the statistically combined solution of the height of the markers. Both combined solutions of the height were found to have a formal sigma of about 1.0 cm.

The scatter of the five daily solutions of the height of the various markers is rather large (rms in Figure 3–5), because the height solutions are highly correlated with the tropospheric zenith delay estimates at Monte Venda and *Acqua Alta*. These daily dry tropospheric zenith delay estimates are shown in Figure 3–6. Because on 14 October GPS data from Graz and Zimmerwald were not available, and Wettzell data of 16 and 18 October were not processed, large 1σ formal error bars occurred for those days

3.3.3.3 Final DUT 1990 GPS coordinates

The final coordinates are computed by combining the single-day arc solutions into a multi-day arc solution. Table B–8 in ANNEX B, "The "Large" GPS Campaign" presents these final marker coordinates of Monte Venda (WM90, TR90 and 7542), and *Acqua Alta* (WM90 and TR90). They are deter-

FIGURE 3–5 Variation of individual daily GPS height solutions with 1σ formal error bars for the SLR marker at Monte Venda (Baiamonte) and the GPS marker at the *Acqua Alta* Tower (Venice). The dashed lines indicate the statistically combined solutions of the height of the markers. (ERS90B reference frame)

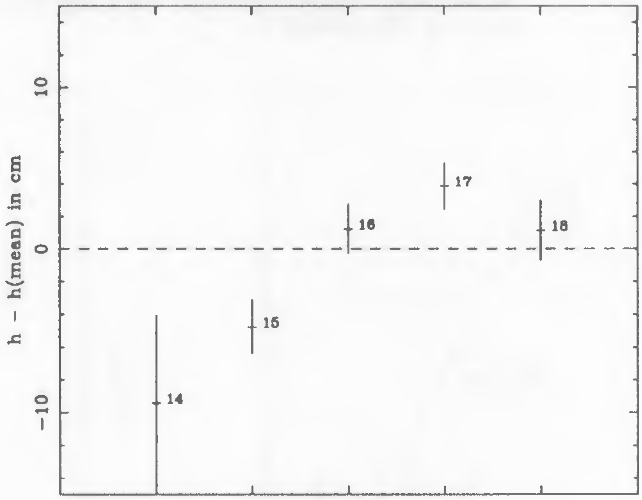

Baiamonte, mean height h = 523.210 m, rms = 3.497 cm

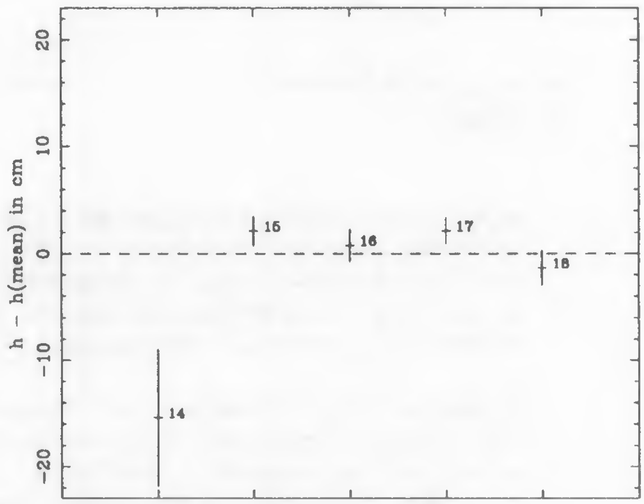

Venice, mean height h = 55.677 m, rms = 2.442 cm

mined in the ERS90B reference frame. A synthesis of all of the solutions will be provided later, in Section 3.3.4.

Table 3–7 presents the differences between the nominal SLR marker coordinates of Monte Venda (based on LAGEOS quick-look SLR data, Table 3–4) and the GPS-estimated SLR marker coordinates. It is shown that the differences enclose 3σ uncertainties and that the estimated height of the SLR marker agrees to within 4.0 cm with the nominal height.

FIGURE 3–6

Daily dry tropospheric delta zenith delay estimates with 1σ formal error bars at Monte Venda (*, WM90; o, TR90), and the Venice Tower (x, WM90; □ TR90) when all five fixed SLR sites were held fixed in the ERS90B reference frame.

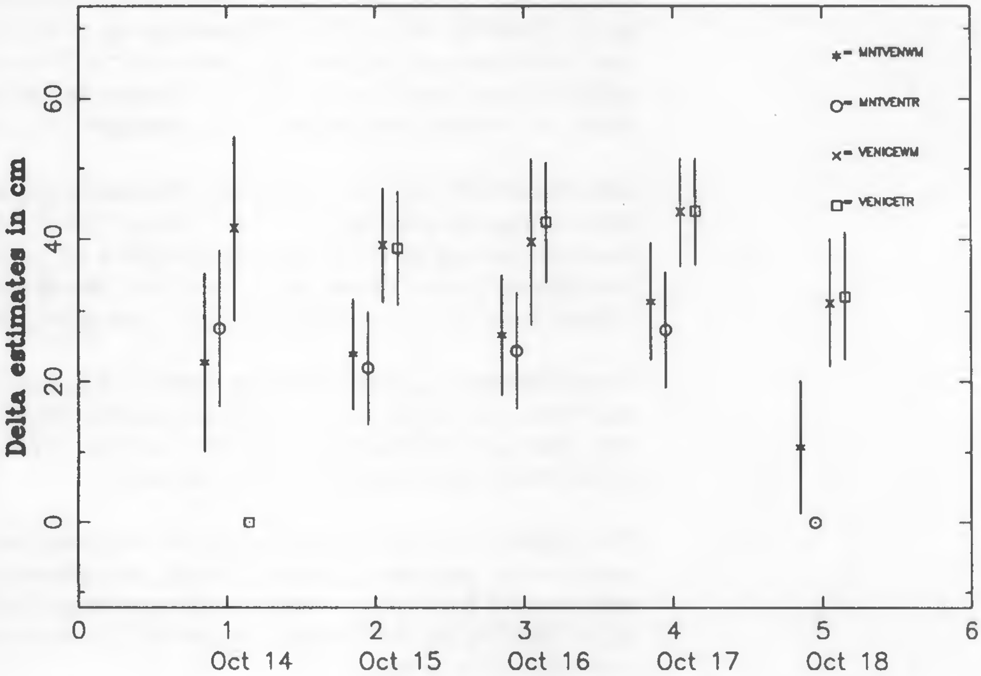

TABLE 3–7

Differences between SLR and GPS derived coordinates of Monte Venda. The height is with respect to the WGS84 ellipsoid.

	x (m)	*y* (m)	*z* (m)	*h* (m)
SLR	4399363.543	910506.419	4512940.880	523.248
GPS	4399363.582	910506.368	4512940.800	523.210
Difference	-0.039	0.051	0.080	0.038

3.3.3.4 Processing at AIUB Using the Bernese GPS Software

The processing of the data at AIUB has been performed on the University's VAX using the *Bernese* GPS Software Version 3.3. In a first step the receiver clock offsets have been computed using the pseudorange observations. These clock offsets are then applied to the receiver time tags to refer the satellite positions to the correct instants, except for the Minimac, where phase observations have already been corrected by the receiver in real-time, so this step had to be skipped for Minimac.

The next step consists in the detection and repair of cycle slips, and the detection and removal of outliers. This data screening is performed on the triple-difference level, simultaneously for L1 and L2 data.

The reference orbit used is a numerically integrated orbit best-fitting, in the least-squares sense, through all transmitted broadcast elements within a given interval (= arc length) of a few hours up to a few days. Two arcs were used, each one covering three successive nights. These *a priori* arcs (*ie* their 6 initial orbital elements plus zero, one or two solar pressure parameters) are subject to improvement by the phase processing program.

The *Bernese* GPS Software uses single-difference files as primary data files for the phase processing. Given n stations then n–1 linearly independent baselines have to be defined for each session. Of course the mathematical correlations between these single- (and later the double-) difference observations are taken into account during the processing step.

The data screening step revealed a number of bad or doubtful data as well as several gaps in the data of up to 20 minutes length. In several cases the files were split at the longer gaps into two files, to make sure that no undetected slips in the gaps remained in the data.

The Rogue receiver in Kootwjik collected very few data only, some of which could not be processed properly due to unexplained systematic errors. It was decided to do all further processing without the Kootwijk data. Two days (289,291) of Wettzell data have not processed either due to unexplained large systematics.

3.3.3.5 Results

As a first check of the data quality daily free solutions are compared, solving for the coordinates of all sites but one, one orbit parameter per satellite, and one zenith delay per station, per day. Table 3–8 shows a seven parameter transformation between the solutions of two consecutive days.

TABLE 3–8 Helmert Transformation Between Days 289 and 290 Including Zenith Delay

Number	Name	Residuals in metres		
835	GRASSE 7835	-0.011	0.020	-0.037
839	GRAZ 7839	0.022	-0.021	-0.010
939	MATERA 7939	-0.006	0.003	0.037
810	ZIMMERWALD 7810	-0.002	0.000	0.082
7	*ACQUA ALTA* WM90	-0.001	-0.005	-0.010
8	MONTE VENDA WM90	-0.002	0.004	-0.063

Further results of the daily repeatability are given in ANNEX B, "The "Large" GPS Campaign"

3.3.3.6 Final AUIB 1990 GPS Coordinates

The solution presented here can be characterized as follows:

- Parameters:
  - Stations : SLR sites kept fixed to their ETRF-89 or ERS90B coordinates
  - Orbits: Two arcs defined for each satellite (days 287-289, 290-292), 6 osculation elements, 1 solar pressure parameter per arc, constraints of the parameters towards the broadcast orbits as shown:

Orbit Parameter		*A priori* Sigma
Semi-major Axis	a	0.50 m
Eccentricity	e	0.0000001
Inclination	i	0.05 ″
Ascending Node	Ω	0.05 ″
Perigee	P	0.02 ″
Argument Of Latitude	U_0	0.10 ″

  - Troposphere: *A priori* atmosphere model, *Saastamoinen* refraction formula, additionally one zenith delay parameter per day per station (except Grasse station).
  - Ambiguities : Introduced as real values, no attempt to resolve the integer ambiguities.
- Observations:
  - Double difference ionosphere free linear combination, minimum elevation angle: 10°.

The coordinates of the WM-102 sites at Monte Venda and *Acqua Alta* refer to the markers on the ground having used the antenna heights of Table B–2 in ANNEX B, "The "Large" GPS Campaign". The Trimble site at *Acqua Alta* is at the end point of a pure Trimble baseline between Monte Venda (TR) and *Acqua Alta* (TR). Monte Venda (TR) has been tied to Monte Venda (WM) using the eccentricities of Table B–1 in ANNEX B, "The "Large" GPS Campaign". The coordinates of the Monte Venda SLR site 7542 have been derived from the WM site adding the local ties of Table B–1 in ANNEX B, "The "Large" GPS Campaign". The resulting solution is shown in Table B–13 in ANNEX B, "The "Large" GPS Campaign" in the ERTF-89 reference frame and in Table B–14 in the ERS90B frame.

The differences between the SLR and GPS derived coordinates of Monte Venda are shown in Table 3–9

3.3.3.7 Final AUIB 1991 GPS Coordinates

The solution presented here can be characterized as follows:

- Parameters:
  - Stations : SLR sites kept fixed to their ETRF-89 coordinates

TABLE 3–9

Differences between SLR and GPS derived coordinates of Monte Venda

	x (m)	y (m)	z (m)	h (m)
SLR	4399363.543	910506.419	4512940.880	523.248
GPS	4399363.527	910506.391	4512940.815	523.186
diff.	0.016	0.028	0.065	0.062

– Orbits: Two arcs defined for each satellite (2 Sept 1991 16:00 – 3 Sept 1991 10:00; 3 Sept 1991 11:00– 4 Sept 1991 05:30) four osculation elements per arc, constrained parameters towards the broadcast orbits as shown:

Orbit Parameter		*A priori* Sigma
Semi-major Axis	a	0.50 m
Inclination	i	0.05 ″
Ascending Node	Ω	0.05 ″
Argument Of Latitude	U_0	0.10 ″

– Troposphere: *A priori* atmosphere model, *Saastamoinen* refraction formula, additionally two zenith delay parameters per session per station (except *Acqua Alta* station).

– Ambiguities : Introduced as real values, no attempt to resolve the integer ambiguities.

• Observations:

– Double difference ionosphere free linear combination, minimum elevation angle: 15°

Again the detailed results are provided in ANNEX B, "The "Large" GPS Campaign", while Table 3–10 shows the differences between the GPS and SLR results for Monte Venda.

TABLE 3–10

Differences between SLR and GPS derived coordinates of Monte Venda

	x (m)	y (m)	z (m)	h (m)
SLR	4399363.543	910506.419	4512940.880	523.248
GPS	4399363.564	910506.408	4512940.772	523.183
Difference	-0.021	0.011	0.108	0.065

3.3.4 Comparisons of all Solutions

Table 3–11 shows a summary of the GPS solutions performed at AIUB (1990/1991) and DUT (1990), as well as the SLR-derived coordinates of Monte Venda 7542 in the system ERS90B, while Table 3–12 shows the baseline components of the individual solutions.

TABLE 3-11

GPS solutions processed at AIUB and DUT; SLR solution processed at DUT (ERS90B System).

Year	Obs	Proc	Station	*x* (m)	*y* (m)	*z* (m)	*h* (m)
1990	GPS	AIUB	MV 7542	4399363.527	910506.391	4512940.815	523.186
1990	GPS	DUT	MV 7542	4399363.582	910506.368	4512940.800	523.210
1991	GPS	AIUB	MV 7542	4399363.564	910506.408	4512940.772	523.183
1991	SLR	DUT	MV 7542	4399363.543	910506.419	4512940.880	523.248
1990	GPS	AIUB	VT WM90	4386229.603	973073.288	4512012.437	55.634
1990	GPS	DUT	VT WM90	4386229.670	973073.271	4512012.435	55.677
1991	GPS	AIUB	VT WM90	4386229.651	973073.347	4512012.393	55.645

TABLE 3-12

Baseline components

Year	Proc	*dx* (m)	*dy* (m)	*dz* (m)	*dh* (m)
1990	AIUB	13133.924	-62566.897	928.378	467.552
1990	DUT	13133.912	-62566.903	928.365	467.533
1991	AIUB	13133.913	-62566.939	928.379	467.538
Average		13133.916	-62566.913	928.374	467.541

3.3.5 Discussion and Conclusions

The results of the various numerical experiments show that the coordinates of the GPS markers at Monte Venda (WM90) and *Acqua Alta* (WM90), and therefore the coordinates of the SLR marker at Monte Venda, have been determined very accurately. It was shown that the processing of the LAGEOS quick-look Monte Venda SLR data has yielded coordinates that agree to within 8 cm with the GPS-computed SLR marker coordinates (after accounting for the known local eccentricity).

The results also compare favorably among those derived independently by the two groups at DUT and AIUB. Differences in the baseline components between the solution are on the centimeter level. Somewhat larger are the differences in the absolute positions of the two baseline endpoints.

Very interesting are the comparisons between the results of the two campaigns of 1990 (WM-102) and 1991 (Ashtech instruments): The agreement is within 6 centimeters in the absolute position and 4 centimeters in the baseline components. The height differences agree within the centimeter.

Formal errors, repeatabilities, and comparisons between the 1990 and 1991 suggest an accuracy of the height difference between Monte Venda and Venice tower of the order of 2 centimeters, therefore easily meeting the requirements for the calibration of the radar altimeter of ERS-1.

3.4 The Local Geoid

Francis and Duesmann (1988) showed that, along the ERS-1 ground track, both the geoid-ellipsoid separation and the slope of the geoid relative to the reference ellipsoid enter into the equation yielding the calibration bias. The geoid-ellipsoid separation, or geoidal height, defines pointwise a "mean sea level" surface by giving its height above the ellipsoid. The scale origin of the tide gauge on the tower and the scale origin of the tide gauges on shore must be points of such a smooth surface. The geoidal slope, or deflection of the vertical, enters the error budget (their eq. 3.5) as a multiplier of the position of the subsatellite point relative to the tower (a dead band of about one km relative to the nominal track through the tower is expected).

A regional geoid in an area approximately 1°×1° around the 'Venice' ground track of ERS-1 has been constructed, thus obtaining the geoidal height and slope, and an estimate of their uncertainties.

Further details may be found in ANNEX C, "Regional Geoid Determination".

3.4.1 Observational Data

The geoid may be described as a surface coinciding with mean sea-level in the oceans, and lying under land at the level to which the sea would reach if admitted by small frictionless channels. Mathematically, the geoid is an equipotential surface of the earth's gravitational and centrifugal potential and coincides with the mean sea level in the open ocean. The undulation of the geoid (geoidal heights) are referred to a spheroidal surface (reference ellipsoid) of semi major axis and flattening such that the undulations have a mean value closest to zero. The deflection of the vertical is the angle of the vertical (direction of gravity) reckoned from the normal to the reference spheroid, and is usually given in terms of N-S and E-W components.The deflection of the vertical thus gives the slope of the geoid to the ellipsoid.

In order to determine the desired geoidal heights and deflections of the vertical along the ground track of ERS-1 direct measurements of these quantities have been made on land. The area in which the observations have been made has an extension of approximately 100×100 km; comparable to the resolution of the most detailed global models of geoid, such as the OSU91A model of the Ohio State University complete to degree and order 360. Then, using a suitable interpolation algorithm (discussed in Section C.2 in ANNEX C, "Regional Geoid Determination") the measured values have been interpolated to the desired zone, *ie* the calibration ground track.

The direct measurement of the geoidal height N is made at any point for which the height above the ellipsoid h and the corresponding height above the geoid H is known:

$$N = h - H$$

Both ellipsoidal and geoidal heights must be referred to some zero. The geoidal heights are generally referred to a tide gauge with a well known and studied record. The ellipsoidal heights are referred to the heights of satellite laser stations. In practice, if one adopts a tide gauge (in this case the one near *Punta Salute* in Venice), one obtains its ellipsoidal height by connecting it via GPS to a nearby laser station, in this case Monte Venda, 64 km west of the *Acqua Alta* tower. Using an origin for which both H and h (and thus N) are known, one can obtain height differences ΔH along the geoid by spirit levelling, and height differences Δh along the ellipsoid by GPS translocation. The corresponding increments ΔN are added to the N of the adopted origin to generate a pointwise sampling of the geoidal height.

The direct measurement of the deflection of the vertical is made at any point for which the latitude and longitude are known on the geoid and on the ellipsoid. The latitude and longitude (Φ, Λ) on the geoid can be obtained by astronomical observations of fundamental stars. The corresponding quantities (ϕ, λ) on the ellipsoid are obtained by connection (*eg* using GPS) to one or more nearby fundamental laser stations. Then the deflection of the vertical (ξ, η) in the meridian and respectively prime vertical planes are obtained from the formulas:

$$\xi = \Phi - \phi \qquad \eta = (\Lambda - \lambda)\cos\phi$$

The two numbers (ξ, η) are the components of a vector resulting from the difference of the vertical to the geoid and the normal to the ellipsoid. Thus a geoid rising from south to north will have a negative ξ. A geoid rising from west to east will have a negative η. In formulas:

$$\xi = -\frac{\partial N}{R\partial\phi} \qquad \eta = -\sec\phi\frac{\partial N}{R\partial\lambda}$$

R being the earth radius.

Different approaches have been discussed in the literature. For example *Engelis et al.* (1985) have used GPS and gravity data to predict orthometric heights over a smaller area of approximately 50×50 km in Germany. The Group of the Polytechnic of Milan (*Benciolini*, 1990) has computed a purely gravimetric geoid for Italy. Other authors (*eg Vanicek and Krakiwski*, 1986, pg.569) suggest that the astrogeodetic methods provide the most accurate geoidal models. Here the option of combining GPS, levelling and astrogeodetic data has been tested.

3.4.2 Origin Tide Gauge and the Geoid

Fundamental to the analysis is the value adopted as origin for N, at Punta Salute. The required numerical value has been obtained by subtracting from the ellipsoidal height of the GPS marker at Punta Salute the orthometric height, which is in turn referred by spirit levelling (a few meters distance) to the nearby tide gauge. The ellipsoidal height has been obtained by GPS in translocation mode, from points of known geocentric coordinates, as discussed earlier. The orthometric height

$$H_{Salute} = 1.1201\,\mathrm{m}$$

is tied to the reference tide gauge labelled "CSO 358/7 IGM CNR73" with a msl (mean sea level) height of 1.2546 m. According to *Cavazzoni* (1977), this tide gauge is connected by precision levelling to the msl of the tide gauge in Genova of 1942 (mean of data from 1937 to 1946). The levelling survey took place in 1968. In analysing the homogenisation of nautical charts for the Venice area, Cavazzoni points out that relative to the zero of the Salute tide gauge of 1897 (mean of 1884 to 1909), in 1942 the Genova msl had a height of 23.56 cm and the Venice msl of 1968 (mean of 1964 to 1973) a height of 22.71 cm. This difference derives from the combination of sea level rising (on a global scale 1-3 mm/yr) and the subsidence of the Venice area. This is a local phenomenon mainly connected with water pumping from the ground. The subsidence stopped in 1980 following suitable regulations. If an overall vertical motion of 3mm/yr with respect to a mean sea level is assumed from 1968 to 1980, followed in 1980-1991 by only sea level rising, then the adopted sea level could be lower than it actually is by $0.3\times12 + 0.13\times11 = 5$ cm. This is considered as an upper limit of the bias in height between the geoid and the mean sea level in 1991.

3.4.3 The Geoid in the Calibration Area

Figure 3–7 shows the geoidal cross section along the calibration track 25 km before and after overflight of the *Acqua Alta* tower. For comparison the cross section predicted by the OSU91A global model is also shown. At the *Acqua Alta* tower the global model predicts $N = 43.09$ m, 19cm lower than the refined local model, $N = 43.28 \pm 0.02$ m.

Consistent preliminary results were obtained by *Weber and Caporali* (1991) and *Scharroo and Overgaauw* (1991) using a "first guess" estimate of $N_{Salute} = 43.29$ m. It is perhaps surprising that the result of the least squares prediction differs by only a few decimetres from the OSU91A prediction. *Rapp et al* (1991) compared a number of global geoidal models finding that the Mediterranean area is one of the regions where the models disagree more—at the level of up a few meters.

The values of (N,ξ,η) at the sites used in the numerical analysis are given by *Caporali et al* (1991). Using these data the observations and the predictions based both on the OSU91A model alone and on this model plus corrections computed with local data ("improved model") are computed. The largest discrepancies between the observed and improved N occur at two nearby sites, Floriano and Feletto, with 18 and –16 cm respectively. The location is on the pre-Alps, with considerable topographic effect expected. The mean and rms discrepancies at the data points (in the sense observed–improved) are 0.8±8.1 cm for N, $-1''.3\pm2''.0$ for ξ and $-2''.2\pm3''.0$ for η.

This along-track geoid determination may be compared with the altimeter profiles, computed with respect to OSU91A, which will be presented in Section 6.2 in CHAPTER 6, "The Satellite and its Measurements". These profiles do not all lie precisely along the ideal track and must be reduced to this position using the cross-track slope of the geoid.

The cross-track geoid slope was measured by astronomical measurements on *Acqua Alta* and can also be derived from the OSU91A geoid and the improved local geoid. The results are given in Table 3–13. This table shows the normal ξ and η components and also the resulting cross-track slope, also expressed in cm/km.

TABLE 3–13 Deflection of the vertical at the *Acqua Alta* platform

Result	ξ	η	Cross-Track	Slope (cm/km)
Observation	– 3″.9±0″.5	– 2″.5±0″.5	-3″.4±0.5	–1.6±0.2
OSU91A	–1″.8	+0″.9	+0″.4	+0.9
Improved local geoid	– 2″.2±0″.2	– 1″.8±0″.2	-2″.3±0″.2	-1.1±0.1

3.5 The Local Survey (*Acqua Alta*)

A full description of the local surveys which were performed at the Monte Venda site and on the Acqua Alta tower is given in ANNEX D, "The Local Surveys". Here only an outline of the *Acqua Alta* survey will be given, as far as determining the vertical reference for the tide gauges is concerned.

Figure 3–7 illustrates a simplified version of the calibration geometry. The altimeter provides a measurement of the vertical distance satellite–sea surface (*s*). This measurement must be compared with an alternative measurement obtained as the sum of the distance *a*, between the satellite and the GPS antenna on board of the tower, and the distance *b*, between the GPS antenna and the actual sea surface at the time of the pass. The determination of *b* is discussed in this section.

It is assumed that the water level inside the tide gauge well is representative of the outside instantaneous sea level, *ie* of the water level present outside, were it not for the wind waves (frequency above 0.015 hz). Note that, as far as the altimeter calibration is concerned, we need to filter out all the waves shorter than the dimension of the altimeter footprint on the surface. Taking this as one kilometre, this corresponds at the tower to waves with a period of 75 seconds. There is virtually no energy in the tidal spectrum in this range (as can be seen in various records in this report) so we are confident that the gauges on the tower effectively provide the correct reference for the evaluation of distance *b*.

A tidal gauge can be placed at any distance above the sea surface, the connection being through a metal ribbon of undetermined length (see Figure 4–2 in CHAPTER 4, "Local Measurements" for a sketch of the system). Generally the interest is only in the oscillations of the surface. Once a sufficiently long record, typically one year, is available, some sort of average is deduced and the tidal values are then conveniently referred to this nominal "zero".

FIGURE 3–7 Schematic diagram of ERS-1 calibration. The satellite range s is the sum of the range to the GPS antenna, a, and b the distance from the GPS antenna to the sea-surface.

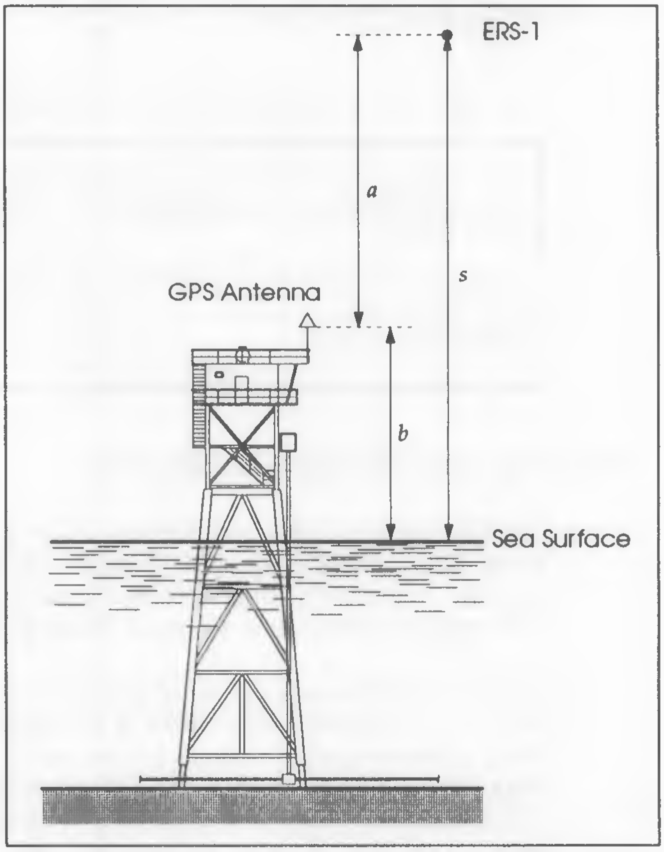

However there is no strict need for this, and furthermore the "zero" changes appreciably from year to year.

In the case of Venice the tidal records of the *Comune di Venezia* are referred to the official "zero" estimated in 1897, which, because of the sinking of the town and of sea level rising, is about 22 cm below the present yearly average. In the case of gauge 1, built for different purposes[1], the values are simply referred to the bottom of the scale (see Figure 4–4 in CHAPTER 4, "Local Measurements").

The sequence of operations required and executed for the determination of the distance b in Figure 3–7 is sketched in Figure 3–8.

1. A description of the two tide gauges on the tower and their characteristics, is given in CHAPTER 4, "Local Measurements". Gauge 1 is an analogue reading device used as the reference for the campaign.

FIGURE 3–8 Scheme for the determination of the distance b (GPS antenna–sea surface) on the tower.

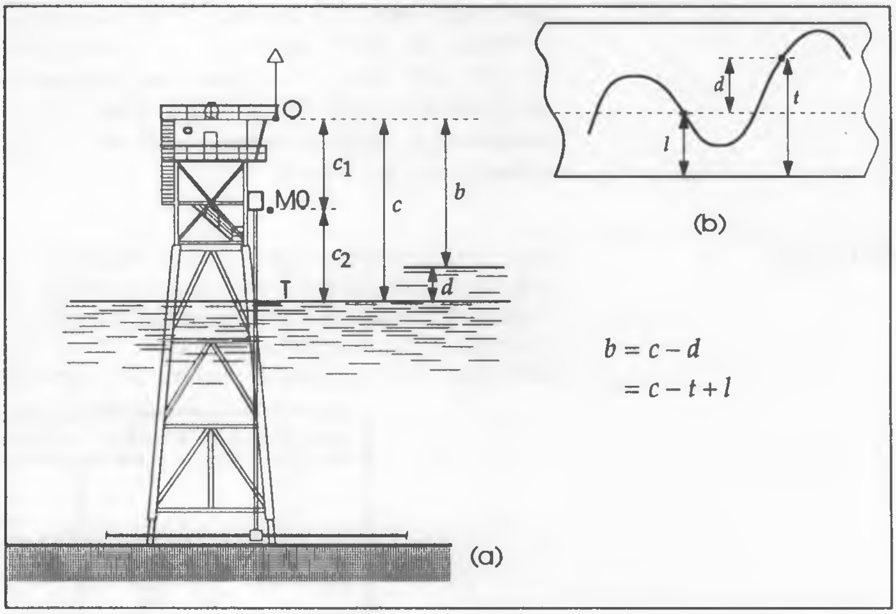

A small reference mark was welded to the tower structure (point T in the figure). When the sea level is exactly at the level of T, the distance b, equal to the distance c, corresponds also to the distance O–T between the GPS antenna and the welded mark T. At this instant a reference level l is read on the tide gauge scale. At any subsequent time the distance b between the GPS antenna and the actual sea level will be given by c minus the difference in tidal level d that can be conveniently read from the tidal record as $t - l$. The distance c was then measured once and for all at a suitable time, *ie* with low tidal level (so that mark T was out of the water) and low waves present. This measurement is described in ANNEX D, "The Local Surveys".

Actually a double check was used in the estimate of c. This distance was measured as a single vertical displacement and as the sum of two separable sections c_1 and c_2 (see Figure 3–8) with respect to an intermediate reference mark M0 on the floor of the terrace hosting the tide gauges. The overall set of measurements is given in Table D–19 in ANNEX D. There were in fact four marks attached to the tower. These were all ultimately referred to a zero on the tide gauge; during these tidal measurements, described in ANNEX D, they were identified as ①, ②, ③ and ④. Of these, two were surveyed relative to the other reference points on the tower, the others being inaccessible, as described in ANNEX D. These surveyed marks were referred to as T1 and T2.

The measured distance of the marks from the GPS reference point were:

T1: 12168.7 mm

T2: 12342.4 mm

with a corresponding vertical separation of 173.8 mm.

Installation of multiple markers, whilst lending security, introduces a risk of confusion—and this initially occurred in establishing the correspondence between the "tidal" marks ①, ②, ③ and ④ and the "survey" marks T1 and T2. The determination of the water reference level at the tidal marks was performed on 23 October 1991 and on 5 November 1992. The tidal values measured on these occasions are shown in Table 3–14, which also shows the correct correspondence.

TABLE 3–14 Tide gauge measurements at the reference marks. The tidal measurements were made in October 1991 and November 1992, and the survey in January 1992. Mark ③ was broken between October 1991 and January 1992, and this prompted the installation of mark "T2", or ④. An estimated measurement, using the stump of mark ③ was made in November 1992.

Survey Mark	Tide Mark	23 October 1991	5 November 1992
"T1"	②		128.0[1]
"T2"	④	not installed	111.5
	①	112.5	108.5
	③	101.5	100.0[2]

1. estimated as tide did not reach this mark.
2. estimated as mark broken.

In October 1991 the measurement of the tidal level at tidal mark ① was wrongly identified as being for tidal mark ②, corresponding to survey mark T1. From thorough investigation of the measurement circumstances and the recollections of the personnel involved this error has been resolved. In fact ②, or T1, was not originally measured, and T2 was not originally installed.

A substantial shift (of 1.5cm and 4cm respectively) appears between the measurements to marks ③ and ①, which were duplicated on the two occasions. While some of this is experimental error, possibly some is also due to a shift in the zero of the tide gauge. To investigate this records from four gauges have been examined:

- Gauge 1 on *Acqua Alta* (the reference);
- The *Commune di Venezia* gauge 2 on *Acqua Alta* (CV2);
- A CNR gauge at Lido (CNR3);
- A *Commune di Venezia* gauge at Lido (CV4).

Contemporary records from three periods have been obtained, corresponding to the calibration campaign in August 1991, the original tidal measurement in October 1991 and the final tidal measurement in November 1992[1]. Hourly values from each gauge during each overlapping period were taken and differences from the reference gauge found (this was necessary to reduce the magnitude of the quantities studied). The results of these comparisons are shown in Table 3–15.

TABLE 3–15

Relative shifts in hourly tide gauge measurements, in centimetres. The final shift during the period is also given. Errors quoted refer to the standard deviation of the measurements.

Difference	August 1991	→	October 1991	→	October 1992	Final shift
Ref – CV2	66.9±1.9	+2.8±2.9	69.7±2.2	–2.7±4.1	67.0±3.5	+0.1±4.0
Ref – CNR3	–46.8±2.7	+2.1±4.2	–44.7±3.2	–2.2±4.4	–46.9±3.1	–0.1±4.1
Ref – CV4	66.0±2.3	+2.2±3.1	68.2±2.1	–0.5±4.1	67.7±3.5	+1.7±4.2

It appears that there has been a consistent shift in the values recorded by the reference gauge 1 in October 1991, by about 2cm relative to the other gauges in the area. However by October 1992 this shift had moved about the same amount the other way. The conclusion which can be drawn from this is that the October 1991 measurements reported in Table 3–14 should be reduced by about 2cm before comparison with the November 1992 values. This tends to bring them into better agreement.

As the final shift between August 1991 and October 1992 is negligible the November 1992 results will be used as the tidal reference value. As an estimate of the error it should be noted that:

- the tidal difference ② – ④ is 16.5 cm, compared with the surveyed difference T1 – T2 of 17.4cm, a combined error of 0.9cm;
- the uncertainty in the zero shift, as reported above, is *at least* 1cm.

Thus the reference will be taken as mark T2, at 111.5±2 cm. That is, following Figure 3–8, the height of the GPS reference above the "zero" reference of the tide gauge is 1234.24+111.5, *ie* 1345.7±2cm.

1. Actually records from the end of October 1992 were used.

CHAPTER 4

Local Measurements

This Chapter primarily addresses the time-dependent part of the system—the part which was measured on each pass, at the tower. It does not address the satellite measurements nor the orbit determination.

4.1 Sea Level

Due to the geometry of the basin of the Northern Adriatic Sea, and to the depth distribution, astronomical and meteorological forcing generate a relatively strong variability of the actual sea level in the northern Adriatic Sea. However, compared to the open ocean, the variation of sea level remains small, justifying the original choice of this region for the altimeter calibration. The astronomical tide is basically bi-diurnal, with dominance of the M2 and S2 component (*Defant*, 1960, p. 400) and a spring overall excursion of 1 metre. The meteorological forcing can produce in a few hours an increase of the sea level up to 1 metre. Obviously, for proper definition of the reference surface, these variations have to be measured and taken into account.

This Section will describe the tide gauges and of their characteristics, and their measurements. The link between their measurement of the local sea level and the corresponding result from the ERS-1 radar altimeter (*ie* their location into the three-dimensional network) is described in Section 3.5 in CHAPTER 3, "The Three-Dimensional Network".

Two tide gauges are present on the oceanographic platform, "*Acqua Alta*", henceforth referred to as 1 and 2 respectively. Gauge 1 is run by the *Istituto Studio Dinamica Grandi Masse* (ISDGM) (see Figure 4–1; see also *Cavaleri and Curiotto*, 1979, for a full description of the instrument). It is the conventional type, *ie* it consists of a vertical well solidly connected to the tower structure that, starting from the second floor, penetrates into the sea for about 3

FIGURE 4–1 A sketch of the tower with the two tide gauges 1 and 2

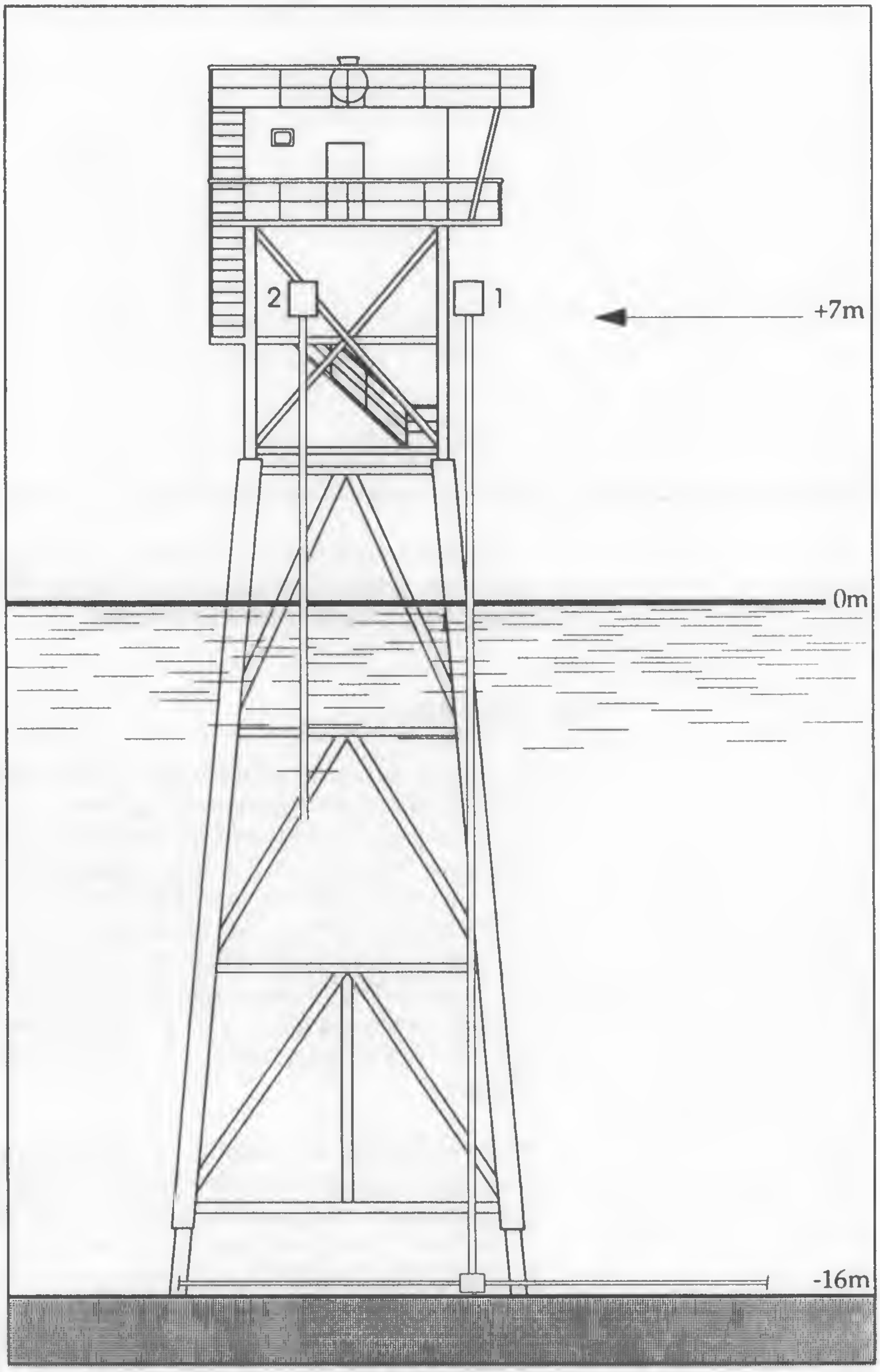

metres. A suitable filter (described below) avoids any appreciable influence of the wind waves (frequency range above 0.05 Hz and mostly above 0.12 Hz) on its inner water level. A float follows the vertical movements of the water level inside the well; its movements are transmitted via an intermedi-

FIGURE 4–2

Working scheme of a conventional tide gauge

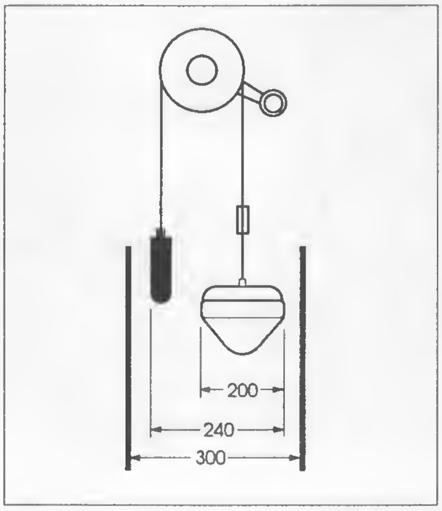

ate metal ribbon, tensioned by a suitable counterweight, to the external wheel of a graphic recorder (Figure 4–2). The actual recording is done directly on paper with an ink pen (see Figure 4–3). Figure 4–4 shows, on a scale of 1:2, a record sample. Each vertical line times one hour, each thick (thin) solid horizontal line represents 10 (2) cm. The reading resolution is estimated at 0.5 cm.

FIGURE 4–3

The recording part of tide gauge 1. The paper height is 25cm, with a scale of 1:10 with respect to the real tidal excursion.

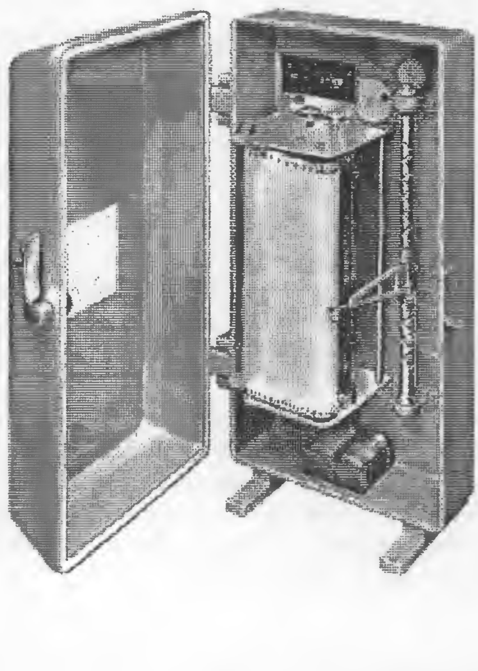

FIGURE 4–4 Graphical record from gauge 1. The scale is 1:2 with respect to the original.

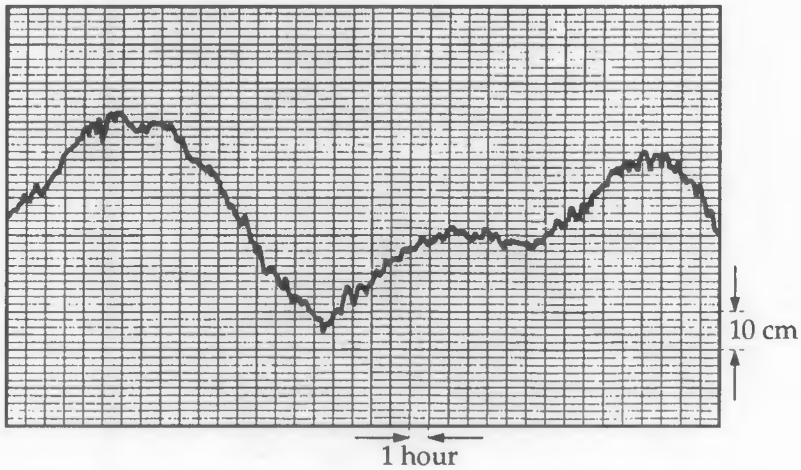

The motivation to build tide gauge 1 was originally to know the actual sea level with an accuracy better than 1 cm. Because under rapid tidal variation differences of up to 30 cm in one hour can be experienced, a time constant of less than a minute was required. In the 16 metres of depth this clashes with the necessity of filtering the relatively high frequency wind waves. The overall requirement was achieved by filtering the wind waves in three different ways:

1. picking up the signal as deeply as possible, namely at the bottom;
2. splitting the gauge pipe at the bottom into six pipes extending horizontally for 40 m along six radial directions at 60° intervals so achieving also a filtering in space;
3. making the pipes large enough (50 mm diameter) to allow an immediate flow for the tidal variations, but allowing the damping of wind wave oscillations by friction and inertia of the water into the pipes.

The resulting filtering characteristics are shown in Figure 4–5.

Gauge 2, run by the *Servizio Previsione Maree* of the *Comune di Venezia* (Tidal Forecasting Centre of the Venice town authorities), has the same basic structure (see Figure 4–1 and Figure 4–2), but the water level is digitally recorded at 5-minute intervals and with a 1 cm resolution, and radio-transmitted in real time to the Forecasting Centre in Venice. For the interested reader a full description of these tidal measurements is given by the *Comune di Venezia* (1989).

The hydraulic filter is the conventional one, *ie* the bottom of the well, at 3 metres depth, is connected to the sea by a very small metal pipe (inner diameter 20 mm). While this is highly effective in filtering out the wind waves, it introduces an appreciable delay between a variation of the outer sea level and the consequent response inside the well. The actual time constant is close to 10 minutes.

In summary the basic differences between the two gauges are the following: gauge number 1 records on graphic paper and gauge number 2 in digital memory. Both are very effective in filtering out the wind waves, but, while gauge number 1 offers an immediate response to tidal variations, number 2 has a delay of more than 10 minutes. The last point becomes particularly important when, as in Figure 4–4, short level oscillations, with periods between 10 and 20 minutes, are superimposed to the main tidal line. These oscillations, with a horizontal scale of 10–20 km, are important for the signal picked up by the radar altimeter. They are usually connected to shelf waves, and are virtually filtered out by gauge 2.

Operational aspects of the tide gauges are described in ANNEX H, "Tower: Modifications and Operations", and the chart records from gauge 1 throughout the campaign are shown in Figure 4–7. The times of the calibration passes are marked.

The full set of tidal values for all the passes is shown in Figure 4–6, together with the values recorded at several other gauges located at the harbour entrances (see Figure H–5 in ANNEX H, "Tower: Modifications and Operations") and at Punta Salute in the town of Venice itself. Note that, once the different reference level and the above mentioned problems are taken into account, the various gauges located in the sea or in the harbour entrances are more or less following each other; on the contrary the gauge at Punta Salute is exhibiting a variable difference. The reason is that, while the other gauges are practically in phase with respect to the tidal cycle, the time

FIGURE 4–5

Filtering characteristics of gauge 1 (from *Cavaleri and Curlotto*, 1979). The overall filtering coefficient is shown in curve χ.

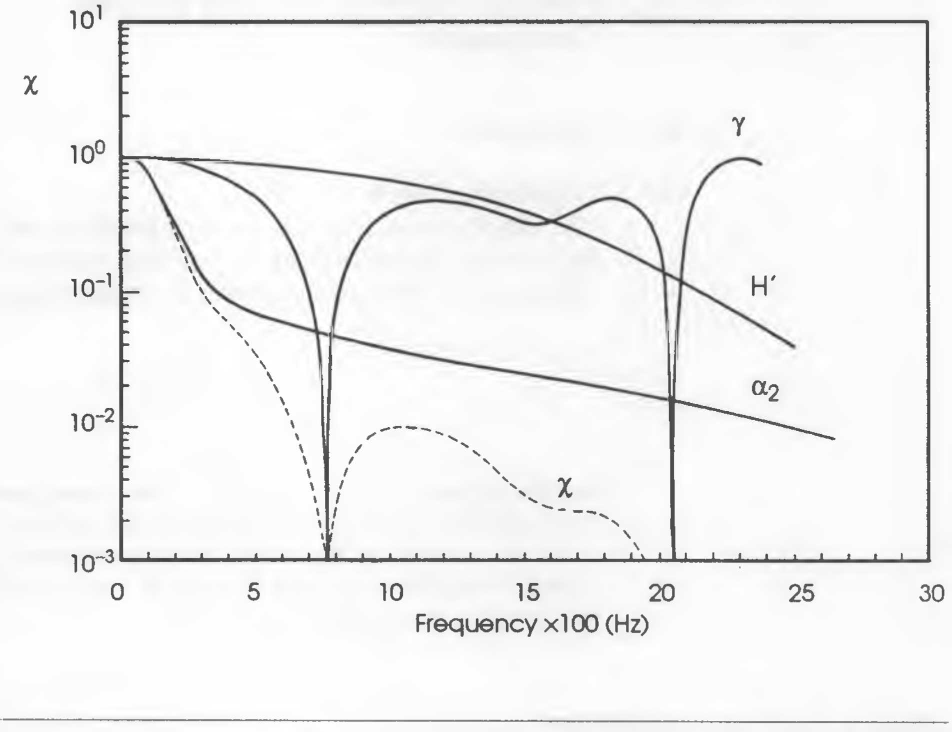

FIGURE 4–6 Tidal values recorded by each of the available tide gauges at the time of each calibration pass.

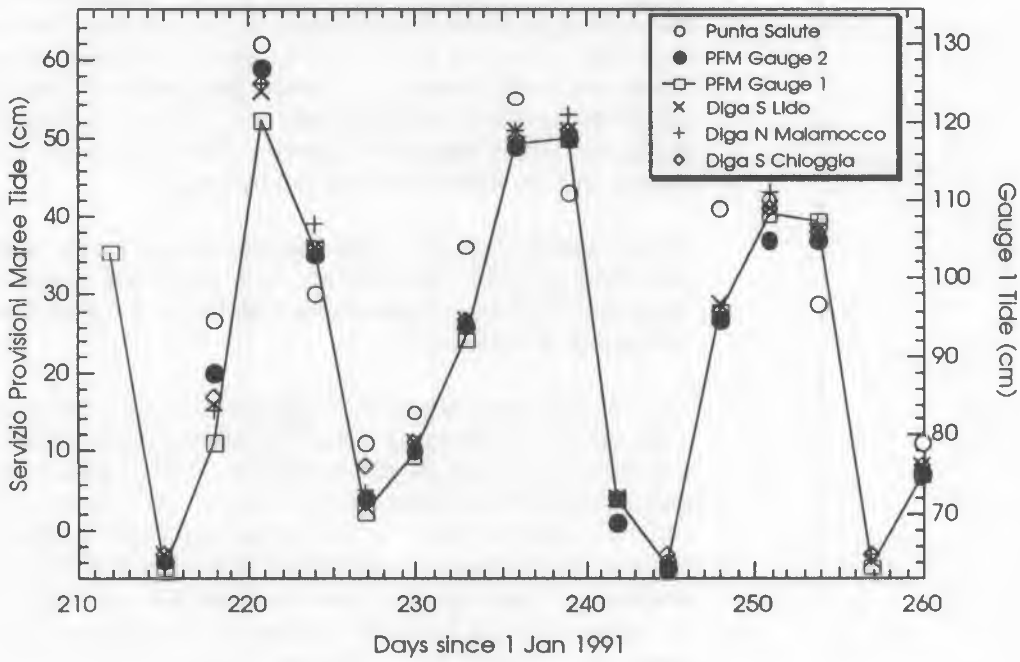

required by the tide to propagate into the lagoon implies about a 40-minute delay for the signal to reach Punta Salute (*Aldighieri et al.*, 1983).

4.2 The Troposphere—the Wet and dry Components

4.2.1 Background

4.2.1.1 Tropospheric Effects

The altitude measurements of a satellite-borne radar altimeter are affected by the time delay due to the atmospheric refraction and need a suitable correction; the radar system observes an apparent range equal to:

$$\int_0^H n(h)\ dh$$

where $n(h)$ is the refractive index of the atmosphere (which is a function of the height h), dh is an increment in path length and the integration extends from the surface of the earth to the maximum altitude H at which the atmosphere affects the altimeter signal. For a vertical path, in the absence of ray bending, the range error is then

$$\delta h = \int_0^H [n(h) - 1]\, dh = 10^{-6} \int_0^H N(h)\, dh$$

where N is the refractivity, $N = (n - 1) \times 10^6$.

FIGURE 4–7 The tidal record from gauge 1 throughout the campaign. The heavy lines indicate a common height reference through the records, and the times of each pass are marked by a cross.

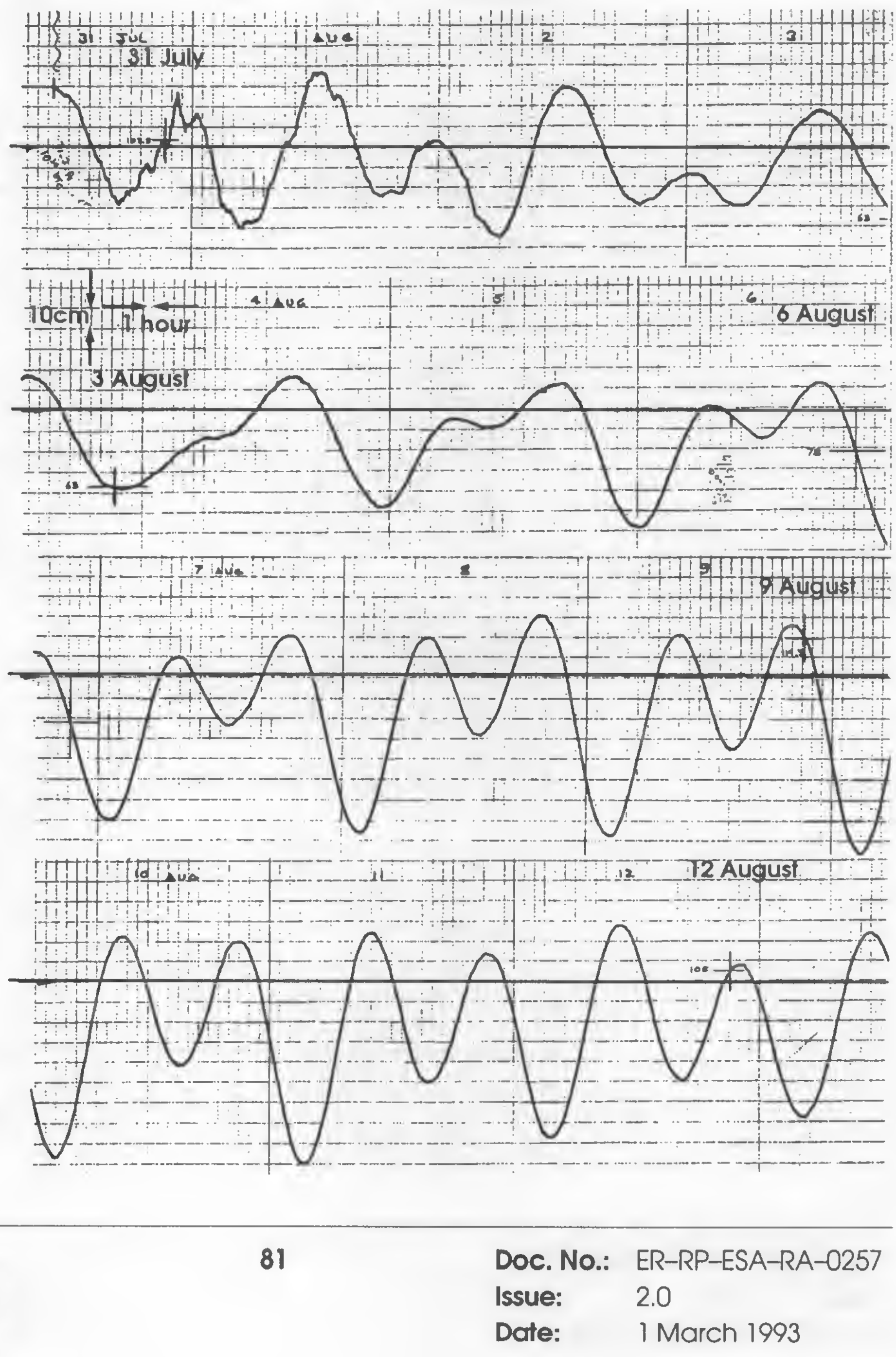

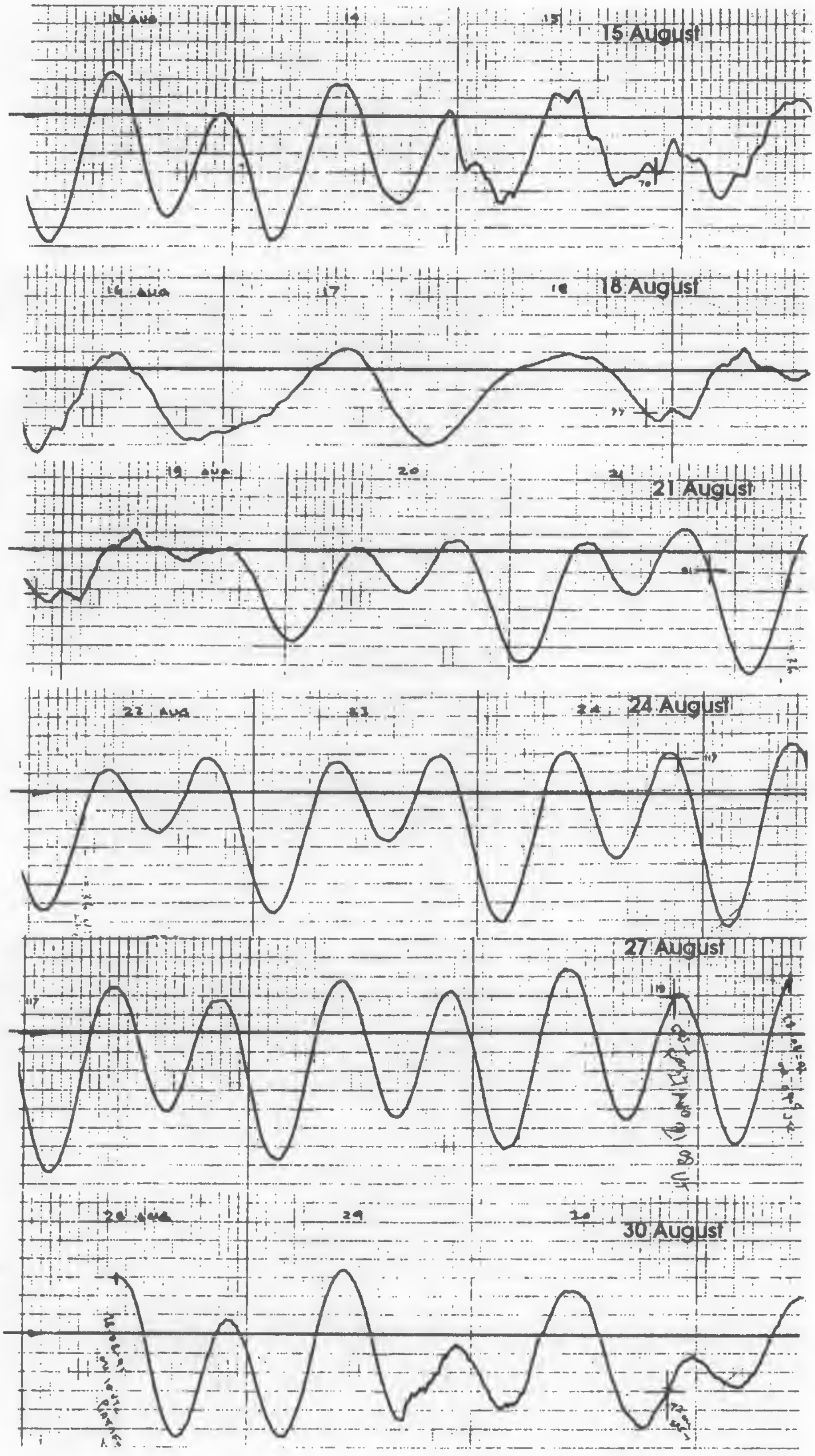
15 August
18 August
21 August
24 August
27 August
30 August

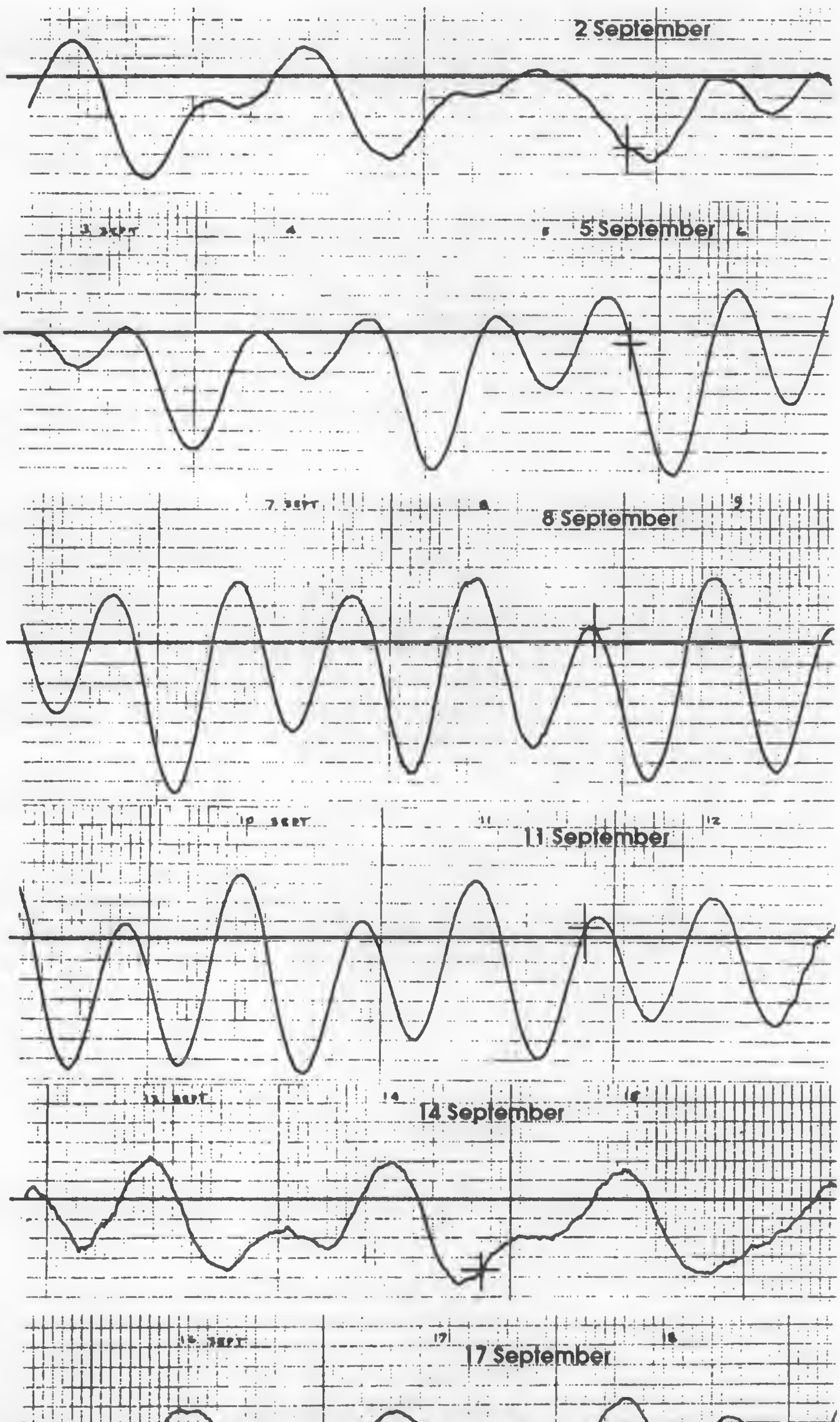
2 September
3 SEPT
4
5
5 September
6
7 SEPT
8
8 September
9
10 SEPT
11
11 September
12
13 SEPT
14
14 September
15
16 SEPT
17
17 September
18

In the troposphere the refractivity can be separated into a dry (and predictable) component and a highly variable wet component, which depends mainly on the water vapour:

$$N = 77.6\left(\frac{P}{T}\right) + 3.73 \times 10^{5}\left(\frac{e}{T^{2}}\right)$$

where P is the total atmospheric pressure [mbar], e the partial pressure of water vapour [mbar] and T the atmospheric temperature [K], and the constants are considered valid to within 0.5% in N for frequencies up to 30 GHz (*Bean and Dutton*, 1978). Correspondingly the range error results in:

$$\delta H = 77.6 \times 10^{-5}\int_{0}^{H}\frac{P}{T}dh + 3.73 \times 10^{-1}\int_{0}^{H}\frac{e}{T^{2}}dh = \delta H_{d} + \delta H_{w}$$

The tropospheric effect produces an altitude overestimate of the order of 2.5m with the predominant part of the error coming from the dry component; however, due to variability in the atmospheric water vapour content, there may be changes in the wet tropospheric correction of 10-20 cm with length scale on the order of 150–500 km. Assuming that the atmosphere follows the perfect gas law and that it is in hydrostatic equilibrium, the dry component can be directly related to the surface atmospheric pressure alone and does not require assumptions on temperature or pressure profiles (*Saastamoinen*, 1972):

$$\delta H_{d} = (2.277 \times 10^{-3} - 1.11 \times 10^{-5}\cos\Phi)\,P_{s} \quad \text{[m]}$$

where P_s [mbar] is the atmospheric pressure at the surface and Φ is the latitude. If we assume, in addition, that the atmospheric temperature decreases linearly with the altitude and that the water vapour partial pressure varies according to the relation:

$$e(h) = e_{s}\left(\frac{T(h)}{T_{s}}\right)^{a}$$

the wet term can be expressed as follows:

$$\delta H_{w} = 2.277 \times 10^{-3}\left(0.05 + \frac{1255}{T_{s}}\right)e_{s}$$

where e_s [mbar] and T_s [K] are, respectively, the water vapour partial pressure and the atmospheric temperature measured at the surface. Due to the significant correlation of P_s and T_s with the actual profiles of pressure and temperature, the dry (hydrostatic) term can be estimated rather precisely from surface measurements. This is not so for the wet term, as the high variability and non uniform mixing with the dry air of water vapour makes it very difficult to predict the altitude distribution of water vapour from a simple ground measurement of humidity.

The correction could be made very accurately only if the value of the atmospheric parameters and then the refractivity $N(h)$ were known along the whole path. In addition the wet term should be also expressed as the sum of two contributions, due to water vapour and cloud liquid water (N_v and N_l respectively), in order to write, for the total refractive range error:

$$\delta H = \delta H_d + \delta H_w = \delta H_d + \delta H_v + \delta H_l = \int_0^H N_d(z)\,dz + \int_0^H N_v(z)\,dz + \int_0^H N_l(z)\,dz$$

These calculations can be carried out straightforwardly from radiosonde data for the first two terms of the equation, while the liquid water contribution δH_l requires the assumption of a suitable cloud model (*Decker et al.*, 1978; *Slobin*, 1982), which could quantify the amount of liquid water in the cloud on the basis of the information introduced by the radio soundings (mainly the distribution of humidity with height). Alternatively the wet refractive range error can be inferred from microwave radiometric observations of brightness temperature at suitable frequencies.

4.2.1.2 Exploitation of microwave radiometric observations

In the microwave region and in non-precipitating conditions, the tropospheric attenuation is mainly due to the spectral absorption produced by oxygen, water vapour and cloud borne liquid water (Figure 4–8). The integrated precipitable water vapour V, the integrated liquid water content L and their contribution to the tropospheric refractivity can be estimated by using a dual-channel ground-based microwave radiometer (with a water vapour and a window channel). Considering an atmosphere without scattering in local thermodynamic equilibrium, the thermal emission is commonly expressed by means of the brightness temperature T_B. In the above conditions, the radiative transfer equation leads to the following expression for the brightness temperature observed by a zenith-viewing microwave radiometer at the frequency f:

$$T_B(f) = T_{BG}\exp\left[-\tau_f(0,\infty)\right] + \int_0^\infty k_f(h)\,T(h)\exp\left[-\tau_f(0,h)\right]dh$$

where

T_{BG} is the cosmic background temperature (2.75 K),
$\tau_f(0,\infty)$ is the atmospheric opacity,
$k_f(h)$ is the atmospheric absorption coefficient [m^{-1}],
$T(h)$ is the absolute physical temperature of the medium and
$\tau_f(0,h)$ is the optical depth:

$$\tau_f(0,h) = \int_0^h k_f(h')\,dh'$$

FIGURE 4–8 Atmospheric attenuation of microwave radiation as a function of frequency

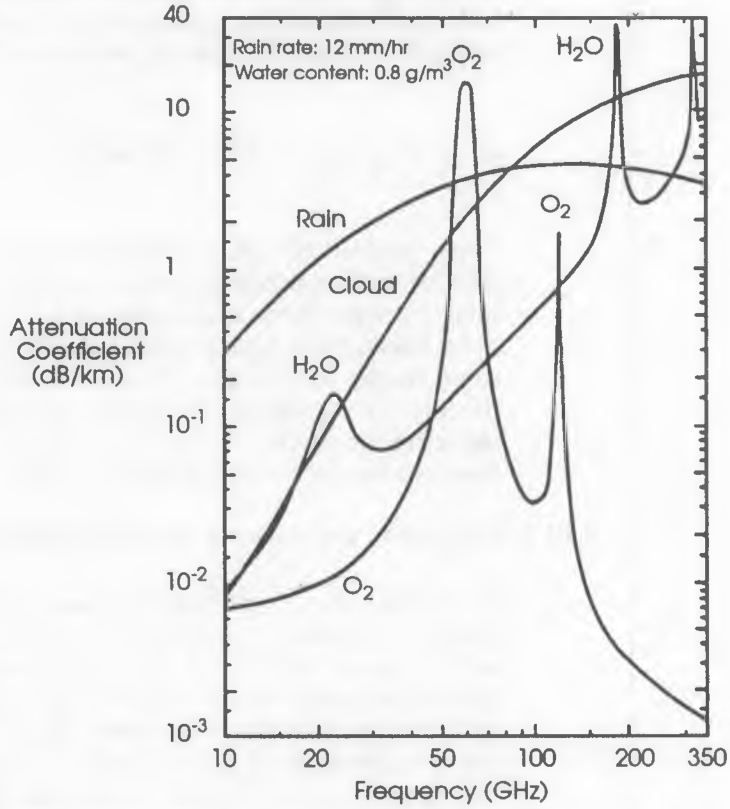

By using the mean radiating temperature T_{mr} (*Wu*, 1979), that summarizes the information on the vertical structure of the atmospheric physical properties

$$T_{mr}(f) = \frac{\int_0^\infty k_f(h)\, T(h) \exp\left[-\tau_f(0, h)\right] dh}{\int_0^\infty k_f(h) \exp\left[-\tau_f(0, h)\right] dh}$$

it is possible to relate the atmospheric opacity to the brightness temperature:

$$\tau_f(0, \infty) = \log \frac{(T_{mr} - T_{BG})}{(T_{mr} - T_B)}$$

In the absence of rain and neglecting the small contribution of ice, the integrated absorption $\tau_f(0, \infty)$ is mainly due to three terms: the water vapour absorption $\tau_v(f)$, the cloud-borne liquid absorption $\tau_l(f)$ and the dry absorption $\tau_d(f)$.

$$\tau(f) = \tau_v(f) + \tau_l(f) + \tau_d(f) = K_v(f)V + K_l(f)L + \tau_d(f)$$

where $K_v(f)$ and $K_l(f)$ are averaged mass absorption coefficients for vapour and liquid, while the integrated vapour and liquid V and L are

$$V = \int_0^\infty v(h)\,dh$$

$$L = \int_0^\infty l(h)\,dh$$

with $v(h)$ and $l(h)$ water vapour and liquid densities. If we measure the atmospheric brightness temperature at two frequencies, a frequency f_1 in the water vapour absorption band and a frequency f_2 in a window band (*eg* 36 GHz which is sensitive to liquid water but is much less so to water vapour), we can write two expressions for these equations and solve for V and L:

$$V = a_0 + a_1\tau(f_1) + a_2\tau(f_2)$$

$$L = b_0 + b_1\tau(f_1) + b_2\tau(f_2)$$

In these equations a_i and b_i are retrieval coefficients for converting atmospheric opacities to integrated vapour and liquid. It has been shown (*Goldfinger*, 1980) that the integrated wet refractivity is in a simple relation with the atmospheric integrated precipitable water vapour V:

$$\delta H_v = \frac{1.79 \times 10^3}{T_s} V$$

The usually small contribution δH_l due to cloud liquid is in linear relationship with L, therefore the correction we require is a linear combination of τ_1 and τ_2.

The required atmospheric opacities can be obtained from measurements of apparent temperatures either ground based or space based. In the latter case the observed brightness temperature is dependent on the upward temperature of the atmosphere (T_{UP}) but includes further contributions due to the downward radiation reflected from the earth surface and the radiation emitted from the surface; these two contributions are further attenuated by the atmosphere: so that, besides the measurements of the space based radiometer, additional information can be useful in improving the tropospheric corrections (*Basili et al.*, 1989). In case a ground based radiometer is considered the measured temperature is simply due to the downward atmospheric brightness temperature (T_{DN}) plus the free space radiation (T_{BG})

attenuated by the atmosphere itself. In this case, considering also that the dry term is simply proportional to P_s, the total (dry plus wet) excess path length can be expressed as a linear combination of the two opacities and of the atmospheric pressure at the surface that is:

$$\delta H = a_0 + a_1\tau_1 + a_2\tau_2 + a_3 P_s$$

The coefficients that appear in the equation retain all the inaccuracies of the assumed models and the uncertainties due to other geophysical variables or parameters not explicitly included and therefore assumed constant on a climatological basis. Without attempting to calculate the coefficients from models, we can derive them by a regression technique, confronting the equation with values of excess length, computed by integrating the atmospheric refractivity for a large set of meteorological data, on a minimum RMS condition. The method retains the main physics of the problem; it also allows adaptation to local climatological characteristics and the exploitation of other measurements which could appear useful for minimizing the total RMS error.

4.2.2 Description of the Equipment

The estimation of the ERS-1 radar altimeter excess path length has been performed by a microwave radiometer system, based on the "*Acqua Alta*" tower, supported by meteorological measurements (air pressure, air temperature and relative humidity) at the radiometer site. The instrument consists mainly of a dual-channel microwave radiometer manufactured by SMA (Florence, Italy), operating at two frequencies, 20.6 and 36.0 GHz respectively (to which we will refer as channel 1 and channel 2).

The equipment operated on top of the tower consisted of the following subsystems:

- microwave radiometer, composed of:
  - two radiofrequency units (for the two frequencies);
  - two control units (for the two frequencies);
  - IF unit.
- two scalar horn lens antennas (for the two frequencies) with a similar beamwidth (about 4.9° for channel 1 and 4.3° for channel 2) and sidelobe level better than –25 dB;
- housing and supporting equipment to protect radiofrequency units and antennas and to allow precise pointing in azimuth and elevation;
- meteorological sub-system composed of:
  - air pressure sensor;
  - air temperature sensor;
  - relative humidity sensor;
  - solar radiation shield;
  - sensor power supply;

FIGURE 4–9 An illustration of the microwave radiometer system during the campaign.

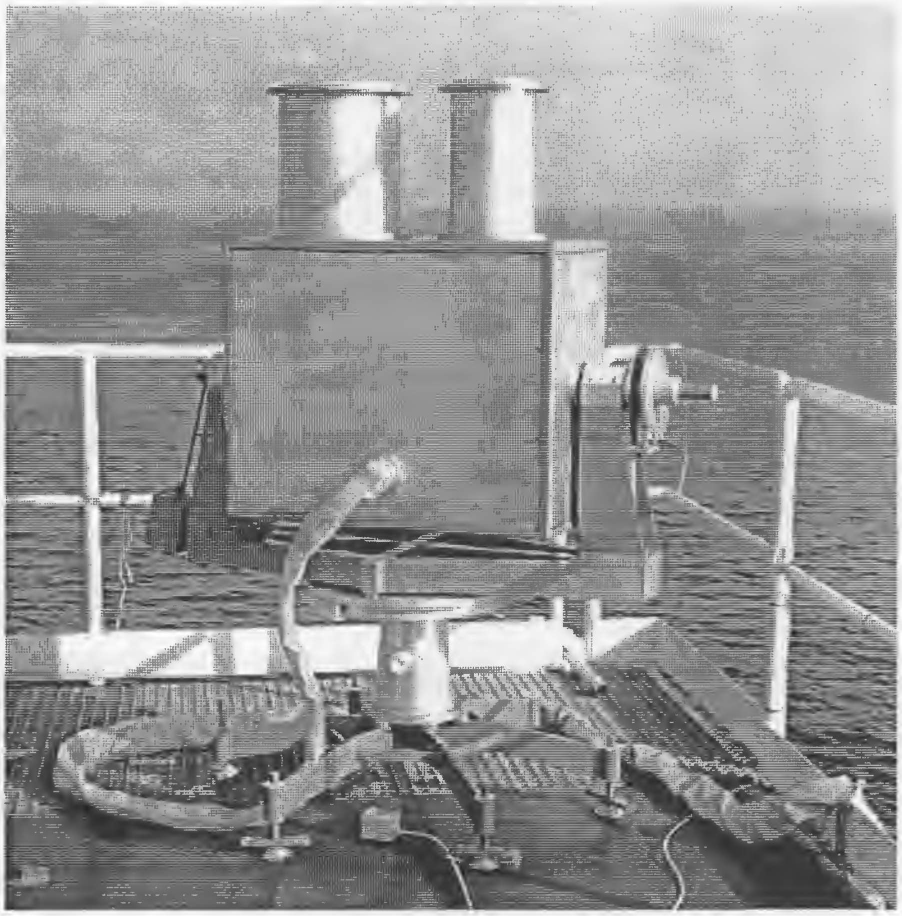

- data acquisition and processing unit for A/D conversion and recording of radiometric and meteorological data and data preprocessing;

An illustration of the microwave radiometer system in place on the tower is shown in Figure 4–9. Details are reported in ANNEX I, "The Microwave Radiometer".

4.2.3 Calibration of the equipment and results

4.2.3.1 Overview of the experimental activity

The radiometer has been operated with the antenna boresights pointed to the zenith when the ERS-1 was passing over the *Acqua Alta* tower. Moreover further activities were performed on the same days with the intention of acquiring a data set useful for instrument calibration and data validation.

The system operated correctly from August 6th to September 17th. All of the ERS-1 passes were covered, except for September 14th because of bad atmospheric conditions. From August 6th to 24th the Dicke operation mode was selected while from August 27th to the end of the campaign data have been acquired in AGC mode which showed better stability in instrument calibration parameters.

4.2.3.2 Instrument Calibration

One of most critical problems in retrieving the excess path length was the absolute calibration of the radiometer which operated in a very uncontrolled environmental condition. Therefore it was necessary to continuously monitor and update the calibration curve.

In the following a brief description of the calibration method is given; further details can be found in ANNEX I, "The Microwave Radiometer".

The objective of instrument calibration was to find the relationship between radiometer output voltage and the apparent brightness temperature at the two frequencies. If this relation can be considered linear it can be described by two coefficients, the gain G and the bias B. That is, we can write for each channel:

$$V = GT_B + B$$

In order to estimate G and B we relied on different kinds of measurements:

- tipping curve calibration performed routinely during the campaign (about 3-4 times each day of the satellite pass);
- absolute calibration by black body at ambient temperature (physical temperature measured by thermometer) performed sporadically.
- laboratory measurements of the instrument linearity by noise injection into the RF unit.

The response to the black body covering the antenna concerns a region of the calibration curve which is far from the range of atmospheric temperature (tens of degrees) so that a check of the instrument linearity within such a large measured range was necessary. This has been performed by injecting a fixed amount of noise into the RF receiver through a directional coupler and a variable attenuator. By switching on and off the noise generator the difference between the corresponding output voltages has been measured for different values of the antenna temperature (obtained by pointing the antenna to different targets). The technique has allowed the measurement of the variation of the calibration curve derivative even if the absolute values of the derivative (that is the instrument gain) could not be measured due to the uncertainties in the injected noise signal. The technique resulted in the estimation of a correction term to be applied to the black body output voltage in order to apply a linear model to the instrument response. Further details are reported in ANNEX I, "The Microwave Radiometer".

As far as the tipping curve calibration is concerned (*Hogg et al.*, 1983), a scanning of the radiometer antennas is required starting from the zenithal position to an elevation angle which is not affected by the earth radiation through the antenna sidelobes. The technique is based on the assumption that the atmosphere is horizontally stratified so that it only varies with the altitude (that is the refraction index is only a function of the z coordinate and remains constant with x, y coordinates).

If this assumption applies, the brightness temperature of the scenario is related to the optical depth τ and the elevation angle θ by the equation:

$$T_B(\theta) = T_{BG}\exp(-\tau m) + T_{mr}(\theta)\,[1 - \exp(-\tau m)]$$

where:

- $T_{BG} = 2.75$ K is the cosmic background noise;
- $T_{mr}(\theta)$ is the mean radiating temperature of the atmosphere;
- $m = \sec(\theta)$ represents the air mass, which is equal to one for zenithal observation, two for 60° and so on.

If the antenna directivity is high the equation also applies to the antenna temperature (see ANNEX I, "The Microwave Radiometer").

Considering the linear relation between antenna temperature and radiometer output voltage, for each scanning step we can write:

$$V_j = G\left[\frac{T_{BG}}{L_j} + T_{mrj}\left(1 - \frac{1}{L_j}\right)\right] + B$$

where:

- j is the scanning step count;
- $L_j = \exp(\tau m_j)$ is the slant atmospheric attenuation factor.

Assuming T_{mrj} can be known from climatological analysis of the radiative properties of the atmosphere, in the geographical area, with some uncertainty, the unknown quantities G, B and τ can be in principle obtained from three elevation measurement steps. This is not feasible in practice because the measurement errors affect the solution of the problem which is inherently ill conditioned.

Therefore the adopted method relied on a number of elevation steps (5 or 6 steps have been adopted at air masses m_j whose output voltage is V_j) plus measurements of the black body radiation output voltage V_{cal} (corrected for the instrument non-linearity) at known ambient temperature T_{cal}. The expression to be minimized was therefore the following (for each of the two channels):

$$\sum_j [A + F\exp(-\tau m_j) - V_j]^2 + g\left[\frac{V_{cal} - B}{G} - T_{cal}\right]^2$$

where:

A $= G\,T_{mr} + B$;

F $= G\,(T_{BG} - T_{mr})$;

g represents the weight of the black body data in the minimization process which constraints the solution.

Different values of the constraint weight have been assessed showing a very high variability of the solutions relying only on tipping curve data. The bias appeared to become stable for small values of the constraint weight, while higher weights were necessary to stabilize the solution for the gain. It should be pointed out that it was not possible to measure the black body temperature T_{cal} with high accuracy, during the campaign on the tower, and that the compensation for the instrument non-linearity could not be perfect, so that using a weight too high could lead to a biased solution of the equations.

The final results showed a quite stable behaviour of the instrument in AGC mode while the Dicke mode was affected by instabilities which could be related to having switched off the instrument during the campaign.

A first validation of the obtained brightness temperatures has been attempted through comparison to radiosonde data acquired by the Italian Meteorological Office around the Adriatic basin (Udine and Brindisi meteorological stations) plus two radiosondes launched from the "*Acqua Alta*" platform on September 5th when the instrument was operating in AGC mode. The instrument brightness temperatures have been compared with those computed from the sounding data through a radiative model (*Liebe*, 1985, 1989). Unfortunately the validation results are affected by the fact that the Meteorological Office soundings are not referred to the radiometer site and that they have been supplied as TEMP data, that is they do not contain all sounding measurement levels, which are made available later on. Therefore at this stage the validation results are only indicative with the exception of the comparison based on the soundings performed at the tower which actually showed a good agreement.

4.2.4 Tropospheric Correction Estimate

Once the calibration of the instrument was performed, the altimeter excess path length was computed straightforwardly from the apparent temperature and surface meteorological data as explained in Section 4.2.1. A four minute averaging of the recorded data stream was performed around the satellite overpass time. The tropospheric correction was computed as a linear combination of the atmospheric opacity τ at the two channels, using also all the available surface meteorological data, that is, the following formula was applied:

$$\delta H = a_0 + a_1\tau_1 + a_2\tau_2 + a_3P_s + a_4T_s + a_5RH$$

where RH is the relative humidity measured at the surface.

Two sets of retrieval coefficients were assumed for clear and cloudy atmospheric conditions respectively (the selection of the correct set of coefficients was based on the information supplied by the experimenter operating on the tower). The opacity was directly computed from brightness temperature T_B:

$$\tau = \ln\left(\frac{T_{mr} - T_{BG}}{T_{mr} - T_B}\right)$$

where T_{mr} was estimated from the surface meteorological data through a linear regression model, tuned by analysing four years of meteorological data coming from the Udine meteorological station. The RMS error in estimating T_{mr} can be assumed to be ±3.5 K.

The coefficients for retrieving δH have been computed by a multivariate analysis of a large set of meteorological data (five years, including data acquired during the ERS-1 campaign) related to the Adriatic basin in the period from July to September. The independent variables of the regression analysis can be obtained from radiosondes either directly (the meteorological parameters) or through a deterministic model (the radiative model which allows computation of the opacity of the atmosphere for each of the radiosonde observations). The quantity to be estimated can be also computed from RAOB's by simply integrating the atmospheric refractivity. This method overcomes the absence of a suitable data set including both radiometric and meteorological observations. The errors associated to each measurement in the real experimental situation are considered in the regression and assumed of Gaussian distribution with a certain variance.

The accuracy of the final estimate can be based on the regression itself. The computed RMS errors were 0.98 cm for clear conditions and 1.3 cm for cloudy conditions (a total of about 2500 RAOB's have been processed).

The excess path length has been also estimated from meteorological data using the algorithms explained in the first paragraph. The comparison with a radiometric estimate shows a RMS difference of 3.3 cm and a bias of 0.9 cm. This must be considered for the ERS-1 passes of July 31th, August 3rd and September 14th, when using meteorological corrections in absence of radiometric data. The difference between these is shown in Figure 4–10.

The final results are reported in Table 4–1 for each ERS-1 pass. Estimates from meteo data and the radiometer are indicated, together with the meteorological measurements and the meteo conditions reported by the operator.

FIGURE 4–10

Variation of the tropospheric measurements during the campaign. The values based on surface measurements and on MWR measurements, together with the values actually used.

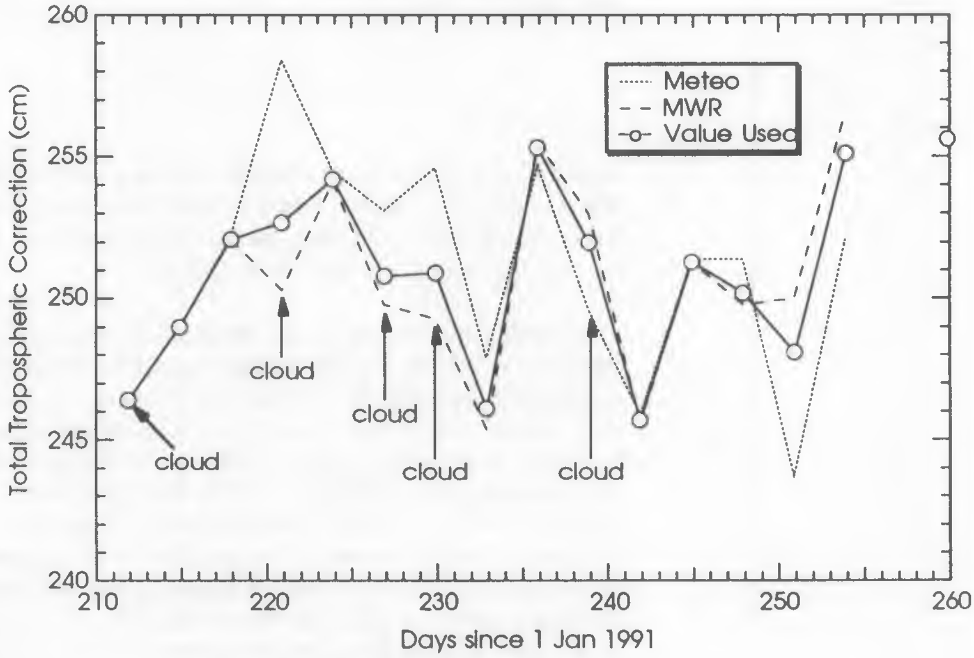

4.3 The Ionosphere

4.3.1 Introduction

The effects of electrons of the ionospheric plasma on an electromagnetic signal travelling from a satellite to ground are the following:

- Phase and group delays;
- Rotation of the polarization ellipse (Faraday Rotation);
- Phase and amplitude scintillations;
- Fluctuations in the angle of arrival.

In the case of the altimeter and of the techniques to be used here, only the first two are relevant and they will be briefly discussed.

The measurement of these ionospheric effects, which in some ways are seen as error sources, provide at the same time a way to determine the status of the ionosphere and consequently the means for correction. In both cases, the ionospheric parameter which directly affects delay and Faraday Rotation is the total number of electrons in an unit cross section column along the ray path from the satellite to the observer or to the target (the sea surface in the case of Radar Altimeter). This parameter is known as Total Electron Content (TEC).

TABLE 4–1 Final results of tropospheric measurements

Date	Day	Total Meteo (cm)	Wet Meteo (cm)	Total MWR (cm)	Wet MWR (cm)	Meteo Conditions	P_s(mb)	T_s (C)	R_h (%)	Total Troposphere (cm)	Estimated Error (cm)
31 Jul	211	246.4	17.2			cloudy	1010.3	20.8	77	246.4	
3 Aug	214	249	18.4			clear	1016.3	25.7	62	249	
6 Aug	217	252.2	21.9	252.1	21.7	clear	1014.9	26.7	71	252.1	1.0
9 Aug	220	258.4	27.7	250.3	19.7	partly	1016.4	27.3	82	252.7	7.0
12 Aug	223	254.5	24.7	254.1	24.3	clear	1012.7	27	80	254.2	1.0
15 Aug	226	253.1	22.8	249.8	19.5	partly	1014.7	26.2	71	250.8	2.0
18 Aug	229	254.6	25.5	249.3	20.2	partly	1009.8	27.3	75	250.9	4.0
21 Aug	232	247.9	17.4	245.4	14.9	clear	1015.7	24.7	62	246.1	1.0
24 Aug	235	254.7	23.6	255.5	24.4	clear	1018.6	26.2	79	255.3	1.0
27 Aug	238	249.6	18.2	253.0	21.6	partly	1019.7	26.3	55	252.0	2.0
30 Aug	241	245.9	13.8	245.6	13.6	clear	1022.6	23	53	245.7	1.0
2 Sep	244	251.4	18.9	251.3	18.8	clear	1024.4	23.9	71	251.3	1.0
5 Sep	247	251.4	20.2	249.8	18.5	clear	1018.9	24	76	250.2	1.0
8 Sep	250	243.7	12	250	18.9	clear	1021.1	22.2	47	248.1	2.0
11 Sep	253	252.1	21.5	256.5	25.9	clear	1016.2	23.7	83	255.1	2.0
14 Sep	256	rain (no data)								247[1]	
17 Sep	259	252.3	21.6	257.1	26.4	clear	1016.6	23.4	85	255.6	2.0

1. Based on measurement of shore-based barometer

Routine measurements using the two effects may be carried out, at the present time, using the satellites of the Navy Navigation Satellite System (NNSS) and the Global Positioning System (GPS). Additionally measurements with the DORIS system on SPOT 2 (which are not generally available) may be used. These provide differential phase (and group for GPS and DORIS), or geostationary beacons providing Faraday Rotation. The main characteristics of these systems are the following:

- NNSS provides accurate relative measurements, by measurements of differential phase, but no continuous time coverage. The column in this case will extend up to NNSS satellite heights (1100 km);
- GPS also provides accurate relative measurements by differential phase, and less accurate absolute measurements by differential group delay, provided delays at the satellite are known. The time coverage will be (and partially is today) continuous. The column extends for GPS up to the satellite height (20000 km) and reaches the plasmasphere;
- geostationary beacons provide accurate relative measurements and continuous time coverage. Although the column extends also to the plasmasphere, Faraday Rotation measurements provide information only up to about 2000 km, as the effect is weighted by the magnetic field of the

Earth. However the availability of suitable geostationary beacons seems problematic for the future.

- DORIS measures the Doppler shift, counting over 10 seconds, at two frequencies (2 GHz and 400 MHz) from a global network of about 50 beacons. The orbital height of SPOT 2 is the same as for ERS-1, and it is also sun-synchronous at about the same local time.

The determination of the ionospheric error (resulting from group delay) affecting the height measurements of the RA requires the knowledge of the TEC in the vertical column from the satellite to ground. The following Sections describe the techniques used and the results obtained.

4.3.2 Faraday Rotation Measurements

At *Istituto di Ricerca sulle Onde Elettromagnetiche* (IROE) determinations of TEC are carried out continuously using the method of Faraday Rotation. This method provides vertical TEC geographically above the subionospheric point. During the campaign the Meteosat 2 beacon has been used; for this satellite and this period, the subionospheric point is located at 40.2° North and 8.5° East. For the extrapolation of the determination of TEC from this point to Venice, take into account of the following points:

- The displacement in longitude is equivalent to about fifteen minutes in time. Therefore it is sufficient to use observations taken at 21:20 (Faraday Observations are taken each minute).
- The displacement of 5° at middle latitudes introduces errors, believed to be comparable to the overall errors involved in the observations and data reduction. This is supported by tests with simultaneous Faraday observations taken with the same type of instruments in Firenze and Trieste, in which no influence due to the difference in latitude (≈2.5°) was noticeable. However since some indication of the ionospheric density gradient is available from the GPS and DORIS results, these have been taken into account in generating the final values.

4.3.2.1 Overall description of the data reduction.

Before a detailed description of the procedure is given, the following summary will be useful to have an overall understanding of the topic.

The steps to evaluate Total Electron Content (TEC) at IROE are the following:

1. Observations of Faraday Rotation from geostationary satellites equipped with a VHF beacon.
2. Operator-attended reconstruction of continuous records of relative polarization angle (PA).
3. Ambiguity resolution by application of semi-empirical models supported by ionosonde measurements.

The raw measurement is the phase angle between the clockwise (cw) and counterclockwise (ccw) components of the incoming VHF beacon, which is twice the PA undergoing Faraday Rotation. The situation is such that several cycles of differential phase (or semicycles of PA) account for normally occurring TEC's. It follows that phase or PA measurements must take into account of the integer number of cycles (or semicycles) elapsed, and this is possible only if continuous observations are carried out, advising the use of geostationary satellite continuously on duty. The basic point to keep in mind is that anyway the ambiguity relative to the integer number of cycles (or semicycles) at the beginning of the observations is still present, what implies an unique offset relative to a period of continuous observations.

Solution of this ambiguity is best done if long, continuous records (some days) are available: this explains why the reconstruction of such records receives so much importance to require the interactive, operator-attended software.

Continuous record of relative PA are then converted into relative vertical TEC (measurements provide information about slant TEC) using standard ionospheric and magnetic field models. TEC's will be expressed in units of vertical TEC (1 TEC unit=10^{16} electrons/m^2).

Finally the third step provides the solution of the ambiguity allowing absolute TEC for all the period covered by the continuous record under investigation to be obtained. During this step, other independent experimental data from ionosonde are used in the reduction. At the end, the user has absolute TEC at any time of the observed record.

In the following, after a more technical description of the technique, some details will be given about the actual work performed for the ERS-1 RA calibration campaign.

4.3.2.2 The Measurement

The instrument to measure Faraday Rotation is the polarimeter. The method used at IROE for many years (*Checcacci et al.*, 1976,1978a,1978b; *Campannini et al.*, 1983; *Campannini and Spalla*, 1988) is reconstruction by a hybrid of the clockwise (cw) and counterclockwise (ccw) circularly polarized components of the incoming electric field, obtained combining the outputs of two crossed dipoles. In this case the phase difference between cw and ccw components provides twice the PA required. This is implemented by the use of a software receiving technique that makes data handling very convenient and rapid (*Ciraola and Spalla*, 1988, 1990). Faraday Rotation observations are carried out on a routine basis according to the availability of VHF beacons.

The error in the measurement of differential phase varies, according to signal to noise ratio (S/N), from 0.2 cycles (Signal power ≈ -130 dBm) to 0.02 cycles (Signal power ≈ -120 dBm).

4.3.2.3 Data Preprocessing

Although the polarimeter at IROE takes into account the integer number of cycles of cw/ccw phase cumulated during the observations, the first step of data analysis is to rebuild an operator-attended continuous record of the observed phase for some given period. Suitable programs display, according to the operator choice, the phase record relative to hours, single days or groups of up to four days. First, individual days are processed. From the display, discontinuities are generally recognized and repaired easily. Operator attendance allows to recover the effect of short signal losses due to interference or satellite and receiver malfunctioning. It is difficult to quantify how short signal losses can be tolerated in order to avoid errors; by past experience gaps up to an half hour can be recovered.

At this point, groups of contiguous days of continuous phase records are joined; they obviously begin and end with gaps that could not be recovered. During this process data are converted from PA into equivalent vertical TEC units, according to the equations from the basic theory.

The orientation of the polarization ellipse of a signal transmitted from a satellite and observed on the Earth (Faraday Rotation), depends on the initial orientation at the satellite, on the satellite-observer geometry, and on the characteristics of the propagation medium, when this medium is magnetoionic (as the ionosphere is). The magnitude of this rotation is given by:[1]

$$\Delta\Omega = \frac{k}{f^2}\int_{\text{Path}} B\cos\theta N\ dl$$

where:

$k = 2.36\times10^{-5}$, from the combination of physical constants;
f = frequency of the incoming signal;
B = Magnetic field along the path;
θ = Angle between B and the propagation vector;
N = electron density along the path;

This is more effectively written in terms of vertical profile of electron density:

$$\Delta\Omega = \frac{k}{f^2}\int_0^{h_{sat}} B\cos\theta N\sec\chi\ dh = \frac{k}{f^2}\overline{M}\text{TEC} \qquad \textbf{(EQ D-1)}$$

where:

χ = angle between the path and the local vertical;
TEC is the vertical Total Electron Content;
$\overline{M} = \overline{B\cos\theta\sec\chi}$ is known as M shape factor, and is computed for the given path according to *Davies* (1980).

It must be kept in mind that the TEC so far obtained is still a relative TEC, as ambiguity remains unknown.

1. in all the equations SI units are used

4.3.2.4 Ambiguity Resolution.

Development of EQ D–1 including the initial polarization angle at the satellite Ω_0, the measured one Ω_{meas} and the ambiguity Ω_{amb}, results in:.

$$\Omega_{meas} = \Omega_0 + \frac{k}{f^2}\overline{M}\mathrm{TEC} + \Omega_{amb}$$

Note at this point that some confusion could arise in the terminology used above: ambiguity refers normally to an integer number of cycles, such that no measurement can fix at the beginning of the observations, and should not refer to the initial polarization angle which is unknown but not ambiguous. The procedures that will be described in the following actually estimate Ω_0 plus Ω_{amb}, although it was reported as an ambiguity resolution.

The most important problem at this point is therefore the evaluation of the additive constant: after this step, TEC at any time in the reconstructed phase record will be given by application of this equation. Several methods are available to solve this problem (*Davies*, 1980)

The so called f_0F_2 method is based on a comparison of Faraday Rotation and ionosonde data collected as closely as possible to the subionospheric point. For the Meteosat–Firenze path, the closest ionosonde is the one operated in Rome by the *Istituto Nazionale di Geofisica* (ING), providing an hourly service. The basic concept is the following, starting with a very simple mathematical approach: provided the maximum electron density N_{Max} is known, there exists an equivalent slab thickness τ' such that:

$$\mathrm{TEC} = \tau' N_{Max}$$

The maximum electron density is proportional to the square of the ionosonde parameter f_0F_2, so that this can be rewritten as:

$$\mathrm{TEC} = \tau' k (f_0F_2)^2 = \tau (f_0F_2)^2 \qquad \text{(EQ D–2)}$$

In principle, fitting relative TEC values *vs* squared f_0F_2 values taken at the same time, one expects a line whose slope accounts for slab thickness and intercept for ambiguity.

In practice, the slab thickness varies during the day, during the season and during the solar cycle according to the actual electron density profile, so that the results of the fitting would be inconclusive. The way to overcome these difficulties is based on some interesting results (*Titheridge*, 1972, 1973): during night-time hours, the slab thickness remains practically constant over very long periods of time. So, if one limits to use data from around 0 to 4h, the fitting is successful, and slope and intercept can be evaluated. Intercept provides directly ambiguity.

Absolute TEC values at any time in the processed period are now available.

4.3.3 Details for the ERS-1 Calibration Campaign.

As already reported, Faraday Rotation observations are carried out at IROE on a continuous basis. So, although not previously mentioned, measurements were available also during the ERS-1 calibration campaign, except on 7 August due to receiver failure.

During this time, attended preprocessing made it possible to extract four periods:

TABLE 4–2 The four distinct periods of faraday Rotation measurements

Period 1	10 Jul to 6 Aug	(191-218)
Period 2	8 Aug to 18 Aug	(220-230)
Period 3	19 Aug to 5 Oct	(231-278)
Period 4	6 Oct to 28 Oct	(279-301)

Continuous relative TEC records are contained in Periods 1, 2 and 4, for which application of the standard f_0F_2 method has been possible. During Period 3 the satellite (Meteosat 2) underwent equinoctial eclipse, so phase records show gaps from about three to six hours at night. In order to have some estimation of TEC during this period, an extension of the standard method has been used. This extension will be reported in the following as the Extended Method.

The fitting procedure was applied to Periods 1, 2 and 4 using proper hours and discarding the magnetically disturbed days. The following results were obtained

TABLE 4–3 Summary of the fitting procedure

Period	Slope	Intercept
1	0.30 ±0.020	-0.55 ±1.4
2	0.28 ±0.035	-2.44 ±1.2
4	0.33 ±0.021	-1.46 ±1.8

Computing the absolute TEC at specified time (21:05) for Venice is performed by reading the relative TEC at 21:20 (at the subionospheric point) and subtracting the intercept relative to the same Period, resulting from straight application of EQ D–2.

This method cannot be applied to discontinuous data of Period 3: each day would have its own non-recoverable intercept, as night-time values are missing. The Extended Method is based on the realization that the assumption of slab thickness constancy, over the considered period, holds satisfactorily, as shown by the results of the fitting given above (Period 4, which does not include any of the days requested, has been processed just for test). This has suggested to assume for Period 3 a constant slab thickness given by a rounded average of the Periods 1, 2 and 4 (τ = 0.3).

Each day, one hour fulfilling these requirements is selected:

- relative TEC and f_0F_2 are available
- to be as close as possible to the time in which the assumption of constancy of slab thickness holds.

The ambiguity is computed at this hour subtracting the relative TEC from the TEC given by EQ D–2. This offset holds for the whole day, so TEC at 21:20 can be computed from the relative TEC at the same hour. For error estimation, Period 3 must still be considered in a different way from Periods 1, 2 and 4, for which the situation is quite simple. For these Periods, as the contribution to errors from raw measurement and associated preprocessing is very small, only the error associated to the intercept, evaluated during the fitting, is considered. These values will therefore be noticed in the column relative to RMS TEC in Table 4–4 for any of the days belonging to that period.

For Period 3, each day will have its own error, which can not therefore be estimated by a statistics over the Period itself. In order to have a reasonable idea about its magnitude, this procedure was applied. During Periods 1, 2 and 4, TEC's obtained by the standard method and considered as reference values, were compared to TEC's computed by the Extended Method, getting for each Period the differences at each hour and then their RMS value. These differences can be considered the errors involved in using the Extended Method during Periods 1, 2 and 4. The statistics for these errors have been assumed to hold, at the corresponding hour, also for Period 3, for which as error estimation at each hour, the maximum RMS difference at the same hour has been taken. It's worth noting that examination of these comparison confirmed that the standard f_0F_2 method can be reasonably used only during night-time hours (0-4), when RMS differences are not much greater than the errors obtained by the standard method. Moving one or two hours from them (5-6 am), RMS differences tend to increase, so that errors for Period 3 are much larger. Still it must be remarked that they are obtained in different Periods, so that they must be considered only an *a priori* evaluation: reporting the results in Table 4–4, they have been flagged by an asterisk.

4.3.4 Ionospheric Errors

In Table 4–4 are reported all the final results for TEC at 21:05 of given days over Venice, the corresponding delay in cm, and the relative errors. The results from the other techniques to be presented are also given in this table. The results from the Faraday Rotation technique have been propagatedto the location of the *Acqua Alta* tower using the longitudinal and latitudinal profiles derived from the GPS technique (see next Section). For the conversion from TEC to delay, the classical formula (*Davies* 1990) has been used.

$$l = \frac{40.3}{cf^2}\mathrm{TEC} \times 100$$

4.3.5 Total Electron Content by GPS Measurements

The GPS phase observations L1 and L2 may also be used to compute a model of the Total Electron Content of the ionosphere above the GPS receiver station. In this case the GPS measurements were performed on the *Acqua Alta* tower for 2 hours centred on each calibration pass. The "*Bernese*" GPS Software contains a module IONEST to compute a polynomial approximation of the total electron content, concentrated into a "single layer", the altitude of which can be selected and is usually set to about 350 km. The two-dimensional polynomial uses as arguments the longitude difference, with respect to the sun, and the latitude. The maximum degrees of the polynomials can be chosen, separately for latitude, longitude, and mixed arguments. The results of the computation contain (among other things) the following information:

Origin of development	Coordinates of Venice Tower; Time should be pass-over time;
Normalization factors	Units for the development in latitude and time *eg* latitude 6 degrees means the development goes in units of 6°; Units for electron content (10^{17});
Coefficients for development	The first coefficient corresponds to TEC at the origin.

As an example of the output:

```
NORMALIZATION FACTORS: LATITUDE (DEGREES)  :  6.00
                       TIME (HOURS)        :  2.00
                       ELECTRON CONTENT    :  0.10E+18
DEG.LAT  DEG.TIME      COEFFICIENT           RMS
0        0              0.14739540E+01   0.58560040E-01
0        1             -0.31182810E+00   0.81083380E-02
0        2              0.33175020E+00   0.28637990E-01
1        0             -0.42722040E+00   0.26803910E-01
1        1              0.13197300E-01   0.19067860E-01
```

This example shows that directly above the origin, assuming the single-layer model, there are 1.47×10^{17} electrons per square meter, while 220 km to the north (2°) the TEC changes by:

$$\frac{2}{6} \times -0.427 \times 10^{0} \times 0.1 \times 10^{18} = -1.42 \times 10^{16}$$

During the calibration campaign the passes with available GPS measurements on the *Acqua Alta* platform are listed in Table 4–4. There were no usable data collected around the pass times on either 2 or 5 September 1991. This corresponded to the end of the availability of the WM102 receiver on loan from Matera, and before the Trimble receiver from Kootwijk could be installed.

Two hours of data, centred around the pass time of ERS-1, have been used to compute the ionosphere models for each of the other days. The results are also summarised in Table 4–4.

4.3.6 Total Electron Content by DORIS Measurements

DORIS is a radiofrequency positioning system designed to enable precise orbit determination for earth-observation missions. The system includes about 50 beacons spread around the world and dual-frequency receivers on board the relevant satellites. The SPOT-2 satellite carried a DORIS receiver during the ERS-1 calibration period. This satellite is in a similar orbit to ERS-1.

The beacons transmit at frequencies of 2 GHz and 400 MHz and the on-board receivers measure the Doppler shift over a counting period of 10 seconds. At each frequency, f_i, DORIS measures N_i, T_{1i} and T_{2i}, where:

$N_i = (f_{ri} - f_{oi})\,dt$: the Doppler count;
$f_{ri} = f_{ei} + \delta f_i$;
f_{ei} is the emitted frequency;
δf_i is the Doppler shift;
f_{oi} is the reference frequency.

The ionospheric quantity measured is:

$$m = \frac{B_1 N_1}{T_{22} - T_{12}} + \frac{B_2 N_2}{T_{24} - T_{14}} + B_3$$

where:

$$B_1 = -\frac{f_{e2}^2}{f_{e1}^2 - f_{e2}^2}$$

$$B_2 = B_1 \frac{f_{e1}}{f_{e2}}$$

$$B_3 = B_1 \left(f_{o1} - f_{o2} \frac{f_{e1}}{f_{e2}} \right)$$

This is related to the electron content by:

$$m = A \left(\frac{I_1 - I_2}{dT f_{e1}^2} \right)$$

where

$A = 40.22$;

I_j is the slant electron content at time T_j;
$dT = T_2 - T_1$: the counting duration.

Following the sub-ionospheric point assumption the ionospheric effect is supposed to be concentrated at the sub-ionospheric altitude, and the slant electron content is related to the TEC at the sub-ionospheric point TEC_j by:

$$I_j = K_j \times \mathrm{TEC}$$

with

$$K_j = \frac{R_e + h_s}{(R_e + h_s)^2 - (R_e \cos S_j)^2}$$

where

R_e is the earth radius;
h_s is the sub-ionospheric altitude (assumed to be 400km);
S_j is the elevation angle at the time T_j

The model used to represent TEC is defined by a latitude–longitude grid and an interpolation method. The TEC values at each grid point is given by a 3rd order polynomial interpolation over the 16 surrounding grid points. The latitude parameter of the grid represents latitude plus local-time variations, while the longitude parameter represents longitude plus absolute time variations.

The unknown parameters are estimated using a least squares fit over the whole set of measurements during two days. Measurements are weighted for measurement noise characteristics. The grid is regular to avoid divergence in areas where there are few DORIS beacons, and a constraint on slope variations is applied.

The results obtained during August 1991 are included in Table 4–4.

4.3.7 Overall Result

The combined results from the different ionospheric measurement techniques used are given in Table 4–4 and shown in Figure 4–11. This diagram also shows the values actually adopted for the ionospheric delay.

The corresponding values of the solar flux $F_{10.7}$, and the sun spot number, are also given, in Figure 4–12.

FIGURE 4–11 Summary of the Ionospheric delay measurements during the campaign

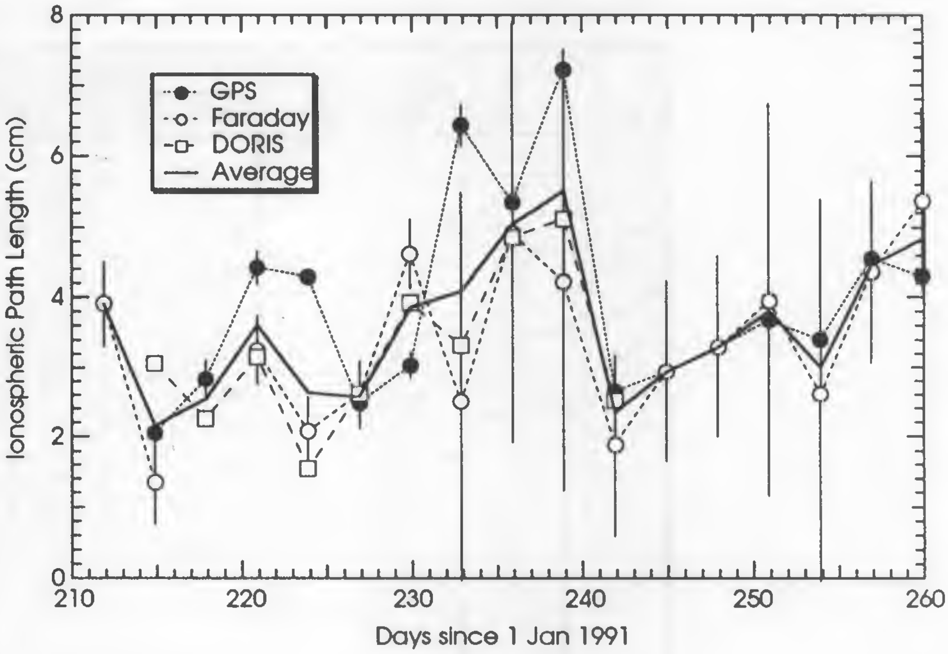

FIGURE 4–12 Solar Activity during the Calibration Campaign

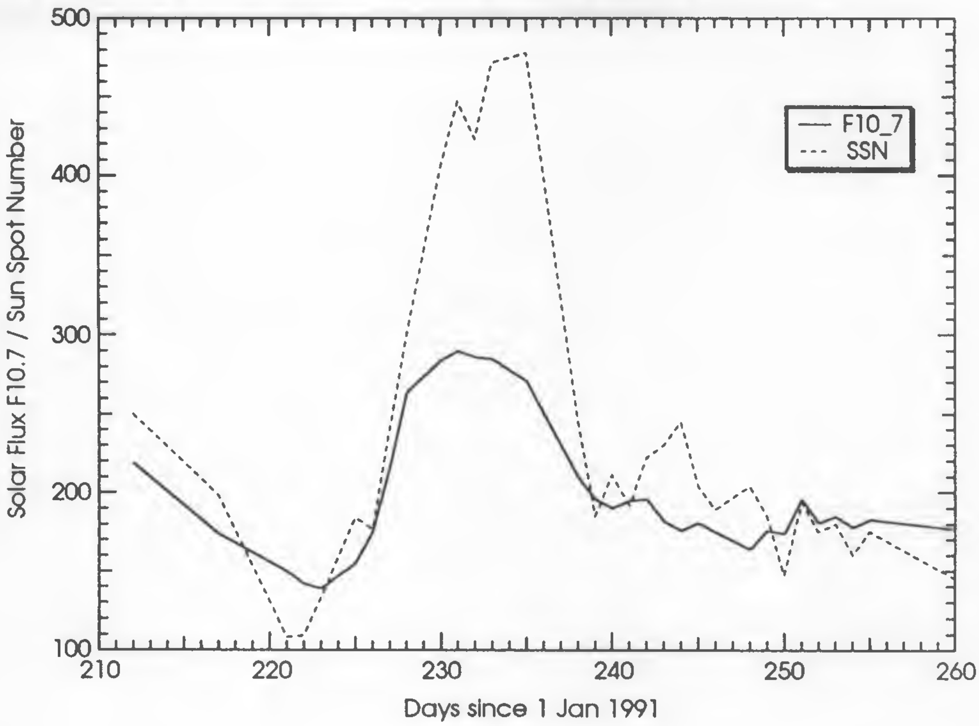

TABLE 4–4

Summary of the Ionospheric measurements and results using the different techniques. The asterisk attached to Fraraday Rotation measurements means that the Extended Method was used in these cases.

Date	Day	Faraday Rotation		GPS			DORIS	Total	
		cm	RMS	Instrument	cm	RMS	cm	cm	error
31 Jul	211	3.91	0.6					3.9	1.0
3 Aug	214	1.35	0.6	WM102	2.05	0.1	3.1	2.1	1.0
6 Aug	217			WM102	2.83	0.1	2.2	2.5	0.5
9 Aug	220	3.25	0.5	WM102	4.43	0.1	3.2	3.6	0.8
12 Aug	223	2.08	0.5	WM102	4.29	0.1	1.5	2.6	1.5
15 Aug	226	2.61	0.5	WM102	2.48	0.2	2.6	2.6	0.4
18 Aug	229	4.62	0.5	WM102	3.03	0.1	3.9	3.9	0.8
21 Aug	232	2.50	3.0*	WM102	6.43	0.2	3.3	4.1	2.0
24 Aug	235	4.91	3.0*	WM102	5.36	0.1	4.9	5.0	0.2
27 Aug	238	4.22	3.0*	WM102	7.22	0.2	5.1	5.5	1.5
30 Aug	241	1.89	1.3*	WM102	2.65	0.1	2.5	2.3	0.4
2 Sep	244	2.94	1.3*					2.9	0.2
5 Sep	247	3.30	1.3*					3.3	0.2
8 Sep	250	3.95	2.8*	TRIMBLE ST	3.68	0.1		3.8	0.2
11 Sep	253	2.60	2.8*	TRIMBLE ST	3.40	0.1		3.0	0.4
14 Sep	256	4.37	1.3*	TRIMBLE ST	4.55	0.1		4.5	0.2
17 Sep	259	5.38	1.3*	TRIMBLE ST	4.30	0.1		4.8	0.4

CHAPTER 5 The Trajectory

This chapter will address all the elements related to the laser tracking and trajectory determination.

5.1 Orbit Determination

The precise orbit for the calibration pass is computed in two steps, both using the DUT/SOM version of the NASA GEODYN II orbit determination software. First, a 4-day long arc solution is generated using ERS–1 so-called quick-look normal points (Section) from a global network of satellite laser ranging systems. Secondly, this orbit serves as *a priori* information for the determination of a short-arc orbit over the Venice Tower and a European Calibration Network (ECN) of fixed laser stations at Matera (Italy), Grasse (France), Graz (Austria), Zimmerwald (Switzerland), Wettzell (Germany) and Herstmonceux (England). This procedure maximises the orbit accuracy over the *Acqua Alta* Tower and minimises the possibility of obtaining an unrealistic or non-converging orbit solution. Once they became available the short-arc orbits were based on high-quality full-rate SLR data. (See Section 5.2.2)

To accurately track the satellite during its pass over the *Acqua Alta* Tower the Dutch Modular Transportable Laser Ranging System (MTLRS–2), which is operated by DUT's Kootwijk Observatory for Satellite Geodesy, arrived on 17 April 1991 at Monte Venda. Between its arrival and the launch of ERS–1 the MTLRS–2 system had already tracked 48 passes of the geodetic satellite LAGEOS from this site. From 17 July until 18 September, when the system returned to The Netherlands, it tracked another 23 LAGEOS passes in between the first-priority ERS–1 passes. Figure 5–1 shows the locations of Monte Venda and the other six ECN laser sites together with the ground tracks of ERS–1 in this area. The calibration pass is shown as a thick line.

For additional tracking two PRARE ground stations were planned to be installed at Monte Venda and the *Acqua Alta* Tower. These stations, which would have been supplied by DUT and *Agenzia Spaziale Italiana* (ASI), would have played a major role in checking the calibration results. However, on 2 August, before the PRARE ground systems were actually delivered to DUT and ASI, it became clear that the PRARE equipment on board of ERS–1 had a serious malfunction and would not provide any useful tracking data. Therefore, the precise ERS–1 orbits had to be computed exclusively from the laser tracking data.

Although, in contrast to the Bermuda approach, none of the tracking systems is vertically beneath the calibration pass, the network of tracking sys-

FIGURE 5–1 The ECN laser sites and the ERS–1 ground-tracks over Europe. The tick marks along the calibration pass over the Venice Tower are drawn at 20-second intervals. The time of overflight is given in UTC.

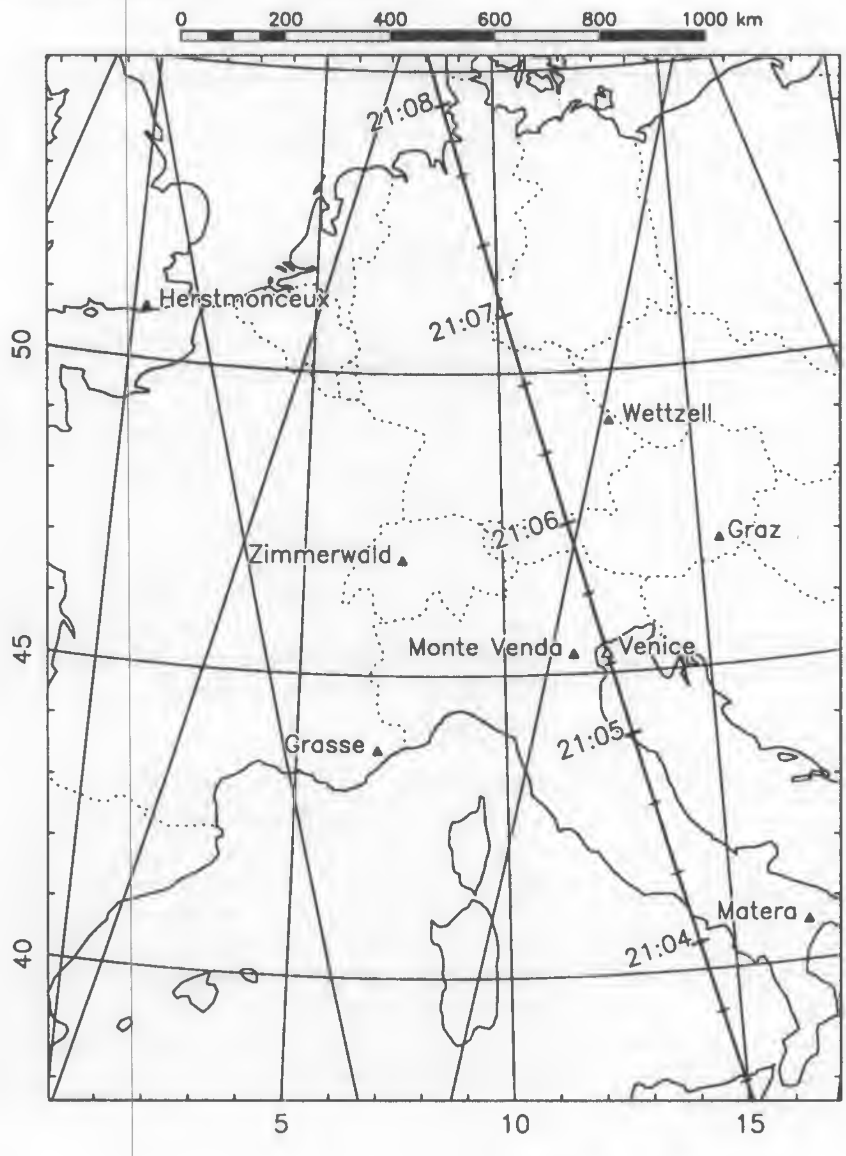

tems is sufficient to ensure an accurate determination of the satellite's height. Many pre-launch simulation studies were performed by ESTEC and DUT/SOM to investigate the radial orbit accuracy achievable with different tracking stations configurations and applying realistic measurement and dynamic error models. Table 5–1 summarises part of the results for 6 possible laser tracking configurations. It shows that the tracking by the Monte Venda laser, which is closest to the pass over the *Acqua Alta* Tower, is essential for achieving a high radial orbit accuracy, especially when some of the fixed laser systems are not able to track ERS–1. Since for this short-arc analysis no dynamic model errors propagate into the radial orbit error budget, it is clear that the dynamical determination of the orbit height is virtually equivalent to any geometrical solution. The results show that if sufficient laser tracking is available a radial orbit accuracy of better than 10 cm may be realised.

TABLE 5–1 Contribution of errors in the measurements and dynamic models to the error in the ERS-1 computed altitude near Venice for different tracking system configurations. Values are listed in centimetres.

Configuration	A	B	C	D	E	F
Monte Venda	•		•		•	
3 fixed sites West of the track	•	•	•	•		
3 fixed sites East of the track	•	•			•	•
Error sources						
Dynamics	0	0	0	0	0	0
Coordinates	2	5	6	15	4	15
Measurements	3	3	7	11	5	11
Refraction	4	4	9	13	6	13
RSS error	5	7	13	24	9	24

To obtain the most accurate orbit determination, high-quality station coordinates are imperative. During the ERS-1 Radar Altimeter Calibration Campaign two alternative sets of coordinates were used.

- ETRF-89: the 1989 set of SLR coordinates published by IERS. Since this set does not include the Monte Venda or *Acqua Alta* tower coordinates, these are obtained from the "Large" 1990 GPS Campaign and the Local GPS Campaign. (See Table 5–2).
- ERS90B: coordinates of the ECN SLR systems converted from the DUT/SOM ERS90 coordinates solution. The SLR marker coordinates of Grasse, Graz, Herstmonceux, Matera and Wettzell are computed from LAGEOS full-rate Release A normal points SLR data, covering the period September to December 1990. The SLR coordinates of Zimmerwald and Monte Venda are computed from quick-look LAGEOS SLR data, acquired until 25 June 1991. All solutions are converted to the epoch 1 September 1991. The position of the *Acqua Alta* tower is deter-

mined by adding the baseline between the *Acqua Alta* tower and Baiamonte obtained from the "Large" 1990 GPS Campaign to the SLR-based coordinates for Baiamonte. (See Table 5–3).

TABLE 5–2 Coordinates of the SLR markers of the ECN lasers in the IERS ETRF-89 frame. The markers of all fixed lasers are per definition at the markers. For the optical centre coordinates of MTLRS-2 the local eccentricity vector was added to the Monte Venda SLR marker coordinates, derived from the 1990 GPS Campaign, as is the *Acqua Alta* WM90 marker. The height *h* of the markers is with respect to the WGS84 ellipsoid

Station		x (m)	y (m)	z (m)	h (m)
7542	Monte Venda	4399363.596	910506.474	4512940.862	523.280
7835	Grasse	4581691.810	556159.420	4389359.400	1322.887
7839	Graz	4194426.720	1162693.899	4647246.558	539.442
7839	Matera	4641965.093	1393069.975	4133262.234	535.866
8834	Wettzell	4075530.074	931781.339	4801618.189	661.141
7810	Zimmerwald	4331283.617	567549.563	4633139.956	951.061
7840	Herstmonceux	4033463.837	23662.378	4924305.031	75.385
	MTLRS-2 optical centre	4399366.355	910507.138	4512939.963	524.635
	Acqua Alta WM90	4386229.673	973073.374	4512012.478	55.725

TABLE 5–3 Coordinates of the SLR markers of the ECN lasers in the DUT/SOM ERS90B frame. The markers of all fixed lasers are per definition at the markers. For the optical centre coordinates of MTLRS-2 the local eccentricity vector was added to the Monte Venda SLR marker coordinates, derived from SLR. The *Acqua Alta* WM90 marker coordinates come from the 1990 GPS Campaign. The height *h* of the markers is with respect to the WGS84 ellipsoid.

	Station	x (m)	y (m)	z (m)	h (m)
7542	Monte Venda	4399363.5434	910506.4196	4512940.8800	523.2483
7835	Grasse	4581691.7390	556159.3355	4389359.3075	1322.7647
7839	Graz	4194426.6561	1162693.8029	4647246.5027	539.3422
7939	Matera	4641964.9980	1393069.8736	4133262.2314	535.7728
8834	Wettzell	4075530.0019	931781.2485	4801618.1924	661.0840
7810	Zimmerwald	4331283.5505	567549.5497	4633139.9254	950.9920
7840	Herstmonceux	4033463.7612	23662.2808	4924305.0003	75.3128
	MTLRS-2 optical centre	4399366.2995	910507.0829	4512939.9714	524.5944
	Acqua Alta WM90	4386229.6174	973073.3156	4512012.5010	55.6944

5.2 ERS–1 Results

As described in CHAPTER 2, "The Problem", the sea level profile for each of the altimeter passes is computed by subtracting the measured altimeter height from the orbital altitude. This orbital height is computed from SLR data in two steps: a global long-arc and local short-arc.Long-Arc Orbits

5.2.1 Long-Arc Orbits

On 17 July 20:29 UTC, only about 18.7 hours after launch, the Grasse laser system acquired the first laser tracking data on ERS–1. The next day both the Grasse and the Zimmerwald lasers tracked the satellite. Then the other lasers stations followed and within 2 weeks a total of 13 stations in Australia, Austria, England, France, Germany, Hawaii, Italy, Japan, Peru, Switzerland, and the USSR had tracked ERS–1. At that time, 30 July, the ERS–1 orbit computation experiments by DUT/SOM started.

Initially, laser tracking data taken during the period 22–25 July were processed to form a 4-day arc, applying the NASA Goddard Space Flight Centre (GSFC) GEM–T2 earth gravity and ocean tides models (*Marsh et al*, 1989). The first computations immediately revealed the relatively poor tracking coverage of the satellite, which was underlined by an unrealistically good orbital fit of the available measurements and a large sensitivity of the recovered parameters to changes in the computation model.

The experiments were repeated with a new data arc, which covered the period 31 July to 3 August and comprised more global tracking data. In this experiment the orbital fit of the laser ranging data decreased to more-realistic levels. However, the results from this experiment also indicated the existence of serious modelling problems, which significant delayed the operational implementation of the orbit computation process at DUT/SOM. For a large part these problems resulted from the fact that the ERS–1 quick-look laser observations retrieved from DGFI were neither corrected for the centre-of-mass offset of the Laser Retro Reflector array, which is the distance between the geometric centre of the array and the satellite's centre of mass, nor for the distance between the array's optical centre and its geometric centre. The pre-launch information available at DUT/SOM showed that the data would have been corrected for these effects. This required a last-minute major modification of the DUT/SOM software.

Apart from software modifications, the major improvements came from the replacement of the GEM–T2 gravity and ocean tides models by the corresponding preliminary GEM–T3 models (PGS4591). The measurements RMS of fit was found to decrease to about 0.6 m for 4-day arcs with a reasonable global tracking coverage, and to about 0.4 m for 4-day arcs with a dominant European systems coverage. Because in the latter case the European tracking data outweigh the amount of tracking data from non-European systems, the orbit determination process leads to better orbits over Europe at the expense of a deteriorated orbit accuracy over the rest of the world.

To get a better insight in the accuracy of the computed orbits a series of overlapping arc analyses were performed. To allow this kind of analysis most of the 4-day orbital arcs were selected such that successive arcs have a 1-day overlap. The RMS orbit differences for that 1-day period were generally found to be about 0.6–1.0 m, 0.6–2.1 m and 1.5–6 m in the radial, cross-track and along-track directions, respectively. The values obtained for the RMS laser range residuals and the RMS orbit differences indicate that the ERS–1 4-day arc orbits computed by DUT/SOM generally have an accuracy of about 0.8 m, 1.5 m and 3 m in the radial, cross-track and along-track directions. This accuracy level is sufficient to use these orbits as *a priori* estimates for the short-arc orbit determination process.

5.2.2 Short-Arc Orbits

For the computation of precise short-arc orbits over the *Acqua Alta* the tracking coverage of the ECN lasers during the ERS–1 zenith pass over the tower is, of course, extremely important. Table 5–4 lists the ECN laser systems which have acquired tracking data for the 15-minute arc in which the satellite passes directly over the *Acqua Alta* Tower.

TABLE 5–4 Tracking coverage by the ECN and other European lasers, and the availability of altimeter data, during the ERS-1 passes over the Venice Tower.

	July		August										September					
Station	28	31	3	6	9	12	15	18	21	24	27	30	2	5	8	11	14	17
Monte Venda				•	•	•	•	•	•		•	•	•	•		•		•
Grasse		•					•	•	•							•		•
Graz					•						•		•	•		•		•
Matera		•				•												
Wettzell																		
Zimmerwald			•	•		•	•		•					•				•
Herstmonceux	•	•				•	•	•	•	•	•	•		•				•
Borowiec						•	•	•										
Potsdam	•	•		•		•	•		•	•	•	•	•	•		•	•	
Riga		•	•			•	•		•	•	•	•	•			•		
Altimeter		•	•		•	•	•	•	•	•	•	•	•	•		•	•	•

This Table illustrates the sparse tracking coverage mentioned above. The altimeter passes of 3 and 6 August are tracked by only one ECN laser, while in many cases only 2 to 3 out of the 7 lasers have acquired tracking data. The Monte Venda laser, which plays a crucial role in the computation of the precise radial position of ERS–1 over the *Acqua Alta* Tower, has tracked the satellite during all zenith passes after 3 August, except for the passes on 24 August, and 8 and 14 September. Since it is known that the orbit accuracy degrades rapidly as less stations track the satellite, it was decided to use only those passes during which the satellite was tracked by the Monte Venda laser and at least one of the other ECN lasers.

From these arguments it may be concluded that the tracking coverage and the amount of tracking data from the ECN laser systems is certainly not optimal to compute precise short-arc orbits for all passes. Apart from that, on three of the passes the ground segment failed to provide the required altimeter raw data to ESTEC for precision reprocessing[1]. Consequently, eight of the eighteen passes have not been analysed, because (in order of frequency of occurrence):

- MTLRS-2 did not contribute to the tracking (6 cases);
- No altimeter data were available (3 cases);

The short-arc orbit computations referred to in this report are all based on the high-quality full-rate laser ranging data available from all ECN SLR sites. These observations are corrected for all known internal and external delays of the laser pulse, which include

- Corrections for tropospheric refraction using the Marini-Murray model;
- Measured system biases;
- Distance from the ERS-1 optical centre of the laser retro-reflector (LRR) to its geometrical centre (See Table 6-2 in CHAPTER 6, "The Satellite and its Measurements").

Table 5-7 lists the amount of full-rate observations (FR) available from each of the tracking ECN lasers and the period in which they were acquired during the ten passes that have been processed. The data come at fairly different rates, ranging from as few as 0.4-per-second (Matera) to as much as 3-per-second (Herstmonceux), depending on the systems architecture and performance.

In order to prevent the high-rate lasers to get a much higher weight in the solution just because of the abundance of data, the full-rate observations are converted into so-called normal points (NP) at 20-second intervals. In this way *over*weighting is overcome, and at the same time the noise of the observations is brought down considerably, without losing information in the original full-rate observations.

Apart from this, the normal points are also attached a system-dependent weight, given in Table 5-5, which is identical for each pass, but differs from one system to the other. The weight, or rather the uncertainty or standard deviation (σ), is the root-sum-square (RSS) of the system noise, varying from 1 to 12 cm, and the overall model uncertainty, which is estimated at 2 cm.

1. These passes were subsequently delivered as off-line data, but none were used due to other reasons, such as insufficient laser tracking data.

TABLE 5–5 Weights attached to the normal points generated from the full-rate observations gathered by each of the ECN laser stations. Uncertainties are in centimetres.

Station	σ_{system}	σ_{model}	σ
Monte Venda	5.0	2.0	5.4
Grasse	2.0	2.0	2.8
Graz	1.0	2.0	2.2
Matera	12.0	2.0	12.2
Wettzell	1.0	2.0	2.2
Zimmerwald	6.0	2.0	6.3
Herstmonceux	4.0	2.0	4.5

For the ten remaining passes the weighted full-rate normal points were processed using the DUT/SOM version of the GEODYN II orbit determination software and a force model as described in Table 5–6. In addition to the observation corrections mentioned above, the fact that they refer to the LRR geometrical centre and not to the satellite's centre-of-mass (CM) is taken into account by adding the distance between the two points in the direction of each observation to the SLR range.

Figure 5–2 and Figure 5–2 portray the SLR range residuals (*ie* the observed minus the computed distance between satellite and tracking station) from the ECN lasers, and Table 5–7 lists their statistics. The RMS of the residuals, which indicates how well the computed orbit fits to the observations, ranges from 0.2–6.2 cm per pass with an average of 1.9 cm, and consists for a large part of remaining system noise in the normal points. The MTLRS–2 system at Monte Venda performs very well with an RMS of fit between 1.0 and 2.5 cm and an average of 1.9 cm. Another important parameter is the mean of the residuals. If stations have a high mean residual for one pass, this means either improper coordinates (*eg* a vertical shift) or an incorrect orbit solution. If this offset is persistent, then the coordinates must be suspect. However, this does not seem the case for any of the stations, giving an indication that both the orbit and the coordinates are accurate.

In order to make a quantitative assessment of the radial orbit accuracy, the orbit determination is also run with the ETRF-89 coordinate set. As can be seen from Table 5–7, this solution gave slightly worse residual statistics than in the former solution, from which we can conclude that the ERS90B solution is a bit more accurate. The level of accuracy can be quantified by comparing the radial position of the satellite over the *Acqua Alta* Tower (which is of the most importance) for all ten passes, listed in Table 5–8.

Surprisingly, the radial orbit difference on 17 September is significantly different from those on other passes. This is not so remarkable if we compare this to Table 5–7. Also here the residuals differ considerably between the two coordinate sets, which makes the ETRF-89 solution of 17 September rather suspect. Of remaining passes the average difference between the sat-

FIGURE 5–2 SLR normal point residuals for processed passes of 12 August, 15 August, 18 August and 21 August.

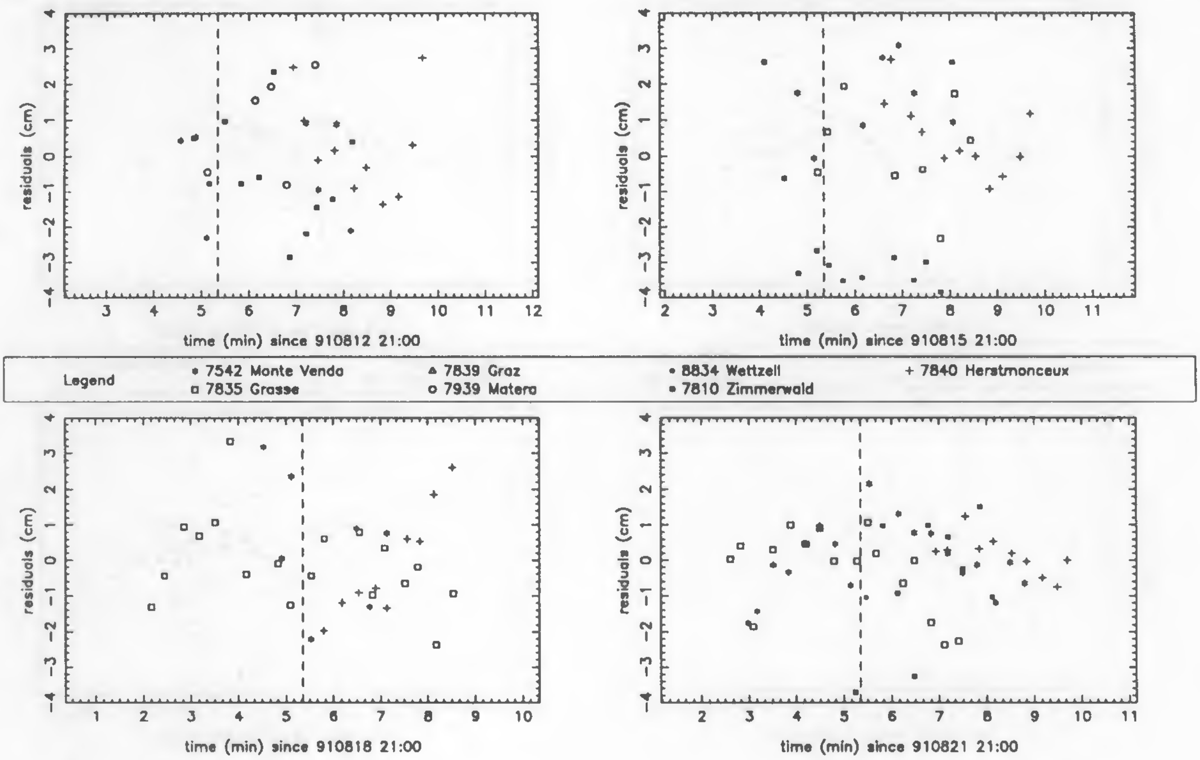

ellite altitude solutions in either frame is 3.6 cm, which corresponds to a similar difference in the height solution of the Venice Tower GPS marker (3.1 cm). Hence, this does not affect the altimeter bias determination. However, the RMS of the radial orbit difference about this mean, being 1.3 cm, is a clear indication of the orbit uncertainty caused by uncertainties in the station coordinates. Since the ETRF-89 and ERS90B sets are independent, we may assume the uncertainty in either solution to be √2 of this, or roughly 1.0 cm. ERS90B, being slightly better that ETRF-89, does produce less than 1 cm radial orbit error.

FIGURE 5–3 SLR normal point residuals for processed passes of 27 August, 30 August, 2 September, 5 September, 11 September and 17 September.

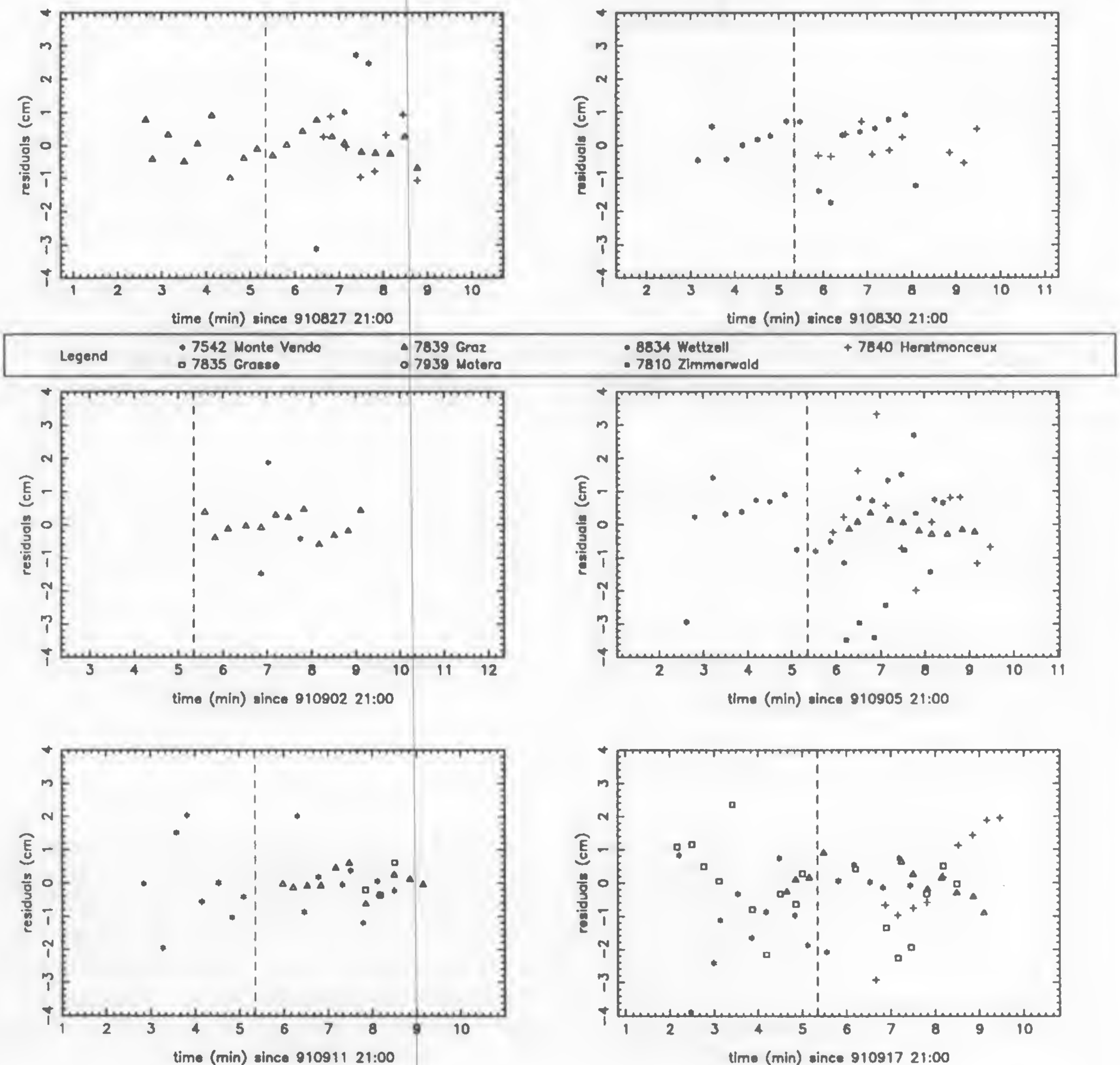

TABLE 5–6

Models and data used to compute the precise short-arc orbits of ERS–1 over the Adriatic and beyond

Measurement Model	
– Observations	Full-rate SLR data retrieved from DGFI, converted to normal points.
– Data weighting	Station dependent (See Table 5–5)
– Tropospheric refraction	Marini Murray model
– Geometric corrections	Offset of LRR optical centre wrt LRR geometrical centre (6.1cm), and the LRR geom. centre offset wrt nominal centre of mass (See Table 5–5)
– Editing	Cutoff elevation set at 20°. Editing at 3.5 times σ.
Dynamic model	
– Gravity Model	NASA Goddard Space Flight Centre PGS4591 model
– Gravitational Parameter	GM = 398600.4360 km^3/s^2
– Speed of light	c = 299792.458 km/s
– Mean equatorial radius	a_e = 6378.1370 km
– Flattening	$1/f$ = 298.257
– Solid Earth tides	Wahr model
– Ocean tides	NASA/GSFC PGS4591 model
– Third body attraction	Sun and Moon, JPL DE200 ephemeris
– Non-gravitational forces	C_D and C_R are solved in a 4-day global arc. A sophisticated multi-element geometric model is used to describe the satellite's shape and reflection properties.
Reference frame	
– Station coordinates	DUT/SOM ERS90B SLR coordinates as described in Table 5–3
– Earth rotation	Values from IERS Bulletin B at 5-day intervals
– CIS	Mean equator and equinox of J2000.0
– Precession	IAU 1976 (Lieske model)
– Nutation	IAU 1980 (Wahr model) plus Herring corrections
– Plate motion	not applied
– Tidal uplift	Love model, including frequency dependent and permanent tides (h_2 = 0.609, l_2 = 0.0852)
– Ocean loading	not applied

TABLE 5–7

Statistics of the SLR normal point residuals from tracking ECN laser systems, per pass and per station. The middle columns list the names of the stations and the number of normal points derived from the full-rate observation taken during the period indicated in the left columns. On the right the number of normal points that had a weight in the orbit solution, the average of the residuals (in centimetres) and their RMS are presented, for the orbit solutions in the ERS90B and ETRF-89 coordinate frames.

	Observation Period		Station		ERS90B Residuals			ETRF-89 Residuals		
Date	(UTC)	(sec)		FR	NP	Mean	RMS	NP	Mean	RMS
12 Aug	21:04:27–21:08:21	233.9	Monte Venda	88	7	-0.4	1.3	7	-0.4	1.5
	21:01:36–21:07:28	352.2	Matera	72	9	2.5	6.2	9	2.6	5.9
	21:04:46–21:08:20	213.6	Zimmerwald	196	11	-0.5	1.5	11	-0.4	1.6
	21:06:52–21:09:40	167.9	Herstmonceux	693	10	0.3	1.4	10	0.3	1.8
	Total			1049	37	0.5	3.3	37	0.5	3.2
15 Aug	21:04:42–21:08:23	221.0	Monte Venda	172	7	1.6	1.9	7	2.0	2.4
	21:04:55–21:09:11	256.4	Grasse	87	8	0.1	1.3	8	0.5	1.5
	21:03:53–21:08:18	264.6	Zimmerwald	469	13	-2.3	3.2	13	-3.3	4.4
	21:05:47–21:09:42	234.8	Herstmonceux	551	11	0.5	1.1	11	0.6	2.4
	Total			1269	39	-0.3	2.2	39	-0.5	3.1
18 Aug	21:04:24–21:07:45	200.9	Monte Venda	102	9	0.3	3.6	9	0.2	3.6
	21:01:03–21:10:59	596.2	Grasse	765	20	-0.0	1.8	20	0.0	1.8
	21:05:42–21:09:08	206.0	Herstmonceux	226	9	-0.1	1.5	9	-0.0	0.6
	Total			1093	38	0.0	2.3	38	0.0	2.2
21 Aug	21:02:57–21:08:56	359.3	Monte Venda	1367	18	0.0	1.0	18	0.4	0.8
	21:02:03–21:09:17	434.0	Grasse	315	17	0.0	1.6	18	0.1	2.4
	21:05:11–21:08:19	188.1	Zimmerwald	320	10	-0.6	1.8	10	-1.9	3.1
	21:06:45–21:09:42	177.5	Herstmonceux	926	10	0.2	0.5	10	0.1	1.9
	Total			2928	55	-0.1	1.3	56	-0.2	2.1
27 Aug	21:06:29–21:08:01	92.4	Monte Venda	39	4	0.8	2.5	3	-0.0	0.9
	21:02:19–21:09:04	405.2	Graz	550	20	-0.0	0.5	20	0.0	0.4
	21:06:38–21:08:51	132.2	Herstmonceux	121	8	-0.1	0.7	8	0.0	0.8
	Total			710	32	0.1	1.0	31	0.0	0.6
30 Aug	21:03:02–21:08:40	337.4	Monte Venda	731	16	0.0	0.8	16	0.0	0.8
	21:05:25–21:09:40	254.7	Herstmonceux	588	10	0.0	0.4	10	0.0	0.4
	Total			1319	26	0.0	0.7	26	0.0	0.7
2 Sep	21:06:47–21:07:49	62.3	Monte Venda	45	3	0.0	1.4	3	0.0	1.4
	21:05:25–21:09:16	230.4	Graz	308	12	0.0	0.3	12	0.0	0.3
	Total			353	15	0.0	0.7	15	0.0	0.7

TABLE 5–7

Statistics of the SLR normal point residuals from tracking ECN laser systems, per pass and per station. The middle columns list the names of the stations and the number of normal points derived from the full-rate observation taken during the period indicated in the left columns. On the right the number of normal points that had a weight in the orbit solution, the average of the residuals (in centimetres) and their RMS are presented, for the orbit solutions in the ERS90B and ETRF-89 coordinate frames.

Date	Observation Period		Station		ERS90B Residuals			ETRF-89 Residuals		
	(UTC)	(sec)		FR	NP	Mean	RMS	NP	Mean	RMS
5 Sep	21:02:03–21:08:42	398.5	Monte Venda	700	20	0.7	1.8	21	0.4	2.3
	21:06:17–21:09:13	176.0	Graz	226	10	-0.1	0.2	10	-0.1	0.3
	21:06:09–21:08:14	125.5	Zimmerwald	437	7	-2.0	2.4	7	-0.7	2.0
	21:05:52–21:09:40	228.2	Herstmonceux	757	12	0.2	1.3	12	0.1	1.3
	Total			2120	49	0.0	1.6	50	0.1	1.8
11 Sep	21:02:51–21:08:35	344.0	Monte Venda	270	16	0.0	1.1	16	-1.6	3.2
	21:07:41–21:10:39	177.6	Grasse	231	3	0.0	0.4	3	1.1	1.3
	21:05:57–21:09:12	194.8	Graz	255	11	0.0	0.3	11	0.2	0.4
	Total			756	30	0.0	0.8	30	-0.7	2.4
17 Sep	21:02:06–21:07:43	336.8	Monte Venda	557	18	-0.4	1.9	18	-4.6	5.3
	21:01:30–21:10:17	527.4	Grasse	706	18	0.1	1.8	18	0.9	2.1
	21:04:38–21:09:14	275.6	Graz	233	11	0.0	0.5	11	0.6	1.1
	21:08:03–21:08:17	13.1	Zimmerwald	18	1	-5.3	5.3	1	-8.6	8.6
	21:06:39–21:09:36	176.5	Herstmonceux	664	10	0.1	1.5	10	-0.3	0.6
	Total			2178	58	-0.2	1.7	58	-1.2	3.4
Overall Totals			Monte Venda	4071	118	0.2	1.9	118	-0.7	2.9
			Grasse	2104	66	0.0	1.7	67	0.4	2.0
			Graz	1572	64	-0.0	0.4	64	0.1	0.6
			Matera	72	9	2.5	6.2	9	2.6	5.9
			Zimmerwald	1440	42	-1.4	2.5	42	-1.9	3.4
			Herstmonceux	4526	80	0.2	1.1	80	0.1	1.4
			Total	13785	379	0.0	1.9	380	-0.3	2.4

TABLE 5–8 Height of the ERS-1 centre of mass (h) above the WGS84 reference ellipsoid at the time of the closest approach (TCA) to the *Acqua Alta* tower and the altitude difference (Δh) between the ETRF-89 and ERS90B solutions.

Date	TCA (UTC)	h (m)	Δh (m)
12 August	21:05:21.9106	784271.287	0.048
15 August	21:05:22.8837	784337.916	0.012
18 August	21:05:23.6536	784297.798	0.027
21 August	21:05:22.9073	784244.115	0.039
27 August	21:05:22.2837	784332.734	0.058
30 August	21:05:22.8475	784310.336	0.032
2 September	21:05:22.1491	784293.975	0.045
5 September	21:05:20.5341	784279.589	0.038
11 September	21:05:21.1293	784329.496	0.022
17 September	21:05:20.8605	784294.757	0.101
Total		Mean	0.042
		RMS about mean	0.023
Total (except 17 Sep)		Mean	0.036
		RMS about mean	0.013

CHAPTER 6

The Satellite and its Measurements

This chapter will address all the elements related to the satellite altimeter measurements of the altitude, and the relevant corrections

6.1 RA Operations

Following the launch of ERS-1 on 17 July 1991 the RA was first switched on for measurements on 25 July 1991. About 6 orbits of data were collected with the instrument being exercised in many of its operational modes. This activity was terminated by an anomaly resulting from attempting a forbidden mode transition. The following day, 26 July 1991, the commissioning phase orbit was acquired, and the planned series of RA activities completed.

Each of the payload instruments was checked out separately in this way, so the RA was not switched on again until 28 July 1991. This was the first day the entire payload was operated together, and was also the first pass over the calibration site after the orbit had been acquired. Unfortunately no RA measurement data were obtained over the site, due to the erroneous inclusion of an on-board software patch which was supposed to be used only during on-ground testing. The effect was to severely reduce the efficiency of the acquisition sequence; as the calibration overpass is only 20sec after a crossing from land to ocean this prevented operation in tracking mode.

This problem was quickly identified and solved and the next pass, on 31 July 1991, became the first pass of the campaign. During the calibration campaign, which lasted from 31 July 1991 until 17 September 1991, the RA operated correctly on all passes. The commanding was adapted so that internal calibration was performed every 30 seconds (instead of the default 2 minutes) in order to ensure internal calibration close to the calibration zone. Furthermore the RA was commanded to "Pause" mode just prior to commencing the calibration pass over the Adriatic, and to "Acquisition" at the coastal crossing. The objective of this was to control the instant when internal calibration occurred, so that there was no chance it would occur during an inconvenient moment.

6.2 RA Measurements

6.2.1 Data Products

The data used for the calibration data processing were a special data product generated at ESTEC in a "reference" processor. This is described later, in Section 6.2.2. This reference processor ingests RA raw data and generates a product containing essentially corrected engineering data. The processor can ingest any RA raw data, but is specifically designed to work with a raw data product called ERAC. This is produced by the Low-Rate Data Processing Facility (LRDPF), a subsystem of the ERS-1 ground stations. The types of RA data products generated by the LRDPF are shown in Figure 6–1.

RA data are received (after decoding) in the form of "source packets". They are generated by the instrument at the rate of one every 980ms in tracking mode, and at no more than one every 490ms in Acquisition mode. Every source packet is 3231bytes long, and has a primary header (identifying the packet and its sequential number), a secondary header (containing the datation, or time-tag, in the form of Satellite Binary Time, SBT), followed by auxiliary data and science or measurement data. In tracking mode the science data are provided as 20 consecutive data-blocks with identical struc-

FIGURE 6–1 The origin and structure of the various altimeter fast delivery products delivered from Kiruna to ESTEC during the Commissioning Phase

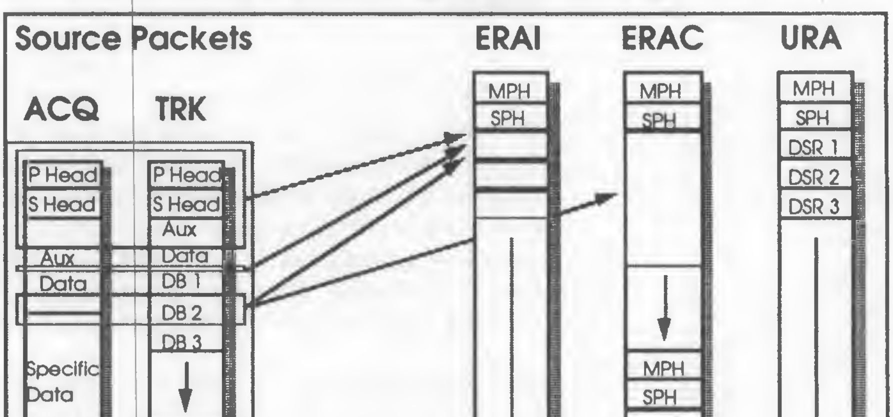

ture. Each of these corresponds to a 50-pulse averaging period and is the fundamental element of the altimeter measurement process.

The primary purpose of the altimeter chain of the LRDPF is to generate the RA fast delivery product for users; a product known as URA whose fundamental size is 80 records of one second each. This corresponds to an along-track size of 500km. The LRDPF also generates two engineering RA fast delivery products called ERAI and ERAC. The ERAI product is generated all around the full orbit and consists of so-called "instrument headers". These are small windows into every source packet which are stripped out and concatenated into one product. There are size limits on the number and size of these windows. The ERAI products have maintained the same window structure since launch: a window collects the primary and secondary headers (and so SBT) and the second data block. This is the one in which internal calibration data appear, when this occurs. All of the orbits dumped at Kiruna are transmitted to ESTEC in ERAI form soon after the dump.

The ERAI products were used during the calibration period to monitor the round-orbit and secular drift of the internal calibration loop, to ensure that the internal calibration records close to the *Acqua Alta* overpass were consistent.

Both the URA and ERAI products have header information prepended to the product (which, it will be recalled, correspond to 500km and one orbit respectively). The header information has two parts. The Main Product Header (MPH) is common to all ERS-1 fast delivery products. This contains much identification information and a number of items essential to the exploitation of the data (when provided in raw form). These latter items include:

- a reference SBT and corresponding reference UTC;
- the frequency of the on-board clock (the "tick" of the SBT);
- the *predicted* state vector and epoch at the ascending node.

There is also a Specific Product Header (SPH) containing further information specific to the type of data product.

The ERAC product which is used by the ESTEC reference processor consists entirely of a raw source packet, preceded by its own MPH and SPH. It is thus a very low-level product and has a natural length of 980ms. The typical length of a file of ERAC products is one minute; though ERACs can be programmed for arbitrary time extents they arrive split into one-minute segments. Constraints on the link capacity from Kiruna to ESTEC limit the total daily and orbital volume of ERAC products quite significantly however.

The RA data used for the calibration were thus all delivered as ERACs from Kiruna, generally within a few hours of the calibration pass itself. The ERAC products were missed on 3 and 6 August 1991, and 8 September 1991, due to computer problems[1]. They were later regenerated at ESRIN, but have not been used in the final analysis due to the relatively poor laser coverage on these dates. In fact on 8 September 1991 no European laser tracked ERS-1, due to an unexpected weekend orbit manoeuvre.

6.2.2 Reprocessing

The RA data used in the calibration processing have been processed at ESTEC, in a reference RA processor developed for the calibration task. Neither the Fast Delivery nor the Off-line products were used. The reason for this is that a retracking scheme was introduced to avoid potential tracking problems over this short stretch of often-calm water. This proved to be a wise precaution. Furthermore detailed control of the relevant characterisation parameters was thereby possible.

The overall procedure required the following steps:

1. Collection of all pre-launch characterisation measurements in numerical form in a database (this step is common to all the RA data processors, including the LRDPF and the Off-line processors);
2. Generation of a second database containing all parameters which vary between passes. This second database contains the internal calibration value (see Section 6.4) determined during preprocessing, measurements of the USO frequency (see Section 6.5) and corrections to the reference times in the MPH (see Section 6.7);
3. Running the reference processor with each of the calibration pass ERACs.

The procedure performed by the reference processor itself has the following steps, of which steps 5. to 10. are performed on every data block (20 per source packet):

1. Correlation of reference times to enable computation of UTC for each data block;
2. Initialisation of the orbit propagator ERSORB, using the predicted orbit (this is used for first-order position determination during data-editing, and not in the calibration process);
3. Opening of the output product file and writing of the file header;
4. Selection of tracking mode data packets (acquisition packets are discarded);
5. Conversion of source packet data to double precision floating point quantities in engineering units;
6. Compensation of the measured waveform for the IF transfer function of the instrument;

---

1. The ERS computer at ESTEC was running in fully automatic mode since the RA switch-on on 25 July 1991, acquiring, logging, processing, plotting and archiving all files (except ERAC processing which was done manually). However the volume of files (including mission planning, orbit restitution, time references, attitude files etc) was enormous and so there were some early problems. These were typically caused by filling of all available disk space before the archive process could intervene.

7. Application of the internal and pre-launch calibration measurements (*ie* the internal delay, see later), and conversion to "calibrated engineering units", according to the algorithms given by *Francis* (1989);
8. Estimation of the offset between the centre of the measured waveform (*ie* the RA tracking point, corresponding to the on-board height measurement) and the estimated mean sea level in the measured waveform. This is done by performing a least-squares fit of the Brown model (*Brown*, 1977) to the measured waveform. The least squares fit is an iterative process performed in three stages. In the first stage uniform weighting is applied to the waveform samples. This stage is intended to find a first estimate of the mean sea level. Based on the results of this stage a "zoned" weighting is applied, in which little weight is given to the echo before the leading edge, maximum weighting is applied to the leading edge itself, and an intermediate weighting is given to the echo plateau. The parameters estimated are Browns quantities τ, σ_s and $\sigma°$ (see the description of the Brown model on page 31). Finally a third stage of estimation is performed in which only Browns parameter ξ, the antenna mispointing, is estimated, with high weighting applied to the plateau of the waveform. In each stage a maximum of 40 iterations is allowed.
9. A range of quality indicators are assembled into a quality word to be associated with the measurement. These are shown in Table 6–1 on page 132;
10. A record is appended to the output product file. This file will have one record per valid data block, with no residue of the original source packet structure;
11. Various additional files, for logging and other analysis functions are also updated as necessary;
12. The output product files header record is completed with the number of valid data blocks, and the file closed.

The full set of RA height measurement data, before and after retracking, is shown in Figure 6–2.

6.2.3 Altimeter Data Processing Per Pass

The reprocessed altimeter data from the ten passes mentioned in CHAPTER 5, "The Trajectory", which had a reasonable ECN laser tracking geometry and good-quality altimeter measurements, have been processed to determine the ERS-1 altimeter bias. Firstly all the altimeter height observations were corrected for:

- offset of the altimeter reference point (the centre of the antenna aperture plane) with respect to the nominal centre-of-mass of the satellite. This distance is 851.9 mm;
- tropospheric and ionospheric propagation delay of the altimeter signal. As described in CHAPTER 4, "Local Measurements", both the dry and the wet component of the tropospheric delay were measured by a zenith looking microwave radiometer and other meteorological instruments placed on the *Acqua Alta* tower. Although these corrections only apply to

FIGURE 6–2

Height profiles from the on-board tracker, for the passes of 31/7, 3/8, 12/8, 15/8, 18/8, 21/8, 24/8, 27/8, 30/8, 2/9, 5/9, 11/9, 14/9 and 17/9, starting with the lowest profile. The upper panel shows the retracked height profiles. An arbitrary offset has been introduced between the profiles to aid visibility.

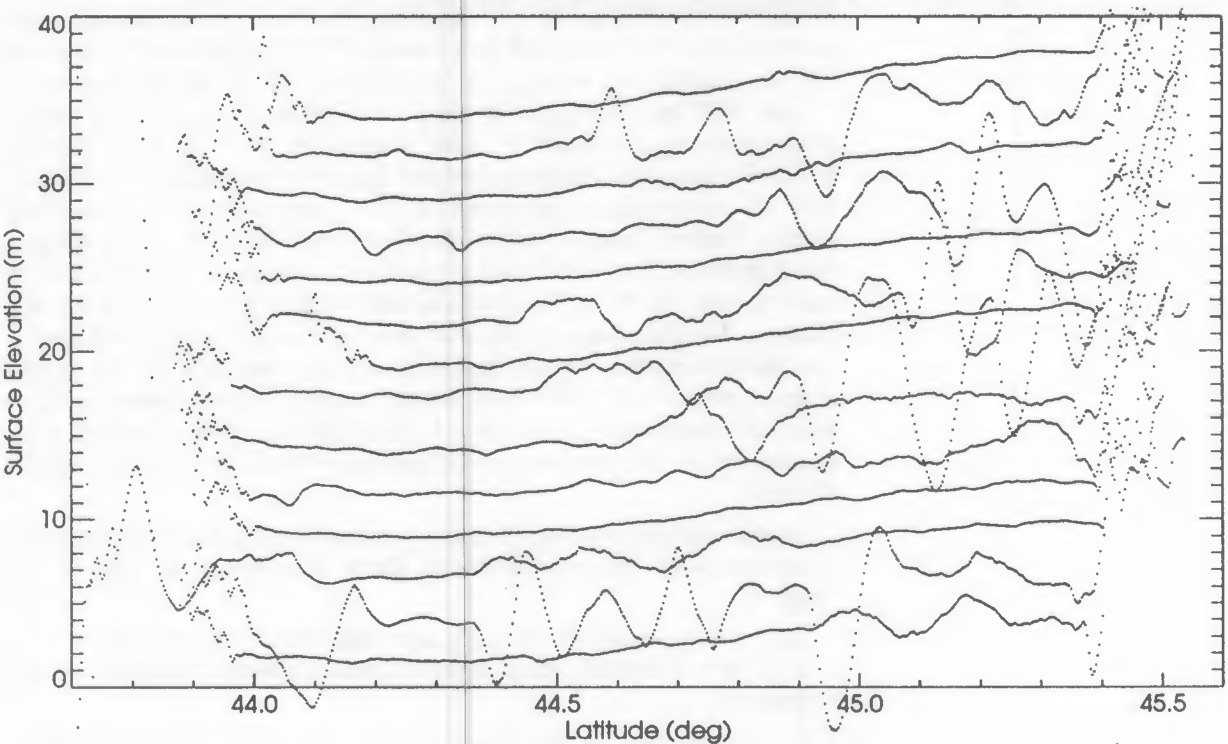

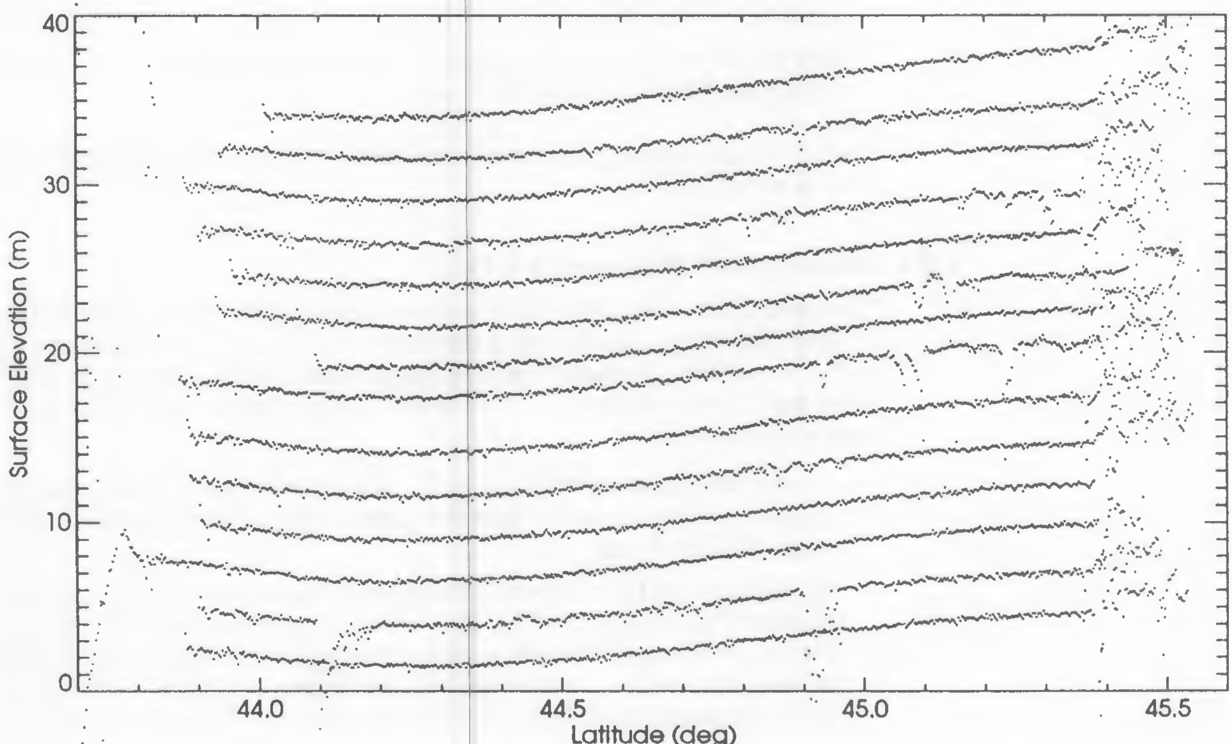

FIGURE 6–3 Smoothing and interpolation of the relative sea surface height derived from ERS-1 20Hz altimeter samples during the Venice passes on 12 August 1991 and 15 August 1991. The upper panel of each pair shows the smoothed altimetric sea surface height, and the lower panel the estimated error.

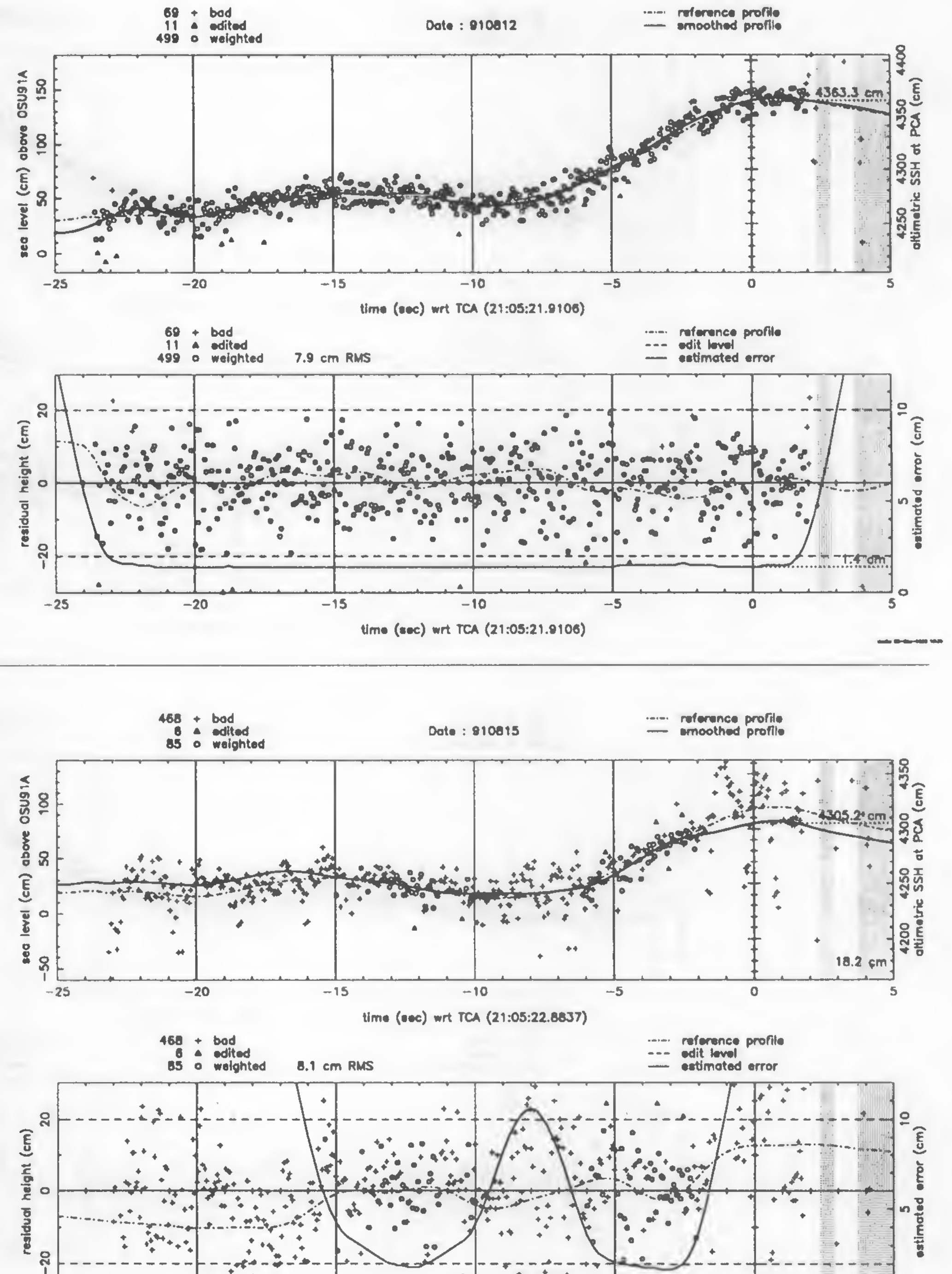

FIGURE 6–4

Smoothing and interpolation of the relative sea surface height derived from ERS-1 20-per-second altimeter samples from the Venice passes of 18 August 1991 and 21 August 1991.

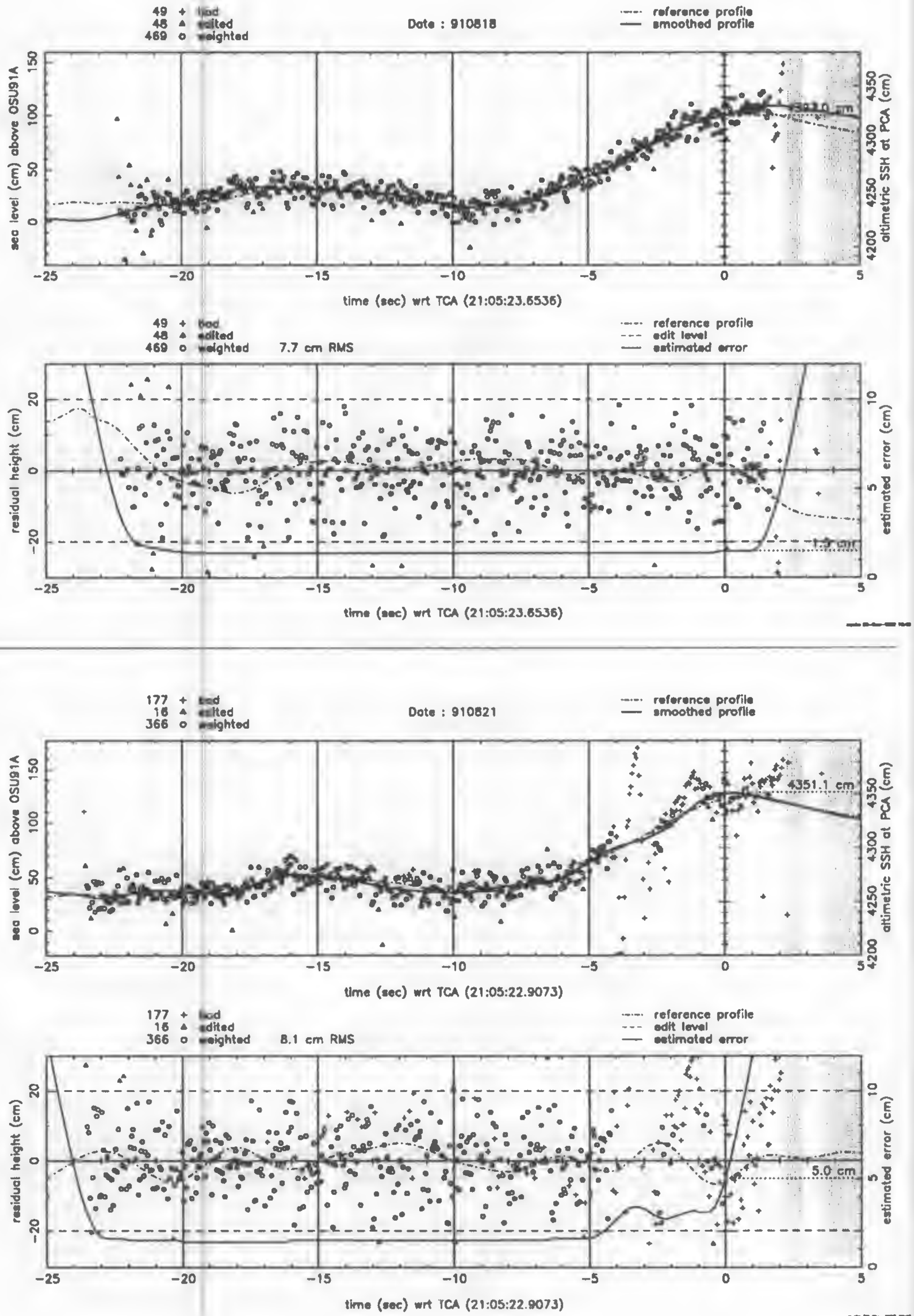

FIGURE 6–5 Smoothing and Interpolation of the relative sea surface height derived from ERS-1 20-per-second altimeter samples from the Venice passes of 27 August 1991 and 30 August 1991.

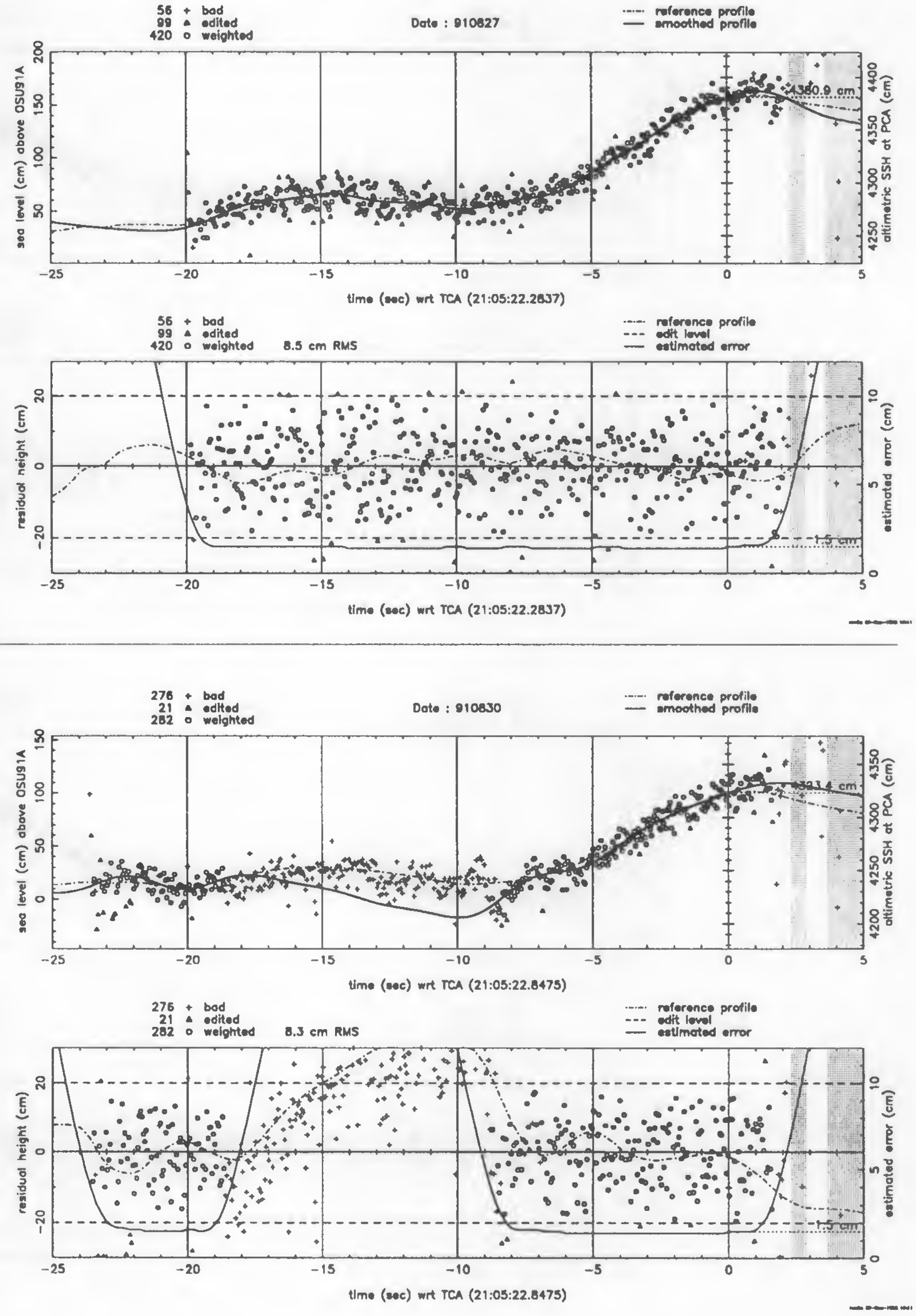

FIGURE 6–6

Smoothing and interpolation of the relative sea surface height derived from ERS-1 20-per-second altimeter samples from the Venice passes of 2 September 1991 and 5 September 1991.

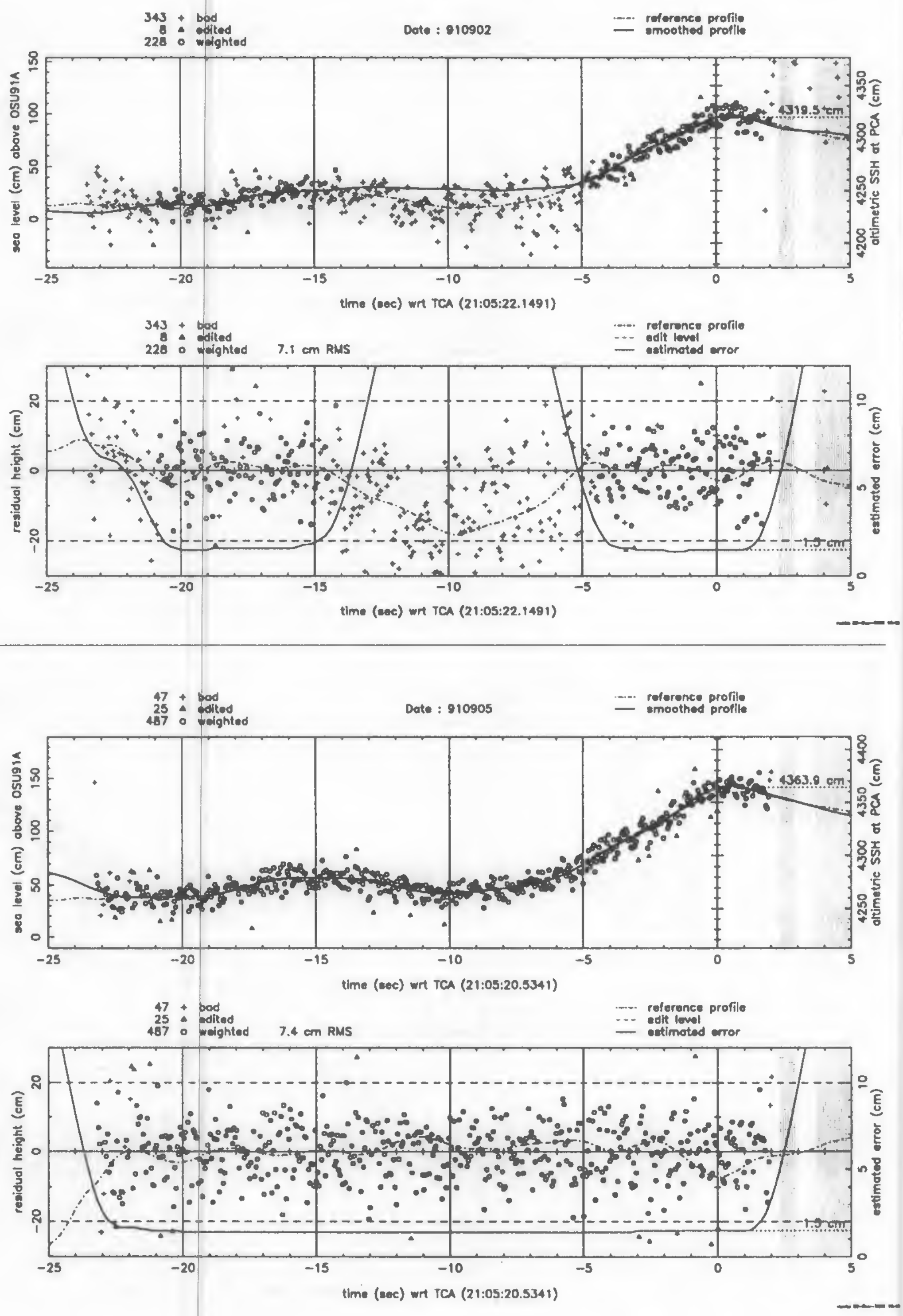

FIGURE 6–7

Smoothing and interpolation of the relative sea surface height derived from ERS-1 20-per-second altimeter samples from the Venice passes of 11 September 1991 and 17 September 1991.

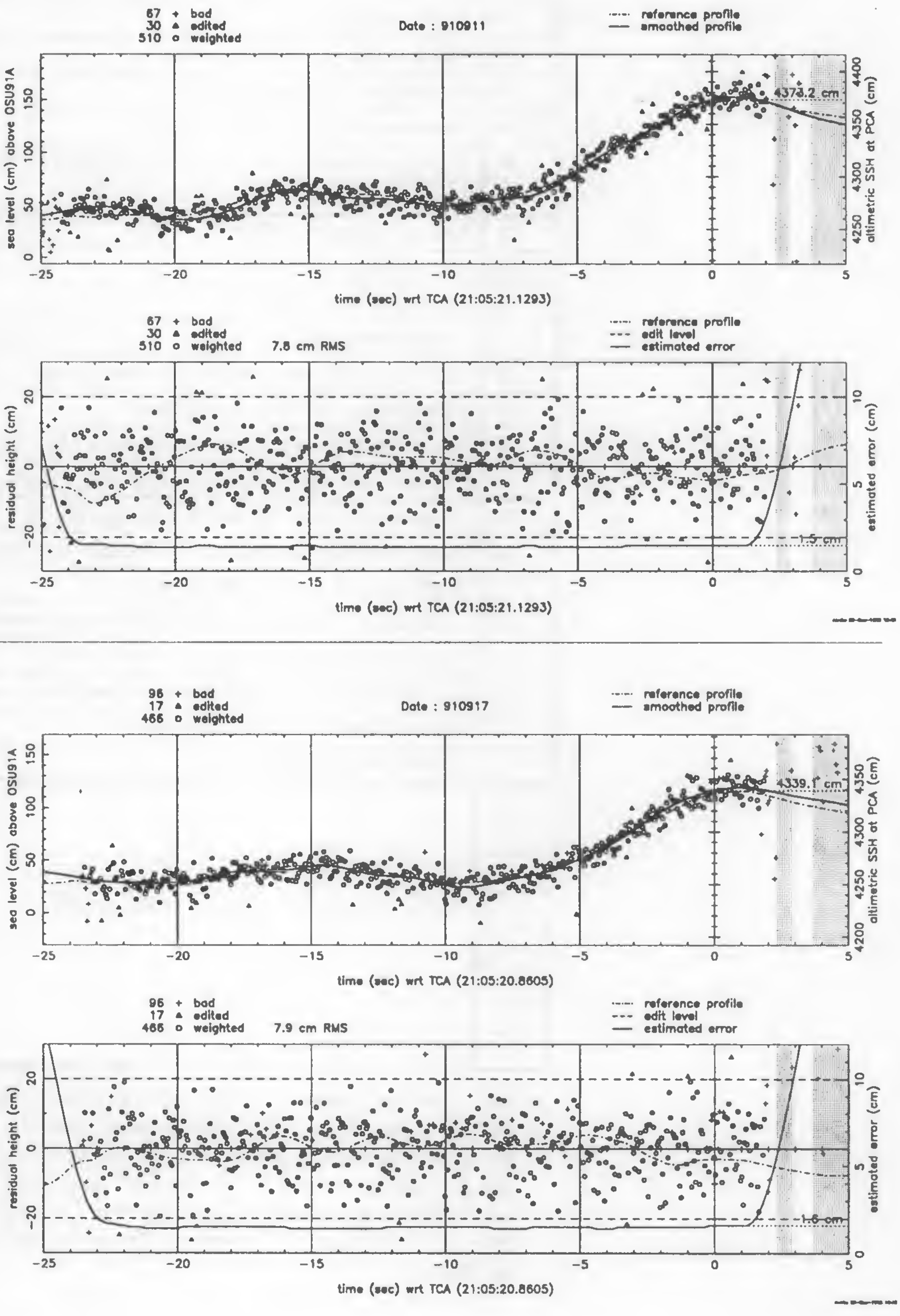

TABLE 6–1 Layout of the quality indicator word

31	PCD Summary
30	Performance of Downlink and X-band acquisition
29	HDDT performance
28	Frame Synchroniser performance
27	Frame Sync to Processor I/F
26	Checksum analysis on LR frames
25	Quality of Downlinked formats and Source Packets
24	Quality of Aux data
23	Orbit propagator IERR(1)
22	Orbit propagator IERR(2)
21	Orbit propagator IERR(3)
20	Orbit propagator IERR(4)
19	Open-loop calibration applied (1 = yes, 0 = no)
18	Open-loop calibration exceeds limit
17	Waveform slightly specular (peakiness > 1.5)
16	Waveform departs significantly from ocean shape
15	Negative root in SMLE waveheight conversion
14	Negative root in least squares waveheight conversion
13	Negative least squares estimated power
12	Number of parameters fitted by least squares less than 4
11	Return code from least-squares fit non-zero
10	Number of points used in waveform less than limit
9	Least squares residual exceeds limit
8	Mispointing exceeds range
7	
6	
5	
4	Mispointing in 0.01 degree units (bits 0 to 7)
3	
2	
1	
0	

altimeter measurements taken vertically above the tower, the same correction is applied to all measurements over the Adriatic sea. Furthermore, a local GPS receiver provides the ionospheric correction through the processing of dual-frequency GPS observations. Additionally ionospheric delays were computed from the Faraday Rotation measured at Firenze (Italy) and TEC measurements provided by the DORIS system on SPOT 2;

- Electro-Magnetic (EM) bias derived by taking 2% of the waveheight measured in-situ. The waveheight values were so small that the altimeter had problems in reliably measuring them;
- Doppler shift due to the vertical velocity of the satellite with respect to the sea surface (See Section 6.3);

Then, the sea surface height profile N_{alt} along the track over the Adriatic Sea is determined by subtracting all 20-per-second fully-corrected altimeter measurements h_{alt} from the orbital height h_{orb}.

Since none of these "full-rate" sea surface heights, which are separated by about 340 m, will actually be made over the tower, and their noise is about 8 cm (compared with the 2 cm obtained with the 1-per-second averages), a smoothing and interpolation has to be performed. The smoothing and interpolation scheme implemented at DUT/SOM is based on the technique of collocation, also known as objective analysis, which makes optimal use of *a priori* information of the expected 'shape' of the altimeter profile. The spatial covariance function was taken to be an isotropic one, based on the expected deviations of the sea level from the 360×360 Ohio State University geoid model OSU91A (*Rapp et al*, 1991). For longer wavelengths (above the spatial resolution of the geoid model) the covariance function was determined by the calibrated degree standard deviation of this model, and for short wavelengths (until 20 km) by Kaula's rule of thumb.

The altimetric sea height profiles of all these passes are shown in Figure 6–3 to Figure 6–7. In order to remove the major slopes in the sea height profiles, they are all plotted with respect to the OSU91A geoid model. The markers in these plots represent the reprocessed samples. Circles indicate samples used to form the smoothed sea surface profile (curved full line). Triangles and crosses indicate erroneous measurements. The time is measured relative to the time of closest approach to the *Acqua Alta* tower. The shaded areas show when the satellite is over land, while the sea in-between is the *Laguna Veneta*.

In order to obtain a reasonable interpolation of the sea height near the tower in cases where there are few proper altimeter measurements in the vicinity (such as on 15 and 21 September), the "average" of the other eight profiles was used as a reference. This reference profile was determined in three steps:

1. a tilt and bias was fitted through each profile and then subtracted;
2. the weighted mean of the eight profiles was computed (the weight along each track being determined by the interpolation error);
3. the profile thus obtained is fitted through the weighted altimetric sea height samples along each track while adding a solved-for tilt and bias, so obtaining ten reference profiles with equal shapes, but a different origin and slope.

Although the altimeter measurements have a noise of about 8 cm, the interpolation of the sea level can be performed to an accuracy of about 2 cm, in general. The interpolated value can be found from the right hand axis.

6.3 Doppler Correction

The vertical relative velocity of the satellite will cause a Doppler shift in the frequency of the returned chirp. Given the way the ERS-1 altimeter operates, registering received frequency as a function of time, a Doppler shift directly introduces an error in the altimeter range measurement.

For a given vertical velocity v and transmitted frequency f (13.8 GHz), the Doppler shift Δf on the two-way signal equals

$$\Delta f = -2\frac{v}{c}f$$

(The minus sign indicates that the frequency decreases for positive altitude rates). A negative change in received frequency with respect to the deramping chirp, having a decreasing frequency, will have the same effect as if the pulse was received earlier, *ie* decrease the IF frequency. The resulting two-way travel time delay thus is

$$\Delta t = \Delta f\frac{T}{B}$$

where B is the chirp bandwidth (330 MHz), and T the chirp duration (20 µs). This two-way time delay then corresponds to a one-way range error

$$\Delta h = \frac{c}{2}\Delta t = -vf\frac{T}{B}$$

Over the *Acqua Alta* tower the altitude rate of the satellite is approximately 12.5 m/s, which results in a Doppler shift of about 10.5 mm to be subtracted from the altimeter range measurements.

6.4 On-Board Calibration

The operation of on-board, or open-loop, calibration has been described in Section 1.2.2 in CHAPTER 1, "ERS-1 and the Radar Altimeter". In this section the way in which the data are used will be described. The block diagram is shown in Figure 6–8. The coarse trigger value is set to a predetermined value (the actual value is 2496) corresponding to the time required for the transmitted signal to pass from the chirp generator, through the delay line, transmitter and front-end to the deramping mixer. At this point the chirp is mixed with the Local Oscillator chirp, generating a so-called "single point target response" in the receiver.

FIGURE 6–8

Block diagram of the internal calibration loop. The timing of radar pulse round trip time is effectively made in the deramping mixer, since here the time to frequency conversion is made. Successive downstream stages have no impact on timing.

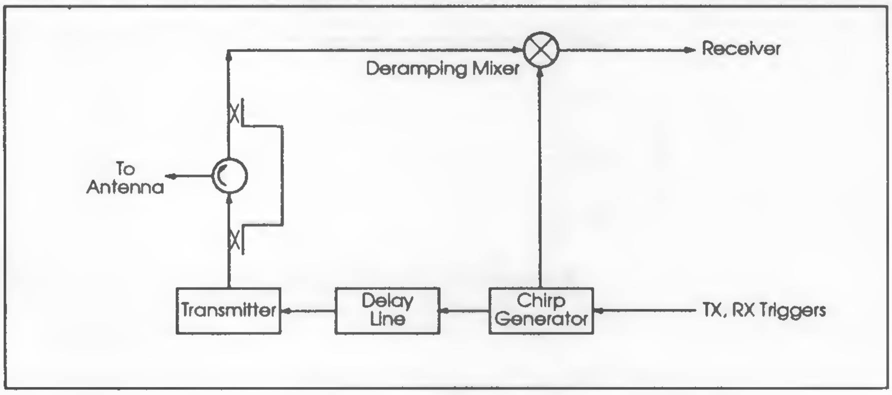

A corresponding signal will appear in the filter bank, as described in Section 1.2.2 in CHAPTER 1, "ERS-1 and the Radar Altimeter". An example of this signal is shown in Figure 6–9, though here the signal has been measured using the "scanning point target" method, in which the fine shift in the FFT is slowly increased giving a complete sampling of the point target response. Note that in open loop calibration only the values falling on the FFT lines are sampled.

The sampled lines are used to find the central point of the point target response, assuming a gaussian shape. By the operating concept of the altimeter the centre of the range window, which corresponds to the zero frequency in the complex spectrum, represents exactly the timing defined by the clock pulse number used (2496 in this case) plus the phase rotation applied in the FFT (zero in this case). Consequently this time, plus the offset of the derived centre of the point target response from the centre of the range window, is the exact time for the signal to travel around the internal loop. It is thus the internal calibration value.

This internal calibration has been performed at 30s intervals during tracking mode since the launch of the satellite. The round-orbit variation has remained at about 1.5cm during this time. The values obtained in one of the calibration orbits are shown in Figure 6–10.

There has been an evolution of the mean value of the internal calibration during the early part of the mission, due to ageing of the delay line. This effect is shown in Figure 6–11, which shows the values of the open-loop calibration during each of the calibration passes. These values are the result of fitting a curve to the round orbit variations.

These values have been included in the altimeter precision processing described earlier.

FIGURE 6–9

Single point target response measured in-flight. The upper panel shows the complete range of the filter bank (in filter number and amplitude), with the SPTR located near filter 40. For comparison the average amplitude of normal ocean echoes is maintained at 7.5 on this scale. The lower panel shows the same SPTR on an expanded scale.

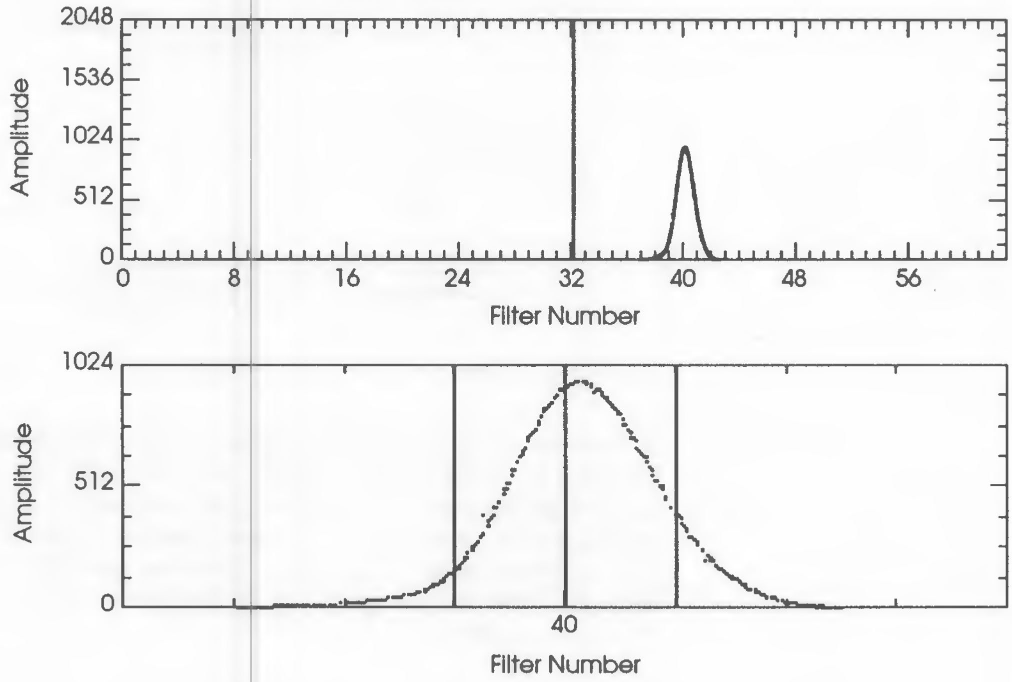

6.5 USO Frequency

The other major element of the altimeter system which must be taken account of during calibration is the frequency of the Ultra Stable Oscillator, or USO. This is measured during passes over the Kiruna station. The technique used is to generate a signal in the altimeter which is frequency locked to the USO, at 15MHz. This signal is passed to the science data telemetry system, where it is used (on command) to drive the bit clock during replay of the tape recorder. The frequency is thus directly recoverable on-ground by extracting the frequency of the real-time bit-synchroniser in the ground station, and measuring it against an atomic frequency standard.

The measured USO frequency and a fitted curve are shown in Figure 6–12. The trend in frequency during the campaign, which was in the early life of the satellite, is characteristic of quartz oscillators. The frequency has since settled to a value of 15000000.2 MHz. The measured values, and the interpolated values when no measurements were available, have been used in the data reprocessing. When the USO is switched off, as with all quartz oscillators, there is a recovery period after switch on, as can be seen in Figure 6–12 at day 257. On this occasion the RA was switched off for two orbits as an automatic safety measure following the loading of erroneous parameters.

FIGURE 6–10 Open Loop calibration values obtained during the calibration orbit on 5 September 1991. The round orbit variation is caused by thermal effects within the instrument, driven by heating and cooling as the satellite passes through eclipse.

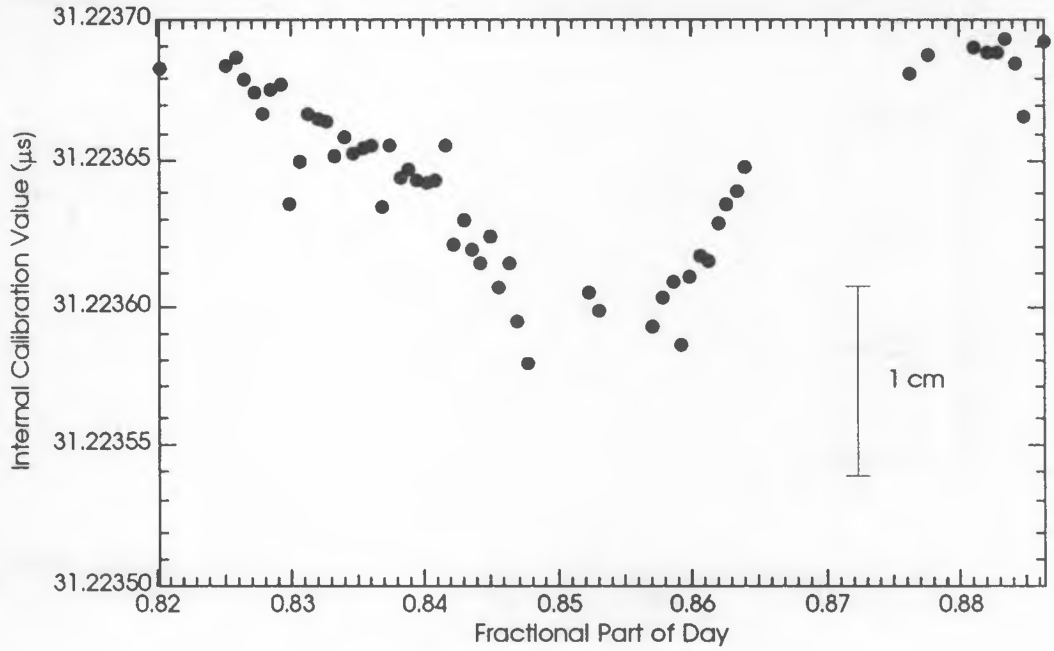

6.6 Reference Data

The positions of all of the elements of the satellite relevant to the altimeter calibration were determined before launch. Drawings showing the various reference points are shown in Figure 6–13 to Figure 6–16.

The antenna of the radar altimeter has its reference point at the centre of the aperture plane, as shown in Figure 6–13. This is different from previous altimeters in which the phase centre of the feed horn has been used. This point was adopted for the following reasons:

- the "electronic" reference point is the deramping mixer, which is within the microwave receiver. Since this point is inaccessible an arbitrary reference point on the antenna is commonly used;
- the centre of the aperture plane is easily definable and measurable.

In defining this point the internal antenna delays were taken into account. This includes the propagation from the feed horn to the reflector and back. These delays are included in the ground calibration value of the instrument. This value, 29.8 ns, represents the measured delay of all components outside the internal calibration loop. It is in fact this value which is being calibrated during the whole height calibration campaign.

FIGURE 6–11

The values obtained by open-loop calibration during each of the calibration passes. The high value (>30μs) is due to the delay line. A conversion to metres is given: the total variation is about 15cm.

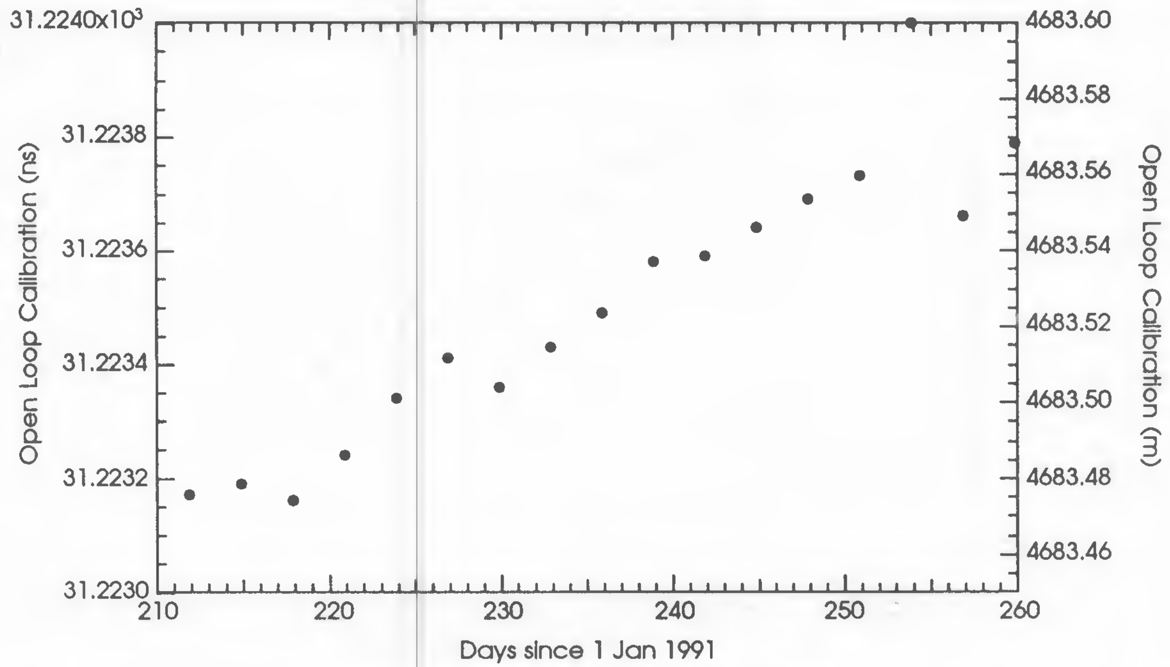

FIGURE 6–12

The difference between the measured USO frequency and its nominal value (15MHz) during the campaign. The corresponding height change is 1.5cm full-scale.

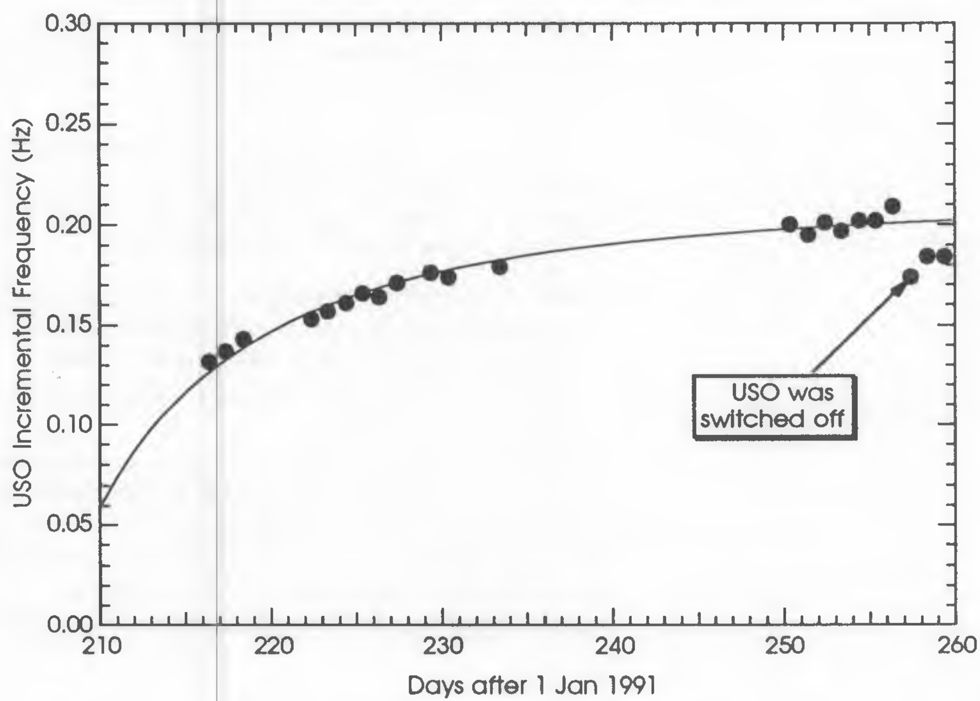

FIGURE 6–13

The location of the reference point for the Radar Altimeter antenna is at the centre of the aperture plane. The path from the feed horn to the reflector surface and back to the reference point is accounted for within the pre-launch characterisation of the instrument.

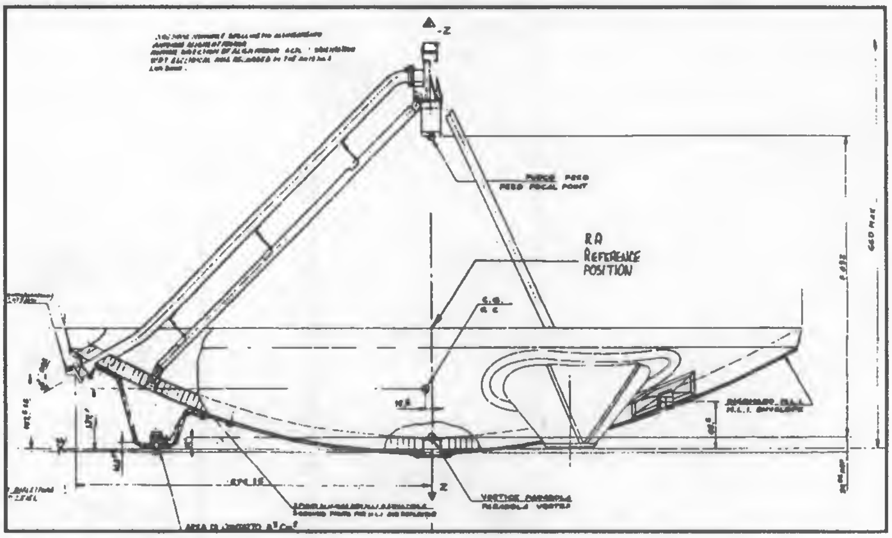

The mounting position of the Laser Retroreflector on the satellite are shown in Figure 6–14 and Figure 6–15. These figures show the position in the satellite frame of reference where the Laser Retroreflector reference point is located.

The position of this reference point on the Laser Retroreflector itself is shown in Figure 6–16. The reference point is not, however, the position where the reflections occur.

FIGURE 6–14

The Laser Retroreflector reference point is at the centre of the central cube of the array of 9 cubes, in the *x-y* plane.

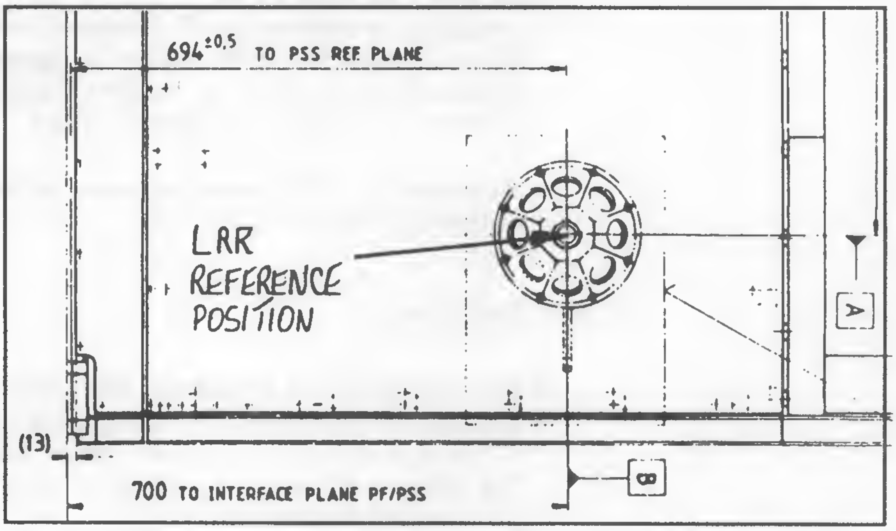

FIGURE 6–15

The reference point of the Laser Retroreflector in the z direction, as mounted on the satellite, is shown; it is 5mm from the panel surface due to the use of mounting washers.

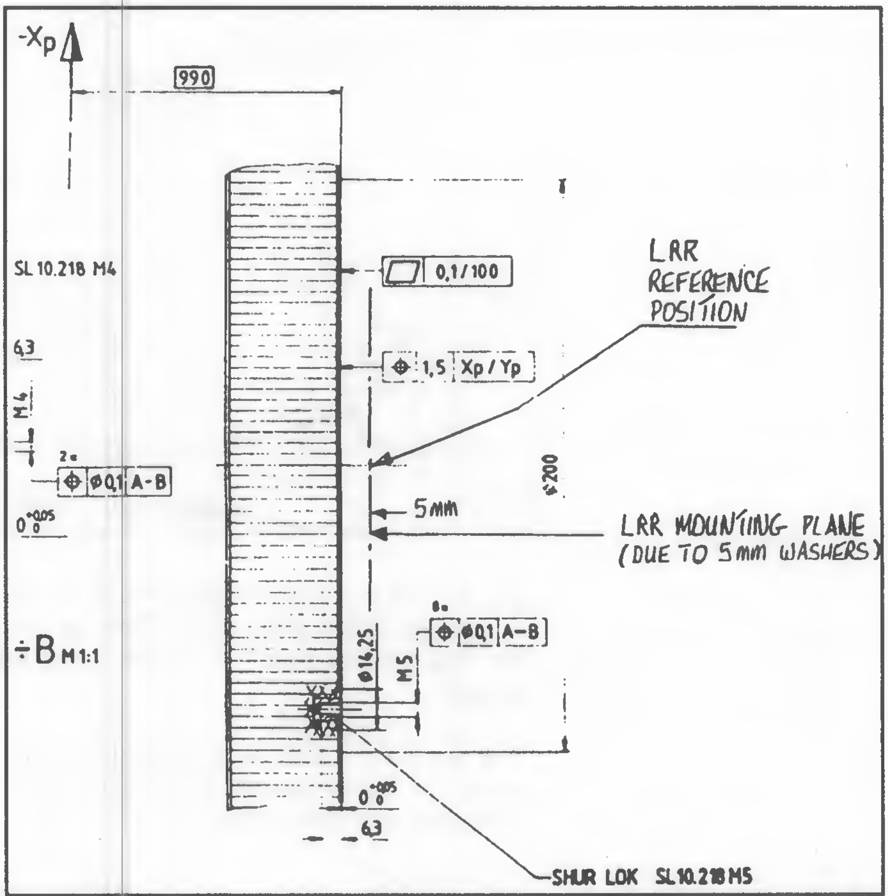

The most significant cube for passes close to zenith is the central cube, which has its front surface 77 mm from the reference point. The construction of a corner cube itself is shown in Figure 6–17. The apex of the cube is 23.3 mm from the front face. Thus the "optical centre" of the Laser Retroreflector is 53.7 mm from the reference point.

A summary of all the reference points, and the sources of the relevant documentation, is given in Table 6–2.

6.7 Datation

Ensuring the correct datation, or time-labelling, of the measurement data is critical to the calibration. The height rate in the Venice area is approximately 12.5 m/s, which corresponds to 1.25 cm for each millisecond of datation. The datation word is acquired every source packet (see Section 6.2.1) in units of Satellite Binary Time (SBT).

FIGURE 6–16

The reference point of the Laser Retroreflector is the centre of the interface plane. The front surface of the central cube is 77mm in the earthward direction from the reference point.

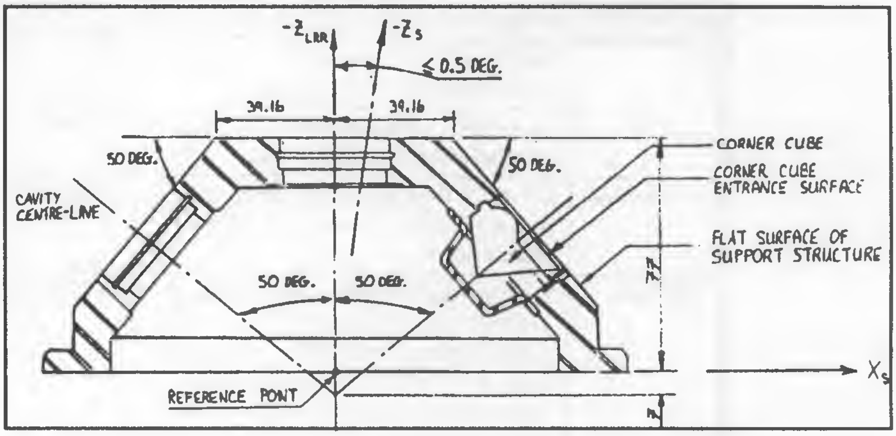

The determination of datation has two elements. The first is the correct identification of the measurement instant, in units of SBT, and the second is the correct conversion of SBT to UTC.

FIGURE 6–17

The corner cubes have a depth of 23.3 mm from the front face to the apex. The reflection is assumed to occur at the apex.

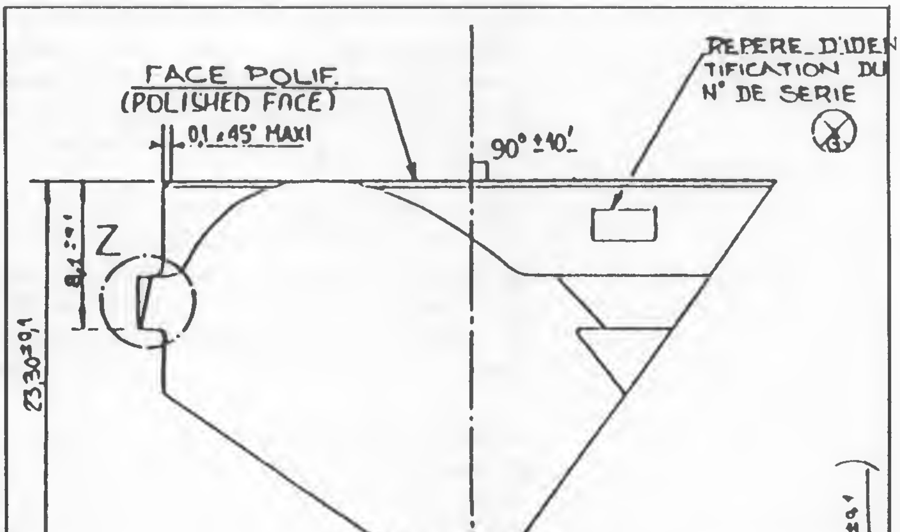

TABLE 6–2 Coordinates of various reference points on ERS-1 in the satellite's body fixed reference frame X_S, Y_S, Z_S. Values are in millimetres.

Ref Point	Description	X_S	Y_S	Z_S	Reference
RA	Radar altimeter reference point (centre of the antenna aperture plane).	-3780	+570	-840	*Francis*, 1991
LRR ref	Laser Retro Reflector reference point (centre of the interface plane)	-2850.4	-700	-995	*Louet*, 1991
LRR centre	Centre of the LRR cavity centre lines, 7 mm in $+Z_S$ direction wrt the LRR reference point	-2850.4	-700	-988	*Louet*, 1991
LRR bias	Distance added to the laser ranges to get from the optical centre of the LRR to the centre of the LRR cavity centre lines. A direct incident in any cube and optimal reflection is assumed, i.e. in the top corner.	= 77 + 7 -23.3 = 60.7			*Louet*, 1991
CM	Nominal position of the satellite's Centre-of-Mass.	-1815.9	+11.8	+11.9	*Louet*, 1991

6.7.1 Datation in Satellite Binary Time (SBT)

The datation is provided once per source packet, each of which contains 20 measurement data blocks. Each data block is assembled from 50 radar pulses. The overall timing of these measurement units is shown in Figure 6–18.

All relevant activities are performed during (or before) the first data block of the packet of 20. The signal which signals the request for a datation time value is the last transmit pulse of the previous packet. Synchronously with the transmit trigger (called TX Trigger) a pulse is sent from the SPSA, which controls all timing, to the ICU, where the datation clock is maintained.

Figure 6–19 shows the way in which this clock is handled inside the ICU. The clock is maintained as a 36 bit counter. The most significant 32 bits are updated synchronously with Satellite Binary Time, which has a nominal clock frequency of 256 Hz. Thus the clock step is approximately 4 ms. Since the altimeter requires more precise datation the RA datation clock maintains a further 4 bits of datation, giving a nominal step interval of 244 µs.

When the datation request arrives from the SPSA it performs two functions. It immediately causes a latch circuit to capture the instantaneous 36-bit value of the datation counter. In parallel it provides an interrupt pulse to the ICU processor. This is handled by a software interrupt handler (slower than the latch) which reads the value in the latch and provides it to the SPSA by a dedicated inter-processor command.

The datation value arrives at the SPSA several pulses after the request, and is inserted into the source packet. The exact time at which this is done is

FIGURE 6–18 Timing diagram of source packet generation and datation.

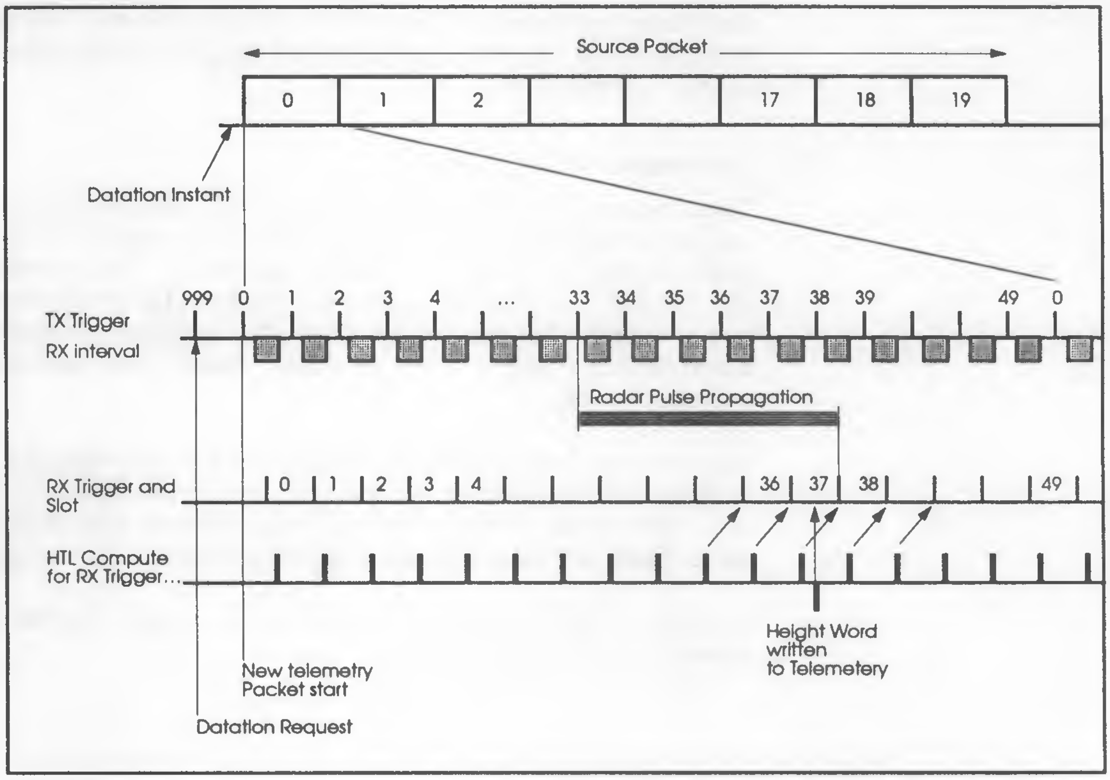

unimportant, since the datation value is the content of the counter at the time the datation request pulse was generated.

The next step is the connection between the datation value and the measurement event. Each 50-pulse measurement block is handled in the same way. The system is interrupt-driven so synchronism is guaranteed. The regular TX triggers are generated at the Pulse Repetition Frequency (PRF) by circuitry locked to the USO. The interval between these is approximately 980.4μs. The system has been designed so that the receive pulses, over the operating range of altitudes, will arrive somewhere during the gaps between TX Trigger pulses. Due to the computations of the height tracking loop (HTL) the arrival time is predicted, and a trigger signal, called RX Trigger, is generated at this time so that the deramping circuits will operate.

This RX Trigger is the interrupt which drives the SPSA processor. The processor thus works in time slots lying between RX Triggers.

The writing of the telemetry packet is performed during slot 37. However this writing is done *after* the update of the HTL, which is always the first task in a slot. Consequently the value which is reported is the value which will be used for RX Trigger 38.

The measurement instant, which corresponds to the time the pulse reflected from the surface, is then easy to calculate. It is the mid point between the time of RX Trigger 38 and the appropriate TX Trigger, which is number 34 since there are 5 pulses in flight before the echo return. This may be seen from the round trip time of about 5.5 ms compared to the pulse interval of slightly less than 1 ms.

6.7.2 Conversion of SBT to UTC

The conversion of SBT to UTC is performed by using *Reference Times*. These are, in principle, measured correspondences between SBT and UTC, as determined at the primary ground station, Kiruna. Two reference times, in SBT and UTC, are provided in the Main Product Header of every data product, as described in Section 6.2.1. The other required information, the onboard clock step length, is also provided. The SBT/UTC conversion then is straightforward.

However, the early period of the life of ERS–1, including the calibration campaign, suffered from procedural problems in the generation of the reference times. These were rectified by going back to the original time measurements made at Kiruna and modelling the performance of the satellite clock.

Analysis of the rectified time references has shown that the 1σ residual errors are approximately 100 μs.

FIGURE 6–19 The operation of the datation counter within the ICU.

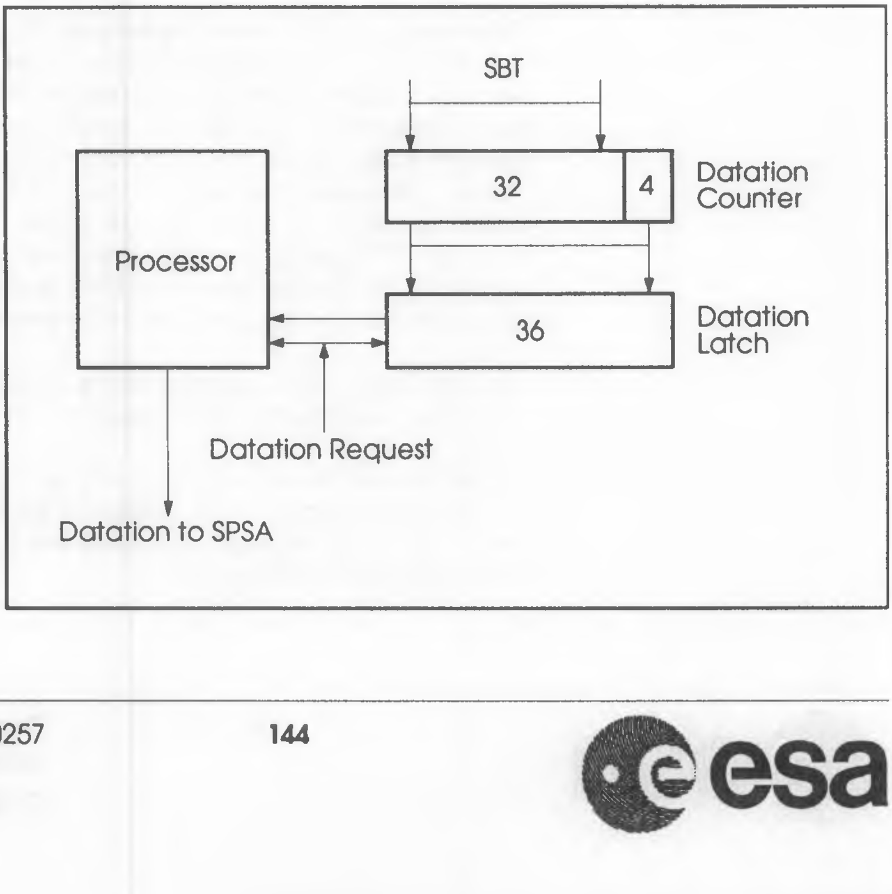

CHAPTER 7

The Results

This Chapter will present the final results of the calibration. It will also present some of the other bias values which have been obtained by independent means. It starts with a discussion of error types and estimaates of the errors in the bias calibration.

7.1 Error Estimation

The errors which will occur in the final value of the bias calibration are of two types. Static errors (also called systematic or bias errors) are errors which are always present, for every pass. They are, for example, caused by wrong measurements of static position or by errors in models. The other type of error is the non-static (or random, or noise) error. These are different from pass to pass, are uncorrelated and can be reduced by increasing the number of calibration passes.

In this Section the budget of static errors will be compiled from the previous Chapters. The non-static error budget will be compiled in the nect Section as part of the overall pass-by-pass evaluation of the overall bias.

The contribution of errors in the measurements and models, as described in the previous Chapters, is given in Table 7–1. This Table is subdivided into the errors affecting the orbit determination, those affecting the altimeter measurement, and those affecting the tidal sea surface height measurement. The static errors are then combined by Root Sum of Squares (RSS) to generate an estimate of the uncertainty which will remain in the final bias value, after taking into accout all of the non-static errors, when processing the final multi-pass result.

This overall uncertainty is ±3.2 cm.

TABLE 7–1

Estimated errors of the various entities building up the bias estimates per pass, in centimeters.

Entity	Method	Static Error
Recorded sea level	Analogue tide gauge	0.0
Height of the zero tide level wrt GPS marker WM90	Local survey	2.0
Height of the GPS marker WM90	GPS	2.0
Local solid Earth tide	Love Model	1.0
Station coordinates	ERS90B coordinate set	1.0
CM correction	Geometry	0.1
Bias estimate per pass	RSS	3.2

7.2 The Final Result

The summary of all of the relevant values leading to the ten independent bias estimates which have been derived during the calibration campaign are given in Table 7–2. The following remarks should be noted:

- The sea level recorded by the tide gauge on the *Acqua Alta* tower is added to the zero reference height of the gauge, which is a fictitious marker on the *Acqua Alta* tower that indicates where the sea level is when the gauge is indicating "0". This level was determined to be 13.457m below the GPS marker WM90, which is at 55.707 m above the reference ellipsoid. Finally, since the sea level rides together with the tower and its tide gauge on the solid Earth tides, the tidal sea level is corrected for the solid Earth tidal elevation computed according to the Love model, including the permanent and frequency-dependent tides.
- The altimetric sea surface height (SSH) comes from the smoothed and interpolated sea surface profiles presented in Section 6.2.1 of CHAPTER 6, "The Satellite and its Measurements". The Table indicates which corrections have been applied and which was the orbital altitude at the time of closest approach, as well as the "raw" (though smoothed and interpolated) altimeter measurement.
- The orbit altitude error, RSS correction error and sea surface height interpolation error are Root-Sum-Squared to form the total error of the single-pass bias estimate.
- A comparison of the altimetric and tidal sea surface height at PCA gives the single-pass bias estimate, as described by EQ 1 of CHAPTER 2, "The Problem". The bias estimates per pass so obtained range from –46.9 cm to –21.1 cm.
- The last part of the table presents some additional information, such as the timing corrections applied to the ERAC product, the deflection of the vertical measured on the tower, the horizontal and vertical velocity of the satellite, the azimuth of the ground-track and the geoid height at PCA with respect to that at the tower.

TABLE 7–3 Summary of the calibration measurements and results for each of the passes used in the final analysis.

	12 Aug	15 Aug	18 Aug	21 Aug	27 Aug	30 Aug	2 Sep	5 Sep	11 Sep	17 Sep
Time of PCA (sec past 21:05 UTC)	21.9106	22.8837	23.6536	22.9073	22.2837	22.8475	22.1491	20.5341	21.1293	20.8605
Location PCA wrt tower (m East)	314	44	-275	-106	187	27	134	520	362	211
Laser Tracking										
7542 Monte Venda	•	•	•	•	•	•	•	•	•	•
7835 Grasse		•	•	•					•	•
7839 Graz					•		•	•	•	•
7939 Matera	•									
7810 Zimmerwald	•	•		•				•		•
7840 Herstmonceux	•	•	•	•	•	•		•		•
Tide gauge										
Recorded sea level	1.040	0.703	0.774	0.924	1.180	0.718	0.634	0.958	1.075	0.749
Height of zero tide *wrt* WM90	-13.457									
Height of the GPS marker WM90	55.708									
Local solid Earth tide	–0.091	–0.111	–0.099	–0.061	–0.043	–0.104	–0.121	–0.038	–0.038	–0.068
Tidal SSH at tower	43.199	42.841	42.925	43.112	43.386	42.863	42.762	43.170	43.287	42.930
Altimeter										
No. of altimeter measurements	579	559	566	559	575	579	579	559	607	579
idem (weighted)	499	85	469	366	420	282	228	487	510	466
RMS of Residuals	0.079	0.081	0.077	0.081	0.085	0.083	0.071	0.074	0.078	0.079
Orbital altitude (784000+)	271.287	337.917	297.801	244.115	332.734	310.366	293.975	279.579	329.496	294.751
Raw altimeter height (784000+)	229.369	296.538	256.267	202.246	290.655	268.768	252.470	237.618	287.490	253.106
Ionospheric delay	0.026	0 .025	0.038	0.040	0.055	0.023	0.029	0.033	0.030	0.048
Tropospheric delay (dry+wet)	2.542	2.508	2.509	2.461	2.520	2.457	2.513	2.502	2.551	2.556
Doppler range error	–0.010	–0.010	–0.010	–0.010	–0.010	–0.010	–0.010	–0.010	–0.010	–0.010
C.M. Correction	0.852									
EM bias	–0.009	–0.002	–0.011	–0.003	–0.017	–0.016	–0.010	–0.005	–0.007	–0.004
Altimetric SSH at PCA	43.633	43.052	43.230	43.511	43.809	43.234	43.195	43.639	43.732	43.391
Error estimates (1σ)										
Orbital altitude	0.020	0.020	0.030	0.015	0.030	0.030	0.030	0.020	0.025	0.020
RA Noise at PCA	0.014	0.182	0.015	0.050	0.015	0.015	0.015	0.015	0.015	0.016
Sea Level	0.005	0.004	0.004	0.007	0.005	0.006	0.003	0.009	0.005	0.005
Ionosphere	0.015	0.004	0.008	0.020	0.015	0.004	0.002	0.002	0.004	0.004
Troposphere	0.010	0.020	0.040	0.010	0.020	0.010	0.010	0.010	0.020	0.020
Datation	0.001	0.001	0.001	0.001	0.001	0.001	0.001	0.001	0.001	0.001
Total σ	0.031	0.184	0.053	0.057	0.042	0.036	0.036	0.029	0.036	0.033
ERS–1 altimeter bias estimate										
From single pass	–0.434	–0.211	–0.325	–0.399	–0.423	–0.371	–0.431	–0.469	–0.445	–0.461
From multi pass	–0.420	–0.416	–0.410	–0.413	–0.418	–0.415	–0.417	–0.423	–0.421	–0.418
Difference	–0.014	0.205	0.105	0.014	–0.005	0.044	–0.016	–0.046	–0.024	–0.043
Fit: bias (m)	–0.415									
Fit: tilt (m/km)	–0.016									

TABLE 7–3 Summary of the calibration measurements and results for each of the passes used in the final analysis.

	12 Aug	15 Aug	18 Aug	21 Aug	27 Aug	30 Aug	2 Sep	5 Sep	11 Sep	17 Sep
Additional information										
Defl. of vertical (SN, arcsec)	–3.87									
Defl. of vertical (WE, arcsec)	–2.48									
Ground speed (km/s)	6.724	6.724	6.724	6.724	6.724	6.724	6.724	6.724	6.724	6.724
Orb. altitude rate at PCA (m/s)	12.462	12.375	12.364	12.357	12.530	12.513	12.500	12.488	12.539	12.520
Azimuth of track at PCA (°)	–14.816	–14.814	–14.815	–14.815	–14.814	–14.812	–14.813	–14.814	–14.811	–14.811
Geoid height wrt tower (m)	0.005	0.001	–0.005	–0.002	0.003	0.000	0.002	0.009	0.006	0.003

Figure 7–1 shows the estimated biases per pass (and their 1σ error bars) as a function of the distance of the PCA to the *Acqua Alta* tower as derived in Table 7–3. The slope of the full line represents the measured slope of the geoid around the tower (see Section 3.4, "The Local Geoid"); the error on this measurement was estimated as ±0.5 arcsec. The origin of the line is determined by the weighted average of the single-pass bias estimates.

The combined bias estimate from this weighted fit is –41.5 ±2.0 cm.

The uncertainty in this fit represents the combination of the non-static errors, which vary pass-to-pass. This must be combined with the estimated

FIGURE 7–1 Results of the bias determination, shown as a function of cross-track distance during the campaign. The fitted line has a slope of 1.6" as measured locally, and intercepts the polstion of the platform, at the zero line, at –41.5 cm.

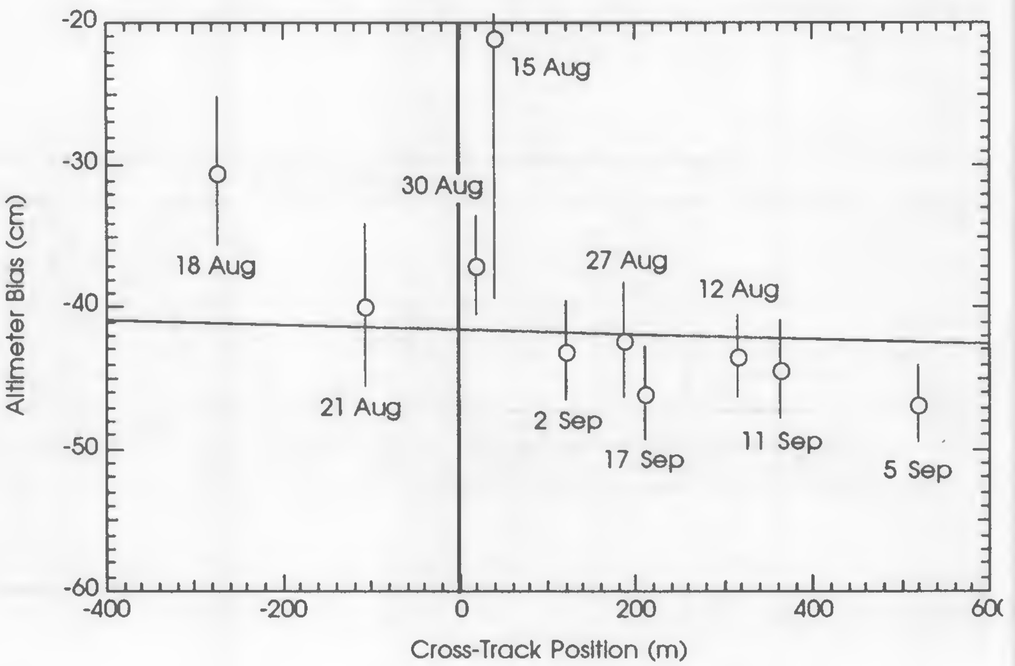

magnitude of the static errors, as derived in Section 7.1, "Error Estimation". The method used to combine these error estimates is Root Sum of Squares.

This results in a final bias estimation, and total uncertainty, of –41.5 ±5.2 cm.

References

Aldighieri, G., G. Biscontin, A. Tomasin and A. Vianello. Convegno di Studi Laguna, fiumi, lidi: cinque secoli di gestione delle acque nelle Venezie, *Atti del Convegno, Magistrato alle Acque*, Venice, Italy, 1983.

Allenby, R., Crustal Dynamics Project Site Selection Criteria. *NASA Technical Memorandum 85084*, August 1983

Astronomisches Rechen-Institut, Apparent places of fundamental stars 1990 Heildelberg: 1973 under auspices of the International Astronomical Union

Basili P., P. Ciotti and G. d'Auria, Improving accuracy in radar-altimetry data correction for tropospheric effects, *Electron. Lett.*, **25**, No. 7, 1989.

Bean B. R. and E. J. Dutton, *Radio Meteorology*, New York, Dover, 1968.

Benciolini, B. ITALGEO 90. *Atti del convegno annuale del Gruppo Nazionale della Terra Solida*, Consiglio Nazionale delle Ricerche, Roma Dicembre 1990.

Bierman, G.J. *Factorization Methods for discrete sequential estimation*, Academic Press, 1977

Blewitt, G., Carrier Phase Ambiguity Resolution for the Global Positioning System Applied to Geodetic Baselines up to 2000 km, *J. Geophys. Res.*, **94** (B8), 10,187-10,203, 1989

Brown, G. S., The Average Impulse Response of a Rough Surface and its Applications, *IEEE Trans. Ant. Prop.*,**AP-25**, 1, p 67, 1977.

Capannini E., Ciraolo L, Spalla P., Use of the VHF Signal of the SIRIO for Ionospheric Investigation. *URSI Symp. on Beacon Satellite Studies on the Earth Environment*, New Delhi, 7/11 Feb, (1983).

Capannini E., Spalla P., Atlante di Contenuto Elettronico Totale della Ionosfera a Medie Latitudini. Consiglio Nazionale delle Ricerche, Roma (1988).

Caporali, A., G.F. Dallaporta, F. Facchinelli and G. Zambon. Rete GPS nel Territorio Veneto. Monografie delle Stazioni di Misura, *TN 126 Consiglio Nazionale delle Ricerche,* Istituto per lo Studio della Dinamica delle Grandi Masse,Venezia, 1990.

Cavaleri, L. and S. Curiotto. A fast response shallow water tide gauge, *Il Nuovo Cimento*, Serie 1, **2C**, pp. 273- 287, 1979.

Cavazzoni, S. Variazioni Batimetriche e Idrografiche nella Laguna di Venezia Intercorse tra il 1933 e il 1971, *Rapporti e Studi della Commissionne di Studio dei Provvedimenti per la Conservazione e Difesa della Laguna e della Citta' di Venezia*, Istituto Veneto di Scienze, Lettere ed Arti, 18 pp., 1977.

Checcacci P.F., Capannini E., Spalla P., Ground Equipment for ATS 6, *Symp. of the Cospar Beacon Satellite Group on "The Geophysical use of satellite beacon observations"*, Boston (USA), Jun (1976).

Checcacci P.F., Capannini E., Spalla P., TEC Results of the ATS 6 Campaign on Italy, *Symp. of the Cospar on Beacon Satellite Measurement of Plasmaspheric and Ionospheric Properties*, Firenze, May 22/25, (1978).

Checcacci P.F., Capannini E., Spalla P., Results on the Operational Test of the IROE ATS 6 Measuring Equipment, *Symp. of the Cospar Beacon Satellite Group on Beacon Satellite Measurement of Plasmaspheric and Ionospheric Properties"*, Firenze, May 22/25, (1978).

Ciraolo L., Spalla P., Ionospheric Instrumentation: a new Approach. *International Beacon Satellite Symp. (IBSS'88) on the Investigation of the Ionosphere by means of Beacon Satellite Measurements*, Beijing (China), 18/21 Apr, (1988).

Ciraolo L., Spalla P., Software Receiver: progress and results. *International Beacon Satellite Symposium 1990*, Tucuman Argentina (1990).

Comune di Venezia, Centro Previsione e Segnalazione Maree. Registrazione ed elaborazione dei valori del livello di marea a Punta della Salute, diga Sud Lido, diga Sud Chioggia e piattaforma *"Acqua Alta"*, Rapporto Interno, 141 pp. 1989

Davies K., Recent Progress in Satellite Radio Beacon Studies with Particular Emphasis on the ATS-6 Radio Beacon Experiment. *Space Science Reviews*, 25, 357-430, 1980.

Davies, K. *Ionospheric Radio*, Peter Peregrinus Ltd., London, 1990

Decker M. T., E. R. Westwater and F. O. Guiraud, Experimental evaluation of ground-based microwave radiometric sensing of atmospheric temperature and water vapor profiles, *J. Appl. Meteor.*, **17**, No. 12, 1978.

Defant A. *Physical Oceanography*, Vol. II, Pergamon Press, London, 598 pp., 1960

Engelis, T., R.H. Rapp and Y. Bock, Measuring Orthometric Height Differences with GPS and Gravity Data, *Manuscripta Geodætica*, **10**, pp.187-194, 1985.

Forsberg, R., A New Covariance Model for Inertial Gravimetry and Gradiometry, *J. Geophys. Res.*, **92**, n.B2, pp.1305-1310, 1987.

Francis, C. R., and E. Attema. ERS-1 Calibration and Validation, *ESA Bulletin*, 80-86, 1991

Francis, C.R. and B. Duesmann, ERS-1 Altimeter Calibration, *ESA ER-TN-ESA-RA-0003*, Issue 3, 128 pp. July 1, 1988.

Francis, C.R., RA Data Chains, *ESA ER-IS-ESA-GS-0001* issue 2B, 12 July 1991.

Francis, C.R., ERS–1 Radar Altimeter Performance, *ESA ER-RP-ESA-RA-0258* issue 1.0, 1993 (in preparation).

Goldfinger A. D., Refraction of microwave signals by water vapor, *J. Geophys. Res.*, **85**, 1980.

Grafarend, E.W., Geodetic Applications of Stochastic Processes. *Phys. Earth Planet. Inter.*, 12, pp.151-179, 1976.

Gurtner, W., Das Geoid in der Schweiz, *Astronomish-geodetische Arbeiten in der Schweiz*, Band 32. Schweizerischen Geodaetischen Kommission, 103 pp., 1978.

Gurtner, W. Notes added to the ERS-1 GPS Calibration data, Bern, 1990

Gurtner, W., The GPS Campaign 1990. *Minutes of the Radar Altimeter Calibration Meeting*, Padova, 9-10 July 1991.

Gurtner, W., The GPS Campaigns 1990/1991, *ERS-1 Radar Altimeter Calibration Team Meeting*, Berne, 20 December 1991.

Heiskanen, W.A. and H. Moritz, *Physical Geodesy*, W.H. Freeman and Co., San Francisco and London, 1967.

Hogg D. C., F. O. Guiraud, J. B. Snider, M. T. Decker and E. R. Westwater, A Steerable Dual-Channel Microwave Radiometer for Measurements of Water Vapor and Liquid in the Troposphere, *J. Appl. Meteor.*, **22**, No. 5, May 1983.

Jordan, S.K., Self-consistent Statistical Models for the Gravity Anomaly, Vertical Deflections and Undulations of the Geoid, *J. Geophys. Res.*, **77**, n.20, pp.3660-3670, 1972.

Kasper, J.F., A Second-Order Markov Gravity Anomaly Model. *J. Geophys. Res.*, **76**, n.32, pp.7844-7849, 1971.

Kerr, D.A. Technical Operating Report for NAVSTAR Block II Satellite Vol. IV: Solar Force Model, *Rep. no. SSD81-0164-4*, Rockwell International, 1982

Kolenkiewicz, R., and C. F. Martin, SEASAT altimeter height calibration, *J. Geophys. Res.*, **87**, C5, 3189–3197, 1982.

Krough, F.T. Changing Stepsize in the Integration of Differential Equations using Modified Divided Differences, JPL Section 914, *Technical Memorandum no. 312*, 1973

Lanyi, G.E. Tropospheric delay effects in Radio Interferometry, *Telecommunications and Data Acquisition Prog. Rept. 42-78:152-159*, 1984

Lichten, S.M. Estimation and filtering for high precision GPS positioning application, *Man. Geod.*, 15, 159, 1990.

Liebe H. J., An updated model for millimeter wave propagation in moist air, *Radio Science*, **20**, No. 5, September-October 1985.

Liebe H. J.,*Int. Journal IR & MMW*, **10**, 1989.

Louet, J., ERS–1 Laser Retro-Reflector (LRR) Characterisation Data, *ESA ER-TN-ESA-LRR-0001* (18-Feb-91).

Marsh, J. G., et al., The GEM–T2 gravitational model, *NASA Tech. Memo. 100746*, Goddard Space Flight Center, October 1989.

Martin, C. F., and R. Kolenkiewicz, Calibration validation for the GEOS 3 Altimeter, *J. Geophys. Res.*, **86**, B7, 6369–6381, 1981.

Melbourne, W., R. Anderle, M. Feissel, R. King, D. McCarthy, D. Smith, B. Tapley, and B. Vincente. Project MERIT Standards, *United States Naval Observatory Circular no. 167*, U.S. Naval Observatory, Washington, D.C., 1983.

Muellerschoen, R.J. Down-dating SRIF arrays, *JPL IOM 314.5-1295*, 1988

Noomen, R. ERS90B SLR reference frame, private communication, Delft, 1991.

Rapp, R.H., Y.M.Wang and N. Pavlis, Geoid Undulation Differences between Geopotential Models. Paper presented at the Congress of the European Geophysisical Society, Wiesbaden 1991.

Rapp, R. H., Y. M. Wang, and N. K. Pavlis, The Ohio State 1991 geopotential and sea surface topography harmonic coefficient models, *Report No. 410*, Department of Geodetic Science and Surveying, The Ohio State University, Ohio, Columbus, August 1991.

Saastamoinen J.,Atmospheric Correction for the Troposphere and Stratosphere in Radio Ranging of Satellites, *Geophys. Monogr.*, **15**, AGU, Washington, D.C., 1972.

Scharroo, R., H. Leenman and K. F. Wakker, ERS–1 Altimeter Calibration Activites at DUT/SOM. First Progress Report, 2 November 1990.

Scharroo, R. and B. Overgaauw, ERS-1 Radar Altimeter Calibration Readiness at DUT/SOM. *Minutes of the Radar Altimeter Calibration Meeting*, Padova, 9-10 July 1991.

Scharroo, R. K. F. Wakker, B. Overgaauw and B. A. C. Ambrosius, Some Aspects of the ERS-1 Radar Altimeter Calibration, *Proc. 42nd IAF*, Montreal, 1991

Shaw, L., I. Paul, and P. Henrikson, Statistical Models for the Vertical Deflection from Gravity-Anomaly Models. *J. Geophys. Res.*, **74**, n.17, 1969.

Slobin, S. D., Microwave noise temperature and attenuation of clouds: statis tics of these effects at various sites in the U.S. Alaska and Hawaii, *Radio Sci.*, **17**, 1982.

Sovers, O.J., and J.S. Border. Observation Model and Parameter Partials for the JPL Geodetic Modeling software 'GPSOMC', *JPL publication 87-21*, Rev. 2, 1990.

Spilker, J.J. GPS signal structures and Performance Characteristics, *Navigation*, **25**:121-146, reprinted in GPS, 1980, Institute of Navigation, Vol. 1:29-54, Washington, D.C., 1978.

Titheridge J.,E.: Determination of Ionospheric Electron Content from Faraday Rotation of geostationary satellite signals. *Planet Space Science*, 20, 353, 1972.

Titheridge J.,E., The slab thickness of the midlatitude ionosphere. *Planet Space Science*, 21, 1775,1973.

Vanicek P., and E. Krakiwsky, *Geodesy. The concepts*, Second Edition, Elsevier Science Publications B.V. 1986.

Vermaat, E., Site Selection for MTLRS. *Release 84.2.1 Reports of the Department of Geodesy* - Mathematical and Physical Geodesy, 1984

Weber. G. and A. Caporali, Combined Regional Geoid Determination for the ERS-1 Radar Altimeter Calibration at Venice. *Minutes of the Radar Altimeter Calibration Meeting*, Padova, 9-10 July 1991.

Wakker, K. F., R. Scharroo and B. A. C. Ambrosius, Some Results of the ERS-1 Radar Altimeter Calibration, *Proc. ESA Symposium on Spacecraft Flight Dynamics*, Darmstadt, *ESA SP-326*, 1991

Wu, S. C., Optimum frequencies of a passive microwave radiometer for tropospheric path-length correction, *IEEE Trans. Antennas and Propagat.*,27, No. 2, 1979.

Zhu and Reigber, Ch., ERS–1 standards used at D-PAF, *D-PAF ERS-D-STD-31101* (25-Jan-91).

GPS Bulletin Vol. 3, No. 3, International Coordination of Space Techniques for Geodesy and Geodynamics, Commission VIII, GPS subcommission, Department of Commerce, Rockville, 1990

ANNEX A

Network Adjustment

This Annex contains many of the background tables related to CHAPTER 3, "The Three-Dimensional Network".

The individual stations of the network, and their UTM coordinates are given in Table A–1.

TABLE A–1 UTM coordinates of the vertices of the local geodetic network

Station	East (km)	North (km)
ADRIA	269.6494571	4992.6169106
AGIP	244.1233755	4985.0554032
BAIAMONTE	240.8250882	5024.0250833
BASSANO	246.5666490	5074.1706231
BELLIERA	268.9622258	4984.8958141
BORGOMOIA	249.3138062	4985.4363986
BOTTRIGHE	270.6759175	4989.7813132
BRONDOLO	286.1975213	5007.0880752
BURANO	298.0371314	5040.3590171
CA VENDRAMIN	287.0177967	4980.9287675
EKAR	233.6010825	5083.0467250
EKAR0691	233.5945203	5082.9280927
ESTE	237.5539169	5014.0177888
FAROROCCHETTA	289.2891272	5024.1653551
FASTRO	245.5785292	5095.8858187
FELETTO	287.0155239	5087.9215975
FLORIANO	290.7735203	5100.4516455

TABLE A–1

UTM coordinates of the vertices of the local geodetic network

Station	East (km)	North (km)
FUSINA	285.5863020	5033.0904212
ISTRANA	273.8074496	5062.4494396
MARCHESI	284.2155825	5047.2341516
MARIAMARE	289.7977104	5023.4295113
MONTEGROTTO	247.1653894	5024.2668055
MOTTEVOLPEGO	285.6509330	5030.1262136
MURANO	292.3928811	5037.2854320
NAGLIATI	249.3423677	4983.3221309
PAPOZZE	265.5595172	4985.5758561
PAPOZZ90	265.5580089	4985.5757021
PENNAR	230.4771558	5084.9842249
POVEGLIA	291.1633344	5028.6974089
PTF_88	304.6958648	5020.8767864
PTF0390	304.6957973	5020.8768194
ROSARA	272.4750924	5019.2142546
SACCASESSOLA	290.5324536	5031.7043787
SALUTE	291.6960149	5034.2727925
SANGIORGIO	288.3839370	5033.7451376
SANMARCO	291.9303642	5034.5185784
SANNICOLO	295.2621928	5034.1516367
SPRESIANO	286.9480821	5073.3796303
STRA	265.6986864	5033.0384242
TESSERA	291.2545476	5040.9940093
TREPALADE	297.8919356	5048.7459753
TREPORTI	300.4482560	5038.4705999
TREVISO	285.8706039	5061.0707882
VENDA	240.6854127	5023.3707845
VILLANOVA	261.4352056	4986.0421615

Table A–2 summarizes the surveyed baselines and polygons which were used in the adjustment of the network. The data and rms entries in this table represent the numbers and rms post-fit residuals, respectively, of the double differences processed.

TABLE A–2

Summary of the measured baselines and polygons used in the adjustment.

Baseline#	Date	# data	rms (m)	Surveyed Baseline or Network
1	02/06/87	484	0.0048	BORGOMOIA, NAGLIATI, AGIP
2	04/06/87	222	0.0034	BELLIERA, PAPOZZE
3	05/06/87	194	0.0055	BELLIERA, BOTTRIGHE
4	25/04/87 26/04/87	863	0.0039	NAGLIATI, BORGOMOIA, AGIP
5	03/06/87	416	0.0046	VILLANOVA, PAPOZZE, BORGO-MOIA
6	29/11/88	1226	0.0129	FELETTO, FLORIANO, SPRESIANO
7	26/11/88	745	0.0048	ADRIA, BRONDOLO, CA VEN-DRAMIN
8	26/11/88	715	0.0058	BRONDOLO, ADRIA,CA VEN-DRAMIN
9	25/11/88	1446	0.0055	ADRIA, BRONDOLO, ROSARA
10	24/11/88	1508	0.0073	ADRIA, MONTEGROTTO, ROSARA
11	23/11/88	1413	0.0091	STRA, ROSARA, MONTEGROTTO
12	19/11/88	835	0.0070	BRONDOLO, MARIAMARE, ROSARA
13	16/11/88	1257	0.0105	SANMARCO, MARCHESI, TRE-VISO
14	17/11/88	1165	0.0092	STRA, MARCHESI, MARIAMARE
15	14/11/88	1399	0.0167	SANMARCO, SALUTE, PTF_88
16	18/11/88	1134	0.0086	ROSARA, STRA, MARIAMARE
17	12/11/88	960	0.0050	SALUTE, MURANO, BURANO, TESSERA
18	11/11/88	1165	0.0067	SALUTE, SANNICOLO, TREPORTI,
19	10/11/88	1278	0.0079	SALUTE, FAROROCCHETTA, POV-EGLIA,SANNICOLO
20	04/11/88	414	0.0049	SALUTE, TESSERA
21	05/11/88	963	0.0063	SALUTE, SANGIORGIO, FUSINA,-SACCASESSOLA
22	14/06/88	459	0.0124	PTF_88, BRONDOLO
23	15/06/88	472	0.0059	PTF_88, SANMARCO, MARIA-MARE
24	16/06/88	511	0.0109	PTF_88, TREPALADE
25	27/06/88	486	0.0062	TREVISO, SPRESIANO, ISTRANA
26	20/06/88	195	0.0093	SANMARCO, TREPALADE
27	22/06/88	357	0.0081	MARCHESI, SANMARCO, MARIA-MARE

TABLE A–2

Summary of the measured baselines and polygons used in the adjustment.

Baseline#	Date	# data	rms (m)	Surveyed Baseline or Network
28	17/06/88	558	0.0078	MARIAMARE, BRONDOLO
29	25/06/88	307	0.0161	SALUTE, SANMARCO, POVEGLIA
30	23/06/88	179	0.0190	MARCHESI, TREVISO
31	24/06/88	436	0.0102	TREPALADE, TREVISO, MARCHESI
32	18/06/88	652	0.0083	SANMARCO, MARIAMARE
33	22/11/88	761	0.0100	MARCHESI, ISTRANA, STRA
34	22/11/88	576	0.0089	STRA, ISTRANA, MARCHESI
35	14/11/88	564	0.0052	SALUTE, SANMARCO, PTF_88
36	14/11/88	828	0.0131	SANMARCO, SALUTE, PTF_88
37	09/11/88	589	0.0138	SALUTE, MOTTEVOLPEGO,SAC-CASESSOLA
38	09/11/88	642	0.0091	MOTTEVOLPEGO, SALUTE, POV-EGLIA
39	28/02/88	599	0.0071	SALUTE, PTF_88
40	15/03/90	998	0.0060	FASTRO, PENNAR, EKAR
41	12/03/90	1662	0.0173	ISTRANA, BASSANO, FELETTO
42	16/03/90	1442	0.0092	FELETTO, PENNAR, EKAR, FAS-TRO
43	17/03/90	1455	0.0172	FELETTO, EKAR, PENNAR, BAS-SANO
44	13/03/90	2651	0.0080	MARIAMARE, VENDA, PTF0390
45	18/03/90	1277	0.0140	STRA, VENDA, MONTEGROTTO, BASSANO
46	19/03/90	1741	0.0069	BORGOMOIA, MONTEGROTTO, VENDA, ADRIA, PAPOZZE90
47	14/03/90	2644	0.0151	MARIAMARE, CA VENDRAMIN, PTF0390
48	15/04/91	1484	0.0070	BAIAMONTE, VENDA
49	16/04/91	1132	0.0093	BAIAMONTE, VENDA
50	31/05/91	1837	0.1901	MONTEGROTTO, EKAR, BAIA-MONTE
51	04/06/91	498	0.0068	ESTE, EKAR0691

The cartesian coordinates of the free stations, after the adjustment, are listed in Table A-3.

TABLE A-3 Adjusted cartesian coordinates, in meters

	X-COORDINATE	Y-COORDINATE	Z-COORDINATE
ADRIA	4413863.5291	944221.1885	4491271.8804
AGIP	4424970.3000	920798.1943	4485246.4659
BAIAMONTE	4399363.6005	910506.4737	4512940.8640
BASSANO	4363208.9986	906770.2705	4547937.0779
BELLIERA	4419304.7341	944968.1417	4485804.4020
BORGO	4423512.8573	925774.6879	4485665.4080
BOTTRIGHE	4415565.4617	945738.7624	4489299.5085
BRONDOLO	4400066.6563	957642.4140	4501882.0936
BURANO	4374400.1663	963014.2913	4525529.3479
CA VENDRAMIN	4417770.8610	963234.7373	4483441.4012
EKAR	4360893.8669	892690.4754	4554619.0318
EKAR0691	4360979.5790	892706.5339	4554538.3277
ESTE	4406672.6576	909101.9432	4505485.9005
FAROROC-CHETTA	4387615.8343	957504.6041	4513967.6587
FASTRO	4348521.7329	901804.1966	4563164.2168
FELETTO	4344262.7196	943528.5505	4558623.8811
FLORIANO	4334633.7843	944838.2443	4567379.3115
FUSINA	4382351.4949	952263.2667	4520144.6410
ISTRANA	4364896.7139	935400.1065	4540424.7639
MARCHESI	4372932.1068	948321.1792	4530023.5993
MARIAMARE	4388000.6842	958133.9256	4513461.9424
MONTEGROTTO	4397410.0374	916558.6689	4512960.0735
MOTTEVOLPEGO	4384375.8793	952872.5647	4518066.5284
MURANO	4377855.0301	958100.2986	4523246.3422
NAGLIA	4424943.3410	926187.9175	4484165.1631
PAPOZZ90	4419633.5351	941535.3191	4486194.7127
PAPOZZE	4419633.0759	941536.7562	4486194.8588
PENNAR	4360048.5775	889247.6914	4555640.1869
POVEGLIA	4384056.8446	958489.9850	4517193.8546
PTF0390	4386229.6730	973073.3740	4512012.4780[1]
PTF_88	4386230.9477	973073.7269	4512013.7696
ROSARA	4394975.3452	942082.7984	4510079.4948
SACCASESSOLA	4382137.3361	957322.9520	4519289.3098
SALUTE	4380093.4828	957979.1553	4521117.0486

TABLE A–3

Adjusted cartesian coordinates, in meters

	X-COORDINATE	Y-COORDINATE	Z-COORDINATE
SANGIORGIO	4381240.6933	954859.8956	4520670.5358
SANMARCO	4379868.5320	958161.3518	4521294.5396
SANNICOLO	4379332.7978	961464.9357	4521114.4720
SPRESIANO	4354251.0722	946140.7219	4548384.0608
STRA	4387061.6983	932953.0089	4519615.2654
TESSERA	4375569.4525	956310.1617	4525818.7170
TREPALADE	4368650.6610	961323.5320	4531397.3394
TREPORTI	4375128.8088	965704.2595	4524260.0430
TREVISO	4362993.4957	947369.9893	4539742.0797
VENDA	4399894.0810	910501.2150	4512527.5090[2]
VILLANOVA	4420279.0247	937444.0319	4486418.6977

1. ETRF89 coordinates held fixed
2. ETRF89 coordinates held fixed

The cartesian coordinates were projected onto the WGS84 ellipsoid and converted to geodetic coordinates, in order to be used as reference for the astronomic latitudes and longitudes, and for the levelled heights. The geodetic coordinates are listed in Table A–4.

TABLE A–4

Adjusted geodetic coordinates on WGS84 (a = 6378137. m; 1/f = 298.257)

	North Latitude		East Longitude		Ellipsoid Height
	dd	mm ss.ssssss	dd	mm ss.ssssss	m
ADRIA	N45	02 58.341338E	12	04 29.333079	45.5820
AGIP	N44	58 22.165466E	11	45 18.008173	48.3057
BAIAMONTE	N45	19 18.623610E	11	41 34.916459	523.2840
BASSANO	N45	46 28.465168E	11	44 24.722122	181.8070
BELLIERA	N44	58 47.647479E	12	04 10.719803	50.3918
BORGOMOIA	N44	58 41.154910E	11	49 13.925387	54.3257
BOTTRIGHE	N45	01 27.766439E	12	05 20.855669	50.5002
BRONDOLO	N45	11 05.443542E	12	16 42.698122	44.2532
BURANO	N45	29 15.062249E	12	24 55.771668	45.8150
CA_VENDRAMIN	N44	56 59.550667E	12	18 00.219161	47.5936
EKAR	N45	50 58.000744E	11	34 07.770753	1410.2413
EKAR0691	N45	50 54.154581E	11	34 07.703246	1413.0690
ESTE	N45	13 50.511926E	11	39 23.959709	63.3693
FAROROCCHETTA	N45	20 21.581611E	12	18 38.128097	45.6763

TABLE A–4 Adjusted geodetic coordinates on WGS84 (a = 6378137. m; 1/f = 298.257)

	North Latitude		East Longitude		Ellipsoid Height
	dd	mm ss.ssssss	dd	mm ss.ssssss	m
FASTRO	N45	58 09.619891E	11	42 57.697766	396.0628
FELETTO	N45	54 42.674540E	12	15 13.450729	261.2752
FLORIANO	N46	01 32.367865E	12	17 47.972842	210.0355
FUSINA	N45	25 06.425876E	12	15 34.226171	45.8184
ISTRANA	N45	40 43.197870E	12	05 44.066569	82.9563
MARCHESI	N45	32 42.691673E	12	14 08.850736	49.5043
MARIAMARE	N45	19 58.312127E	12	19 02.596531	44.6403
MONTEGROTTO	N45	19 34.769118E	11	46 25.241273	57.4433
MOTTEVOLPEGO	N45	23 30.553055E	12	15 41.836690	45.7415
MURANO	N45	27 29.609064E	12	20 40.700716	45.8051
NAGLIATI	N44	57 32.779463E	11	49 19.009719	44.5605
PAPOZZ90	N44	59 05.635090E	12	01 34.351382	46.9240
PAPOZZE	N44	59 05.641865E	12	01 34.419907	46.9214
PENNAR	N45	51 56.292201E	11	31 39.284999	1086.2498
POVEGLIA	N45	22 50.301001E	12	19 57.255471	45.8603
PTF0390	N45	18 51.172292E	12	30 30.015202	55.7251
PTF_88	N45	18 51.171293E	12	30 30.018344	57.5722
ROSARA	N45	17 22.438837E	12	05 54.692969	47.0119
SACCASESSOLA	N45	24 26.956267E	12	19 23.680805	45.9041
SALUTE	N45	25 51.345033E	12	20 13.240734	44.5717
SANGIORGIO	N45	25 30.685147E	12	17 41.795225	46.1345
SANMARCO	N45	25 59.552213E	12	20 23.640464	44.1269
SANNICOLO	N45	25 51.215448E	12	22 57.374295	44.8958
SPRESIANO	N45	46 51.949922E	12	15 33.481501	99.8633
STRA	N45	24 41.782385E	12	00 20.434030	52.3943
TESSERA	N45	29 28.430594E	12	19 42.668812	45.8660
TREPALADE	N45	33 46.403772E	12	24 36.631720	44.4325
TREPORTI	N45	28 16.427823E	12	26 49.500982	45.7456
TREVISO	N45	40 12.370133E	12	15 03.216369	58.2891
VENDA	N45	18 57.270672E	11	41 29.744544	593.8993
VILLANOVA	N44	59 15.787607E	11	58 25.551695	50.2033

Table A–5 gives the error ellipses for the network after the adjustment. In this table the sites marked with "N" were not used in the geoid computation, because of lack of levelled height or because judged bad. The expected correlation between the size of the error ellipse and the number of baselines to the given point may be noted in Figure 3–1 on page 48. The sites marked with "V" were used as vertical deflection points.

TABLE A–5

Error ellipses (2 σ) of the adjustment

Identification	Semi-major axis	Semi-minor axis	Azimuth of major axis	Vertical	Notes
	metres	metres	degrees	metres	
ADRIA	0.0525	0.0444	49.59	0.0827	
AGIP	0.0775	0.0584	38.97	0.1039	
BAIAMONTE	0.0118	0.0086	175.10	0.0224	N[1]
BASSANO	0.0691	0.0641	109.66	0.1155	
BELLIERA	0.0981	0.0748	19.65	0.1327	
BORGOMOIA	0.0758	0.0555	36.48	0.1002	
BOTTRIGHE	0.1155	0.0781	12.23	0.1543	
BRONDOLO	0.0514	0.0430	74.57	0.0781	
BURANO	0.1196	0.0924	114.52	0.2043	N
CA VENDRAMIN	0.0654	0.0404	48.68	0.0755	
EKAR	0.1714	0.0928	49.50	0.1655	N
EKAR0691	1.1207	0.3187	159.47	1.8306	V[2]
ESTE	1.5881	1.0192	99.91	1.8810	V
FAROROCCHETTA	0.1349	0.1053	115.09	0.2322	N
FASTRO	0.1706	0.0909	50.11	0.1602	
FELETTO	0.0853	0.0817	69.88	0.1414	
FLORIANO	0.2720	0.1762	58.22	0.3600	
FUSINA	0.1698	0.0995	108.30	0.2202	N
ISTRANA	0.1296	0.0769	40.07	0.1441	
MARCHESI	0.0602	0.0582	20.32	0.1116	
MARIAMARE	0.0115	0.0086	12.54	0.0205	
MONTEGROTTO	0.0659	0.0556	32.23	0.1081	
MOTTEVOLPEGO	0.1759	0.1419	135.81	0.2913	N
MURANO	0.1189	0.1069	144.92	0.2284	N
NAGLIATI	0.0767	0.0565	36.22	0.1024	
PAPOZZ90	0.0779	0.0581	36.80	0.1048	
PAPOZZE	0.0971	0.0706	18.77	0.1288	
PENNAR	0.1861	0.1203	45.02	0.1853	N
POVEGLIA	0.1374	0.1176	142.72	0.2526	N
PTF_88	0.0779	0.0631	134.21	0.1438	V
ROSARA	0.0482	0.0451	35.32	0.0867	
SACCASESSOLA	0.2518	0.2014	2.84	0.4415	N
SALUTE	0.0946	0.0742	127.64	0.1739	

TABLE A–5

Error ellipses (2 σ) of the adjustment

Identification	Semi-major axis	Semi-minor axis	Azimuth of major axis	Vertical	Notes
	metres	metres	degrees	metres	
SANGIORGIO	0.2587	0.1310	152.29	0.5538	N
SANMARCO	0.0680	0.0590	147.89	0.1318	
SANNICOL	0.1523	0.1234	117.29	0.2393	N
SPRESIANO	0.1318	0.1130	41.33	0.2244	
STRA	0.0419	0.0357	167.11	0.0743	
TESSERA	0.1166	0.0912	124.93	0.2058	N
TREPALADE	0.1584	0.1025	171.94	0.2797	
TREPORTI	0.1499	0.1032	108.83	0.2212	N
TREVISO	0.1650	0.1196	22.50	0.2292	
VILLANOVA	0.0798	0.0635	45.34	0.1109	

1. N means "Not used in the geoid computation"
2. V means "Vertical deflection point"

ANNEX B

The "Large" GPS Campaign

This Annex contains many of the details from CHAPTER 3, "The Three-Dimensional Network".

B.1 The 1990 Campaign

Table B–1 presents the local survey information between the fixed SLR marker and the GPS marker at the various SLR sites, and the eccentricity vector between the SLR marker and the GPS marker at Monte Venda. This local tie has been provided by A. Caporali using a WM- 102 baseline (mean of 3 sessions). The local survey between the WM-102 GPS markers and the Trimble GPS markers at Monte Venda and the Venice Tower are also presented in Table B–1.

Table B–2 presents the antenna heights of the GPS antennas at the various sites. A zero height indicates that the antenna has been fixed directly at the marker.

Table B–3 presents the phase centre offsets (*Gurtner*, 1990). The phase centre offset is defined as the vector from antenna base to the antenna phase centre. The fictitious phase centre offset, Lc, indicates the ionosphere-free linear combination of the two frequency-dependent phase centre offsets L1 and L2, defined as (*Blewitt*, 1989):

$$Lc = 2.5457 \cdot L1 - 1.5457 \cdot L2 \qquad \text{(EQ B–1)}$$

The Wettzell GPS marker 1100 has been defined by the Institut für Angewandte Geodsie (IfAG) to be the L1 phase centre.

TABLE B–1 Local Ties 1990

GPS Monument	Reference Monument	*dN* (m)	*dE* (m)	*dh* (m)
GRASSE M001	GRASSE 7835	-29.517	-21.559	-4.819
GRASSE M004	GRASSE 7835	-2.666	-24.990	-4.206
GRAZ	GRAZ 7839	-0.759	8.864	0.806
KOSG 24	KOOTWIJK 8833	38.496	-1.020	2.266
MATERA 7541	MATERA 7939	-33.624	-33.719	-7.450
WETTZELL 1100	WETTZELL 7834	-43.084	38.263	-1.235
ZIMMERWALD GPS87	ZIMMERWALD 7810	-9.442	-9.063	3.212
MONTE VENDA TR90	MONTE VENDA WM90	3.24	-3.22	-0.125
VENICE TOWER TR90	VENICE TOWER WM90	1.332	1.381	1.825
		dx (m)	*dy* (m)	*dz* (m)
MONTE VENDA WM90	MONTE VENDA 7542	530.485	-5.259	-413.353

TABLE B–2 Antenna Heights 1990

Station Name	Receiver	Antenna	*h* (m)
ZIMMERWALD GPS87	WM-102	WM-102	0.000
GRASSE M001	WM-102	WM-102	1.332
GRASSE M004	WM-102	WM-102	1.199
MATERA 7541	WM-102	WM-102	1.578
GRAZ GPS	WM-102	WM-102	0.000
KOSG 24	ROGUE / SNR 8	DMC 14	0.000
WETTZELL 1100	MIMIMAC 2816AT	MINIMAC L1 CNTR	0.000
VENICE TOWER TR90	TRIMBLE 4000SST	TRIMBLE SST	0.000
VENICE TOWER WM90	WM-102	WM-102	1.893
MONTE VENDA TR90	TRIMBLE 4000SST	TRIMBLE SST	0.160
MONTE VENDA WM90	WM-102	WM-102	
Day 287			1.296
288			1.373
289			1.335
290			1.240
291			1.242

B.1.1 Data Preprocessing

The raw data files have been converted into the exchange format RINEX

TABLE B–3 Phase Centre Heights 1990

Receiver	Antenna	L1 (m)	L2 (m)	Lc (m)
WM-102	WM-102	0.066	0.066	0.066
MINIMAC 2816AT	MINIMAC L1 CNTR	0.000	-0.015	0.023
TRIMBLE 4000 SST	TRIMBLE SST	0.069	0.068	0.071

files by different groups:

Station	Group	Program
GRASSE	EPFL Lausanne	W2RINEXO
GRAZ	ETH Zürich, AUIB	W2RINEXO
KOOTWIJK	Kootwijk Observatory	RGRINEXO
MATERA	Telespazio, Matera	W2RINEXO
MONTE VENDA	Telespazio, Matera	W2RINEXO
ACQUA ALTA	Telespazio, Matera	W2RINEXO
WETTZELL	IfAG (→NGS format)	ARGO
	AUIB (→RINEX)	NGSRXO
ZIMMERWALD	EPFL Lausanne	W2RINEXO

ARGO is a program provided by the US National Geodetic Survey (NGS) to reformat raw data file into the NGS exchange format still used by the international GPS tracking network CIGNET. The other programs have been developed at AIUB to directly reformat raw data files into RINEX or to transform NGS files into RINEX files.

The WM-102 data first had to be run through the data transfer part of the WM program system *PoPS*. As *PoPS* can only handle a maximum of 500 epochs at a time, most of the data had to be split into two or three files. In order to facilitate the subsequent processing step, we concatenated such multiple (RINEX) files into one file per session, as soon as they had been sent to AIUB.

All the (concatenated) daily RINEX observation and navigation message files have been redistributed to other groups, as well.

B.2 The 1991 Campaign

Table B–4 contains the local tie information from the 1991 campaign, Table B–5 contains the instrument types and the heights of the antenna above the markers and Table B–6 the antenna phase centre offsets.

TABLE B–4 Local Ties 1991

GPS Monument	Reference Monument	*dN* (m)	*dE* (m)	*dH* (m)
GRASSE M004	GRASSE 7835	-2.666	-24.990	-4.206
GRAZ ASHTECH	GRAZ 7839	2.606	9.768	0.784
KOSG ROGUE	KOOTWIJK 8833	26.910	-36.049	8.257
WETTZELL 7597	WETTZELL 7834	-106.825	27.948	-0.820
ZIMMERWALD LT88	ZIMMERWALD 7810	-14.737	4.183	5.250
MONTE VENDA P	MONTE VENDA 7542	14.876	-12.403	2.559
VENICE TOWER GPS	VENICE TOWER WM	5.191	-8.921	1.286

TABLE B–5 Antenna Heights 1991

Station Name	Receiver	Antenna	*h* (m)
GRAZ ASHTECH	L-XII	MICROSTRIP	0.000
KOSG ROGUE	ROGUE / SNR 8	DMC 14	0.105
WETTZELL 7597	L-XII	MICROSTRIP	1.663
after 16:00 UT	on day 246		1.535
ZIMMERWALD LT88	LM-XII	MICROSTRIP	0.000
MONTE VENDA P	LM-XII	MICROSTRIP	0.040
VENICE TOWER GPS	LM-XII	MICROSTRIP	0.000
GRASSE M004	L-XII	MICROSTRIP	1.547

TABLE B–6 Phase Centre Heights 1991

Receiver	Antenna	L1 m	L2 m
ROGUE / SNR 8	DMC 14	0.059	0.083
LM-XII	MICROSTRIP	0.064	0.064
L-XII	MICROSTRIP	0.064	0.064

B.3 DUT Results, 1990

Table B–7 summarizes the daily and mean delta estimates, with 1σ formal errors, and the weighted RMS about the mean (repeatability), of the baseline components of the baseline Monte Venda (WM90)—*Acqua Alta* (WM90).

This weighted rms about the mean is defined as:

$$\text{rms} = \sqrt{\left(\frac{N}{N-1}\right)\frac{\sum_{i=1}^{N}\frac{(R_i - \langle R\rangle)^2}{\sigma_i^2}}{\sum_{i=1}^{N}\frac{1}{\sigma_i^2}}}$$

where N is the number of samples, R_i and σ_i are the estimate and formal error of the baseline component on the ith day, and $\langle R \rangle$ is the weighted mean.

TABLE B–7

Daily and mean delta estimates with 1σ formal errors, and the weighted rms about mean (repeatability) of the baseline components of the baseline Monte Venda (WM90)—Venice (WM90), when all fixed SLR marker coordinates were held fixed in the ERS90B reference frame.

Days	*dE* (cm)	*dN* (cm)	*dV* (cm)	*dL* (cm)
Oct 14	-913.802	434.674	-1487.337	-893.221
	2.380	0.680	3.260	2.370
Oct 15	-911.028	430.106	-1474.489	-890.626
	1.820	0.760	2.720	1.810
Oct 16	-915.000	433.627	-1481.849	-894.494
	1.390	0.530	2.410	1.390
Oct 17	-915.878	436.032	-1483.108	-895.350
	1.330	0.480	2.250	1.330
Oct 18	-911.307	432.249	-1483.914	-890.776
	1.440	0.470	2.540	1.450
mean ($\langle R \rangle$)	-913.681	433.650	-1481.969	-893.176
($\sigma\langle R \rangle$)	1.534	0.544	2.556	1.536
rms	2.277	2.099	4.293	2.254

Table B–8 presents these final marker coordinates of Monte Venda (WM90, TR90 and 7542), and *Acqua Alta* (WM90 and TR90), and also presents the 1σ formal errors based on the multi-day arc solution. They are determined in the ERS90B reference frame. The coordinates of the Monte Venda SLR site (7542) have been derived from the WM site (WM90) by adding the local ties.

TABLE B–8

Marker coordinates and 1σ formal errors of Monte Venda (WM90, TR90 and 7542), and *Acqua Alta* (WM90 and TR90) after combining the single-day arc solutions into a multi-day arc solution. The coordinates are computed in the ERS90B reference frame, whereas the height of the markers is with respect to the WGS84 ellipsoid.

Station	*x* (m)	*y* (m)	*z* (m)	*h* (m)
Monte Venda	4399894.067	910501.109	4512527.447	593.830
(WM90)	0.007	0.006	0.006	0.007
Monte Venda	4399363.582	910506.368	4512940.800	523.210
(7542)	0.007	0.006	0.006	0.007
Monte Venda	4399892.378	910497.421	4512529.581	593.659
(TR90)	0.009	0.006	0.008	0.008
Venice	4386229.670	973073.271	4512012.435	55.677
(WM90)	0.007	0.006	0.005	0.006
Venice	4386229.635	973074.668	4512014.584	57.393
(TR90)	0.010	0.007	0.008	0.009

B.4 AUIB Results 1990

B.4.1 Daily Repeatability

As a first check of the data quality daily free solutions are compared, solving for the coordinates of all sites but one, one orbit parameter per satellite, and one zenith delay per station, per day. Table B–9 shows a seven parameter transformation between the solutions of two consecutive days.

TABLE B–9

Helmert Transformation Between Days 289 and 290 Including Zenith Delay

Num	Name	Residuals in metres		
835	GRASSE 7835	-0.011	0.020	-0.037
839	GRAZ 7839	0.022	-0.021	-0.010
939	MATERA 7939	-0.006	0.003	0.037
810	ZIMMERWALD 7810	-0.002	0.000	0.082
7	VENICE TOWER WM90	-0.001	-0.005	-0.010
8	MONTE VENDA WM90	-0.002	0.004	-0.063

The daily solutions were also compared with given SLR/VLBI coordinates, *eg* the ETRF-89 coordinates, as shown in Table B–10.

The next test examines the daily repeatability of the baseline Monte Venda - *Acqua Alta*, now keeping all SLR sites constrained to their ETRF-89 coordinates, solving for 3 orbit parameters per satellite (U_0, node, inclination) and a zenith delay for all sites but one. Table B–11 shows the daily variations of the heights at Monte Venda and *Acqua Alta* (differences to average value).

TABLE B–10 Helmert Transformation Between Day 290 and ETRF-89 Including Zenith Delay

Num	Name	Residuals in metres		
835	GRASSE 7835	0.016	-0.043	0.069
839	GRAZ 7839	-0.005	0.023	0.056
939	MATERA 7939	-0.082	0.003	-0.037
834	WETTZELL 7834	0.073	0.090	-0.005
810	ZIMMERWALD 7810	-0.003	-0.073	-0.083

TABLE B–11 Daily height variations (m)

Day	Monte Venda (WM)	*Acqua Alta* (WM)	*Acqua Alta* (TR)
287	-0.035	-0.034	
288	-0.011	-0.026	-0.019
289	-0.022	-0.015	-0.037
290	0.059	0.060	0.057
291	0.009	0.015	

Although there are quite large variations in the heights of the sites, the end points of the baseline show the same behaviour, *ie* the height difference between Monte Venda and Venice Tower turn out to be rather constant, as shown in Table B–12.

TABLE B–12 Daily Variations of the Baseline Height Difference and Length (m)

Day	WM-102	Baseline	Trimble	Baseline
	D(HGT)	D(LGT)	D(HGT)	D(LGT)
287	-0.001	0.014		
288	0.015	-0.011	0.000	0.003
289	-0.006	-0.004	-0.007	-0.003
290	-0.002	-0.012	0.006	0.000
291	-0.006	0.013		

B.4.2 AUIB 1990 Solution

The AUIB 1990 solution is given in Table B–13, in the ETRF-89 reference frame.

The solution given in Table B–14 has been performed using SLR fixed coordinates provided by DUT (Solution ERS90B).

TABLE B–13 Final AIUB GPS Coordinates (1990, ETRF-89)

Station	*x* (m)	*y* (m)	*z* (m)	*h* (m)
MONTE VENDA WM90	4399894.081	910501.215	4512527.509	593.898
MONTE VENDA TR90	4399892.391	910497.577	4512529.698	593.773
MONTE VENDA 7542	4399363.596	910506.474	4512940.862	523.279
ACQUA ALTA WM90	4386229.673	973073.374	4512012.478	55.724
ACQUA ALTA TR90	4386229.670	973074.844	4512014.725	57.544

TABLE B–14 Final AIUB GPS Coordinates (1990, ERS90B)

Station	*x* (m)	*y* (m)	*z* (m)	*h* (m)
MONTE VENDA WM90	4399894.012	910501.132	4512527.462	593.806
MONTE VENDA 7542	4399363.527	910506.391	4512940.815	523.186
ACQUA ALTA WM90	4386229.603	973073.288	4512012.437	55.634

B.4.3 AUIB 1991 Solution

The AUIB 1991 solution is given in Table B–15 and Table B–16 in the ERTF-89 and ERS90B reference frames respectively.

TABLE B–15 Final AIUB GPS Coordinates (1991, ETRF-89)

Station	*x* (m)	*y* (m)	*z* (m)	*h* (m)
MONTE VENDA 7542	4399363.599	910506.492	4512940.823	523.256
ACQUA ALTA WM90	4386229.678	973073.435	4512012.439	55.709

TABLE B–16 Final AIUB GPS Coordinates (1991, ERS90B)

Station	*x* (m)	*y* (m)	*z* (m)	*h* (m)
MONTE VENDA 7542	4399363.564	910506.408	4512940.772	523.183
ACQUA ALTA WM90	4386229.651	973073.347	4512012.393	55.645

ANNEX C

Regional Geoid Determination

This annex is a modified form of the report by Caporali et al, *1992, cited in , "References". It fills in details omitted from CHAPTER 3, "The Three-Dimensional Network".*

C.1 Observational Data

C.1.1 Definition of the Observed Quantities

The direct measurement of the geoidal height N is done at any point for which the height above the ellipsoid h and the corresponding height above the geoid H is known:

$$N = h - H$$

Both ellipsoidal and geoidal heights must be referred to some zero. The geoidal heights are generally referred to a tide gauge with a well known and studied record. The ellipsoidal heights are referred to the heights of satellite laser stations. In practice, if one adopts a tide gauge (in our case the one near Punta Salute in Venice), one obtains its ellipsoidal height by connecting it via GPS to a nearby laser station, in our case Monte Venda, 64 km west of the tower. Using an origin for which both H and h (and thus N) are known, one can obtain height differences ΔH along the geoid by spirit levelling, and height differences Δh along the ellipsoid by GPS translocation. The corresponding increments ΔN are added to the N of the adopted origin to generate a pointwise sampling of the geoidal height.

The direct measurement of the deflection of the vertical is made at any point for which the latitude and longitude are known on the geoid and on the ellipsoid. The latitude and longitude (Φ, Λ) on the geoid can be obtained by astronomical observations of fundamental stars. The corresponding quantities (ϕ, λ) on the ellipsoid are obtained by connection (*eg* using GPS) to one or more nearby fundamental laser stations. Then the deflection of the vertical (ξ, η) in the meridian and respectively prime vertical planes are obtained from the formulas:

$$\xi = \Phi - \phi \qquad \eta = (\Lambda - \lambda)\cos\phi$$

The two numbers (ξ, η) are the components of a vector resulting from the difference of the vertical to the geoid and the normal to the ellipsoid. Thus a geoid rising from south to north will have a negative ξ. A geoid rising from west to east will have a negative η. In formulas:

$$\xi = -\frac{\partial N}{R\partial\phi} \qquad \eta = -\sec\phi\frac{\partial N}{R\partial\lambda}$$

R being the earth radius.

C.1.2 Measurement Campaigns

Figure C–2 shows the geographical distribution of the sites at which the observations of N and/or (ξ, η) have been made. As shown in Figure C–2, fault lines are suspected, but are largely inactive, across the Colli Euganei in the NNW direction. Overall the area is mostly flat and indicates a smooth equipotential in the neighbourhood of the calibration area. Consequently, it is reasonable to expect that geoidal heights and slopes observed on land can be interpolated to the sea with sufficient accuracy.

Most of the points shown in Figure C–1 belong to existing levelling lines which are monitored and catalogued by the *Istituto per lo Studio della Dinamica Delle Grandi Masse* of CNR in Venice (*Caporali et al.* 1990). A number of these levelled points have been occupied by GPS receivers generating the network shown in Figure 3–1 in CHAPTER 3, "The Three-Dimensional Network".

We used single and dual frequency receivers (Wild Magnavox WM 101 and 102 respectively) during several campaigns from 1987 through 1991. In addition, dual frequency Trimble receivers have been used to monitor the critical baseline Monte Venda–tower. At Monte Venda, the Dutch mobile laser system MTLRS 2 operated very successfully from April through September 1991 and provided a tie to the rectangular reference system of the laser ranging network. This tie was strengthened in the October 1990 "large GPS campaign" where dual frequency GPS receivers occupied Monte Venda, the tower and a number of European laser sites. This resulted in very accurate reference coordinates for these two key sites. The individual baseline vectors of the local GPS network (mean distances in the order of 15 km) were computed from the GPS phases by standard data reduction programs (PoPS for the WM's and TRIMVEC for the Trimble's). The network was least squares adjusted on the WGS84 ellipsoid using the program Geolab. In the adjustment, the coordinates of Monte Venda and tower resulting from the "Large campaign" mentioned earlier were held fixed to the follow-

FIGURE C-1 Geography of the area covered by the survey

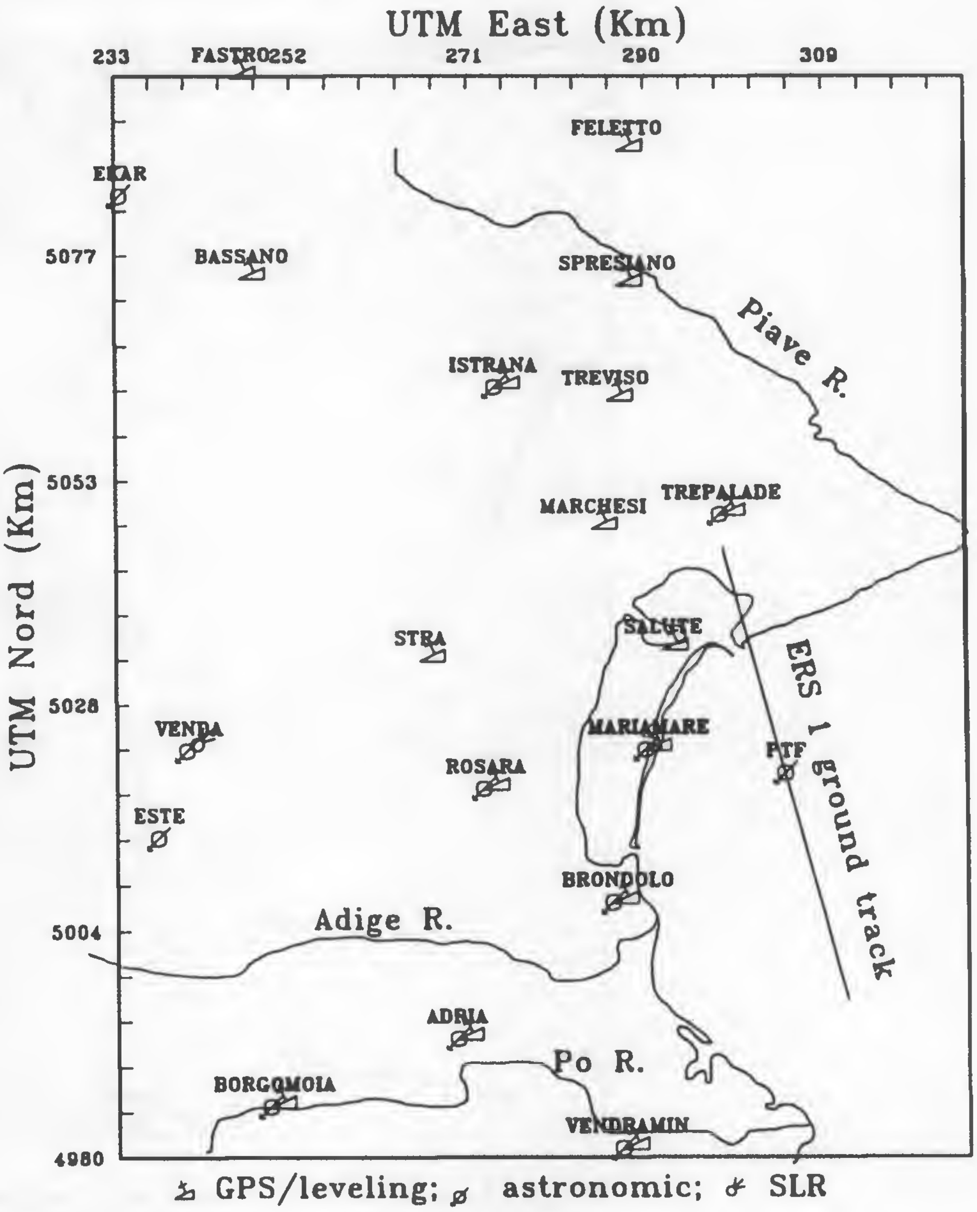

ing values (*Gurtner*, 1991; *Scharroo and Overgaauw*, 1991), which are consistent with the coordinates ETRF 89 of the five Satellite Laser Ranging stations Grasse (7835), Graz (7839), Matera (7939), Wettzell (7834) and Zimmerwald (7810):

	X (m)	*Y* (m)	*Z* (m)
Monte Venda	4399894.081	910501.215	4512527.509
Tower	4386229.670	973073.374	4512012.478

FIGURE C–2

Major geological features of the surveyed area. Stars indicate the location of a number of astrogeodetic and GPS/leveling sites.

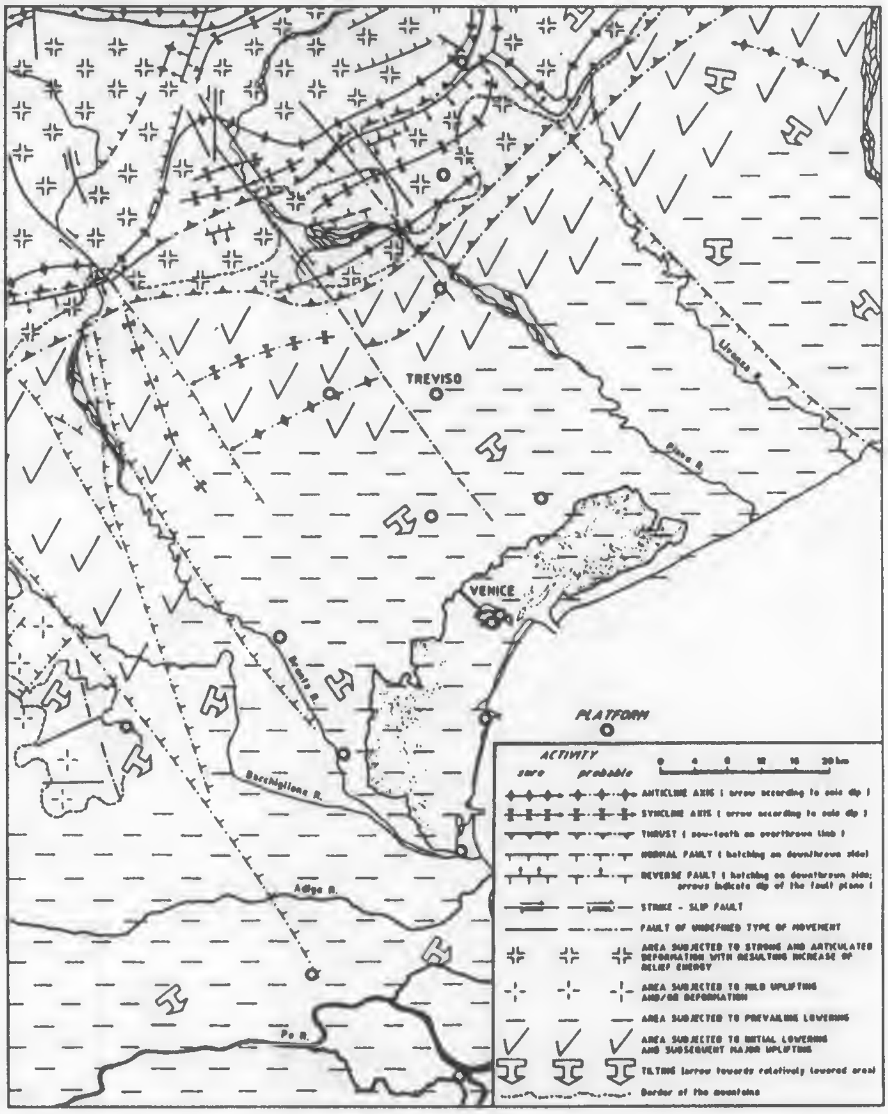

The geographical coordinates result from the mapping of the cartesian ones on the WGS84 ellipsoid (a = 6378137 m; $1/f$ = 298.257):

	f	l	h
Monte Venda	45° 18′ 57″.2707	11° 41′ 29″.7445	593.899 m
Tower	45° 18′ 51″.1723	12° 30′ 30″.0152	55.725 m

Constraining the coordinates of the two sites gave to the adjustment enough control to solve for a scale factor, in addition to the WGS84 coordinates of all the remaining sites. The scale factor between the GPS baselines of the local network and the baseline tower-Monte Venda, which is matched to the scale distance of the SLR stations, resulted in:

scale factor = -0.43 ± 0.24 ppm (1.96 σ)

(ppm = parts per million) which is thus marginal.

As a result of the adjustment, the least squares adjusted network is rigidly tied to the laser tracking network in the sense that the local (GPS) and global (Satellite Laser Ranging) networks are matched in origin, scale and orientation. The least squares adjusted ellipsoidal heights have an estimated formal uncertainty typically below 10 cm. The corresponding planar coordinates are a factor of two more precise.

It should be remarked that the coordinates of Monte Venda given above refer to the Helipad. The connection from the Helipad to the laser ranging site in Baiamonte (always on the Monte Venda) was done in April 1991 by Telespazio personnel using GPS. The resulting coordinates of the reference marker at the laser site in Baiamonte are:

	X (m)	*Y* (m)	*Z* (m)
Baiamonte	4399363.6005	910506.4737	4512940.8640
	f	l	h
Baiamonte	45° 19′ 18″.6236	11° 41′ 34″.9165	523.284 m

The astronomical campaigns were carried out in summer 1990 and 1991 using the method of equal heights. This consists in timing the transits of fundamental stars through an *almucantar* of nominal radius 30° from the local vertical. The equipment used was developed by the Institute of Geodesy and Photogrammetry of the ETH in Zurich and was operated by personnel of the *Istituto Geografico Militare Italiano*. The equipment consisted of an electronic theodolite of type Wild T2002, a Time Digitising Unit synchronised to UTC by means of a radio receiver and by a Personal Computer for preparation of the observing session, data acquisition and real time data processing. By observing 20 to 30 stars per station, typical formal errors of 0″.5 could be routinely achieved.

Table 1 of *Caporali et al* (1992) provides a summary of the available observational data. We give ellipsoidal and astronomic coordinates, ellipsoidal and orthometric heights, and the resulting "observed" geoidal heights and deflections. The corresponding quantities computed, on the same WGS84 ellipsoid, using the OSU91A model complete to degree and order 360 are also given. This model, which is based on an expansion of the terrestrial gravity field in spherical harmonics, is rather accurate and can be conveniently used as a starting point. Thus the interpolation algorithm discussed in the next section will be applied to reduced (*ie* observed minus model) data to locally improve on the starting model. As an alternative we have also used a terrain reduction and carried out the interpolation with data reduced to a co-geoid. However the final results are virtually identical.

C.2 Mathematical Algorithm for Geoid Computation

In this section we discuss how pointwise samples of the geoidal height and vertical deflection can be rigorously interpolated to other points where no data are available, in particular along the calibration ground track. The corresponding propagation of the measurement errors will be discussed as well.

Because the data set consists of heterogeneous data (geoidal heights and deflections of the vertical) it is convenient to use the algorithm called "least squares prediction" (*Heiskanen and Moritz*, 1967). For completeness we summarise the algorithm, with particular emphasis to our specific case.

Suppose that we have geoidal heights at points $Q1\ldots Qn$ and deflections of the vertical at points $Q'1\ldots Q'm$ which may or may not coincide with the Q's. Let us introduce the measurement vector of n+$2m$ elements

$$x = (N_1\ldots N_n, \xi_1\ldots\xi_m, \eta_1\ldots\eta_m)$$

Let P be a point at which (N, ξ, η) are to be predicted. The three dimensional array at P

$$\hat{y} = (\hat{N}, \hat{\xi}, \hat{\eta})$$

contains the predicted values and

$$y = (N, \xi, \eta) \qquad \text{(EQ C-1)}$$

contains the actual ("true") values, or "signals".

Accordingly

$$\varepsilon = y - \hat{y}$$

is the prediction error at P.

In a linear approximation we represent the prediction y at P as a linear combination of the heterogeneous observations x at points Q, Q':

$$\hat{y} = \mathbf{H}x \qquad \text{(EQ C-2)}$$

H being a $3\times(n+2m)$ matrix with elements independent of the measurements x. We assume that the measurements are zero mean random variables and without error (the extension to measurements with errors will be dealt with in section C.2.2, "Inclusion of Measurement Errors"). At the desired point P the measurement error is

$$\varepsilon = y - \mathbf{H}x$$

By squaring we find

$$\varepsilon^2 = y^2 - 2\,(y)\,(\mathbf{H}x) + (\mathbf{H}x)^2 \qquad \text{(EQ C-3)}$$

Denoting by M the averaging operator, we introduce the autocovariances of, and the crosscovariances between, the observations, the signals and the prediction errors:

$M(y_P y_i) = C_{y_P y}$	is the autocovariance between the signal at P and the signals at the data points
$M(y_P x_i) = C_{y_P x}$	is the crosscovariance between signal at P and measurements at points Q, Q'
$M(x_i, x_j) = C_{xx}$	is the autocovariance of the measurements

The variance of the prediction at P is

$$m^2 = M(\varepsilon^2) \qquad \text{(EQ C-4)}$$

By inserting EQ C-3 into EQ C-4 we find

$$m^2 = \mathbf{C}_{y_P y_P} - 2\mathbf{H}\mathbf{C}_{y_P x} + \mathbf{H}\mathbf{C}_{xx}\mathbf{H}^{\mathrm{T}}$$

where $\mathbf{H}^{\mathrm{T}}$ denotes the transpose of $\mathbf{H}$.

So far the interpolation coefficients $\mathbf{H}$ are arbitrary. We can determine them unequivocally by a minimum variance criterion, *ie* by imposing that they are such that the variance of the predictions (EQ C-4) intended as a functional of $\mathbf{H}$ has a minimum. The necessary condition is given by the algebraic system

$$\frac{\partial m^2}{\partial \mathbf{H}} = -2\mathbf{C}_{y_P x} + 2\mathbf{C}_{xx}\mathbf{H} = 0$$

If C_{xx} is invertible (*ie* there exist no duplicate points), then the minimum variance estimate of $\mathbf{H}$ is

$$\mathbf{H} = \frac{\mathbf{C}_{y_P x}}{\mathbf{C}_{xx}}$$

Accordingly, the minimum variance prediction and prediction errors for the desired quantities $y = (N, \xi, \eta)$ are

$$\hat{y} = \frac{\mathbf{C}_{y_P x}x}{\mathbf{C}_{xx}} \qquad \text{(EQ C-5)}$$

$$m^2 = \mathbf{C}_{y_P y_P} - \mathbf{C}_{y_P x}\mathbf{C}_{xx}^{-1}\mathbf{C}_{y_P x}^{\mathrm{T}} \qquad \text{(EQ C-6)}$$

We would like at this stage to apply this general formulation to our specific case. We introduce the autocovariance of the observed geoidal height

$$C^{NN} = \begin{bmatrix} C_{11}^{NN} & \dots & C_{1n}^{NN} \\ \dots & \dots & \dots \\ C_{n1}^{NN} & \dots & C_{nn}^{NN} \end{bmatrix}$$

and of the deflections

$$C^{\xi\xi} = \begin{bmatrix} C_{11}^{\xi\xi} & \dots & C_{1m}^{\xi\xi} \\ \dots & \dots & \dots \\ C_{m1}^{\xi\xi} & \dots & C_{mm}^{\xi\xi} \end{bmatrix}; \qquad C^{\eta\eta} = \begin{bmatrix} C_{11}^{\eta\eta} & \dots & C_{1m}^{\eta\eta} \\ \dots & \dots & \dots \\ C_{m1}^{\eta\eta} & \dots & C_{mm}^{\eta\eta} \end{bmatrix}$$

The cross covariances of geoidal heights and deflections are given by rectangular matrices:

$$C^{N\xi} = \begin{bmatrix} C_{11}^{N\xi} & \dots & C_{1m}^{N\xi} \\ \dots & \dots & \dots \\ C_{n1}^{N\xi} & \dots & C_{nm}^{N\xi} \end{bmatrix}; \qquad C^{N\eta} = \begin{bmatrix} C_{11}^{N\eta} & \dots & C_{1m}^{N\eta} \\ \dots & \dots & \dots \\ C_{n1}^{N\eta} & \dots & C_{nm}^{N\eta} \end{bmatrix}$$

The cross covariances between deflections are given by the square matrix

$$C^{\xi\eta} = \begin{bmatrix} C_{11}^{\xi\eta} & \dots & C_{1m}^{\xi\eta} \\ \dots & \dots & \dots \\ C_{m1}^{\xi\eta} & \dots & C_{mm}^{\xi\eta} \end{bmatrix}$$

The autocovariance of the heterogeneous data has thus the symbolic expression

$$C_{xx} = \begin{bmatrix} C^{NN} & C^{N\xi} & C^{N\eta} \\ C^{\xi N} & C^{\xi\xi} & C^{\xi\eta} \\ C^{\eta N} & C^{\eta\xi} & C^{\eta\eta} \end{bmatrix}$$

It is a matrix of dimension (2m+n)×(2m+n) and symmetries discussed in section C.2.3, "The Selection of the Correlation Function".

The predicted ($\hat{N}$, $\hat{\xi}$, $\hat{\eta}$) at a point P are, according to EQ C–5:

$$\hat{N}_p = C_{N_p x} C_{xx}^{-1} x \qquad \text{(EQ C–7)}$$

where:

$$\mathbf{C}^{\mathrm{T}}_{N_px} = \left[c^{NN}_{N_p1}\ldots c^{NN}_{N_pn}c^{N\xi}_{N_p1}\ldots c^{N\xi}_{N_pm}c^{N\eta}_{N_p1}\ldots c^{N\eta}_{N_pm}\right]$$

is the transposed of the vector $\mathbf{C}_{N_px}$ of the cross covariances between the geoidal height at P and heterogeneous data (geoidal height and deflections) at the observation points (thus $\hat{\vartheta}_P = \hat{N}_P$).

The variance of the predictions is, according to EQ C–6:

$$m^2_{N_p} = \mathbf{C}^{NN}_{N_pN_p} - \mathbf{C}_{N_px}\mathbf{C}^{-1}_{xx}\mathbf{C}^{\mathrm{T}}_{N_px} \qquad \text{(EQ C–8)}$$

Likewise for the deflections at P (thus $\hat{\vartheta}_P = \hat{\xi}_P$):

$$\hat{\xi}_P = \mathbf{C}_{\xi_px}\mathbf{C}^{-1}_{xx}x \qquad \text{(EQ C–9)}$$

where, in this case,

$$\mathbf{C}^{\mathrm{T}}_{\xi_px} = \left[c^{\xi N}_{\xi_p1}\ldots c^{\xi N}_{\xi_pn}c^{\xi\xi}_{\xi_p1}\ldots c^{\xi\xi}_{\xi_pm}c^{\xi\eta}_{\xi_p1}\ldots c^{\xi\eta}_{\xi_pm}\right] \qquad \text{(EQ C–10)}$$

and the variance of the prediction is:

$$m^2_{\xi_p} = \mathbf{C}^{\xi\xi}_{\xi_p\xi_p} - \mathbf{C}_{\xi_px}\mathbf{C}^{-1}_{xx}\mathbf{C}^{\mathrm{T}}_{\xi_px} \qquad \text{(EQ C–11)}$$

Similar formulas apply for the prediction of η, by replacing ξ with η in equations EQ C–9–EQ C–11.

Hence, from the computational viewpoint, the least squares prediction algorithm requires pointwise evaluation of functions and some matrix algebra, in particular the inversion of matrix $\mathbf{C}_{xx}$ of size equal to the total number of observations.

C.2.1 Absolute versus Relative Geoidal Heights

From EQ C–7 it follows that measurements of (ξ, η) only, with no information on N, enable N to be computed. This fact must be examined with care as the deflections represent spatial increments of N and carry no information on the origin of N. As *Gurtner* (1978) has shown in some examples, computing N at a number of points using EQ C–7 with only deflection data results in a surface which has a correct slope but height scale strongly dependent on the input observations. In our situation we have several origins available, as N is known at several points. We select one, *Punta Salute,* and from there work by differences:

$$N_P = N_{Salute} + (\hat{N}_P - \hat{N}_{Salute}) \qquad \text{(EQ C–12)}$$

where each term in parentheses is computed using EQ C–7 while, according to table 1, N_{Salute} is held fixed at 43.45 m.

If we have only geoidal heights and no deflection data, then the predicted N's will coincide with the original data. When, in a more general case, there are heterogeneous data, this will not be exactly satisfied because of the contribution of the observed vertical deflections via the crosscovariances $C^{N\xi}$, $C^{N\eta}$. Likewise for the prediction of the deflections from deflection and geoidal heights data or, at least in principle, even deflections of different type (η data to predict ξ, or *vice-versa*) due to the action of $C^{\xi\eta}$.

C.2.2 Inclusion of Measurement Errors

For measurements with noise EQ C–2 modifies to

$$\hat{y} = \mathbf{H}x + n$$

where n is the measurement noise. It can be shown that the fundamental computational equations EQ C–7 and EQ C–8 remain formally unchanged, with the replacement

$$\mathbf{C}_{xx} \rightarrow \mathbf{C}_{xx} + n_{xx}$$

where n_{xx} is the noise covariance matrix. For our applications n_{xx} can be assumed diagonal, *ie* the measurements are uncorrelated. The diagonal elements are the variances of the measurements

$$n_{xx} = \begin{bmatrix} \sigma^2_{N_1} & & & & & & & & 0 \\ & \dots & & & & & & & \\ & & \sigma^2_{N_n} & & & & & & \\ & & & \sigma^2_{\xi_1} & & & & & \\ & & & & \dots & & & & \\ & & & & & \sigma^2_{\xi_m} & & & \\ & & & & & & \sigma^2_{\eta_1} & & \\ 0 & & & & & & & \dots & \\ & & & & & & & & \sigma^2_{\eta_m} \end{bmatrix}$$

For our analysis it will be a good starting assumption that all measurements of the same type have equal variance. However the computational algorithm is from the very start flexible enough that individual measurements, or group of measurements, can be down-weighted, enabling particular types of solutions (*eg* a purely astrogeodetic geoid) to be investigated.

Finally, the inclusion of measurement noise produces a smoothing effect in the interpolated surface, which otherwise (*ie* in the absence of noise), would be forced through the data points. Thus the smoothing is a desirable effect as it permits large discrepancies to be identified.

C.2.3 The Selection of the Correlation Function

The previous section described an interpolation algorithm which is implemented on the basis of statistical criteria (minimum variance) by means of algebraic relations. No reference is made to the fact that the observational data, whether geoidal heights or deflections of the vertical, are attributes of an equipotential surface $W(x,y,z)$ satisfying the field equation on the boundary surface, *ie* the Poisson equation:

$$\nabla W = 0 \qquad \text{(EQ C-13)}$$

The question of how to construct a covariance function such that the interpolation procedure described in the previous section generates points which globally define a surface W = const. satisfying EQ C–13 does not seem to have been fully answered yet. However a number of investigations (*eg Jordan*, 1972; *Kasper*, 1971; *Shaw et al.* 1969; *Grafarend*, 1976; *Forsberg*, 1987) have addressed the constraints put on the autocovariance of the observations by the harmonicity condition EQ C–13 in order to identify covariance functions which are, in some sense, "physical" or "self consistent". We here summarise the basic formulas, as they will be used later in our work.

Let (e,n) represent the coordinate differences in the east and north direction between any two points. If C^{NN} (e,n) is the autocorrelation of the geoidal heights, then it can be shown that the auto and cross-correlations of the deflection are obtained by

$$\begin{aligned} C^{\xi\xi}(e,n) &= -\frac{\partial^2 C^{NN}}{\partial n^2} \qquad & C^{\eta\eta}(e,n) &= -\frac{\partial^2 C^{NN}}{\partial e^2} \\ C^{N\xi}(e,n) &= -\frac{\partial C^{NN}}{\partial n} \qquad & C^{N\eta}(e,n) &= -\frac{\partial C^{NN}}{\partial e} \\ & & C^{\xi\eta}(e,n) = -\frac{\partial^2 C^{NN}}{\partial e \partial n} \end{aligned} \qquad \text{(EQ C-14)}$$

In the appendix of his 1972 paper, Jordan has shown that the following symmetry properties are satisfied:

$$\begin{aligned} C^{N\xi}(e,n) &= C^{N\eta}(n,e) = -C^{\xi N}(e,n) = -C^{\eta N}(n,e) \\ C^{\xi\eta}(e,n) &= C^{\eta\xi}(e,n); \qquad C^{\eta\eta}(e,n) = C^{\xi\xi}(n,e) \end{aligned} \qquad \text{(EQ C-15)}$$

In practice it is often assumed that the autocovariance function of scalar quantities, such as the geoidal heights or the gravity anomalies, is isotropic, that is it depends only on the relative distance between two points:

$$C^{NN}(e,n) = C^{NN}(r) \qquad \text{with } r = \sqrt{e^2+n^2}$$

In particular, Jordan has shown that a third order Markov statistical model of the geoidal heights

$$C^{NN}(r) = \sigma_N^2\left(1+\frac{r}{D}+\frac{r^2}{3D^2}\right)e^{-\frac{r}{D}} \tag{EQ C-16}$$

with

$s^2{}_N =$ variance of the observed geoidal heights;

$D =$ scale distance

is such that necessary conditions for the undulation model to be "physically realistic" are satisfied. With EQ C–16, theEQ C–14 takes the form

$$C^{\xi\xi}(r,\theta) = \sigma_\xi^2\left[1+\frac{r}{D}+\frac{r^2}{D^2}\cos^2(\theta)\right]e^{-\frac{r}{D}}$$

$$C^{\eta\eta}(r,\theta) = \sigma_\eta^2\left[1+\frac{r}{D}+\frac{r^2}{D^2}\cos^2(\theta)\right]e^{-\frac{r}{D}}$$

$$C^{\xi\eta}(r,\theta) = -\frac{\sigma_\xi\sigma_\eta}{2}\frac{r^2}{D^2}\sin 2\theta \tag{EQ C-17}$$

$$C^{N\xi}(r,\theta) = \frac{\sigma_N\sigma_\xi}{\sqrt{3}}\frac{r}{D}\left(1+\frac{r}{D}\right)e^{-\frac{r}{D}}\cos\theta$$

$$C^{N\eta}(r,\theta) = \frac{\sigma_N\sigma_\eta}{\sqrt{3}}\frac{r}{D}\left(1+\frac{r}{D}\right)e^{-\frac{r}{D}}\sin\theta$$

where the azimuth θ is reckoned clockwise from north:

$$\sin\theta = \frac{e}{r} \qquad \cos\theta = \frac{n}{r} \tag{EQ C-18}$$

and

$$\sigma_\xi = \sigma_n = \frac{\sigma_N}{\sqrt{3}D}$$

(the notations for the east coordinate and exponential sign are in conflict but there ought to be no confusion).

Equations EQ C–16 through EQ C–18, with the symmetry relations EQ C–15 will be the statistical complement of the observational data, which are given in table 1 of the report by *Caporali et al* (1992). They form the basis for the interpolation of the geoidal heights and vertical deflections at the desired locations, as it will be discussed in the following section. It must be emphasized that the choice of the covariance function is not unique. For example *Forsberg* (1987) has suggested a planar logarithmic covariance function with a different parametrization than the Markov process EQ C–16. Although this approach is theoretically more sound, the numerical difference in using one or the other covariance functions is expected to be negligible, in our case.

C.3 Numerical Results

C.3.1 Origin Tide Gauge and the Geoid

Fundamental to our analysis is the value adopted as origin for N, *ie* the value N_{Salute} in EQ C–12. As shown in table 1 (*Caporali et al*, 1992), the required numerical value has been obtained by subtracting from the ellipsoidal height of the GPS marker at Punta Salute the orthometric height, which is in turn referred by spirit levelling (a few meters distance) to the nearby tide gauge. The ellipsoidal height has been obtained by GPS in translocation mode, from points of known geocentric coordinates, as discussed earlier. The orthometric height

$$H_{Salute} = 1.1201\,\mathrm{m}$$

is tied to the reference tide gauge labelled "CSO 358/7 IGM CNR73" with a msl (mean sea level) height of 1.2546 m. According to *Cavazzoni* (1977), this tide gauge is connected by precision levelling to the msl of the tide gauge in Genova of 1942 (mean of data from 1937 to 1946). The levelling survey took place in 1968. In analysing the homogenisation of nautical charts for the Venice area, Cavazzoni points out that relative to the zero of the Salute tide gauge of 1897 (mean of 1884 to 1909), in 1942 the Genova msl had a height of 23.56 cm and the Venice msl of 1968 (mean of 1964 to 1973) a height of 22.71 cm. This difference derives from the combination of sea level rising (on a global scale 1-3 mm/yr) and the subsidence of the Venice area. This is a local phenomenon mainly connected with water pumping from the ground. The subsidence stopped in 1980 following suitable regulations. If an overall vertical motion of 3mm/yr with respect to a mean sea level is assumed from 1968 to 1980, followed in 1980-1991 by only sea level rising, we conclude that our adopted sea level could be lower than it actually is by 0.3×12 + 0.13×11 = 5 cm. We take this as an upper limit of the bias in height between our geoid and the mean sea level in 1991.

C.3.2 The Geoid Along the Calibration Ground Track and Surrounding Areas

Figure 3–7 in CHAPTER 3, "The Three-Dimensional Network" shows the geoidal cross section along the calibration track 25 km before and after overflight on the tower. For comparison the cross section predicted by the OSU91A global model is also shown. At the tower the global model predicts $N = 43.09$ m, 19cm lower than the refined local model, $N = 43.28 \pm 0.02$ m. A quick check of this result is made by means of the measured (ξ,η) at the tower and (N,ξ,η) at the nearby sites of Mariamare, Brondolo and Trepalade, indicating that N at the tower should be greater than the 43.09 m predicted by the global model:

TABLE C–1 Comparative check of Geoid Height

Site	N (m)	ΔN (m)	N_{Tower} (m)
Mariamare	43.25	0.27	43.52
Brondolo	42.90	0.45	43.35
Trepalade	43.65	-0.53	43.12
Mean			43.33

Here ΔN is given by the classical formula of astrogeodetic levelling:

$$\Delta N = -<\eta>\Delta e - <\xi>\Delta n$$

where $\Delta e,\Delta n$ are the easterly and respectively northerly separation of the tower from the site and $<\xi>,<\eta>$ are the arithmetic means of the deflections at the tower and the site.

Consistent preliminary results were obtained by *Weber and Caporali* (1991) and *Scharroo and Overgaauw* (1991) using a "first guess" estimate of $N_{Salute} = 43.29$ m. It is perhaps surprising that the result of the least squares prediction differs by only a few decimetres from the OSU91A prediction. *Rapp et al* (1991) compared a number of global geoidal models finding that the Mediterranean area is one of the regions where the models disagree more—at the level of up a few meters.

Table 2 of *Caporali et al* (1992) gives the numerical results of the application of the least square prediction method to the data. The formal errors are computed by assuming a noise of 3 cm in the observations of N and 0".5 for the deflections (ξ,η). In the correlation function of the N's, a scale distance D = 40 km has been assumed. This figure results from the analysis of the behaviour of the actual autocorrelation of the values of N, after subtraction of the arithmetic mean, averaged over bins of 10 km. Furthermore it is consistent with the fact that we work with data from which all the wavelengths down to 100 km have been preliminarily subtracted out.

Table 2 of *Caporali et al* (1992) gives the values of (N,ξ,η) at the sites used in our numerical analysis as observed data and predictions based both on the

OSU91A model alone and on this model plus corrections computed with local data ("improved model"). We remark that the largest discrepancies between the observed and improved N occur at two nearby sites, Floriano and Feletto, with 18 and -16 cm respectively. The location is on the pre-Alps, with considerable topographic effect expected. The mean and rms discrepancies at the data points (in the sense observed–improved) are 0.8±8.1 cm for N, $-1''.3\pm2''.0$ for ξ and $-2''.2\pm3''.0$ for η.

Figure C–3 shows the geoid predicted on the area by the starting field OSU91A. The general structure is an increasing geoid-ellipsoid separation from south to north and closely associated with isostatic compensation of the Alpine chain. At sea the level curves tend to be more separated and the geoid becomes more flat.

Figure C–4 shows the result of the local geoid determination. The most relevant difference from Figure C–3 is the westward shift of the undulation which in Figure C–3 appears east of the ground track of ERS-1.

Figure C–5 shows those features which have been added to the predictions of the global model in Figure C–3 to generate Figure C–4. The excursion is from -30 to +30 cm. The signal resulting from the local data appears to be supported by a reasonable number of well distributed observing stations.

C.4 Conclusion

A local geoid model has been generated for an area of approximately 1°×1° by interpolating samples of the geoidal height and slope using a minimum variance algorithm. Proper alignment and scale is ensured by connecting the local network used for the measurements to the fiducial network of the laser ranging stations which track ERS-1. The inclusion, in the local network, of the tide gauge at Punta Salute, in Venice, provides appropriate vertical origin and relation to a mean sea level. To ensure the most favourable conditions for interpolation, geoidal heights and deflections from the global model OSU91A have been subtracted from the data and later, *ie* after the interpolation, restored at the interpolated points.

Throughout the surveyed area, including the section along the "Venice" ground track of ERS-1, the formal errors associated with the interpolation algorithm are of up to few centimetres. Comparison of the observed and computed geoidal heights show a mean difference virtually zero and a rms discrepancy of 8 cm, which we consider a realistic estimate of the accuracy of the computed model.

FIGURE C–3 The geoid predicted by the global model OSU91A. Contour distance 10 cm.

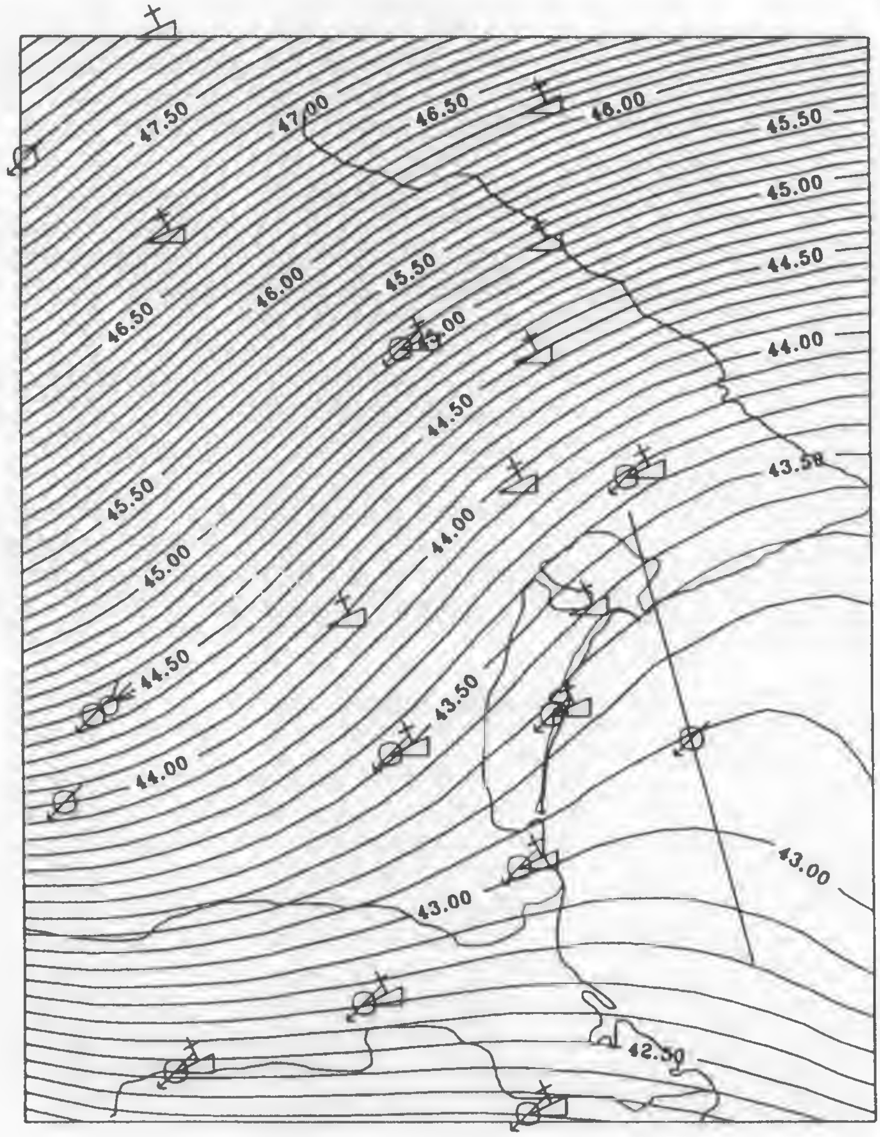

FIGURE C-4

The local geoid model resulting by complementing the predictions of the global model with local astrogeodetic, GPS and levelling data

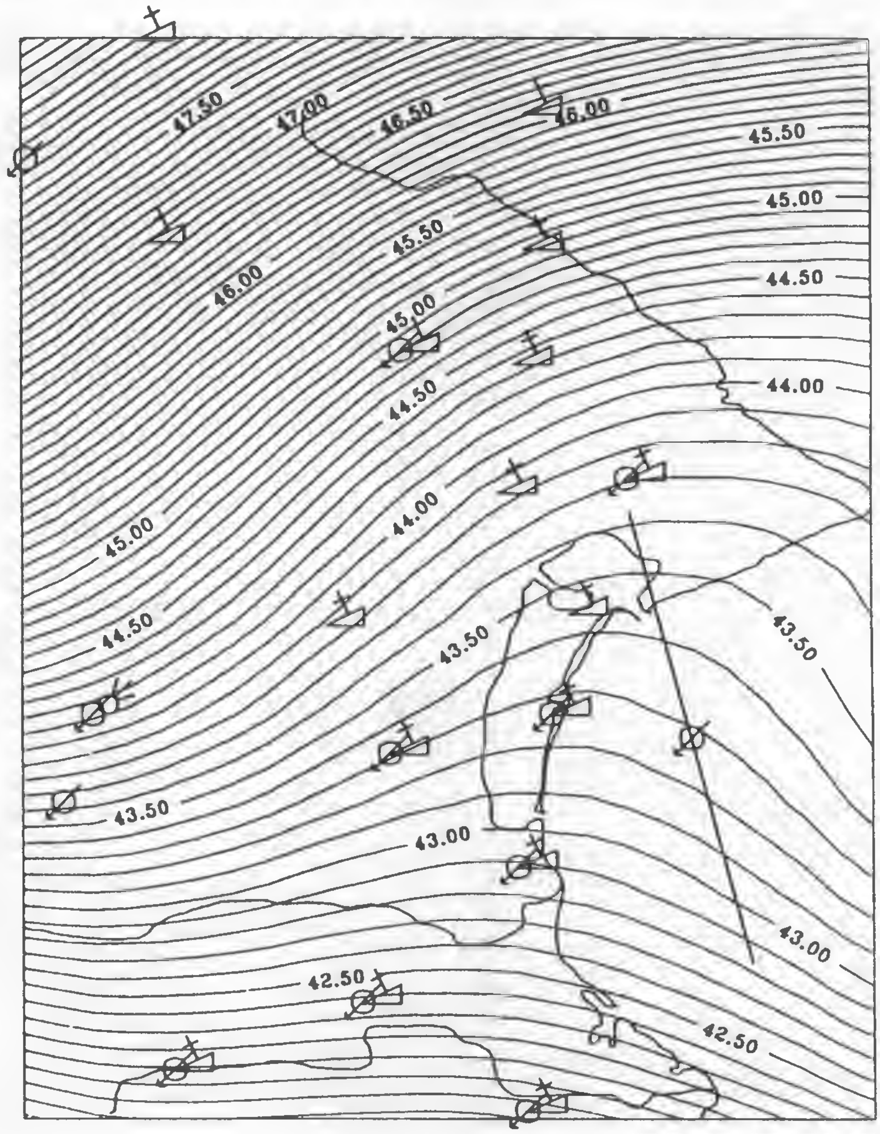

FIGURE C–5

The information content of local observations in terms of geoid undulations. This figure is the difference between Figure C–4 andFigure C–3.

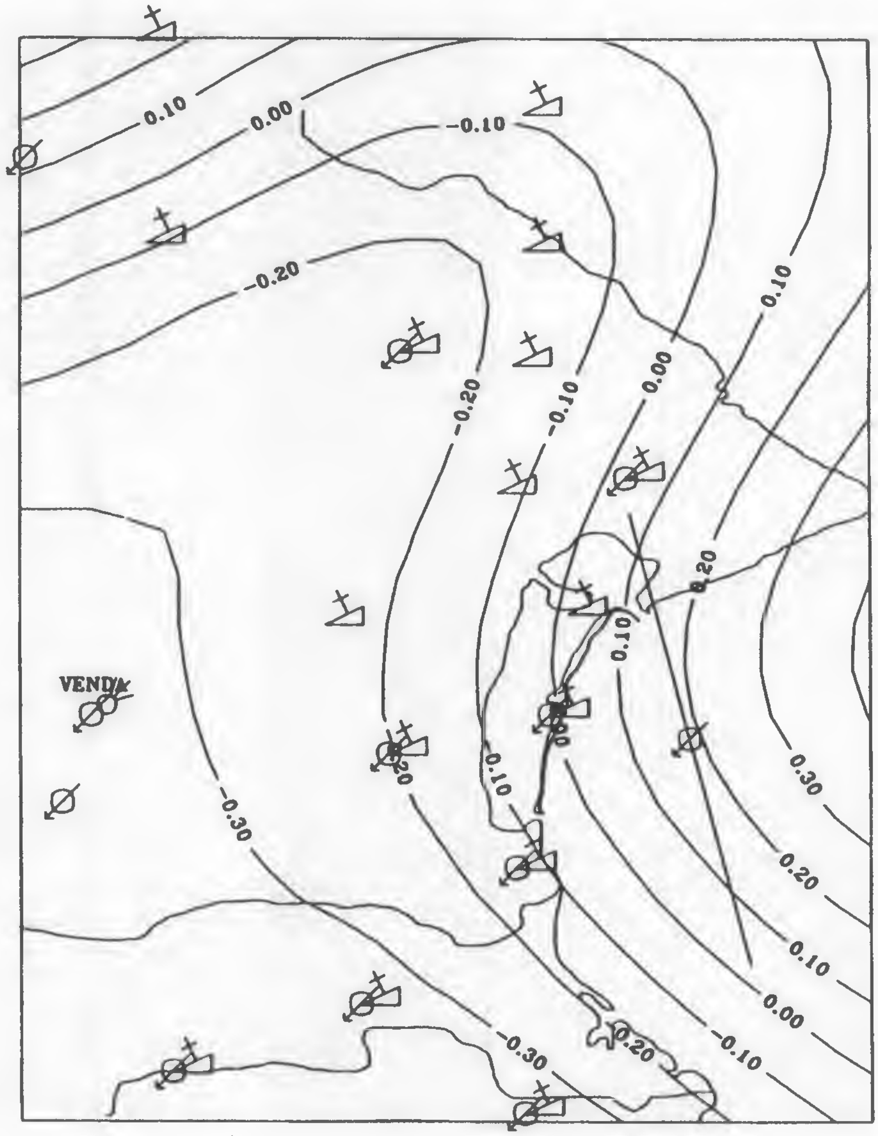

FIGURE C–6 A 3-dimensional picture of the geoid in Figure C–4

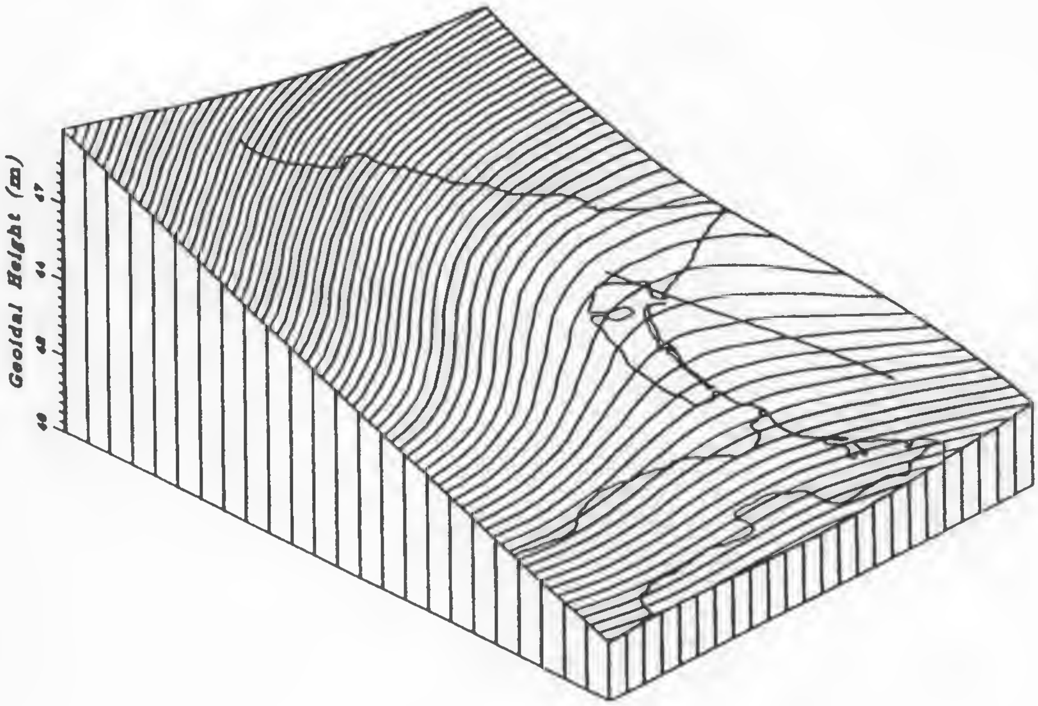

ANNEX D

The Local Surveys

This Annex describes the geodetic survey performed at Monte Venda (Baiamonte), Padova, from March 19 to March 22 1991 and at the Oceanographic Tower "Aqua Alta" from August 08 to August 10 1991 and from January 30 to January 31 1992. The measurements and data analysis have been performed by the Telespazio (Matera) operational team. The software packages used for data processing has been developed by Cenci, and is presently running on a VAX 11/730 at Matera. Moreover GPS raw data were analysed with the PoPS 3.4 software. This annex describes the analysis procedures, the methods adopted during the survey and contains a full characterization of the site.

D.1 Monte Venda

D.1.1 Monte Venda Site Description

The Monte Venda SLR site, a facility of the *Aeronautica Militare,* is located close to Teolo town in the Colli Euganei area, south west of the city of Padova at a distance of about 70 km from the CNR tower *"Aqua Alta"*. Figure D–1 shows the plan of the station site, including the SLR universal pad, located south-east of the transmitting house. The site is capable of hosting a transportable Laser Ranging System (MTLRS/TLRS).

Five reference markers are located on the pad and five additional brass markers have been installed for the local geodetic survey. The reference point "O" is the main marker of the pad (monument number 7542)

The five markers, called "A", "B", "C", "D" and "E", are located as additional reference points for reconstruction of all previous markers (*Allenby,* 1983). Table D–1 and Figure D–2 show the complete survey network with the coordinates obtained from the final analysis.

FIGURE D–1

Plan of the Monte Venda site

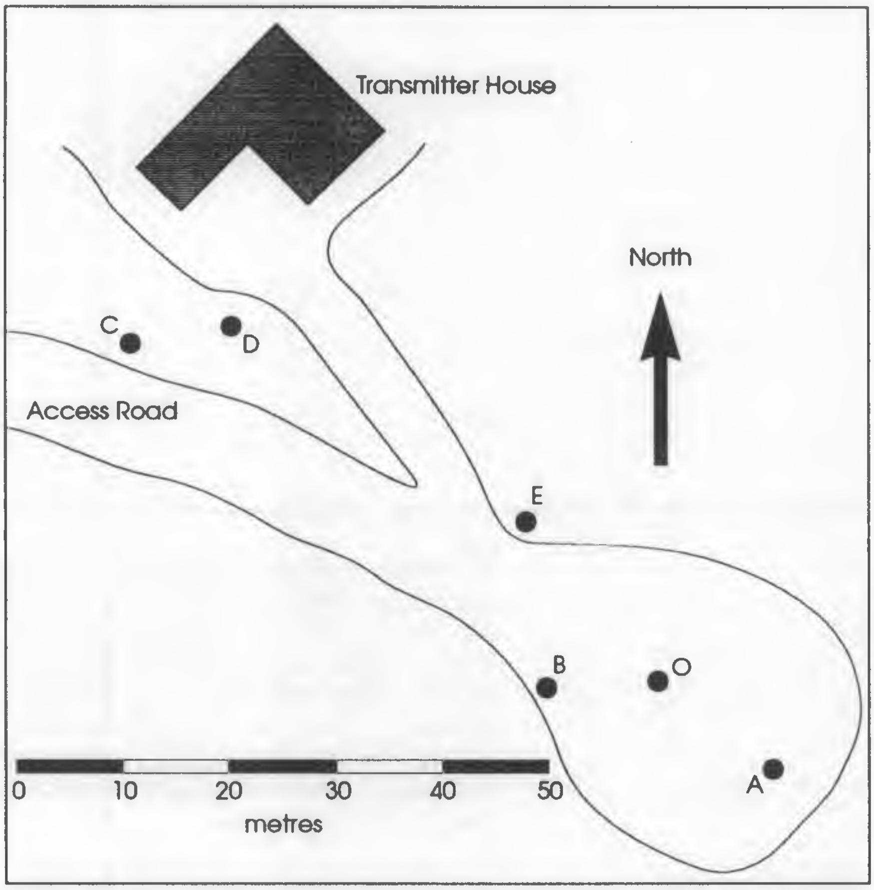

TABLE D–1

Monte Venda local network vectors in the local reference system (m)

	Up	East	North
"O"	0.0000	0.0000	0.0000
"A"	1.2583	10.7426	-8.1912
"B"	-0.1355	-10.2956	-0.6495
"C"	-0.5359	-49.2951	31.7134
"D"	2.5843	-39.9014	33.2103
"E"	1.9870	-12.3994	14.8739

D.1.2 Summary of the Results

Table D–2 to Table D–6 show the final coordinate values of the twelve vectors of the network, in the local reference system, taking the point "O" as

FIGURE D–2 Monte Venda Survey Network

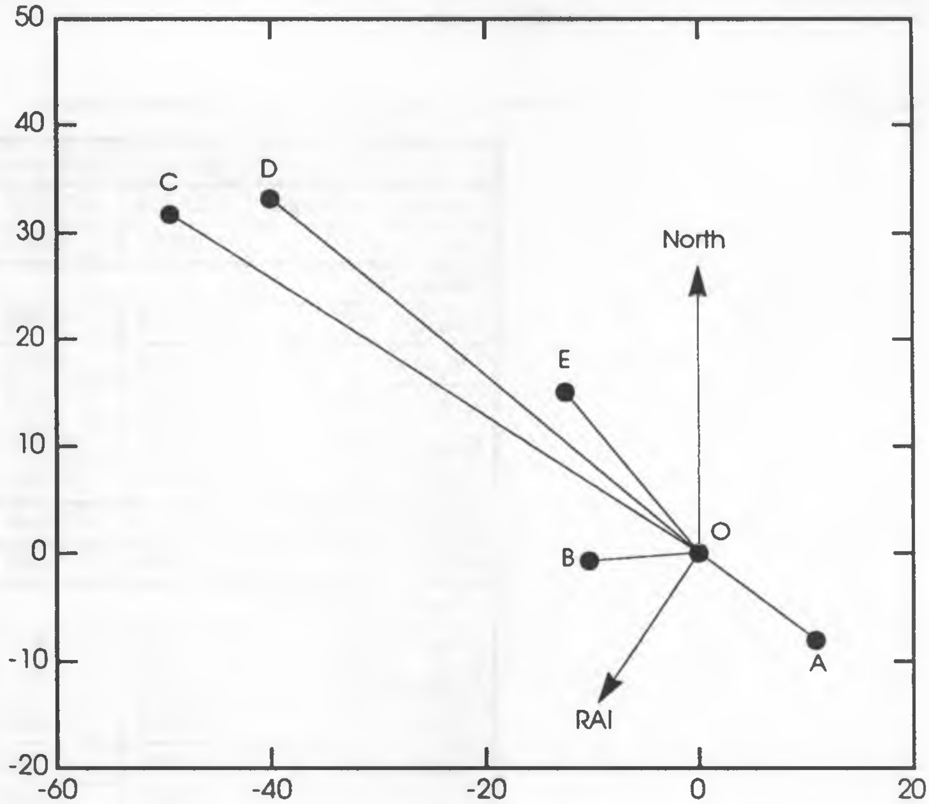

origin. The *a priori* input errors are the following

Azimuth:	3 mgrades
Elevation:	3 mgrades
Distance:	3 mm
Height Differences:	2 mm
Astronomical Latitude:	2 mdegrees
Astronomical Longitude:	2 mdegrees

The obtained *a priori* errors along the Up, East and North axes were used as weights for the weighted averages and rms calculation. It should be noted that the rms's of the coordinates are always lower than the *a priori* errors, being normally less than 3 mm for all vectors. This indicates a good repeatability of the measurements.

The final values (arithmetic averages) of the vectors in both local and global system are summarized in Table D–8 and Table D–8. The latitude and longitude used are:

Lat = 45.321958° = 45° 19′ 19″

Lon = 11.693108° = 11° 41′ 35″

The overall error budget, including systematic and random errors, remains within 5 mm.

TABLE D–2 Summary of Vector A–O from 5 measurements

	Up (m)	East (m)	North (m)	Distance(m)
Arithmetic Averages	1.258332	10.742598	-8.191205	13.567706
rms	0.0007	0.0021	0.0016	0.0026
Residuals				
Origin in "O"	0.0014	0.0024	-0.0017	0.0030
Origin in "A"	-0.0005	0.0027	-0.0020	0.0033
Origin in "B"	-0.0006	-0.0021	0.0019	-0.0029
Origin in "D"	-0.0001	-0.0013	0.0004	-0.0013
Origin in "E"	-0.0002	-0.0016	0.0013	-0.0021
Weighted Averages	1.258473	10.743483	-8.191233	13.568759
Weighted rms	0.0008	0.0021	0.0018	0.0026
Weighted Residuals:				
Origin in "O"	0.0012	0.0015	-0.0017	0.0020
Origin in "A"	-0.0006	0.0018	-0.0019	0.0022
Origin in "B"	-0.0008	-0.0030	0.0019	-0.0039
Origin in "D"	-0.0002	-0.0022	0.0005	-0.0024
Origin in "E"	-0.0003	-0.0025	0.0014	-0.0032
A Priori Errors	0.0057	0.0033	0.0026	0.0030

D.1.3 GPS Results

D.1.3.1 Heliport Site (Monte Venda).

During the initial measurements at Monte Venda, to tie it to the local reference system for the first time, a site at the heliport as used, as the final site for the MTLRS2 pad was unknown at that time. The measurements and results at the heliport are given here. Marker "A" was occupied by the WM102 GPS receiver, while marker "B" by the Trimble (see Figure D–3). The relative positions of these are given in Table D–3.

D.1.3.2 Baiamonte - Monte Venda measurement

The measurements between marker "A" on the heliport (Monte Venda) and marker "O" on the pad (Baiamonte) have been performed from April 15 to April 17, 1991 with two WM-102 GPS receivers The data were analysed by Telespazio with POPS 3.4 software. Table D–9 and Table D–10 summarize the results of the observation.

FIGURE D–3 The Heliport Site

	dN	dE	dUp	dX	dY	dZ
Marker "A"	0.000	0.000	0.000	0.000	0.000	0.000
Marker "B"	3.121	-3.335	-0.125	-1.583	-3.733	2.106

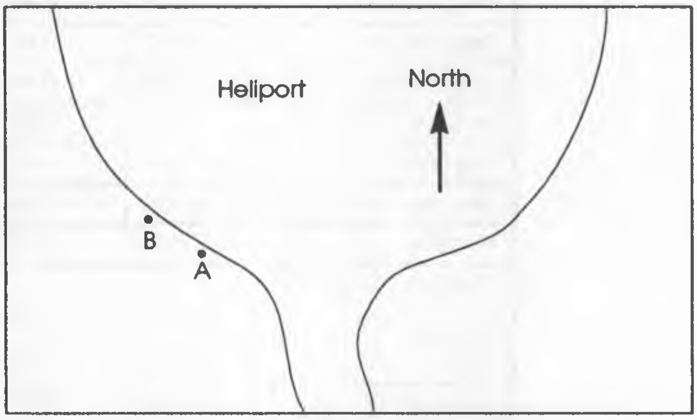

TABLE D–3 Summary of Vector B–O from 5 Measurements

	Up (m)	East (m)	North (m)	Distance(m)
Arithmetic Averages	-0.136388	-10.294872	-0.650091	10.316279
rms	0.0013	0.0018	0.0035	0.0017
Residuals				
Origin in "O"	0.0008	-0.0015	0.0034	0.0012
Origin in "A"	0.0009	0.0021	-0.0005	-0.0021
Origin in "B	-0.0021	-0.0023	0.0034	0.0021
Origin in "D"	0.0014	0.0020	-0.0002	-0.0020
Origin in "E"	-0.0010	-0.0003	-0.0061	0.0007
Weighted Averages	-0.136652	-10.295223	-0.646867	10.316888
Weighted rms	0.0014	0.0015	0.0011	0.0016
Weighted Residuals:				
Origin in "O"	0.0011	-0.0011	0.0002	0.0006
Origin in "A"	0.0012	0.0024	-0.0037	-0.0027
Origin in "B"	-0.0019	-0.0020	0.0002	0.0015
Origin in "D"	0.0017	0.0023	-0.0034	-0.0026
Origin in "E"	-0.0008	0.0000	-0.0094	0.0001
A Priori Errors	0.0055	0.0032	0.0022	0.0030

TABLE D–4

Summary of Vector C–O from 5 Measurements

	Up (m)	East (m)	North (m)	Distance (m)
Arithmetic Averages	-0.535952	-49.295132	31.713464	58.617754
rms	0.0014	0.0023	0.0040	0.0040
Residuals:				
Origin in "O"	-0.0005	-0.0024	0.0025	0.0034
Origin in "A"	-0.0002	0.0043	-0.0072	-0.0075
Origin in "B"	-0.0015	-0.0006	-0.0013	-0.0002
Origin in "D"	0.0026	0.0003	0.0025	0.0011
Origin in "E"	-0.0003	-0.0016	0.0035	0.0033
Weighted Averages	-0.535986	-49.295584	31.714005	58.618333
Weighted rms	0.0013	0.0023	0.0034	0.0038
Weighted Residuals:				
Origin in "O"	-0.0005	-0.0020	0.0019	0.0028
Origin in "A"	-0.0002	0.0048	-0.0078	-0.0081
Origin in "B"	-0.0015	-0.0001	-0.0019	-0.0008
Origin in "D"	0.0026	0.0007	0.0020	0.0005
Origin in "E"	-0.0003	-0.0012	0.0030	0.0027
A Priori Errors	0.0063	0.0038	0.0031	0.0030

D.1.4 Geodetic Information and Pad Measurements

Figure D–5 shows the results of the measurements made to uniquely define the SLR universal pad built at MONTE VENDA for MTLRS, TLRS and other transportable systems (*Vermaat*, 1984). The measurements of the distances between the five brass markers on the pad have been made using measuring tape, while levelling has been performed to obtain the height differences. The estimated accuracy for all measurements is better than 1 mm. Table 1.4 gives also the geodetic coordinates of the monument number 7542 (the main marker of the pad). These values are referred to the WGS 84 international ellipsoid and are obtained by using a GPS receiver (Magnavox WM102).

D.1.5 Astronomical Azimuth Orientation

The astronomical azimuth orientation of the network has been determined by observations of the Polaris star, from the monument "O" on March 20 1991. Table 1.5 summarizes the results of these observations. Marker "C", has been used as terrestrial reference. The columns MARKER "C" show the azimuth values (grades) of reference points with respect to the astronomical north, taking into account the calculated anomaly of the star, corrected with astronomical tables (*IAU*, 1990). The rms of 1.0 mgrades indicates a good repeatability of the measurements.

FIGURE D–5 Definition of 7542 MONTE VENDA

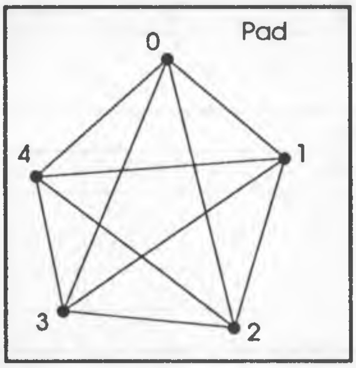

GPS Coordinates:

Lat = 45° 19′ 19.05″
Lon = 11° 41′ 35.19″

Astronomical Coordinates:

Lat = 45° 19′ 14″
Lon = 11° 41′ 43″

Pad Measurements:

	Distance(m)	Height(m)
1-0	2.421	-0.001
2-0	4.382	+0.002
3-0	4.301	+0.003
4-0	2.777	+0.004
2-1	2.782	
3-1	4.232	
4-1	3.919	
3-2	2.731	
4-2	3.950	
4-3	2.164	

	dN	dE	dUp
Marker "0"	0.000	0.000	0.000
Marker "1"	-1.579	1.835	-0.002
Marker "2"	-4.252	1.061	0.000
Marker "3"	-3.969	-1.656	0.002
Marker "4"	-1.846	-2.075	0.004

	dX	dY	dZ
Marker "0"	0.000	0.000	0.000
Marker "1"	0.726	2.024	-1.112
Marker "2"	2.746	1.652	-2.989
Marker "3"	3.101	-1.049	-2.790
Marker "4"	1.708	-1.765	-1.295

D.1.6 PRARE Antenna Support

On marker "E" was installed a pillar for the PRARE antenna. This pillar was included in the local survey as marker "P". Note that the height is the top of the pillar flange. The results are given in Table D–11.

TABLE D–5 Summary of Vector D–O from 5 Measurements

	Up (m)	East (m)	North (m)	Distance (m)
Arithmetic Averages	2.584377	-39.901382	33.210322	51.978118
rms	0.0002	0.0037	0.0033	0.0049
Residuals:				
Origin in "O"	0.0004	0.0014	0.0002	-0.0009
Origin in "A"	0.0000	0.0041	-0.0054	-0.0066
Origin in "B"	0.0000	-0.0040	0.0032	0.0051
Origin in "D"	-0.0002	0.0034	-0.0015	-0.0035
Origin in "E"	-0.0001	-0.0048	0.0034	0.0059
Weighted Averages	2.584398	-39.900945	33.210642	51.977889
Weighted rms	0.0003	0.0035	0.0029	0.0044
Weighted Residuals:				
Origin in "O"	0.0004	0.0009	-0.0001	-0.0007
Origin in "A"	0.0000	0.0036	-0.0057	-0.0063
Origin in "B"	-0.0001	-0.0044	0.0029	0.0054
Origin in "D"	-0.0003	0.0029	-0.0018	-0.0033
Origin in "E"	-0.0002	-0.0053	0.0031	0.0061
A Priori Errors	0.0059	0.0034	0.0030	0.0030

D.1.7 Survey Data Processing

The Telespazio procedure for the computation and analysis consists of the following steps:

1. To process input data obtained by the measuring station located above one single marker in order to obtain vectors in a topocentric polar reference system (azimuth, elevation, distance). During this step, the data are corrected for the height differences between the instruments (theodolite and reflector) and the markers.
2. To convert the vectors from the topocentric polar reference system into a topocentric rectangular reference system (north east, zenith).
3. To convert the topocentric rectangular vector into global geocentric vectors, taking into account the latitude and longitude of the origin of the topocentric system (optional)
4. Steps 1,2, (3) are repeated for all the measurement configurations, while the survey equipment past all markers.
5. Statistical analysis of the result from steps 1 to 4 is made to obtain arithmetic and weighted averages and rms of the local and/or global coordinates X, Y, Z for each vector of the network. *A priori* errors are defined in the input in order to estimate the errors in the local or global geocentric reference frame.

TABLE D–6

Summary of Vector E–O from 5 Measurements

	Up (m)	East (m)	North (m)	Distance (m)
Arithmetic Averages	1.987052	-12.399414	14.873946	19.466076
rms	0.0016	0.0032	0.0042	0.0051
Residuals:				
Origin in "O"	0.0008	-0.0031	0.0019	0.0035
Origin in "A"	0.0005	0.0033	-0.0045	-0.0055
Origin in "B"	0.0009	-0.0030	0.0067	0.0071
Origin in "D"	0.0010	0.0045	-0.0042	-0.0060
Origin in "E"	-0.0033	-0.0016	0.0001	0.0008
Weighted Averages	1.986667	-12.400543	14.874276	19.466926
Weighted rms	0.0019	0.0027	0.0037	0.0044
Weighted Residuals:				
Origin in "O"	0.0012	-0.0020	0.0016	0.0027
Origin in "A"	0.0009	0.0044	-0.0048	-0.0063
Origin in "B"	0.0013	-0.0019	0.0064	0.0063
Origin in "D"	0.0014	0.0056	-0.0046	-0.0068
Origin in "E"	-0.0029	-0.0005	-0.0002	-0.0001
A Priori Errors	0.0055	0.0029	0.0029	0.0030

TABLE D–7

Vectors in the local reference system (m)

MARKER	Up	East	North	Distance
"O"	0.0000	0.0000	0.0000	0.0000
"A"	1.2583	10.7426	-8.1912	13.5677
"B"	-0.1363	-10.2948	-0.6501	10.3162
"C"	-0.5359	-49.2951	31.7134	58.6177
"D"	2.5843	-39.9013	33.2103	51.9781
"E"	1.9870	-12.3994	14.8739	19.4660

TABLE D–8 Vectors in the Global Reference System (m)

MARKER	X	Y	Z	Distance
"O"	0.0000	0.0000	0.0000	0.0000
"A"	4.3928	11.8794	-4.8646	13.5677
"B"	2.4452	-10.0069	-0.5540	10.3162
"C"	-12.4608	-52.9187	21.9173	58.6177
"D"	-13.2585	-43.4910	25.1885	51.9781
"E"	-6.4757	-14.0024	11.8711	19.4660

TABLE D–9 Summary of Measurements between Heliport ("A") and Balamonte ("O").

	X	Y	Z	Sigma				
	Lat (N)	Long (E)	Height (m)	*d*Lat	*d*Lon	*d*Ht	Distance (m)	rms (m)
15/04/91								
"O"	4399368.582	910501.955	4512952.328	0.001	0.001	0.002	627.530	0.001
	45°19'18.7929"	11°41'34.6669"	534.213					
"A"	4399899.065	910496.697	4512538.979					
	45°18'57.4401"	11°41'29.4951"	604.834					
16/04/91								
"O"	4399368.582	910501.955	4512952.328	0.001	0.001	0.001	672.540	0.001
	45°19'18.7929"	11°41'34.6669"	534.213					
"A"	4399899.065	910496.697	4512538.973					
	45°18'57.4399"	11°41'29.4951"	604.830					
17/04/91								
"O"	4399368.582	910501.955	4512952.328	0.001	0.001	0.002	672.539	0.001
	45°19'18.7929"	11°41'34.6669"	534.214					
"A"	4399899.070	910496.696	4512538.972					
	45°18'57.4398"	11°41'29.4950"	604.833					

TABLE D–10 Summary of the relative positions of Monte Venda and Balamonte

	*d*N	*d*E	*d*Up	dX	dY	dZ
Marker "O"	0.000	0.000	0.000	0.000	0.000	0.000
Marker "A"	-659.263	-112.661	70.584	530.485	-5.258	-413.353
Sigma				0.003	0.001	0.004

STATION:	BAIAMONTE MARKER "O"
OBSERVERS:	DEL ROSSO/AMBRICO
TERR.DIRECT:	MARKER "C"
OBSERVED STAR:	POLARIS 907
DATE:	20 MARCH 1991
LAT:	45° 19′ 19″
LON:	11° 41′ 35″

UT TIME	MARKER "C"
20:32:16	336.3948
20:45:37	336.3952
20:52:10	336.3941
20:59:48	336.3954
21:10:00	336.3941
21:17:06	336.3956
21:22:10	336.3949
21:25:45	336.3928
AVERAGE:	**336.3950**
STD DEV:	0.0010

TABLE D–11 Summary of the PRARE antenna pillar survey

MARKER	Up(m)	East(m)	North(m)	Distance(m)
P–O	2.5590	-12.4031	14.8765	19.5370
P–B	2.690	-2.1037	15.5233	15.8945

D.2 Venice Tower "*Aqua Alta*"

D.2.1 Venice Tower Site Description

The Venice Tower "*Acqua Alta*" is situated at about 15 km off the coast of Venice. It is about 14 meters high and the sea in that area is about 16 meters deep. This site is connected to the existing ground network using the GPS technique. Figure D–6 shows the plan of the tower and Figure D–7 shows the top floor plan of the tower. There are six reference markers located on the upper deck for the local survey plus other markers:

- marker "O" as reference marker;
- marker "W" for GPS measurement;
- marker "P" for the PRARE receiver pillar;
- markers "A", "B", "R" as additional reference points;
- Marker M0 is located on the first floor near the tide gauge;
- Markers T1 and T2 are located on the structure of the tower, within the tidal range, near the access ladder of the tower.

Figure D–8 shows the references for the markers "P" and "W" and Figure D–9 shows the complete survey network with the coordinates obtained from the final analysis.

	Up	East	North
"O" =	0.0000	0.0000	0.0000
"A" =	0.0194	-2.1333	6.1757
"B" =	-0.0079	-5.7130	4.3039
"W" =	1.2865	-8.9211	5.1910
"P" =	0.7087	-7.8459	3.6989
"R" =	0.0158	1.3807	1.3318

D.2.2 Summary of the Results

Table D–12 to Table D–16 show the final coordinate values of the twelve vectors the network, in the local reference system, taking the point "O" as origin. The *a priori* input errors are the following:

Azimuth:	3 mgrade
Elevation:	3 mgrades
Distance:	3 mm
Height Differences:	2 mm
Astronomical Latitude:	2 mdegrees
Astronomical Longitude:	2 mdegrees

The obtained *a priori* errors along the Up, East and North axes were used as weights for the weighted averages and rms calculation. It should be noted

FIGURE D–6 Schematic diagram of the Venice Tower

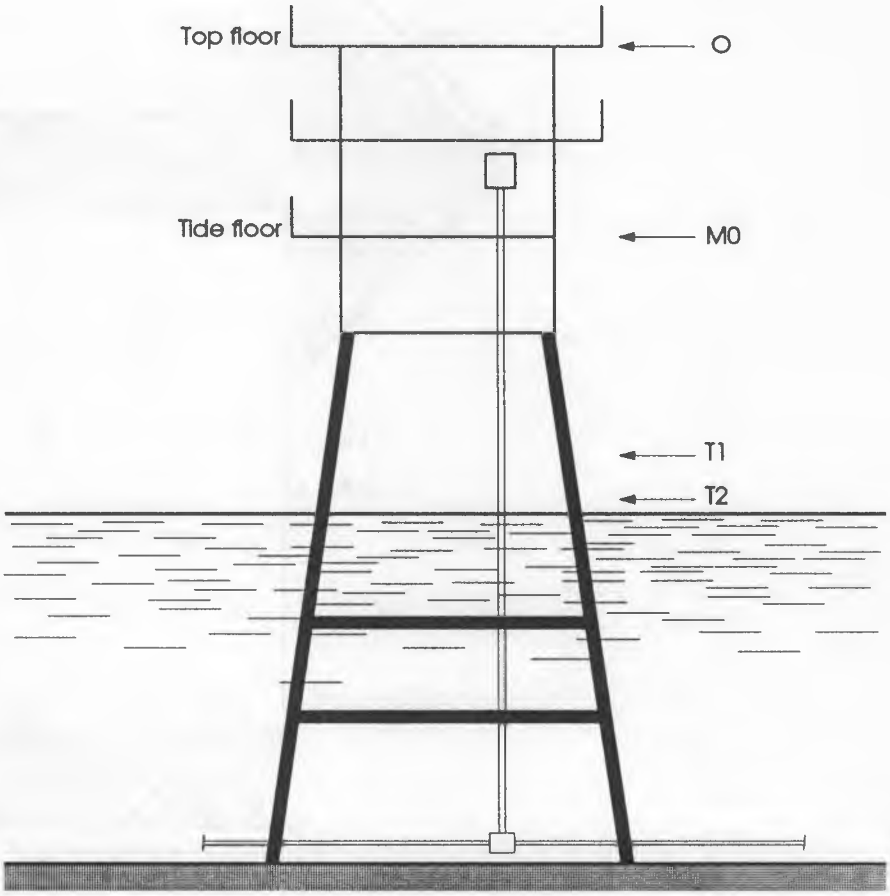

that the rms's of the coordinates are always lower than the *a priori* errors, being normally less than 3 mm for all vectors. This indicates a good repeatability of the measurements.

The final values (arithmetic averages) of the vectors in both local and global system are summarized in Table D–17 and Table D–18, where the latitude and longitude values are:

Lat = 45.314167° = 45° 18′ 51″

Lon = 12.508333° = 12° 30′ 30″

The overall error budget, including systematic and random errors, stays within 5 mm.

FIGURE D–7 Plan of the top floor

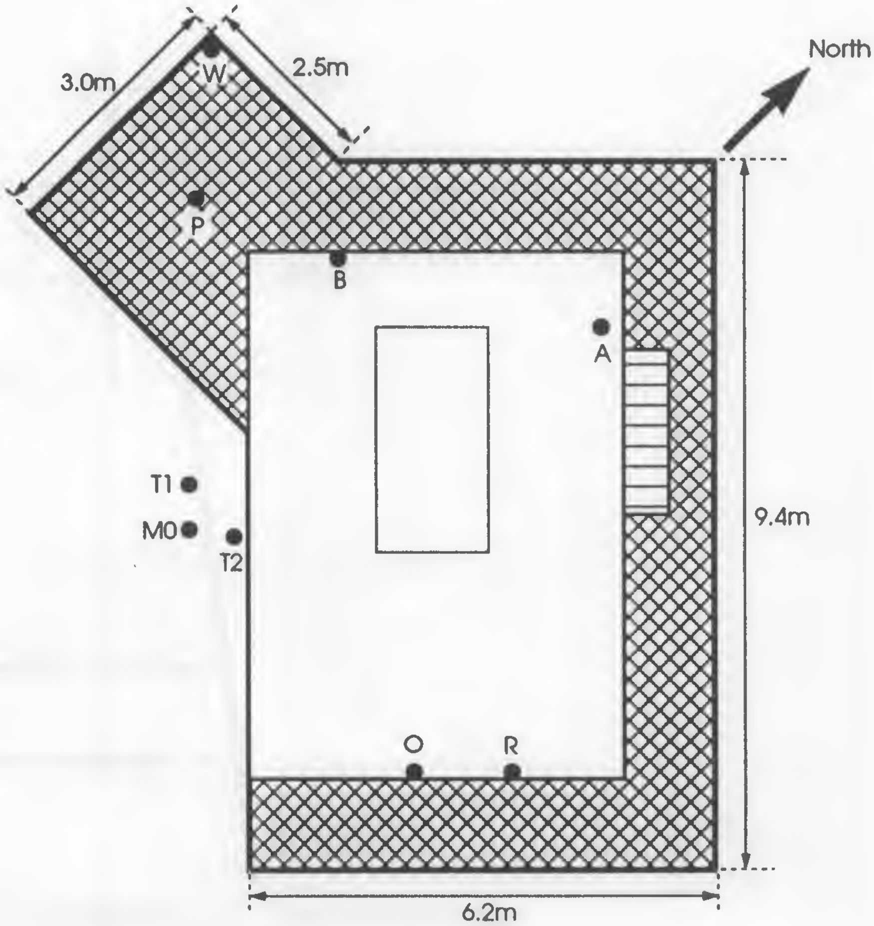

FIGURE D–8 Identification of the Tower reference points

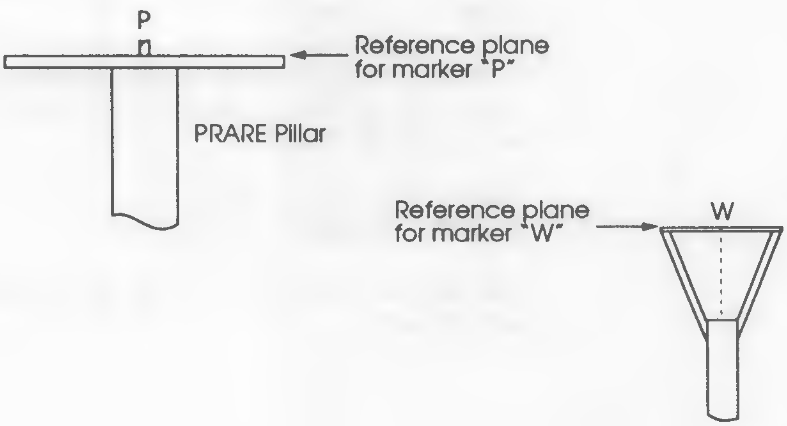

FIGURE D–9 Vectors in the local reference system

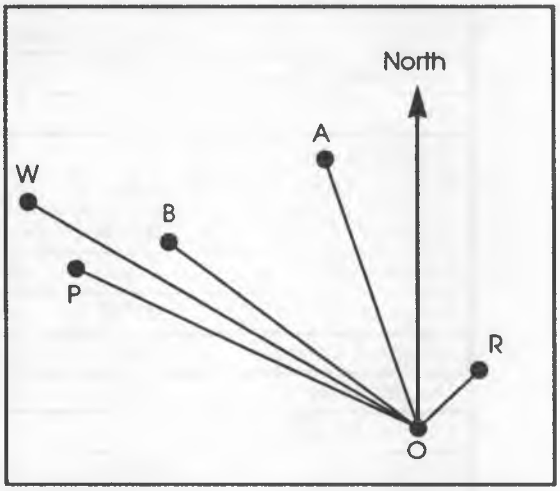

TABLE D–12 Summary of vector A–O from 4 measurements

	Up (m)	East (m)	North (m)	Distance (m)
Arithmetic Averages	0.019444	-2.133278	6.175697	6.533796
rms	0.0014	0.0031	0.0019	0.0028
Residuals:				
Origin in "O"	-0.0002	-0.0018	0.0012	0.0017
Origin in "A"	-0.0021	-0.0019	0.0016	0.0021
Origin in "B"	0.0006	0.0053	-0.0033	-0.0048
Origin in "O"	0.0017	-0.0015	0.0005	0.0009
Weighted Averages	0.019357	-2.134867	6.175346	6.534493
Weighted rms	0.0015	0.0011	0.0021	0.0023
Weighted Residuals:				
Origin in "O"	-0.0001	-0.0002	0.0016	0.0010
Origin in "A"	-0.0020	-0.0004	0.0019	0.0014
Origin in "B"	0.0007	0.0069	-0.0029	-0.0055
Origin in "O"	0.0018	0.0000	0.0008	0.0002
A Priori Errors	0.0047	0.0017	0.0027	0.0030

TABLE D–13 Summary of vector B–O from 4 measurements

	Up (m)	East (m)	North (m)	Distance (m)
Arithmetic Averages	-0.007936	-5.713047	4.303917	7.152809
rms	0.0011	0.0036	0.0018	0.0039
Residuals:				
Origin in "O"	-0.0007	0.0004	0.0005	0.0000
Origin in "A"	-0.0008	-0.0053	0.0017	0.0053
Origin in "B"	-0.0005	0.0049	-0.0029	-0.0057
Origin in "O"	0.0020	0.0000	0.0008	0.0005
Weighted Averages	-0.007830	-5.712592	4.303571	7.152046
Weighted rms	0.0012	0.0034	0.0017	0.0036
Weighted Residuals:				
Origin in "O"	-0.0008	-0.0001	0.0008	0.0008
Origin in "A"	-0.0009	-0.0058	0.0020	0.0060
Origin in "B"	-0.0006	0.0045	-0.0026	-0.0050
Origin in "O"	0.0019	-0.0004	0.0011	0.0012
A Priori Errors	0.0047	0.0025	0.0022	0.0030

TABLE D–14 Summary of vector P–O from 4 measurements

Up	(m)	East (m)	North (m)	Distance (m)
Arithmetic Averages	0.708721	-7.845904	3.698890	8.703004
rms	0.0011	0.0070	0.0028	0.0074
Residuals:				
Origin in "O"	-0.0003	0.0075	-0.0040	-0.0085
Origin in "A"	-0.0009	-0.0113	0.0039	0.0118
Origin in "B"	-0.0007	0.0033	0.0007	-0.0028
Origin in "O"	0.0019	0.0005	-0.0007	-0.0006
Weighted Averages	0.708990	-7.845803	3.697486	8.701474
Weighted rms	0.0012	0.0071	0.0023	0.0068
Weighted Residuals:				
Origin in "O"	-0.0006	0.0074	-0.0026	-0.0069
Origin in "A"	-0.0012	-0.0114	0.0053	0.0133
Origin in "B"	-0.0010	0.0032	0.0021	-0.0012
Origin in "O"	0.0016	0.0004	0.0007	0.0010
A Priori Errors	0.0051	0.0031	0.0019	0.0030

TABLE D–15 Summary of the vector W–O from 2 measurements

	Up (m)	East (m)	North (m)	Distance (m)
Arithmetic Averages	1.286566	-8.921131	5.191056	10.401389
rms	0.0001	0.0016	0.0015	0.0021
Residuals:				
Origin in "O"	0.0001	0.0016	-0.0015	-0.0021
Origin in "B"	-0.0001	-0.0016	0.0015	0.0021
Weighted Averages	1.286602	-8.920500	5.190720	10.400683
Weighted rms	0.0001	0.0014	0.0015	0.0020
Weighted Residuals:				
Origin in "O"	0.0001	0.0009	-0.0012	-0.0014
Origin in "B"	-0.0001	-0.0022	0.0019	0.0028
A Priori Errors	0.0051	0.0033	0.0018	0.0030

TABLE D–16 Summary of vector R–O from 2 measurements

	Up (m)	East (m)	North (m)	Distance (m)
Arithmetic Averages	0.015852	1.380695	1.331822	1.918417
rms	0.0017	0.0010	0.0002	0.0009
Residuals:				
Origin in "A"	-0.0017	0.0010	0.0002	0.0009
Origin in "O"	0.0017	-0.0010	-0.0002	-0.0009
Weighted Averages	0.016422	1.380741	1.331714	1.918129
Weighted rms	0.0016	0.0010	0.0002	0.0008
Weighted Residuals:				
Origin in "A"	-0.0022	0.0010	0.0003	0.0011
Origin in "O"	0.0011	-0.0010	-0.0001	-0.0006
A Priori Errors	0.0051	0.0022	0.0029	0.0030

TABLE D–17

Vectors in the local reference system (m)

MARKER	Up	East	North	Distance
"O"	0.0000	0.0000	0.0000	0.0000
"A"	0.0194	-2.1333	6.1757	6.5338
"B"	-0.0079	-5.7130	4.3039	7.1528
"P"	0.7087	-7.8459	3.6989	8.7030
"W"	1.2865	-8.9211	5.1910	10.4014
"R"	0.0158	1.3807	1.3318	1.9184

TABLE D–18

Vectors in the global reference system (m)

MARKER	X	Y	Z	Distance
"O"	0.0000	0.0000	0.0000	0.0000
"A"	-3.8111	-3.0306	4.3567	6.5338
"B"	-1.7554	-6.2414	3.0209	7.1528
"P"	-0.3816	-8.1213	3.1050	8.7030
"W"	-0.7877	-9.3128	4.5652	10.4014
"R"	-1.2126	1.1453	0.9478	1.9184

D.3 Tide Gauge Reference

On the first floor are located the two tide gauge recorders. The marker "M0" is located as an intermediate reference point compared to marker "O". Marker T1 is the main reference marker for the tidal measurement and marker T2 is an additional reference marker. The measurements have been done with a calibrated meter, with 2.0 millimetre accuracy over a 10 meter range. Figure D–6 shows the location of the markers M0, T1, T2. The results of the measurements are shown in Table D–19

TABLE D–19 Summary of the tide gauge measurements (mm)

	Time	M0–T1	M0–T2	O–M0	O–T2	O–A	O–B
08/08/91				6005.0		-19.4	8
30/01/92	16:30	6160.8					
	18:00	6164.0	6337.0				
	19:00	6163.3	6337.5				
31/01/92	09:00		6336.5	6005.5	12342.0	-19.0	10
	10:00		6335.0	6006.5	12341.5	-19.0	10
	11:30	6162.5	6337.0	6006.5		-19.5	9
	12:00	6163.0	6336.5				
	13:00		6335.5	6005.5	12341.0		
Average		6162.7	6336.4	6006.0	12341.5		
Std. Dev.	1.2	0.9	0.6	0.6			

The calculated distances resulting from these measurements are:

T1–T2 = 173.8±0.7mm

O–T1 = 12168.7mm

O–T2 = 12342.4mm

The measurement of the reference level was done in the following way. A sketch of the reference mark with centrally the exact target P is shown in Figure D–10. A rigid plastic transparent cover (also shown in Figure D–10) was placed against the supporting steel beam. The circular closure *r* in Figure D–10 is made of rubber, but at two opposite points a small passage was left, so that, if done on a calm day, the water level inside was calm, and perfectly representative of the actual sea level outside. Figure D–11 shows all of the reference marks which were installed, while Figure D–12 shows the mark ① uncovered and Figure D–13 shows the plastic cover in position.

The horizontal surface of the mark, about 4×4 cm, is slightly inclined with a slope of approximately 1:20. This allows a much higher sensitivity in establishing the moment at which the edge of the water reaches the reference notch P at the centre of the "horizontal" surface. Assuming a sensitivity of 5 mm in establishing the position of the water edge, this corresponds to

FIGURE D–10 The reference plate welded to the tower structure. The dimensions are 4 x 4 cm. The exact target is the central notch P. (b) The plastic transparent cover around the plate.

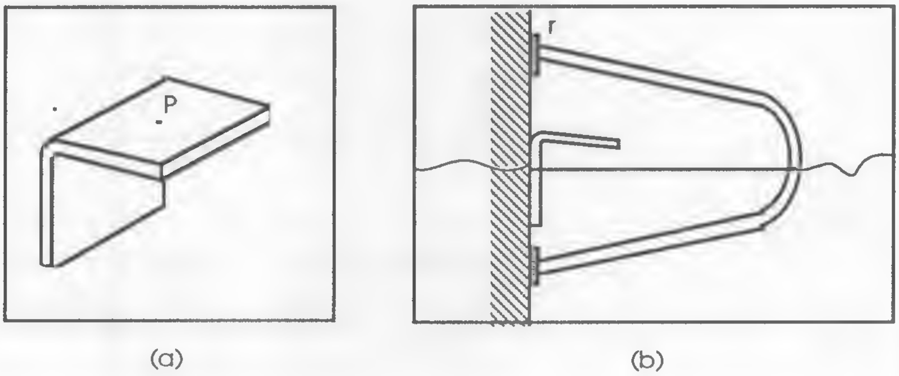

0.35mm in the determination of the actual sea level. Figure D–14 shows the position of the survey mark T1 (corresponding to the "tidal" reference mark ②) with respect to the structure of the tower. Note that two further marks (① and ③) had been prepared, but ① was unusable because of its position, and ③ was broken by an unknown vessel before the corresponding measurement of its position by Telespazio could be done.

D.3.1 Astronomical Azimuth Orientation

The astronomical azimuth orientation of the network has been determined by observations of Polaris, from the monument "O", performed on 9

FIGURE D–11 Positions of the reference marks T1 and T2, and the other marks 2 and 3.

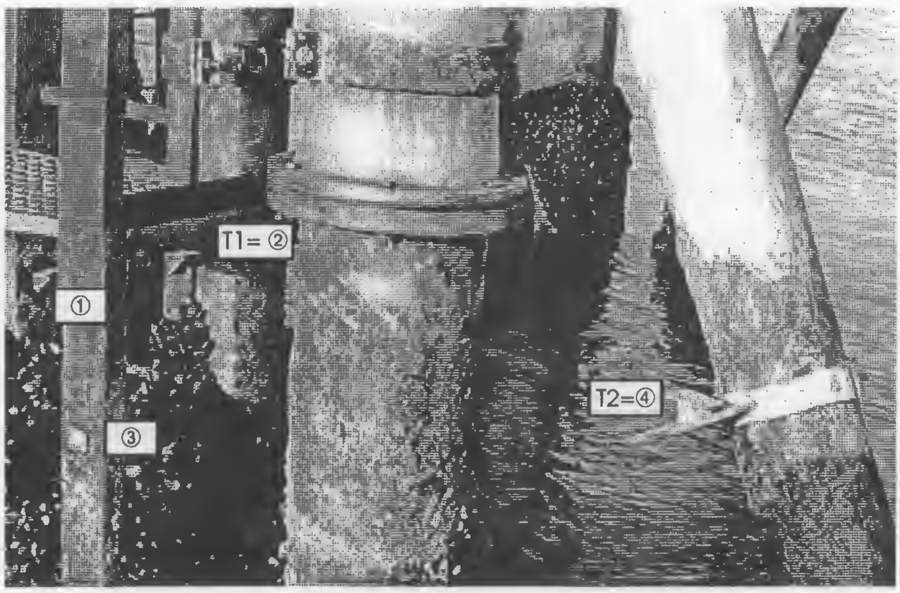

FIGURE D–12

The reference mark ① uncovered, in a view looking down the access steps.

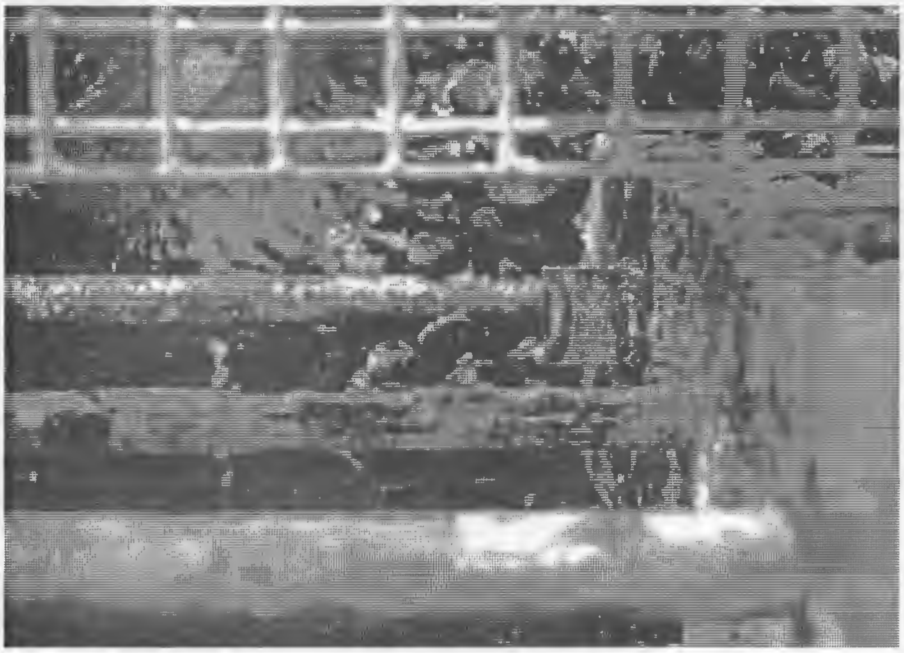

August 1991. The results of these observations are summarised below. Marker "A", has been used as the terrestrial reference. The columns MARKER "A" show the azimuth values (grades) of reference points with respect to the astronomical north, taking into account the calculated anom-

FIGURE D–13

The plastic cover over the reference plate.

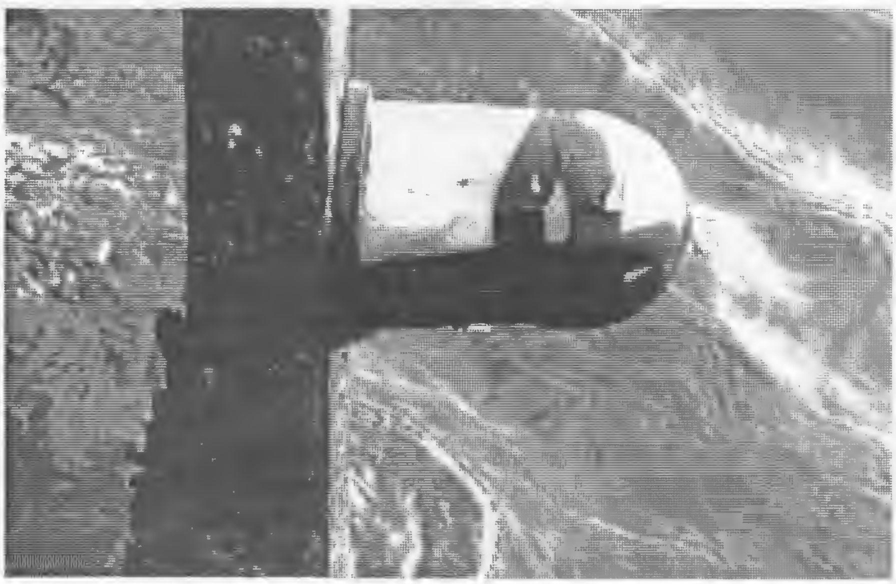

FIGURE D–14

Position of three mof the marks on the structure of the tower. Of the three present, T1 (②)is the primary reference, ① was not used, and ③ was broken off. The ladder is the one between the two tide wells.

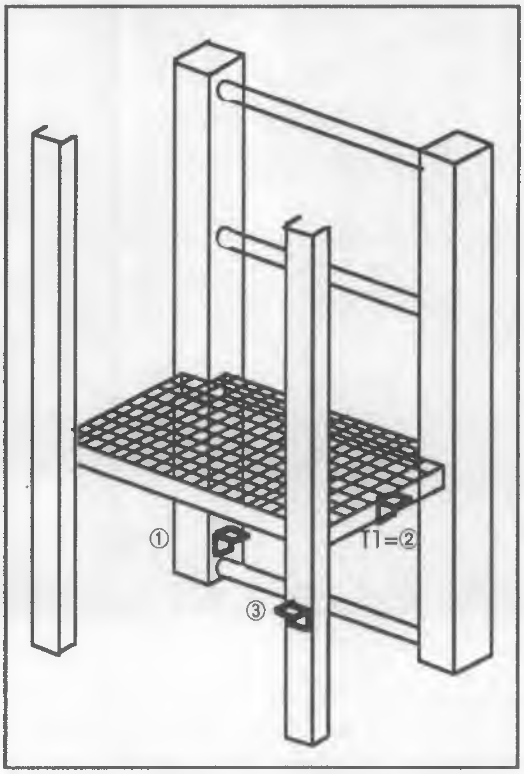

aly of the star, corrected with astronomical tables (IAU, 1990). The rms of 2.2 mgrades indicates a good repeatability of the measurements.

STATION:	BAIAMONTE MARKER "O"
OBSERVERS:	DEL ROSSO/AMBRICO
TERR.DIRECT:	MARKER "A"
OBSERVED STAR:	POLARIS 907
DATE:	09 August 1991
LAT:	45° 18′ 51″
LON:	12° 30′ 30″

UT Time	MARKER "A"
21:07:26	378.8144
21:19:51	378.8160
22:15:54	378.8122
22:28:05	378.8102
22:32:13	378.8138

AVERAGE = 378.8133

STD DEV = 0.0022

D.4 Equipment Description and Calibrations

The following instruments have been used for the survey measurements:

- Theodolite KERN, model DKM2-AE
- Distance meter KERN, model DM503
- WM 102 and TRIMBLE 4000 GPS RECEIVER

The distance meter is mounted directly on the theodolite; therefore the readings are referred at theodolite reference. The distance meter with guaranteed accuracy of ±3 mm ±2 ppm has been checked by comparison with a measuring tape at distances between 5 and 20 meters, and differences less than 3 mm have been found.

ANNEX E

Site Selection and Preparation

E.1 Summary

For the calibration of the ERS-1 Radar Altimeter, the Satellite Laser Ranging (SLR) system should ideally be located directly on the ground track at the calibration point. In the Venice scenario, where this calibration point is located at the CNR tower off the coast near Venice, this ideal situation is impossible to realize, because the SLR system comprises one truck-load of equipment which cannot possibly be deployed at the CNR tower.

The selection of the Baiamonte site for the mobile laser site has proven to be, *a posteriori*, a very successful one in spite of the fact that other sites were originally considered more suitable. The choice of Baiamonte resulted from compromising on a number of constraints, some of which were well known in advance, others came in somehow unexpected. Basic scientific and logistic considerations indicated that the Colli Euganei were suitable to host the selected site. The necessary (though not sufficient) conditions to be fulfilled by the selected site were, in fact, nearness to Venice, to the highway system, airport and hotels, reasonable elevation and sky visibility. Alternative areas, such as Lido of Venice or the Asiago Observatory were also considered but, after careful examination, were put on a lower priority level because failed to meet all the necessary conditions.

Finding a suitable place on the Euganei Hills was not a simple task: the ideal place had to be owned by a Organization willing to work with us, had to be safe for the crew and the equipment, geologically stable and with clear sky down to 15-20° elevation. The presence of a large installation of the Italian Air Force on the highest hill, Monte Venda (601 m) on the one side, and the existence of an official agreement of general cooperation between the Italian Air Force and the *Consiglio Nazionale delle Ricerche* on the other side suggested that, while working on parallel options, a negotiation had to be started with the Military Authority to find out whether we could have positioned the laser site within the military area. The delicate task of the negotiation was undertaken by Franco Dallaporta, Director of the *Instituto per lo Studio della Dinamica delle Grandi Masse* of CNR in Venice, who fortunately interfaced with enthusiastic, very practical and cooperative Officers.

Below the activities related to the site selection are summarized. The following persons have participated in one or more field trips for this selection: Dr. Giuseppe Bianco (*Agenzia Spaziale Italiana*), Prof. Alessandro Caporali and Prof. Roberto Sedea (University of Padova), Dr. Alberto Cenci (Telespazio, SpA.), Dr. Richard Francis (ESTEC), Ing. Danny van Loon and ir. Erik Vermaat (Delft University of Technology). Telespazio SpA. has been responsible for the implementation of the laser site.

E.2 Chronology of the field trips and related activities

E.2.1 Colli Euganei

On 11 April 1990, the Colli Euganei area was visited to explore the feasibility of a laser site at any of the accessible hills. During the visit to Monte Venda, the party was accompanied by Dr. Gianfranco Dallaporta (ISDGM) and Prof. Roberto Sedea (University of Padova). Prof. Sedea gave a brief overview of the geological history of the area.

E.2.1.1 Geology

The Colli Euganei are of tertiary volcanic origin and occur in the foreland of both the south Alpine and Appennine thrust belts, suggesting a large stability. Most parts are covered with mesozoic and tertiary limestone. As could be seen during the trip, this limestone appears rather undisturbed, mostly horizontally stratified, but quite strongly weathered and broken. Solid volcanic bedrock is covered by a thin quaternary layer. The Colli Euganei are technically speaking enclosed between two strike-slip fault lines, extending SE-NW at the west side and S-N at the east side of the hills. However in the area no significant seismicity is noted. Towards the north east, the northernmost part of the Adriatic Promontory is tectonically overlaid by the South-Vergent Pre-Alpine units. There, seismicity is quite evident, increasing further north.

During the field trip, practically every accessible hilltop of the Colli Euganei was visited and inspected for feasibility for a SLR site.

E.2.1.2 Monte Grande (481 m)

The access road uphill is of dubious quality, especially the upper part. At the top of the hill a large spherical radome is situated, which houses a weather radar system, according to our escort. Immediately next to this construction a hole had been dug out to about 2 meters depth, as it appeared to install drain pipes, showing highly fractured material all the way down with occasional larger limestone blocks. Constructing a stable site here would be a major technical problem. At the hill top there is no space for a site and the view is severely obstructed by the radar. About 50 m downhill there is a plateau which is marginally accessible, but from there the view is blocked by the hill top in approximately northern direction (50 or 60 degrees elevation).

E.2.1.3 Monte Madonna (526 m)

At the top a monastery is located, which is well kept and obviously drawing a great deal of tourism. The remaining area is taken by a radio and/or TV broadcast station. There is no option for a laser site.

E.2.1.4 Monte Gallo (385 m)

As a typical example of a commercial radio/TV broadcast station (on private property) the facility at Monte Gallo was visited. The installation included omni-directional VHF/UHF antenna's and point to point microwave antenna's. Additional microwave antenna's were being installed. There is a reasonable clearance at the hill top but the view is severely obstructed by the antenna's and by some power lines. Private ownership makes near term availability unlikely.

E.2.1.5 Monte Gémola (415 m)

Near the hill top a farmhouse with additional buildings and an enclosed yard is situated (*Villa Beatrice d'Este*) which is managed by the *Consorzio per la Valorizzazione dei Colli Euganei*, an organization of the local government of Veneto. Nearby, at the hill top there is a clear area covered with grass, bordered on the south side by a vineyard. The clear view all around is excellent with only a few trees giving some obstruction at low elevation. The major problem at this location is caused by the fact that the only access is through two gates, the lower one of which limits the vertical clearance to 3.52 m or less, and the other one limiting the horizontal clearance to 3.00 m. A stable pad construction appears to be feasible because a large quite horizontal area is available, although similar precautions would have to be taken as described for Monte Venda. It could not be expected that there would be any kind of facility available, apart from some minor support (sanitary, telephone?) at the farmhouse. A power generator running continuously at the hill top, might cause quite an annoyance to inhabitants of the area. With the restrictions as indicated, this location was initially considered to be an option for the SLR site.

E.2.1.6 Monte Cinto (283 m)

This hill is located immediately west of Monte Gémola and is almost completely covered with trees. We were informed that this is not government property and therefore no further investigations were made.

E.2.1.7 Monte Cero (415 m)

This hill is at the top completely occupied by a major radio/TV broadcast facility, together with directional microwave installations. Downhill no options for a site could be found.

E.2.1.8 Monte Lozzo (324 m)

The hill top is inaccessible. A road of dubious quality reaches a quarry which is obviously still in production. In that area no realistic options for a site could be found.

E.2.1.9 Monte Venda (601 m).

Preparatory contacts had been made by Dr. F. Dallaporta and Prof. A. Caporali with the Italian Air Force group, operating a military facility on the upper part of Monte Venda. The party was welcomed by Major Vincenzi, who escorted us during the visit of the facility. The hill top is occupied with antenna's of various kind, together with small buildings for equipment. Although no specific information could be obtained, the facility appears to be a communication site deploying VHF/UHF omni-directional broadcast and many point to point microwave antenna's. Vincenzi referred to a commercial broadcast transmitter, 1 km away at 9 kW power. At the west side of the hill top, outside the military area, commercial TV broadcast antenna's could be seen (omni-directional, VHF and/or UHF). In between the military antenna's a primary triangulation point is located. A new fence was being installed immediately surrounding the military installations at the hill top, leaving only a small, quite strongly sloped area, cut in two by the access road, as an option for a laser site. There is practically no space for manoeuvring the truck of the SLR system, and the view is severely obstructed by the antenna's to at least 45 degrees elevation in westerly direction. If there is a problem with RF interference in the SLR system at all, it is likely to occur at this location in view of the nearness of the radio antenna's. About 50 m downhill, south of the main access road, a quite horizontal clearance of about 30×100 m can be found, bordered at the end by the ruins of an old monastery. At the entrance to the clearing, next to the main road, there is a small building used for storage. This small plateau definitely is an option for a SLR site, although the exact location of the platform must be chosen very carefully, in view of the necessity of a clear view down to 20 degrees elevation in all directions. Potential obstruction is caused by the monastery (south) and the hilltop itself, covered with trees on this side (west) and trees across the road (north). Of major importance also is the stability of the platform and in particular its monumentation, requiring removal of all loose surface material during the site construction. Access to this potential site location is excellent. There is an asphalt road at moderate slopes all the way to the site and even a parking facility very nearby.

At about 100 m further downhill, approximately at the north side of Monte Venda, a heliport can be found, where a GPS point has been secured which was observed recently. This location is excellent for its clear view in all directions, but the idea of a SLR site here was abandoned because the area is artificially constructed from dumped material on top of the natural slope of the hill, and no long term stability can be expected there.

Of major importance for a SLR site at Monte Venda is the accessibility in connection with the security regulations at this military facility. Imperative for operating the SLR system is access to the site by the crew at any time during night or day, without any prior notice. *A priori* identification of the individual crew members will of course be supported. Data communication with the external world can be accomplished via modem and commercial telephone, if a telephone connection will be made available to the site.

E.2.2 Asiago

On 12 April 1990 two locations of the Asiago Astrophysical Observatory were visited. Asiago is a small town located in the Altipiano di Asiago, about 50 km north of the town of Vicenza. The Asiago highland belongs to the active south-vergent thrust system of the South-Alpine border zone. The Observatory represents the major astronomical facility in Italy. There are two locations, the Pennar site and the Ekar site. Previous contacts had been made by Prof. A. Caporali (University of Padova) and Dr. G. Bianco (ASI) independently with the Director of the Observatory, Prof. Cesare Barbieri.

E.2.2.1 Pennar (1000 m)

This is a major facility with office buildings, a lodging house and two observatory facilities with astrodomes. We made no contact with anyone at this site, but we were informed that the major instruments deployed are a 0.67 m Schmidt camera and a 1.22 m telescope. There are expected to be various technical facilities (workshop, etc.) and we were told there is a VAX computer facility with DECNET connection to the outside world. A recently observed GPS point is located on a grass covered knoll in between the two astronomical domes. This knoll represents about the highest point in the area and would in principle be quite well suited for a SLR site. There is a clear view around and still some shielding from strong winds by trees from two sides. The area makes a well kept and friendly impression. Outcrop could not be seen at the surface and the stability issue requires further investigations, although no major problems are foreseen. Access to this area is of excellent quality, by asphalt road all the way.

E.2.2.2 Ekar 1360 m)

This site is dominated by a large observatory building with an astrodome housing the 1.82 m Cassegrain Astronomical telescope. There is also a facility for refurbishing the primary and a reasonably equipped mechanical workshop. This building is situated at the highest point in the area. Other facilities include some microwave directional antenna's and small buildings of various kind. In westerly direction the foundation has been constructed for an accommodation for the 1.22 m telescope at Pennar, which may eventually be moved to this site. Especially at this construction site it is evident that solid bedrock is not immediately available. The first few meters of the subsurface typically consist of strongly stratified, weathered limestone (*"arenaria"*). A stable construction would require careful removal of all loose and brittle material. The major problem at this location for a SLR site will be the absence of any shielding against strong winds, blizzards and thunderstorms. If an SLR site would have to be installed here, a semi-stationary setup would be advisable, with a housing of some kind to provide effective shielding, preferably including a dome.

E.3 Initial conclusions

In view of the ERS-1 calibration, the Euganei hill area is preferable for its occurrence in the stable foreland of the South-Alpine and Appennine thrust belts, for its nearness to the Venice tower and for the fact that accurate vertical geodetic connection to the Venice tower is available or can easily be obtained through GPS measurements. With respect to this vertical connection, Asiago would impose major problems because of the large elevation above sea level. In view of possible later use for Crustal Dynamics studies, the Euganei Hill area provides in principle stable opportunities with low seismicity, whereas the Asiago site would typically represent the mobile outer zone of the Pre-Alpine compression belt. Application to Crustal Dynamic studies requires an overall network planning for the whole Alpine region, in which Asiago could play an important role, together with a stable fiducial site in the Euganei hills. In view of its elevation Asiago would give excellent data yield with an optical technique such as SLR, while the Euganei hills, although at much lower elevation, are expected to be quite favourable too, because of the local elevation of a few hundred meters above the Po-plain area.

Consultations after the first field trip with representatives of the *Consorzio per la Valorizzazione dei Colli Euganei* made it clear that the prospect for a site at Monte Gémola had to be abandoned. Consequently the decision was made to give preference to the Monte Venda. The field trip to Monte Venda had confirmed that the Monte Venda had an excellent potential from the point of view of safety, lodging, access, local facilities, elevation and visibility (immunity from fog). However it was also rather clear that since the Monte Venda Base is deeply involved in Air Traffic Control and Military Communications, EMC (Electro-Magnetic Compatibility) could have posed a serious, perhaps insoluble problem. Additional concerns were: getting a timely formal approval from the Ministry of Defence, identifying the exact spot and doing all the necessary civil works in time for the launch. Finally, the practical implications of the rather strict regulations for the access to the area, though enforcing safety for the crew, their belongings and the equipment, were carefully examined.

E.4 A conflict of interests

After having obtained an informal and uncommitting "go ahead while the paper work is being done", the potential candidates for the final site within the Monte Venda base were checked for visibility, accessibility and EMC. Broad band surveys were done by Telespazio (see ANNEX F, "EMC Issues at Monte Venda") and the major noise sources (from our view point) were identified in space, time and frequency. Eventually an easily accessible site near the ruins of an old monastery was found to have the lowest level of EMC, though still high by normal standards. As soon as the civil works for the pad construction started, it was discovered that the selected site lay above ruins associated with the old monastery and therefore of archeological interest. The site had to be abandoned at once.

E.5 Baiamonte

There were not many options left. A new field trip was made on 14 November 1990, which suggested one alternative site, Baiamonte, which was very attractive on most aspects except access and EMC. It was decided to work on these two problems. Additional EMC measurements indicated that the ERP (effective radiated power) could have reached very high levels (1 kw) at unpredictable times, the transmitters being omni-directional and located about 10 m from the candidate site. However the statistics indicated that the events were mostly in day time and occasional, approximately 1/month, for a few minutes. Therefore it was decided to take the risk. In any case all the sensitive equipment was checked in The Netherlands with the help of ESTEC, simulating the EMC environment of Monte Venda on the basis of the field data, and the necessary countermeasures were identified and implemented on the laser station (see ANNEX F, "EMC Issues at Monte Venda").

The access to the site was of concern because of a sharp U-turn uphill, the view at the site was obstructed by some trees in the easterly direction and the site area would have to be flattened to permit manoeuvring of the truck of the laser ranging system. These problems were considered to be solvable and the construction of this site at Baiamonte started as soon as possible. By mid January 1991 the platform together with the required monumentation were available.

When on January 16, the Dutch laser ranging system MTLRS-2 arrived at the site, it became clear that the truck of that system could not pass the U-turn. This access problem was solved by downloading the equipment in parts to a medium size truck (see ANNEX G, "MTLRS2 Operational Aspects"). The subsequent operations at the Baiamonte site turned out to be very successful, and demonstrated that the selection of this site had been the right choice, although it resulted from compromising on a variety of different constraints.

ANNEX F

EMC Issues at Monte Venda

F.1 Introduction

A considerable electromagnetic compatibility (EMC) effect on the space-geodetic equipment being used in the calibration campaign, such as the Dutch transportable satellite laser ranging system MTLRS-2, GPS receivers and the PRARE transponder, could be expected during operations at Monte Venda caused by various powerful transmitters in the area. In view of the multitude of transmitter antenna's and their nearness to the site, the susceptibility of the equipment used has been of major concern from the onset of planning the campaign.

At Monte Venda itself various VHF/UHF omni-directional antenna's and many point-to-point microwave antenna's could be seen. The transmitting frequencies probably include 3 GHz and 12 GHz with unknown transmission power (military facility). RAI radio and TV transmitter antenna's are located in a tall mast at the west side of Monte Venda. The location at Baiamonte faced an antenna farm with omni-directional antenna's of a military installation less than 100 meters from the site location.

A local electromagnetic field could affect the equipment in three ways:

- introduce a bias and an increase in noise (RMS) in the laser ranging data;
- introduce high frequency disturbances in the mount servo motors of the telescope;
- prevent or disturb the reception of the GPS and PRARE signals.

To understand the real impact of the local RF field on the laser instrumentation, the following strategy has been followed:

1. a broad band frequency investigation was conducted at Monte Venda by Telespazio, utilizing an omni-directional wideband antenna and spectrum analyser;
2. test measurements with MTLRS-2 were made at the Kootwijk Observatory for Satellite Geodesy in The Netherlands, utilizing an interference probe, to check the response to the major spectral components found;
3. a pre-launch *in-situ* test was performed with MTLRS-2 at the Baiamonte site after applying grounding and shielding modifications to the system.

F.2 Broad band survey

Concerning GPS, the simplest thing was to bring a receiver to Monte Venda, turn it on and let it acquire data simultaneously with other receivers at sufficiently large distances, monitor the receiver during the tracking and check for suspicious noise in the data in comparison with the data collected by the other receivers. This was done during the October 1990 when the "Large GPS campaign" was performed, and no interference problem was reported. In any case a frequency survey was scheduled also for the L1 (1575 MHz) and L2 (1227 MHz) frequencies. PRARE was considered to be not a problem, as a directional antenna is used and the signal (as for GPS) is broad band.

Telespazio was asked to take action on the EMC measurements, since it had the necessary equipment and trained personnel to do this type of measurements. The instrumentation used was ADVANTEST model 4136 spectrum analyser coupled with a broadband, omnidirectional antenna. The measurements were done by Mr. di Giannantonio. The advice and contribution of Mr. Van Essen is also gratefully acknowledged.

The surveys took place on 26 May 1990 and 7 November 1990. The May survey covered two sites, "Hilltop" and "Monastery". The results indicated that, from the EMC viewpoint, Monastery, being out of line of sight to the transmitters located on the hilltop, had to be preferred to Hilltop, where several beacons and omnidirectional transmitters operated on commercial and military frequencies. Because this indication agreed with other indications of logistic and scientific nature, the Monastery site was put on top of the list of preferred sites. However this site was later found to fail to comply with archeological constraints and had to be abandoned. This is why a new survey was made in November 1990. The new candidate site was Baiamonte and data were taken there, as well as on the Monastery and Hilltop. RF–wise Baiamonte was the worst possible selection: about 10 transmitters were located in the small building at about 70 m distance, the nearest antenna being some 20 m from the candidate site. However the site was on bed rock, grounding from old, dismantled antennas was available, distance from Hilltop was about 1 km and other problems appeared solvable.

FIGURE F–1 EMC survey at the Monastery site, in the frequency range 0–500MHz

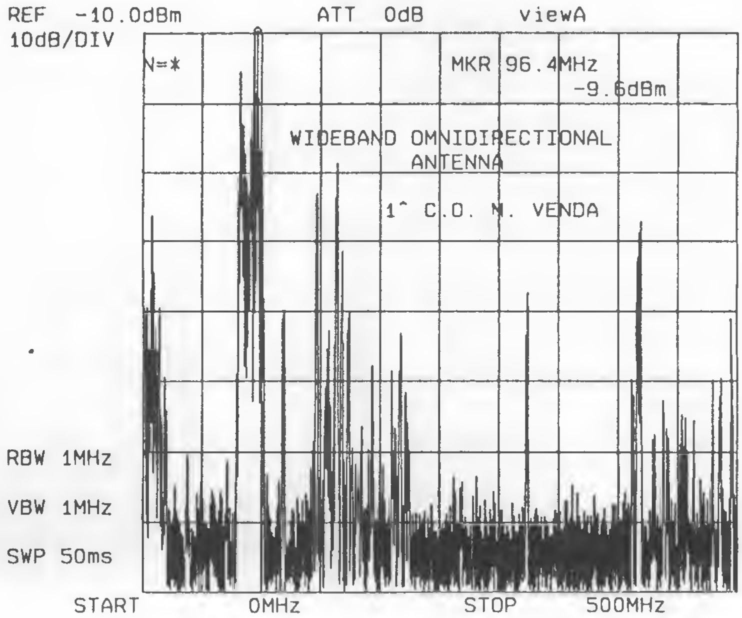

The surveyed frequency windows are listed in Table F–1, with reference to the figures containing the spectrum.

TABLE F–1 Cross reference of test measurements and sites

Site	Frequency (MHz)						
	0 – 500	500 – 1000	1000 – 2000	4 – 30	6.64 – 8.50	83 – 113	120 – 220
Monastery	Figure F–1	Figure F–4	Figure F–4	Figure F–4		Figure F–4	Figure F–4
Hilltop	Figure F–2	Figure F–4	Figure F–4	Figure F–4		Figure F–4	Figure F–4
Baiamonte	Figure F–3	Figure F–4	Figure F–4	Figure F–4	Figure F–4	Figure F–4	Figure F–4

Quite remarkable are Figure F–4 and Figure F–4, both referring to Baiamonte, without and respectively with the nearby transmitters broadcasting at full power (2kW).

Table F–2 summarizes the power and field associated with the most relevant spectral lines in Figure F–1 through Figure F–4. The worst case, (*ie* with the transmitters switched on) is indicated. In all frequency bands the EMC levels at Baiamonte are the highest among the three surveyed sites.

FIGURE F–2 EMC survey at the Hilltop, in the frequency range 0–500MHz

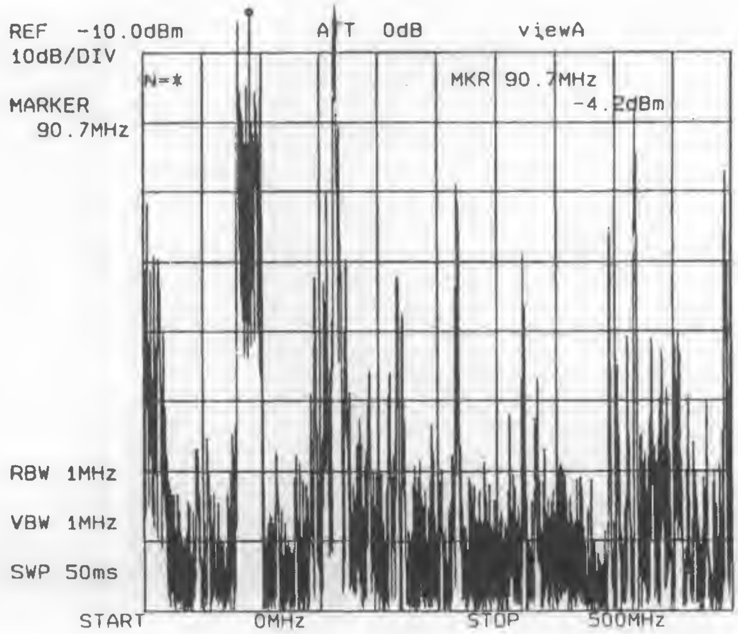

FIGURE F–3 EMC survey at Balamonte, in the frequency range 0–500MHz

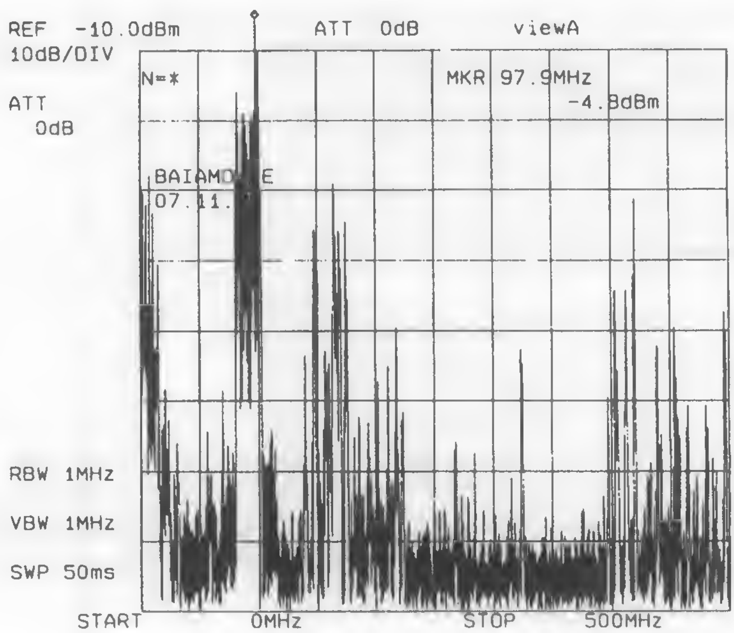

FIGURE F–4

EMC survey at the Monastery, in the frequency range 500–1000MHz

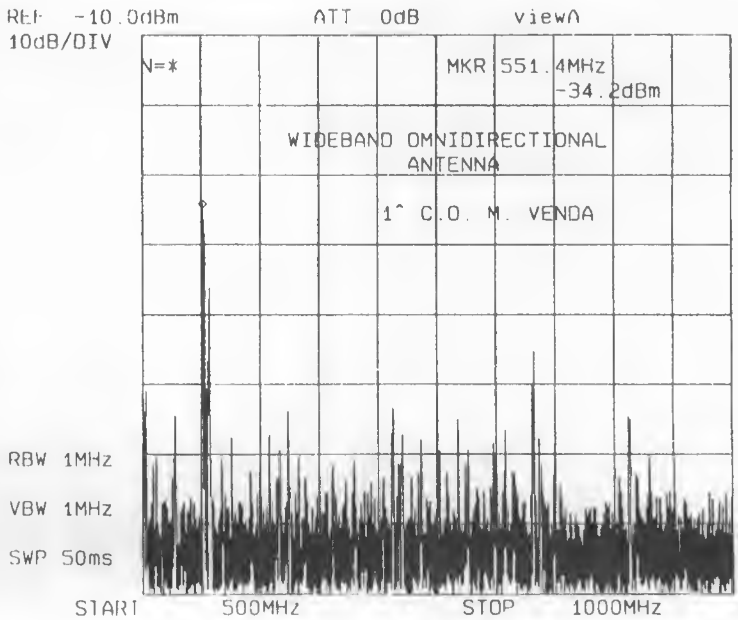

FIGURE F–5

EMC survey at the Hilltop, in the frequency range 500–1000MHz

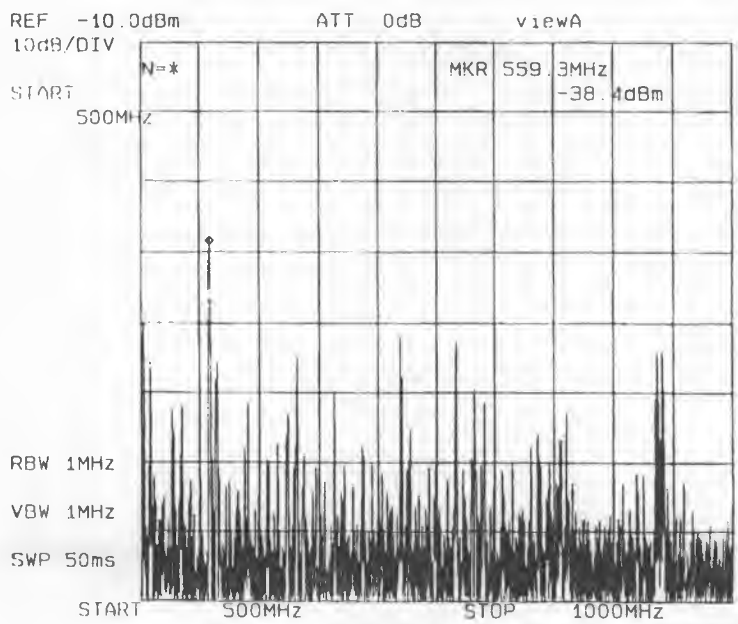

FIGURE F–6 EMC survey at Baiamonte, in the frequency range 500–1000MHz

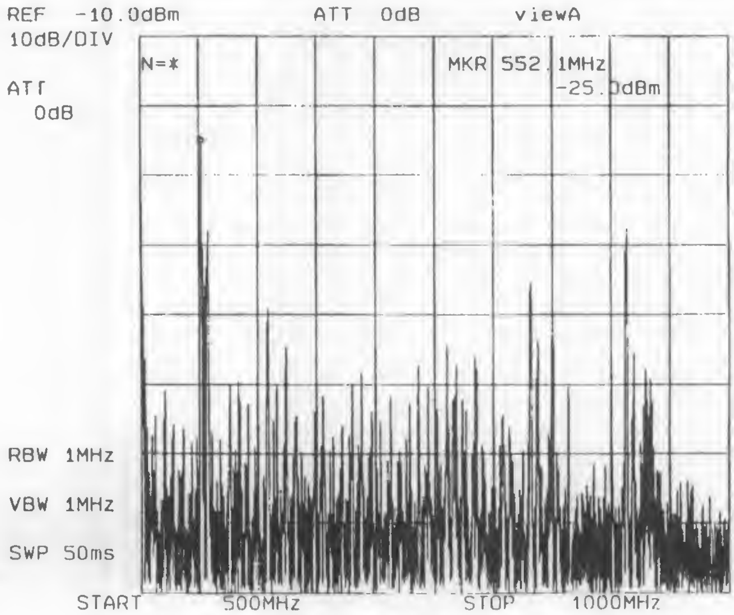

FIGURE F–7 EMC survey at the Monastery, in the frequency range 1000–2000MHz

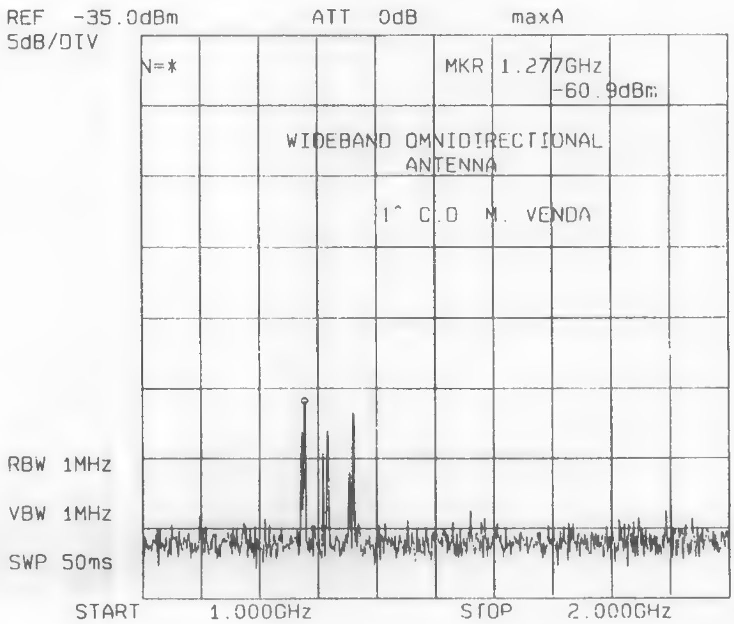

FIGURE F–8 EMC survey at the Hilltop, in the frequency range 1000–2000MHz

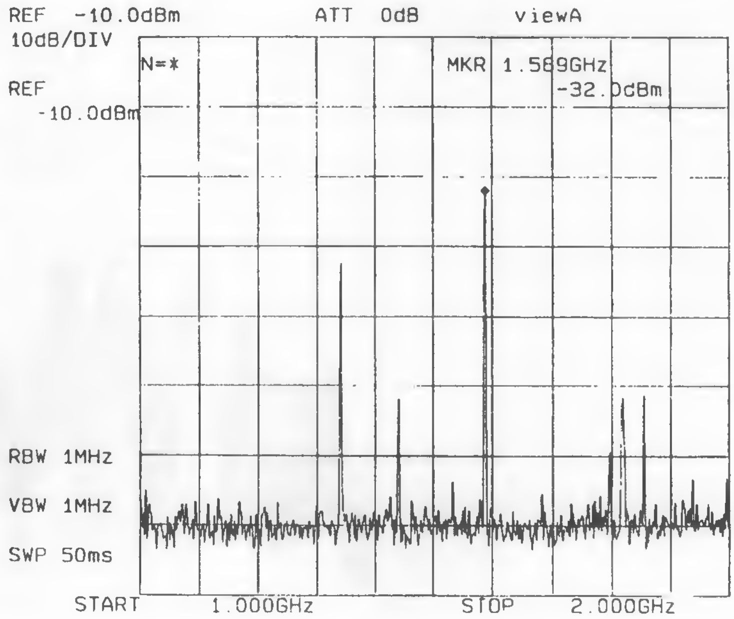

FIGURE F–9 EMC survey at Balamonte, in the frequency range 1000–2000MHz

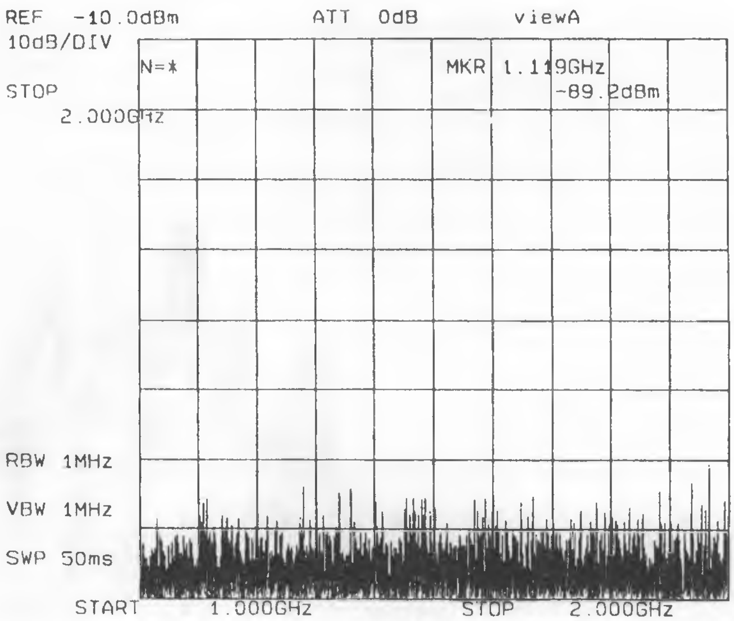

FIGURE F–10 EMC survey at the Monastery, in the frequency range 4–30MHz

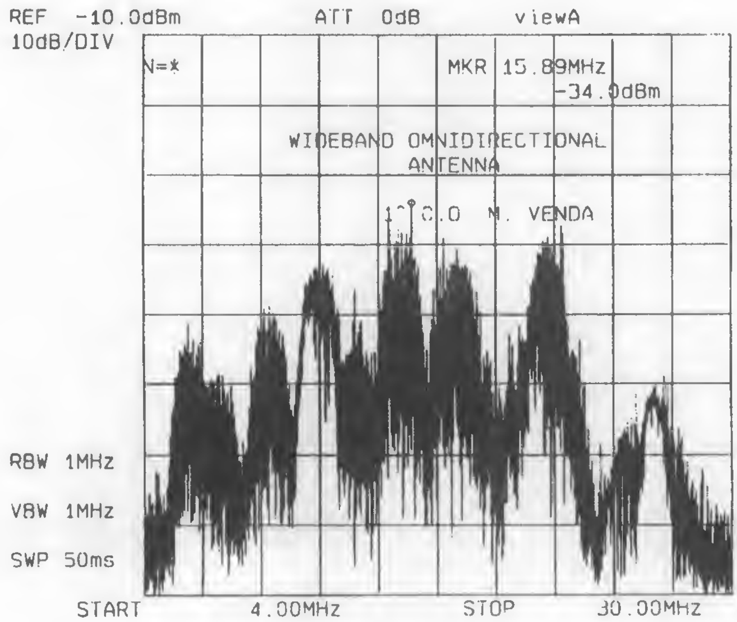

FIGURE F–11 EMC survey at the Hilltop, in the frequency range 4–30MHz

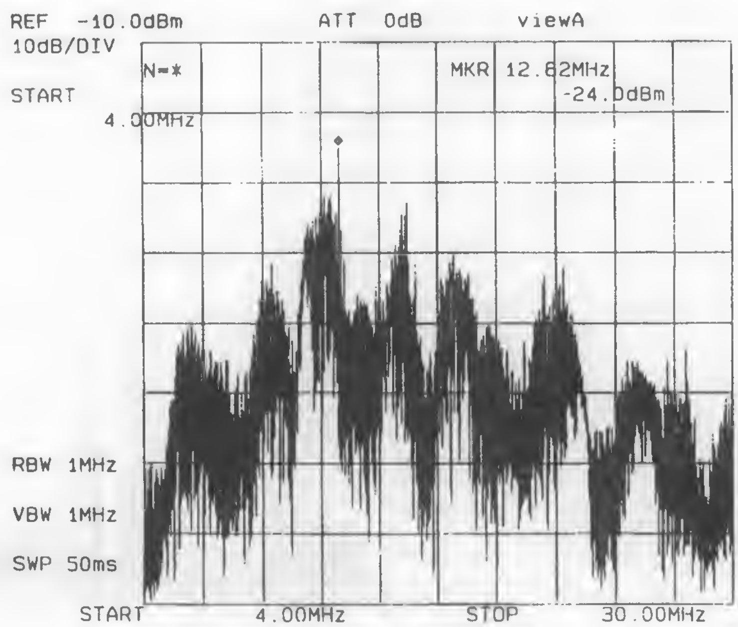

FIGURE F–12

EMC survey at Balamonte, in the frequency range 4–30MHz

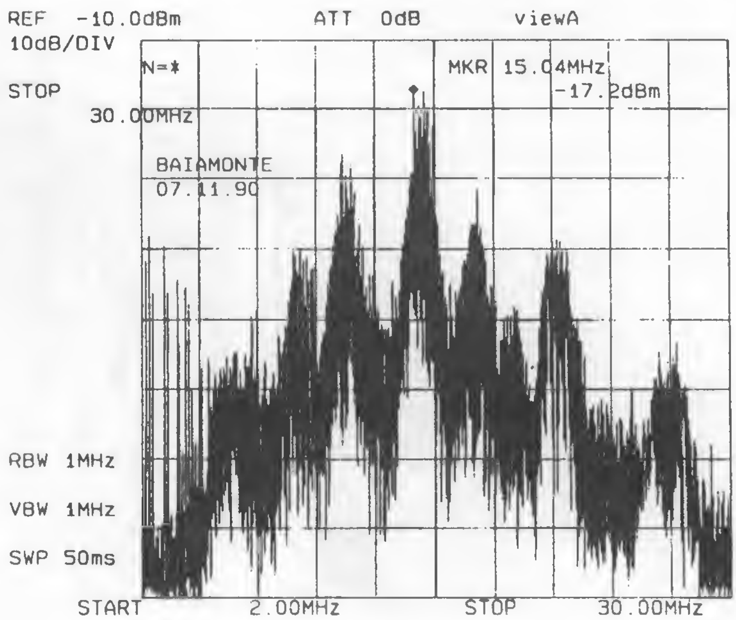

FIGURE F–13

EMC survey at Balamonte, in the frequency range 6.64–8.50MHz

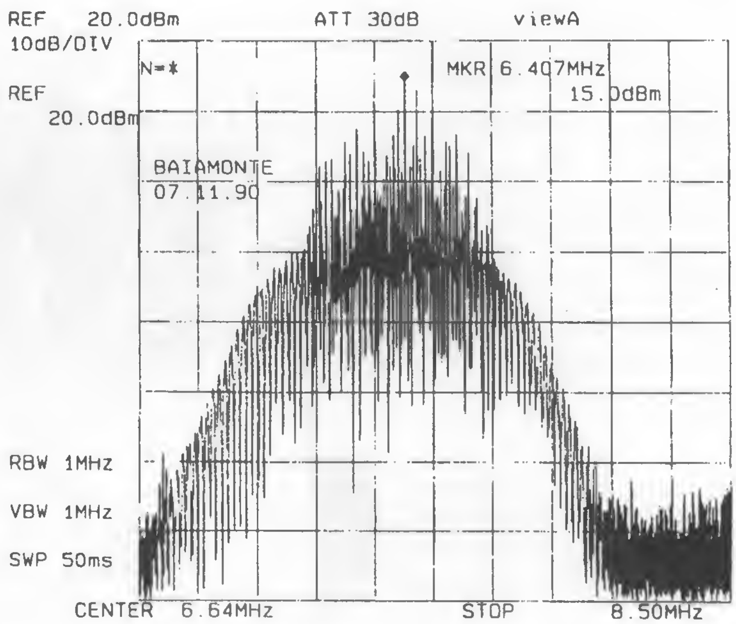

FIGURE F–14 EMC survey at the Monastery, in the frequency range 83–113MHz

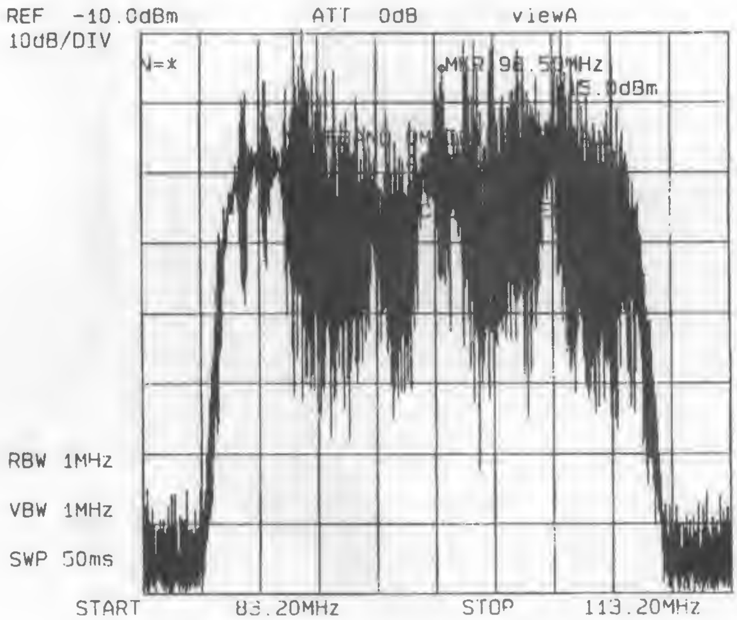

FIGURE F–15 EMC survey at the Hilltop, in the frequency range 83–113MHz

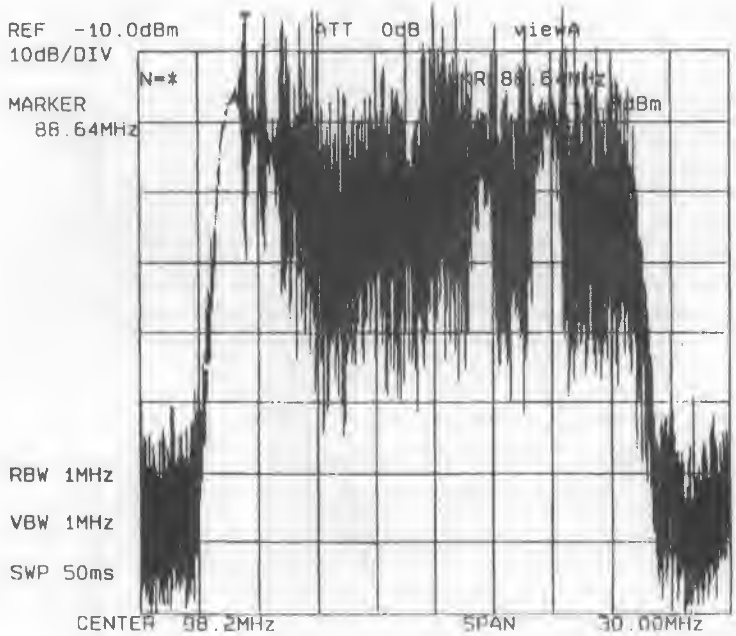

FIGURE F–16

EMC survey at Balamonte, in the frequency range 83–113MHz

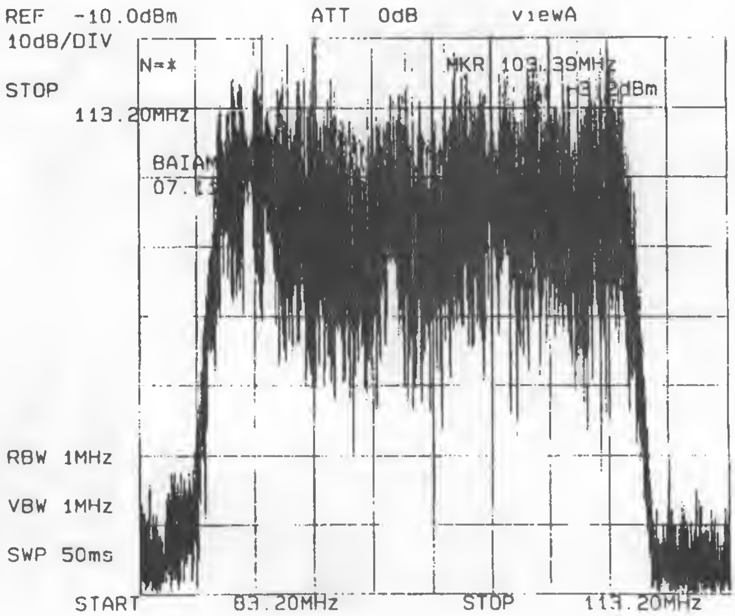

FIGURE F–17

EMC survey at the Monastery, in the frequency range 120–220MHz

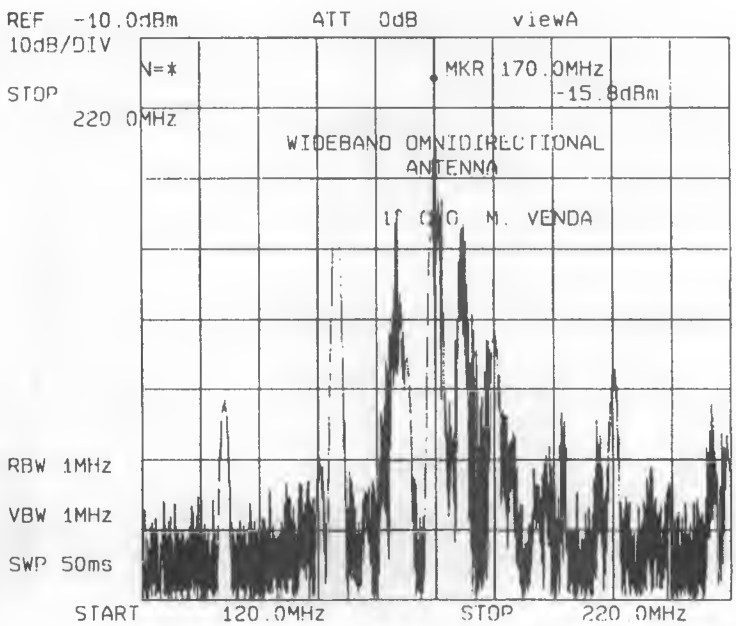

FIGURE F–18 EMC survey at the Hilltop, in the frequency range 120–220MHz

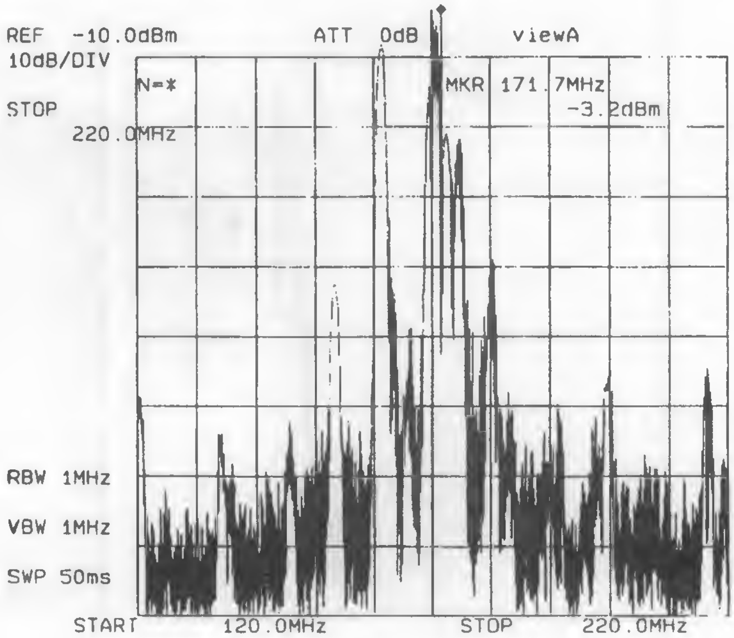

FIGURE F–19 EMC survey at Balamonte, in the frequency range 120–220MHz

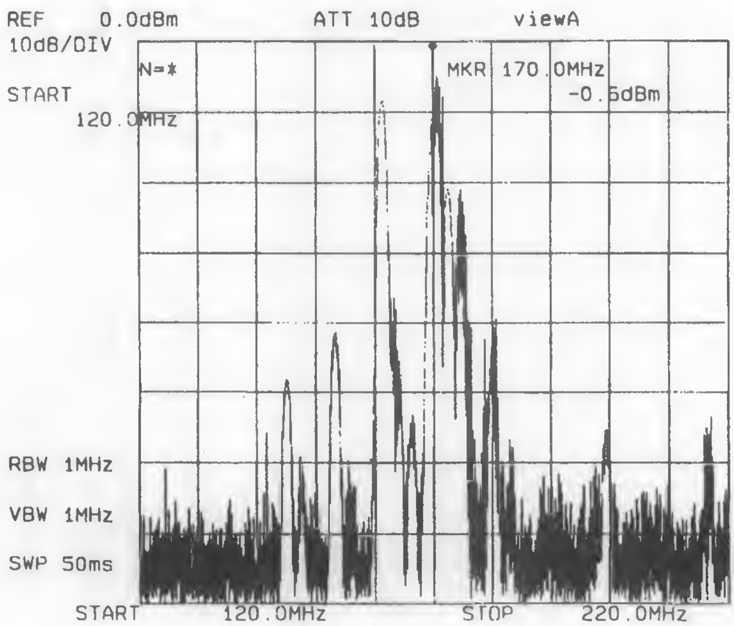

TABLE F–2 Summary of the radio interferences at Monte Venda

	Power (dBm)			Electric Field (mV/m)		
Frequency (MHz)	Monastery	Top of Hill	Baiamonte	Monastery	Top of Hill	Baiamonte
6.0			+15[1]			260[1]
12.6		-24			6	
16.0	-33		-17	2.5		16
88.0	-20	-4	-15	64	404	112
96.0	-7	-5	-4	320	402	450
103.0	-20	-10	-3	75	237	530
170.0	-12	-3	-1	303	875	1100
384.0	-40			28		
420.0	-29			110		
551.0	-25	-38	-25	228	51	228
1277.0	-45			52		
1589.0		-32			10	

1. with local antennas transmitting

F.3 Susceptibility tests with MTLRS-2 at Kootwijk

On 11 October 1990 test measurements were conducted at the Kootwijk Observatory for Satellite Geodesy (KOSG) to investigate the susceptibility of the MTLRS-2 to the level of RF interference which could be expected at the laser calibration site at Baiamonte. These test measurements were designed on basis of the information obtained from the spectrum measurements made earlier by Telespazio together with a listing of all critical cable connections between the cabin and the telescope cart (concerning frequency range, signal strength and trigger levels) made by the KOSG technical staff. The scenario for these tests was prepared by ESTEC technical staff in consultation with the technical staff at KOSG during the summer of 1990. Clearly the MTLRS has not been designed to minimize its sensitivity to EMC under such adverse RF conditions and therefore effects in many different parts of the system could be expected. Of major concern were the 11 meter long cables between the telescope cart and the control electronics of the system. During the tests, various frequencies in the range of 100-500 Mhz were injected utilizing a calibrated interference loop-probe connected around the signal cables simulating a 10 V/m field strength while the system was ranging in internal calibration mode.

Table F–3 represents the observed effect in calibration distances and RMS values when noise was induced in the signal cable at different frequencies, as compared to the noise-free reference measurement.

A slight increase in noise level and range bias could be noted at a frequency around 100 MHz which reflects the maximum frequency of the Constant

TABLE F–3 Results of radiated susceptibility tests on MTLRS-2

Frequency (MHz)	Distance difference (ns)	RMS difference (ns)
96	0.26	0.25
170	0.04	0.05
384	0.18	0.02
420	0.01	0.07
551	0.12	0.01

Fraction Discriminator (CFD) used in the range measurement. The CFD's compensate for amplitude variations of the start and stop pulse. These tests led to the general conclusion that maximum shielding should be realized by re-configuring the system according to the list below.

1. The control electronics should be placed inside a (fortunately available) small container made of aluminium sandwich panelling, which should be properly grounded.
2. The 11 meter connecting cables between the telescope cart and the control electronics should be replaced by a new set with minimum length of 2 meters, inserted in a shielded metal tube.
3. A special 30 meter DRACOVO 3-phase computer power cable should be used between the diesel power generator and the system. This cable contains five power wires which are doubly shielded by a copper and a steel mantle.
4. All shields used in the system should be connected to one 'star'-point. This point should be connected to an existing grounding point (fortuitously) available several meters from the platform, which had served as the ground for an old antenna. This connection itself should also be shielded. The entire grounding circuit is depicted in Figure 20.
5. It was also recommended to perform *in-situ* tests at Baiamonte with the modified configuration.

F.4 *In-situ* test measurements at the Baiamonte site

In the period of 16–29 January 1991 MTLRS-2 was installed at the Baiamonte site in the modified configuration and prepared for test measurements to investigate any further susceptibility of the system to the RF environment. The system was set up according to the recommendations above, with the telescope cart in its normal position on the platform and the small cabin, housing the electronics, placed nearby with a connecting 2 meter long metal tube through which the new short cable set was installed. These features are visible in Figure F–21. The two mains-power cables between cart and cabin were connected outside the metal pipe. The power generator was located at about 20 meters from the cabin and its 30 meter shielded power cable was laid out in a wide curve.

FIGURE F–20 The EMC Grounding Circuit

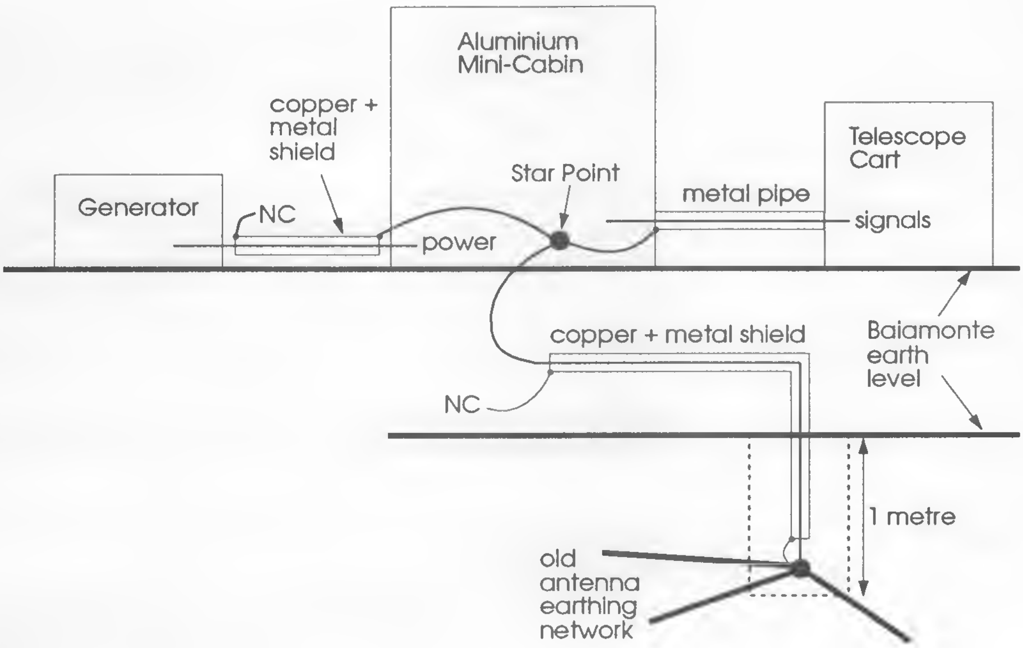

FIGURE F–21 MTLRS2 deployed at Monte Venda. The small enclosure for the electronics equipment, and the metal pipe through which the cables were run are easily visible

Basically two things have been tested:

- the range noise level (RMS) together with the range bias;
- the pointing stability of the telescope.

The measurements were performed while in internal calibration mode. Simultaneously the least significant digits of the mount positioning displays were monitored for jitter and independently the analog output signals for elevation and azimuth of the servo-amplifier were observed. Several 30 minute tests were made in the period of 24–26 January.

Ideally the nearby transmitters at Baiamonte should have been switched on and off during the tests, but some of these were remotely controlled and therefore, in spite of the support obtained from the military, only two of the transmitters were known to be on or off. Transmitter #1 radiated at a power of 2 kW and transmitter #2 with the nearest antenna at about 20 meters from the system, was low power, according to the available information.

Table F–4 represents the test results of the internal calibration distance and RMS at different field strengths generated by transmitters #1 and #2

TABLE F–4

Test results of the MTLRS2 internal calibration when transmitters #1 and #2 were operating.

Day	No.	Time	RMS (ns)	Calibration distance (ns)	Transmitters	
					# 1	# 2
24	1	10.15	.31	121.14	on	off
24	2	10.40	.32	121.22	on	off
24	3	11.00	.34	121.24	on	on
24	4	15.15	.32	121.27	off	off
24	5	15.37	.32	121.25	on	off
24	7	15.45	.32	121.25	off	off
25	1	09.55	.31	121.41	off	off
25	2	10.05	.32	121.42	on	on
25	3	10.10	.35	121.43	off	off
26	1	09.45	.32	121.42	off	off

Generally these results were better than those from the tests made at KOSG, which indicated that the modifications to the system configuration had been significant. The range bias and range noise appeared to be at the usual level and the mount positioning unit gave fluctuations of plus and minus 0.001° as normally expected. Noticeable fluctuations of plus and minus 0.003° have been noticed during only one of the tests. This effect could not be correlated to any of the switchable transmitters near the site because they were said to be switched-off at that particular time.

With the launch date of ERS-1 still being uncertain at that time and the necessity of starting the LAGEOS and STARLETTE campaigns, it was decided to maintain MTLRS-2 in the current configuration and to continue the remaining preparations for the mission.

Throughout the entire operational period at Baiamonte, which lasted from April until mid-September, no significant disturbances in the system were noted, in relation to RF interference, which demonstrated that the provisions taken, had been successful and sufficient.

ANNEX G

MTLRS2 Operational Aspects

The Satellite Laser Ranging (SLR) observations in support of the calibration of the Radar Altimeter of ERS-1 were planned to start as shortly as possible after launch, but in addition observations to the LAGEOS satellite were necessary for the determination of the Baiamonte position in the SLR frame of reference. These observations from Baiamonte could commence at earliest convenience and would continue side by side to the ERS-1 observations if necessary. In addition the German Processing and Archiving Facility, D-PAF, organized a pre-launch test campaign of SLR observations to the STARLETTE satellite, in order to test the various communication links with respect to the global SLR network. D-PAF started this pre-launch test campaign on 25 April 1991 and it would last until the launch of ERS-1. In view of these duties the Dutch transportable satellite laser ranging system, MTLRS-2, arrived at the calibration site at Baiamonte on 17 April 1991. At that time an ERS-1 launch on 3 May 1991 was still expected and therefore MTLRS-2 was installed at the site and made operational as soon as possible.

G.1 Access

The first visit of the Dutch transportable satellite laser ranging system MTLRS-2 to the newly selected and prepared site at Baiamonte had been in January 1991, for the EMC test measurements (see ANNEX F, "EMC Issues at Monte Venda"). During that visit it had turned out to be impossible to bring the standard configuration (truck with main cabin) up to the actual site area. The road towards the Baiamonte site was too narrow with a sharp U-turn just before the entrance gate. After consulting with the military, the truck had been brought up to a parking area at the Monte Venda main military facility, where the telescope unit, the electronics unit and the power generator, together with other necessary equipment had been off-loaded. A separate cooling unit, which is necessary when the main cabin with its air-conditioning system is not available, had been brought in immediately from the Kootwijk Observatory for Satellite Geodesy (KOSG) in The Netherlands. These individual components of the ranging system had been transported to the site area in a small truck and the hoisting had been done with a mechanical shovel. This operation was carried out successfully with support from a local construction firm and with great care, although the equipment used had not been well suited for the job.

Arriving now for the second time at Baiamonte on 17 April 1991, although it had not been possible to make any modifications to improve the access to the site, the off-loading and transportation of the sub-systems of MTLRS-2 had been much better prepared. A modern crane was available and the telescope unit was transported on a small truck, utilizing an air-cushion suspension system, which had been brought in from KOSG. This device had been used earlier in 1985 at Monte Generoso, Switzerland, when MTLRS-2 had been transported by rack-and-pinion railway.

Thus, the problem of access to this site has been solved adequately for MTLRS-2. Nevertheless it must be concluded that other space-geodetic equipment of similar dimensions, in particular SLR and VLBI systems, are likely to encounter access problems as well. If the Baiamonte site is to be used in the future for similar campaigns or if this site is to be included in a network of fiducial stations, *eg* for monitoring crustal motions, the accessibility will have to be addressed.

G.2 Installation

The installation of MTLRS-2 at the site includes the determination of the eccentricity vector of the system's mechanical reference point with respect to the site's reference point (the main marker on the platform) as well as the orientation of the telescope with respect to astronomical north. For these purposes star observations were performed in the night of 19 April 1991. The definitive eccentricity vector in the global reference frame from the system's reference point, *ie* the intersection of the telescope axes, towards the site's reference point (marker "A") on the platform, is:

$$dX = -2.759$$

$$dY = -0.664$$

$$dZ = +0.899,$$

where the units are in meters. The station position derived from the laser range data has been corrected for this eccentricity to relate it to the site reference point.

G.3 Observation programme

Observations on the LAGEOS satellite were started as soon as the system was operational. The first acceptable pass was observed when the weather permitted on 29 April 1991. The aim of this LAGEOS campaign was to obtain a precise position determination of the Baiamonte site in the SLR frame of reference. The internationally accepted criterion for a successful position determination is a dataset of 50 well distributed passes of this satellite together with an acceptable sky coverage. This will expectably result in a determination of the site coordinates with an accuracy of about one cm. The LAGEOS observations were continued throughout the entire campaign. In Table G–1 a summary of the observed LAGEOS passes is given, while Figure G–1 shows the sky coverage of these observations.

FIGURE G–1 The sky coverage of the LAGEOS observations from Monte Venda, within a 20° horizon.

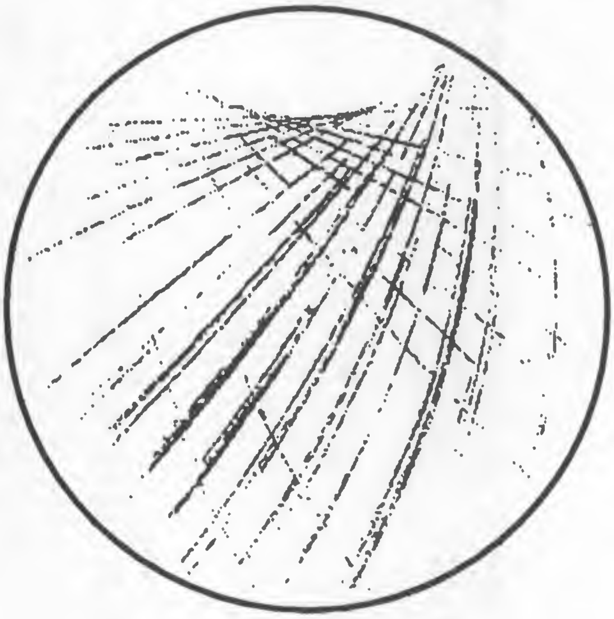

The STARLETTE campaign, which was organized by D-PAF, started on April 25. In addition to the purpose of testing the communication links for rapid data transfer with the global network of SLR stations, this campaign enabled the crews to refresh their experience with tracking a low satellite. A summary of the observed STARLETTE passes is given in Table G–2.

As soon possible after the launch of ERS-1 on 17 July 1991 the SLR tracking started and when the weather permitted, on 29 July 1991, the first pass from Baiamonte was observed. It turned out that ERS-1 was a much more difficult satellite to observe than STARLETTE. The ERS-1 predictions submitted by D-PAF were accurate enough if the date of observation was close to the epoch of the last computed predictions. However in a few days time, the time correction to these predictions became quite unpredictable because of the satellite's air drag component.

The highest priority for MTLRS-2 was to observe the calibration pass occurring once every three days at 20:02 UTC. Furthermore tracking of all other

TABLE G–1

Summary of LAGEOS observations at Balamonte

SAT	STAT	START TIME YYMMDD	START TIME HHMMSS	STOP TIME YYMMDD	STOP TIME HHMMSS	NO. OF OBS
7603901	7542	910429	103748	910429	111106	98
7603901	7542	910430	022642	910430	024816	165
7603901	7542	910430	060357	910430	063236	401
7603901	7542	910513	055654	910513	061444	168
7603901	7542	910517	073127	910517	075343	106
7603901	7542	910519	044512	910519	051812	1456
7603901	7542	910519	081031	910519	084113	93
7603901	7542	910520	103042	910520	104122	33
7603901	7542	910521	015719	910521	023458	959
7603901	7542	910521	053711	910521	060715	889
7603901	7542	910521	124052	910521	124247	32
7603901	7542	910522	041530	910522	044343	1551
7603901	7542	910522	075007	910522	075855	36
7603901	7542	910523	024956	910523	032009	82
7603901	7542	910524	084117	910524	085410	59
7603901	7542	910524	115132	910524	121624	220
7603901	7542	910525	035259	910525	041120	969
7603901	7542	910525	102848	910525	105554	162
7603901	7542	910525	140739	910525	141111	44
7603901	7542	910526	090932	910526	092637	118
7603901	7542	910527	075948	910527	082146	78
7603901	7542	910527	111658	910527	112253	25
7603901	7542	910528	025644	910528	034123	1785
7603901	7542	910528	063603	910528	070559	344
7603901	7542	910528	100258	910528	101939	179
7603901	7542	910529	120819	910529	121448	31
7603901	7542	910530	034440	910530	042432	1493
7603901	7542	910530	072322	910530	074514	221
7603901	7542	910530	105816	910530	110600	69
7603901	7542	910531	060248	910531	062406	357
7603901	7542	910531	093451	910531	093654	22
7603901	7542	910603	085847	910603	091330	28
7603901	7542	910610	025302	910610	033159	605
7603901	7542	910613	022301	910613	024658	97
7603901	7542	910614	010941	910614	013144	148
7603901	7542	910615	032319	910615	034140	252

TABLE G–1

Summary of LAGEOS observations at Baiamonte

SAT	STAT	START TIME YYMMDD	START TIME HHMMSS	STOP TIME YYMMDD	STOP TIME HHMMSS	NO. OF OBS
7603901	7542	910618	023007	910618	030647	820
7603901	7542	910618	125126	910618	131000	93
7603901	7542	910622	004118	910622	010617	460
7603901	7542	910622	231456	910622	232655	22
7603901	7542	910629	014408	910629	015724	279
7603901	7542	910630	003713	910630	004138	179
7603901	7542	910630	225423	910630	231807	65
7603901	7542	910701	023509	910701	030128	88
7603901	7542	910701	093911	910701	094416	42
7603901	7542	910707	013101	910707	015121	222
7603901	7542	910707	235913	910708	003024	154
7603901	7542	910709	022707	910709	024248	339
7603901	7542	910710	232359	910710	234818	122
7603901	7542	910711	031614	910711	033045	47
7603901	7542	910712	015239	910712	020639	147
7603901	7542	910802	235823	910803	000450	200
7603901	7542	910807	013118	910807	015720	321
7603901	7542	910810	005503	910810	011800	293
7603901	7542	910810	234426	910811	000348	176
7603901	7542	910815	234815	910815	235217	268
7603901	7542	910816	223712	910816	225219	146
7603901	7542	910818	003947	910818	004946	81
7603901	7542	910819	215129	910819	215511	27
7603901	7542	910821	001404	910821	002642	764
7603901	7542	910821	223932	910821	231039	922
7603901	7542	910831	003033	910831	005746	1075
7603901	7542	910831	225810	910831	234110	1603
7603901	7542	910901	215437	910901	220833	323
7603901	7542	910903	222249	910903	230443	1277
7603901	7542	910904	205938	910904	212615	84
7603901	7542	910905	232741	910905	233845	59
7603901	7542	910906	215715	910906	222730	201
7603901	7542	910909	211624	910909	215059	349

ERS-1 passes was important for supporting the determination of the ERS- 1 orbit. Because of the delay in the launch of ERS-1, the period planned originally for the deployment of MTLRS-2 at Baiamonte had to be extended.

TABLE G–2 Summary of STARLETTE observations at Baiamonte

SAT	STAT	START TIME YYMMDD	START TIME HHMMSS	STOP TIME YYMMDD	STOP TIME HHMMSS	NO. OF OBS
7501001	7542	910519	052215	910519	052420	393
7501001	7542	910519	070704	910519	071349	616
7501001	7542	910519	085652	910519	090524	567
7501001	7542	910520	091618	910520	092524	579
7501001	7542	910521	040944	910521	041536	961
7501001	7542	910528	062738	910528	063206	557
7501001	7542	910531	072358	910531	072525	88
7501001	7542	910612	210147	910612	210808	389
7501001	7542	910614	195038	910614	195225	60
7501001	7542	910614	213846	910614	214603	182
7501001	7542	910614	232854	910614	233558	210
7501001	7542	910615	201045	910615	201701	136
7501001	7542	910615	215816	910615	220637	1101
7501001	7542	910615	234737	910615	235554	237
7501001	7542	910618	191813	910618	192433	46
7501001	7542	910619	194054	910619	194613	510
7501001	7542	910619	212650	910619	213612	1723
7501001	7542	910619	231620	910619	232537	1130
7501001	7542	910620	214619	910620	215511	1286
7501001	7542	910620	233541	910620	234530	624
7501001	7542	910621	201701	910621	202527	948
7501001	7542	910621	220555	910621	221350	1530
7501001	7542	910621	235525	910622	000419	557
7501001	7542	910622	165947	910622	170333	378
7501001	7542	910622	185233	910622	185321	38
7501001	7542	910622	203555	910622	204412	1460
7501001	7542	910622	222510	910622	223448	1211
7501001	7542	910623	001743	910623	002144	172
7501001	7542	910623	205636	910623	210107	766
7501001	7542	910623	224738	910623	225205	14

Fortunately the system could be made available until 18 September 1991. Then, because of urgent refurbishments in preparation of the its mission for 1992, MTLRS-2 had to terminate the calibration campaign and leave the Baiamonte site. In total 44 ERS-1 passes, including the calibration passes directly over the Venice tower, were observed.Table G–3 summarizes the ERS-1 data obtained.

TABLE G–3 Summary of ERS-1 Observations at Balamonte

		START TIME		STOP TIME			
SAT	STAT	YYMMDD	HHMMSS	YYMMDD	HHMMSS	NO. OF OBS	CAL. PASS
9105001	7542	910729	203446	910729	203538	50	
9105001	7542	910802	102203	910802	102324	195	
9105001	7542	910802	213922	910802	214013	134	
9105001	7542	910806	210737	910806	210835	92	•
9105001	7542	910808	213747	910808	214127	109	
9105001	7542	910809	210420	910809	210632	53	•
9105001	7542	910810	203201	910810	203311	46	
9105001	7542	910812	210426	910812	210820	88	•
9105001	7542	910813	203133	910813	203420	26	
9105001	7542	910815	210442	910815	210823	172	•
9105001	7542	910816	203127	910816	203320	144	
9105001	7542	910817	195852	910817	200042	64	
9105001	7542	910817	213831	910817	214145	47	
9105001	7542	910818	210424	910818	210744	102	•
9105001	7542	910819	203102	910819	203537	457	
9105001	7542	910819	221052	910819	221348	69	
9105001	7542	910820	213916	910820	214145	156	
9105001	7542	910821	210256	910821	210856	1367	•
9105001	7542	910822	202934	910822	203440	100	
9105001	7542	910827	210628	910827	210801	39*	•
9105001	7542	910828	202946	910828	203448	47	
9105001	7542	910830	210302	910830	210839	731	•
9105001	7542	910831	105301	910831	105519	67	
9105001	7542	910831	202928	910831	203535	157	
9105001	7542	910831	221004	910831	221254	165	
9105001	7542	910901	195807	910901	200111	68	
9105001	7542	910901	213525	910901	214146	703	
9105001	7542	910902	210646	910902	210748	45	•
9105001	7542	910903	202953	910903	203529	468	
9105001	7542	910903	220959	910903	221247	65	
9105001	7542	910904	195828	910904	200115	26	
9105001	7542	910904	213520	910904	214100	505	
9105001	7542	910905	210203	910905	210841	700	•
9105001	7542	910906	203026	910906	203519	120	
9105001	7542	910909	203050	910909	203528	222	
9105001	7542	910909	221001	910909	221308	116	

TABLE G–3

Summary of ERS-1 Observations at Baiamonte

SAT	STAT	START TIME		STOP TIME		NO. OF OBS	CAL. PASS
		YYMMDD	HHMMSS	YYMMDD	HHMMSS		
9105001	7542	910910	213543	910910	214055	215	
9105001	7542	910911	210250	910911	210834	270	•
9105001	7542	910913	195916	910913	200032	10	
9105001	7542	910913	213537	910913	214120	138	
9105001	7542	910915	203050	910915	203519	574	
9105001	7542	910915	221006	910915	221339	49	
9105001	7542	910916	213757	910916	214104	54	
9105001	7542	910917	210206	910917	210743	557	•

During the field operations, the Dutch team of observers was supported by personnel from Telespazio SpA., in the framework of an already long-standing cooperation between Delft University of Technology and the *Agenzia Spaziale Italiana*.

TABLE G–4

Totals of SLR Observations at Baiamonte

SATELLITE	PASSES	OBSERVATIONS
7501001	30	18469
7603901	69	24623
9105001	44	9582

G.4 Data acquisition, review of the results

An optical technique such as SLR, is susceptible to cloud cover and haze. In this respect it can be concluded that the weather circumstances generally have been quite reasonable throughout the campaign. Mostly during day-time a light haze or thin clouds limited the data acquisition. It must be considered fortunate that the calibration passes occurred at night time, when generally these conditions were much more favourable. From time to time rain or heavy overcast prevented satellite observations. The laser ranging system generally functioned very well during the campaign. Only minor problems inhibited the observations a few times. In this respect it can be concluded that the preventive maintenance which had been carried out at Kootwijk Observatory, prior to the campaign, had been successful.

Summarizing, of all overflights of ERS-1 over Baiamonte, 54% could not be observed due to weather circumstances, and 8% was missed due to instrument failure. The total data yield for the ERS-1 satellite has been 12 out of the 18 possible calibration passes and 32 additional passes. In addition 69

LAGEOS and 30 STARLETTE passes have been observed. These statistics must be considered to be quite favourable, as compared to many years of experience with field deployed SLR systems and the general weather situation at Baiamonte.

G.5 Other operational aspects

G.5.1 Data communication

MTLRS-2 is not equipped with a mobile data communication system such as the Inmarsat satellite communication system, by means of which data can be transferred from and to the site, independently from local connections. An alternative, which is generally applied by MTLRS-2, is the use of an ordinary commercial telephone connection at the site. Together with a modem connected to the system's PC, data can usually be transferred quite easily at a rate of up to 2400 Baud. For a very low satellite like ERS-1 (in terms of SLR tracking), frequent updates of the orbit information are required at the site, to be able to find the satellite within the narrow laser beam. In preparation of this campaign it was therefore imperative that a good facility for data communication would be established with the German Processing and Archiving Facility (D-PAF), which issued the orbit predictions for ERS-1.

G.5.1.1 Original setup

In spite of all the efforts to organize a telephone connection at the Baiamonte site, this facility was not available when MTLRS-2 arrived there in April. As the only possible alternative, a PC together with a 2400-Baud modem was installed in the hotel room of one of the crew members in Albano Terme, where a telephone outlet was available. From the start of the operations this setup has been utilized as the data communication facility to receive orbit predictions and to relay quick-look datasets from the site.

In principle, with this setup ASCII data transfer was possible from and to the mailbox at D-PAF, while binary and ASCII data could be transferred from and to KOSG by using QMODEM software with the XMODEM protocol on both sides. However the quality of the telephone connection caused the datalink to fail in about ninety percent of the attempts. The connection to the mailbox at D- PAF turned out to be practically impossible, because no error checking protocol could be used. The standard procedure therefore became to communicate with D-PAF through KOSG, mostly at night time. Data transfer between MTLRS-2 and the PC in the hotel room took place by means of floppy diskettes. This procedure worked most of the time, but caused frequent delays in the communication. Besides it was very time consuming and costly, and caused additional workload for the operators. With this experience, still before the launch of ERS-1, it was evident that an alternative procedure would have to be found, to enable fast data communication between the site and D-PAF directly.

G.5.1.2 Use of the PRODAT system

Recognizing this urgent situation, ESTEC proposed to use ESA's experimental mobile satellite communication system PRODAT. This system was installed at Baiamonte on 26 July 1991. The PRODAT system is a system for communicating small ASCII datasets between a mobile terminal and stationary terminals connected to the Fucino ground station by means of public data networks, including the telex network. In this campaign, the telex link was used, to which D-PAF as well as KOSG are connected. With this system, although experimental, a direct communication facility between the site and D-PAF became available, with improved reliability and with much less delay. The PRODAT system is however limited in some respects, such as the low data speed of 200 bits/second and the maximum file size of 1935 bytes per message. The system is a store-and-forward system with the consequence that the delivery of a message is not always certain. This support from ESTEC nevertheless very significantly enhanced the opportunities for tracking ERS- 1, based on new orbit information received almost daily at the site.

G.5.2 Electrical power

As soon as the Baiamonte site was selected, attempts were made to obtain a 380 V, 20 kVA power outlet to accommodate the MTLRS-2 requirements. Such support avoids the continuous operation of a diesel power generator Even an outlet of 6 kVA would have been sufficient to support the stand-by equipment, *eg* the temperature control unit and the station clock together with the time calibration system, to permit switching off the power generator between range observation sequences. Unfortunately such electrical power connection has not been available and therefore the MTLRS-2 diesel generator had to be operated continuously during the entire campaign. The contingency procedure in case of a serious malfunctioning of the generator was to rent a spare unit and to fly it in from The Netherlands. Fortunately the generator functioned well and such action has not been necessary.

ANNEX H

Tower: Modifications and Operations

H.1 Modifications to the Structure

The following new instruments were expected to be placed and operational on board for the calibration phase:

1. GPS antenna and receiver;
2. microwave radiometer;
3. PRARE station.

Of these, number 3 was never taken on board due to the failure of PRARE on ERS-1. The associated modifications were nevertheless done, as they were executed prior to the launch of the satellite.

Figure H–1 shows a schematic view of the upper floors of the tower before the modifications. The main room L includes the living quarters and the instrumental area, C contains the cooking facilities. M is the high extending mast, P is the wind power generator. The main diesel power generators, together with the long term battery storage, are located on the lower floor, below the living quarters.

The expected extended duration of the campaign, and the possibility of a large number of people on board at the same time, suggested to separate the areas devoted to instruments and to living quarters. Therefore (see Figure H–1) a further small room I was added. This implied a change of position of the staircase from the third (living) floor to the fourth one (terrace), and the completion of the grid path all around the floor.

The radiometer had to be located at a position where it could explore the sky at different angles, and also with the possibility of pointing towards the sea. It was conveniently located in the south corner (above room I in Figure H–1). The extension of the terrace was completed with a grid exten-

FIGURE H-1 A schematic view of the upper floors of the tower before the modifications. The main room L includes the living quarters and the instrumental area, C contains the cooking facilities. M is the high extending mast, P is the wind power generator.

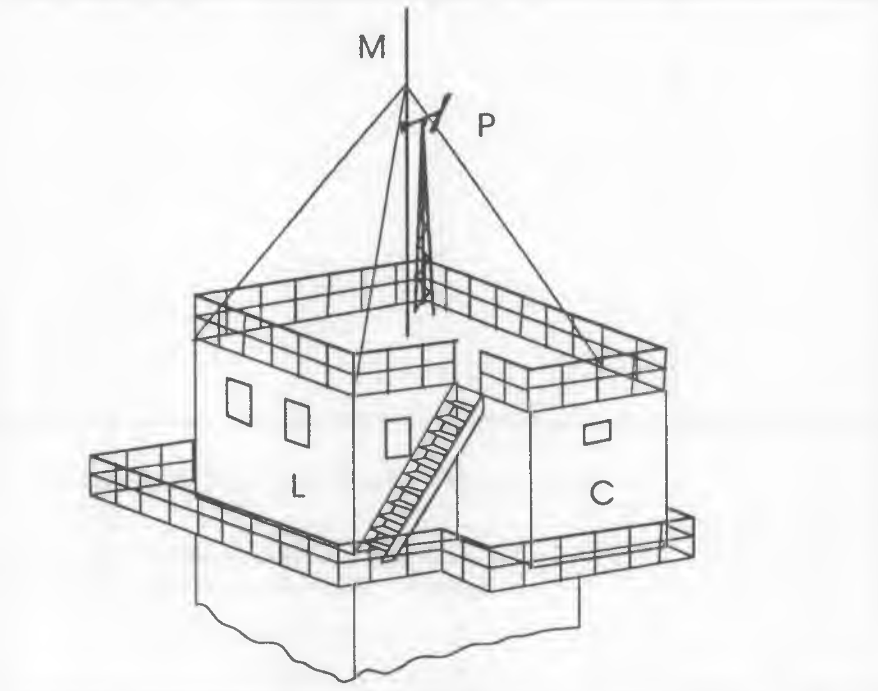

sion repeating the lower one, with the exception, for logistic reasons, of the south-west side.

The PRARE had to be located at a position where its view of the satellite during its necessary 180° rotation on the vertical plane was not obscured by any overhead structure. A terrace was therefore purpose-built, about 3.5×3.5 m wide on the west corner (to the left in Figure H–1) of the terrace. The whole is highly rigid, and a special support was manufactured and located at its centre to hold the PRARE antenna.

An overall view of the tower, fully equipped during the calibration campaign, was shown in Figure 2–2 in CHAPTER 2, "The Problem".

H.2 Operational Aspects

During the calibration campaign both the tide gauges on the tower (see Section 4.1, "Sea Level") were operated without any interruption. Taking the different filtering characteristics into account (which leads to a slight delay of 2 with respect to 1, and the absence in 2 of the short period oscillations) for most of the period the two traces can be almost superimposed on each other. However problems arose on two occasions. Around the 6th of August (see Figure H–3; the problem did not arise suddenly, but appeared gradu-

FIGURE H–2

A schematic view of the upper floors of the tower after the modifications. The instrument room is marked I.

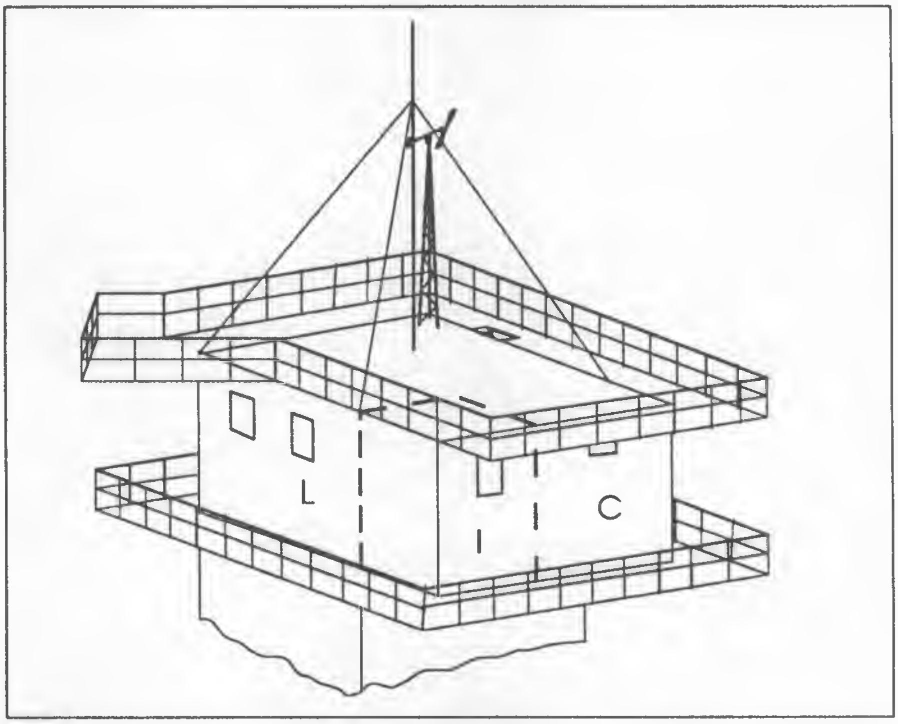

ally) gauge 2 began showing an increased filtering capability, cutting off crests and troughs, sticking to a fixed level for a while, then suddenly running after the actual sea level. Figure H–3(a) offers a clear visualization of the situation. The reason turned out to be *mucillagine*, an algae product that on some occasions in the recent years has suddenly shown a tremendous increase in population, filling up the whole depth from surface to bottom. In these cases it is sometimes referred to as "sea snow". Apparently the "snow" had occluded the small filter of 2, while gauge 1, due to the large size of its pipes, was still working correctly. Confirmation in this sense came from the cleaning of the filter of 2, after which (see Figure H–3(b)) everything went back to normal.

The second problem arose on 29th of August (see Figure H–4) when again gauges 2 showed another evident malfunctioning. The bad tracing lasted only a few hours, but the main worry came from an evident shift between the reference lines of gauge 1 and 2. By comparing Figure H–4 with Figure H–7, the relative displacement, estimated at about 2 cm, is fairly evident.

The malfunctioning set obvious suspicion on 2, but a further check was carried out by comparing 2 against another gauge, referred to as 3, also run by the Venice City Authority, and located (see Figure H–5) at 14 km distance at the end of the south jetty of the Lido entrance to the Venice Lagoon. In usual

FIGURE H–3

Malfunctioning of gauge 2 due to occlusion of its filter by algae (a). After cleaning its filter on 12 August (b) everything returned to normal

(a)

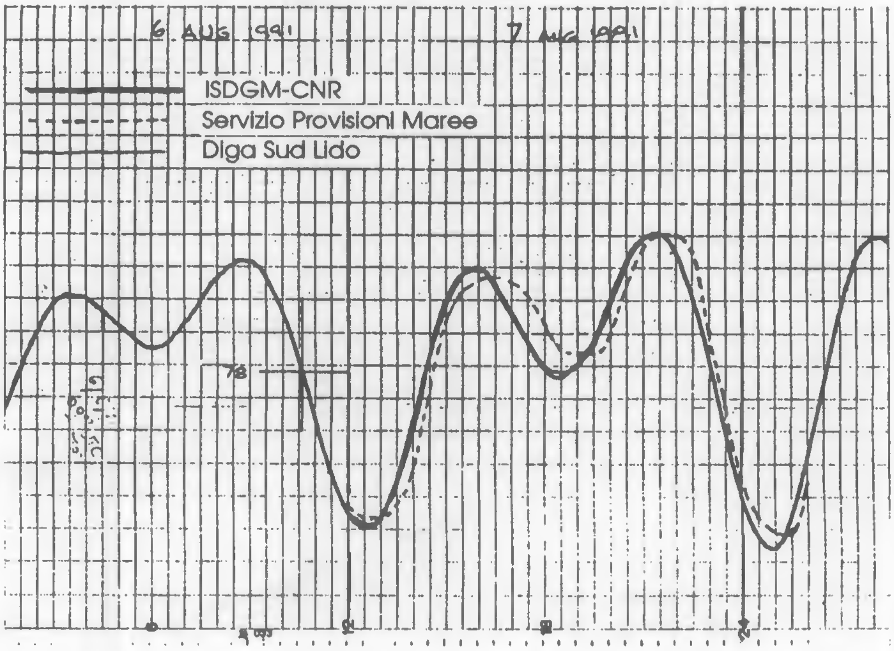

(b)

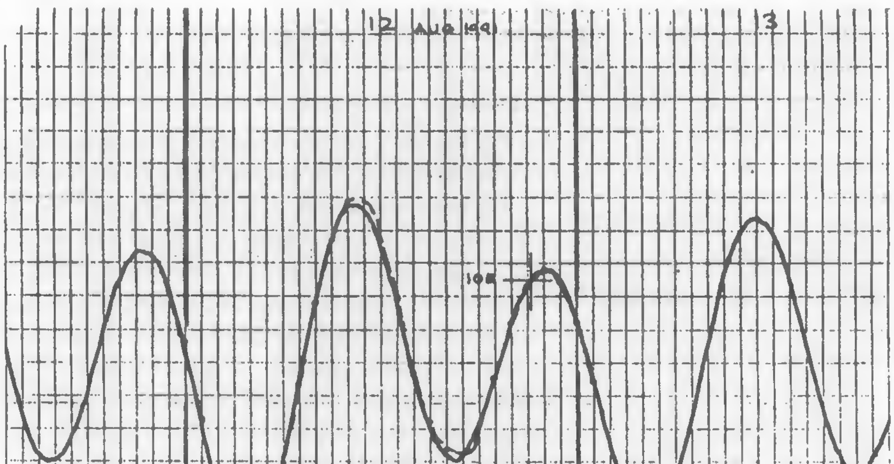

conditions the record of gauge 3 does not differ much from those of 1 and 2, except for the possibly different filtering characteristics and the higher excursions shown in case of shelf waves.

Figure H–4 shows the trace of gauge 3 superimposed to those of 1 and 2, with a reference chosen before the event of 29 August. It is evident that 1 and 3 follow smoothly each other, with a clear offset of gauge 2. In more

FIGURE H-4 On 29 August 1991 gauge 2 showed a malfunction (a), after which the two gauges showed an offset of about 2cm.

(a)

(b)

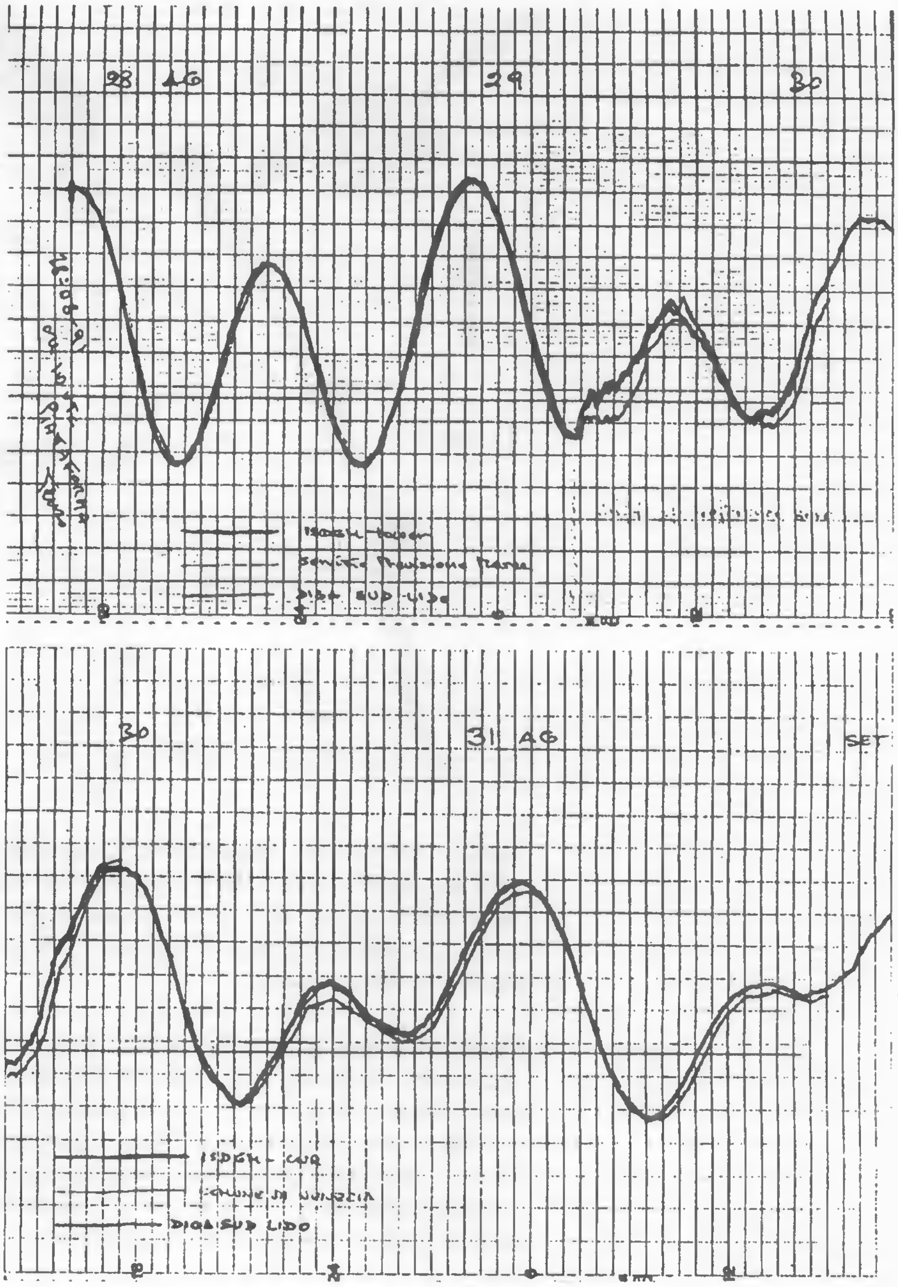

numerical terms we have evaluated the daily mean average value of 2 and 3, as the average of 24 hourly values, and plotted them in Figure H-6. While from 6 to 12 August, notwithstanding the filtering problem of 2, the two means follow each other exactly, there is an obvious shift after the 29th. In the lower diagram the difference has been plotted on an expanded scale. We have also drawn the overall average value of the difference for each of the

FIGURE H–5

Geographical distribution of tide gauges 1 and 2, on the tower, and 3, at the end of the south jetty bordering the harbour.

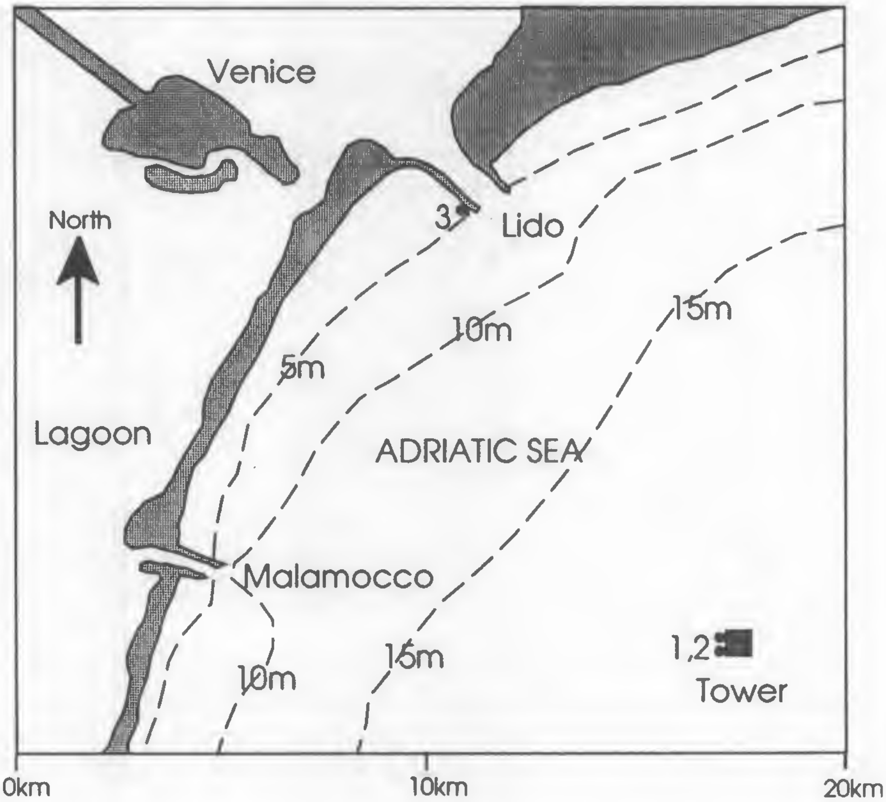

periods, which were respectively 0.2 and 1.8 cm. We concluded, coherently with the results suggested by Figure H–7, that gauge 2 had suffered a shift of its reference zero of –1.6 cm. A later inspection revealed the likely reason in that the metal ribbon had slipped out of position; it was later set again in place to work properly.

Operatively the tidal value at the time of each satellite pass had to be obtained from both gauges 1 and 2. The data of gauge 2 were usually made available at a later time, and the proper tidal level, referred to the official reference zero of the city of Venice (see Section 3.5 in CHAPTER 3, "The Three-Dimensional Network"), was deduced by interpolation between the two data taken at 5 minutes interval across the pass. Actually, since the pass was at 21:05, no interpolation was required.

The datum from gauge 1 had to be read directly from the graph. However it was soon evident after the first few passes that, due to the very compact time scale, exact timing was difficult to achieve. The diagram has a few time markers every now and then, which also reveal a slight shift of the clock of the recorder. This was duly taken into account while estimating the time of the passes on the diagram, but the obvious way out, taking advantage of the operator on board of the tower during each pass, was to mark the dia-

FIGURE H-6

Daily means of 24 hourly values from gauge 2 and 3, and the difference between them. Note the shift after 29 August (day 240).

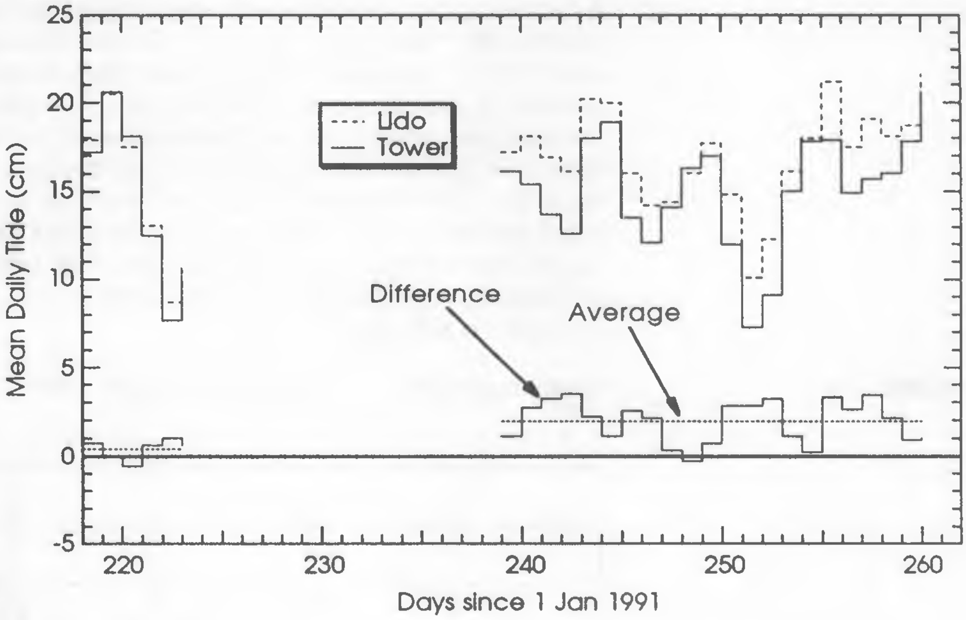

FIGURE H-7

Superposition of the diagrams from gauges 1 and 2, in September 1991

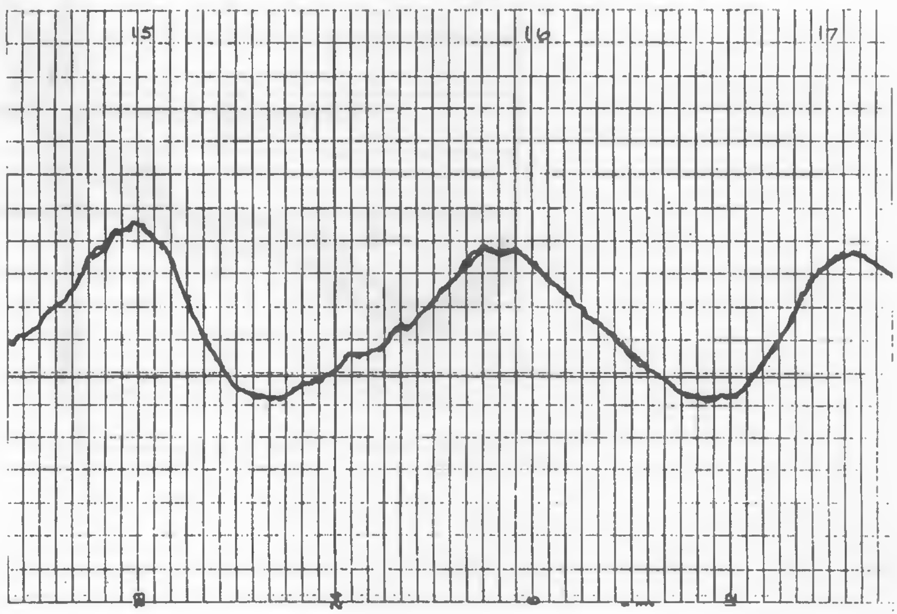

gram at the time of the pass itself. In a few occasions in the first part of the campaign, if no clouds were present, the pass was visually observed. Later on, when at the tower position ERS-1 was in the darkness of the Earth's shadow, the correct timing was established by clock. All the marked passes on the diagram from gauge 1 are shown in Figure 4–7 in CHAPTER 4, "Local Measurements".

A certain degree of uncertainty in determining the correct tidal level is associated to the thickness of the trace. The uncertainty can be estimated at about 0.5 cm. However this figure can be reduced by referring to the centre of the trace after proper magnification (see example in Figure H–8), because the actual pen is very thin and the thickness of the trace on paper is mainly due to the porosity of the paper itself. This has been verified by direct reading of the value on board (both from the pen position as from the decimal position counter at the top of the recorder (see Figure 4–3 in CHAPTER 4, "Local Measurements"), and later reading of the centre of the trace. The two estimates were within 0.2 cm, which we then took as representative of the accuracy of each reading.

FIGURE H–8 An enlargement of the tidal diagram at the pass of ERS-1 on 14 September 1991.

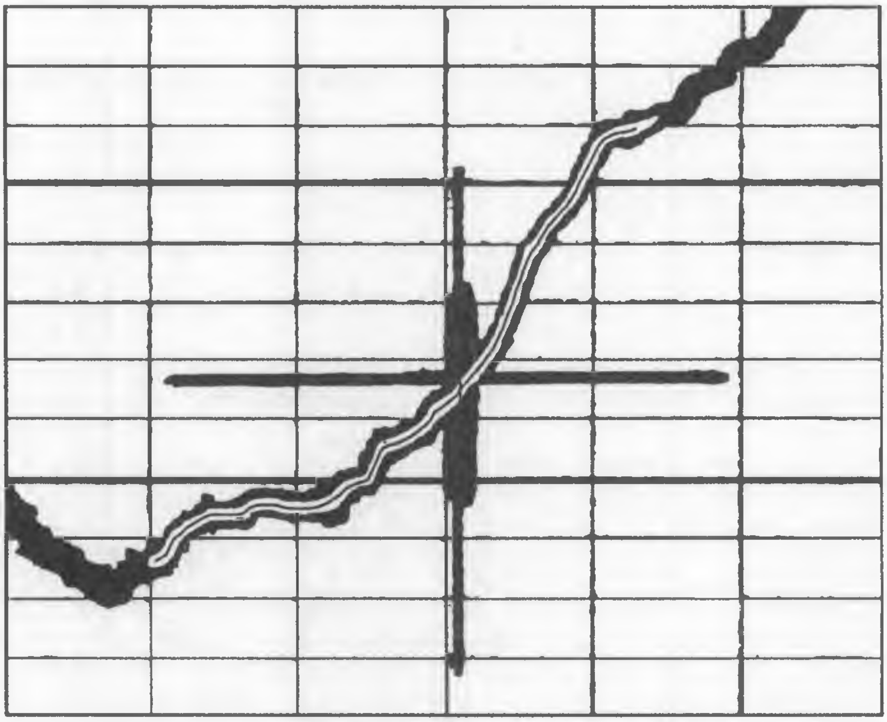

ANNEX I

The Microwave Radiometer

I.1 Description of the equipment

A few details of the various pieces of equipment used for estimating tropospheric corrections are reported in the following.

I.1.1 Microwave radiometer

The instrument employs double side-band receivers with a band of approximately 2 GHz. Each receiver can be used in three different modes: total power, Dicke and automatic gain control (AGC). In the Dicke and AGC mode ferrite switches are used in order to connect the receiver alternatively to the antenna and to the cold or both the reference loads respectively. Cold and hot reference temperatures are kept at nominal values of 303K and 373K. Three different integration time constants are selectable for each mode of operation: 10, 1 and 0.1 seconds. The radiometric resolution depends on operational mode; 0.5K is the value for AGC mode while a 0.1K resolution is achieved in Dicke mode.

I.1.2 Antennas

The antennas are manufactured by Alpha Industries (Woburn, Massachusetts). The TRG Series 858 Scalar horn lens antennas have been selected based on their high beam efficiency and negligible sidelobes and cross polarized lobes over the full waveguide frequency range. They are composed of a Scalar Feed horn which is held at the focus position of a Rexolite lens by a light-weight plastic housing. The dielectric constant and the loss tangent of the lens material at millimetre wave frequencies are 2.53 and approximately 0.001 respectively. The Scalar Feed horn overcomes the deficiencies of the more common horn feeds achieving radiation patterns almost identical in all axial planes, essentially constant bandwidths, extremely low sidelobes and back-lobes, a true fixed phase centre and an inherently low SWR.

The antenna performances measured at 23.8 GHz and 36.0 GHz are reported in Table A–1.

TABLE A–1 Antennas characteristics

	23.8 GHz		36.0 GHz	
	E-plane	H-plane	E-plane	H-plane
Beamwidth	4.25°	4.25°	4.25°	4.30°
Sidelobe level	-26dB	-27.3 dB	-25 dB	-28.7 dB
Effective diameter	22.9 cm		15.2 cm	
Physical diameter	27.9 cm		19.3 cm	
VSWR	1.4:1 Max		1.4:1 Max	
Efficiency	> 55%		> 55%	
Axial ratio	< 1 dB		< 1 dB	
Waveguide	WR 42		WR 28	
Operating range	18–26.5 GHz		26.5–40 GHz	

Operating the lower frequency antenna at 20.6 GHz results in a slightly broader beamwidth which can be estimated from the above measured parameters through a simple scaling in the frequency domain. A beamwidth of about 4.9° can therefore be assumed for channel 1 (20.6 GHz).

The three-dimensional antenna directivity has been computed based on the directivities measured in the E-plane and H-plane and using an appropriate resampling algorithm. The resulting antenna patterns are reported in Figure I–1 as a function of the u, v coordinates ($u = \sin\Theta \cos\Phi$, $v = \sin\Theta \sin\Phi$ where Θ, Φ represent the observing direction in the antenna reference system).

I.1.3 Housing and supporting equipment

The radiofrequency sub-systems and the antennas are enclosed in an aluminium box designed to protect them against the marine environment. The box is connected to a mechanical support able to provide scanning of the entire box both in azimuth and in elevation. The pointing device has a precision of 2.5′ in both directions. The accurate pointing of the antenna boresight can be achieved by referring the pointing device setting to a known boresight direction. This is usually done for the zenithal direction by adjusting the lens planarity using a level meter. The maximum error in antenna pointing can be assumed of about 6′.

FIGURE I–1 Antenna Patterns in *u, v* coordinates, for the 20.6GHz antenna on the left, and the 36.0GHz antenna on the right. The scale on the gain axis is from –25 to +35dB.

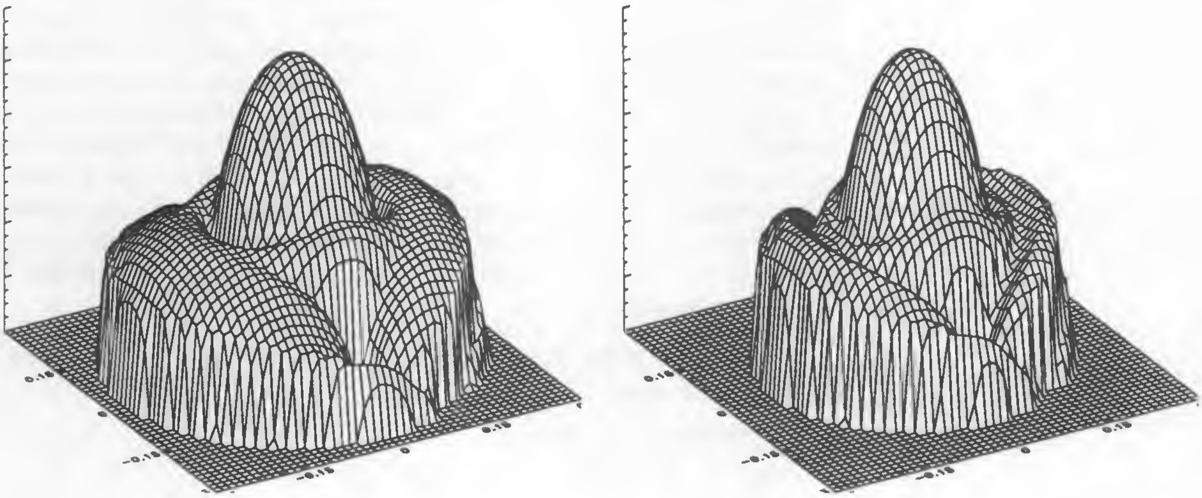

I.1.4 Meteorological sub-system

The temperature and relative humidity transducers are installed inside an anti-radiation shield providing a forced air flux. The main characteristics of the meteorological sensors are the following:

- Temperature
  - transducer: compensated thermistor
  - measurement range: –30°C – +50°C
  - accuracy: ±0.15°C
- Relative humidity
  - transducer: Hygrometer C-83-N Rotronic
  - measurement range: 0 – 100%
  - accuracy: ±1.5%
  - repeatability: 0.5%
  - hysteresis error: better then 0.5%
- Air pressure
  - transducer: piezoelectric
  - measurement range: 860 – 1060 mbar
  - accuracy: ±0.2% of the measurement range

I.1.5 Data acquisition and processing unit

The acquisition of analog signals from the microwave radiometer and meteorological sensors is performed by a Compaq SLT/286 portable personal computer and a DAS-16G1 12 bit data acquisition and control interface board (by Metra-Byte Corporation, Taunton, Massachusetts) connected to the computer bus. The acquisition and preprocessing software have been developed in an Asyst software environment (Asyst Scientific System is a product by Asyst Software Technology, Rochester, NY). Data are stored in ASCII files which include 10 records of ancillary information (*ie* start time of acquisition, meteo condition flag, instrument electrical offsets, *etc.*) and a variable number of records which contain samples of each acquisition channel output voltage with a 1 second sampling rate. Each sample is coded as a 2 byte integer number. The record structure is different for the Dicke and AGC mode of operation of the radiometer (the two modes used during the ERS-1 calibration experiment). For the AGC mode each record contains the following data items:

#1 output voltage channel 1
#2 output voltage channel 2
#3 cold reference channel 1
#4 cold reference channel 2
#5 hot reference channel 1
#6 hot reference channel 2
#7 air pressure
#8 air temperature
#9 relative humidity
#10 time of data record (# of seconds from acquisition starting time)

As far as Dicke mode is concerned the hot loads temperatures are not present. A remote control of the data recording as been also implemented in order to allow special operations on the instrument on top of the tower. The data acquisition and processing unit is also able to perform preliminary estimation of the excess path length plus some utilities useful during the operational data collection.

I.2 Acquired data overview

Table A–2 summarizes the main events occurred during the campaign. It should be noted that most of the ERS-1 passes have been covered. Data are not available for the first two passes of July due to a failure in the data acquisition board and on September 14th because of bad atmospheric conditions. As far as data quality is concerned, when the radiometer was operating in Dicke mode a few data acquisitions should be considered less reliable. In particular on August 9th and 21th the ERS-1 pass follows a change in the instrument configuration due, respectively, to operations on the tower and a recovery of an instrumental drift; however data processing has not shown evident anomalies. On August 18th the meteorological conditions were very bad so that radiometer calibrations close to the ERS-1 pass are not available; final results should therefore be considered questionable.

TABLE A–2 Summary of events during the calibration campaign

Date of Event	Date of Pass	Event Report	Quality
30–31 July 1991		Radiometer and Meteo sensors installation: acquisition board failure	
	31 July 1991	Rain; meteo data by manual acquisition only	no data
1 August 1991		Radiometer problems, probably due to power supply	
	3 August 1991	Meteo data by manual acquisition only	no data
6 August 1991		Acquisition board reinstalled; rearrangement of power supply and grounding	
	6 August 1991	Regular Acquisition; clear conditions	good
9 August 1991		Radiometer displacement for GPS measurements	
	9 August 1991	Regular acquisition; partly cloudy	apparently good
12 August 1991		Antenna alignment; software upgrading	
	12 August 1991	Regular acquisition; clear	good
	15 August 1991	Regular acquisition; partly cloudy; apparent drift of 20GHz during pass	apparently good
	18 August 1991	Regular acquisition; partly cloudy; no calibration close to pass	questionable
21 August 1991		Instrument bias variation (36 GHz)	
	21 August 1991	Regular acquisition after bias adjustment	apparently good
24 August 1991		Instrument bias recovery (supply problem)	
	24 August 1991	Regular acquisition after bias re-adjustment	good
27 August 1991		Change to AGC mode of operation	
	27 August 1991	Regular acquisition; radio disturbances; cloudy	good
	30 August 1991	Regular acquisition; clear	good
	2 September 1991	Regular acquisition; clear	good
	5 September 1991	Regular acquisition; clear; 2 radiosondes launched from tower	good
	8 September 1991	Regular acquisition; clear	good
	11 September 1991	Regular acquisition; clear	good
	14 September 1991	Rain at satellite pass; no data	no data
	17 September 1991	Regular acquisition; clear	good

I.3 Calibration of the equipment

I.3.1 Tipping curve examples

Figure I–2 shows an example of data coming from operating a tipping curve calibration. The output of the two channels are showed as a function of the recording time (the time needed for operating the pointing device at each calibration step is not considered). The different steps in the figure correspond to different elevation angles changing from 0° to 65° and back to 0°, that is to air masses from 1 to about 2.3 and *vice-versa* (in particular the steps at 0°, 40°, 50°, 60°, 65° are present). The average output voltages are computed for each step and processed as explained in Section 4.2.3.2. The output of the black-body calibrator has not been measured during the tipping curve shown in Figure I–2 so that values coming from previous measurements are used. The calibration algorithm estimates the gain *G* and bias *B* of the instrument such that the atmospheric brightness temperature at each calibration step better approximates an exponential dependence on air mass; moreover the brightness temperature which corresponds to the output voltage of the blackbody approximates its physical temperature. This is shown in Figure I–3 where the atmospheric opacity computed at each step by using the retrieved calibration coefficients is shown as a function of air masses. The points are fairly well aligned along a straight line as expected

FIGURE I–2 Example of tip-curve calibration data

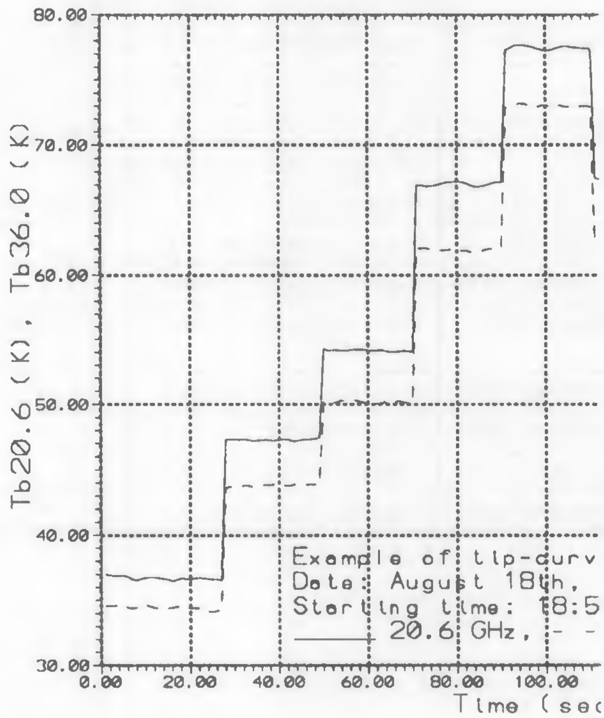

FIGURE I–3 Atmospheric opacity as a function of air mass resulting from tip-curve calibration processing

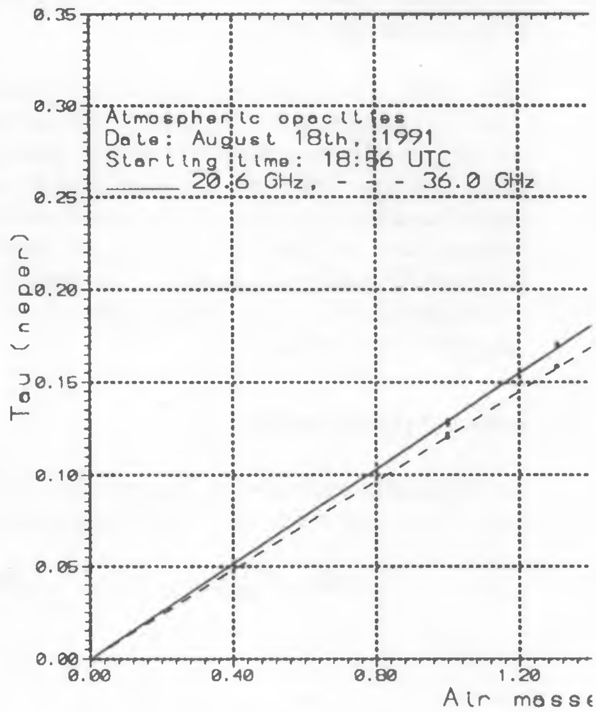

considering that the exponential behaviour of the brightness temperature would result in a linear dependence of the opacity (computed as explained in Section 4.2.4).

I.3.2 Correction of the non-linearity of the instrument

The calibration algorithm assumes that the response curve of the radiometer (*ie* the relation between output voltage and brightness temperature) is a straight line. Since non linearity could be present the method used for measuring and correcting it is explained with some details in the following.

The data used for this purpose come from injecting a fixed amount of noise into the antenna waveguide by a directional coupler. The noise is produced by a noise generator whose output passes through a variable attenuator. The apparent temperature of the antenna is changed from the lower value (corresponding to zenithal pointing to a clear sky) to a maximum value (which can be obtained by pointing an object at ambient temperature) performing a number of intermediate steps.

At each step (i) the voltage increment (δV_i) due to the switching on of the noise generator is measured. The quantity δV_i is proportional to the derivative of the instrument response curve which cannot be computed because of the uncertainties on the level of the injected noise (due to uncertainties on the noise generator itself, attenuation and coupling factor). Therefore we only know the variation of the response curve slope, so that we can plot δV_i normalized to the first value, δV_1 (that is the quantity $\delta V_i / \delta V_1$) as a function of the radiometer voltage (V_i).

This is shown in Figure I–4 for AGC and Dicke operation and both frequencies. The increasing of the normalized gain with the output voltage indicates a consistent non-linearity in AGC mode for both channels. The Dicke operation does not seem to be affected by appreciable non-linearity. The points have been fitted by a polynomial in order to allow integration of the normalized gain between the voltage V_1 and the voltage of the black-body response. The integral provides a correction to the output voltage associated with the black-body itself needed to apply a linear model in a wider range of temperatures.

I.3.3 Antenna pattern effect

The algorithm explained in Figure 4.2.3.2 is based on the equation which gives the brightness temperature along a direction Θ, Φ, that is:

$$T_B(\Theta) = T_{BG}\exp(-\tau m) + T_{mr}(\Theta)\,[1 - \exp(-\tau m)]$$

FIGURE I–4 Results of instrument linearity test

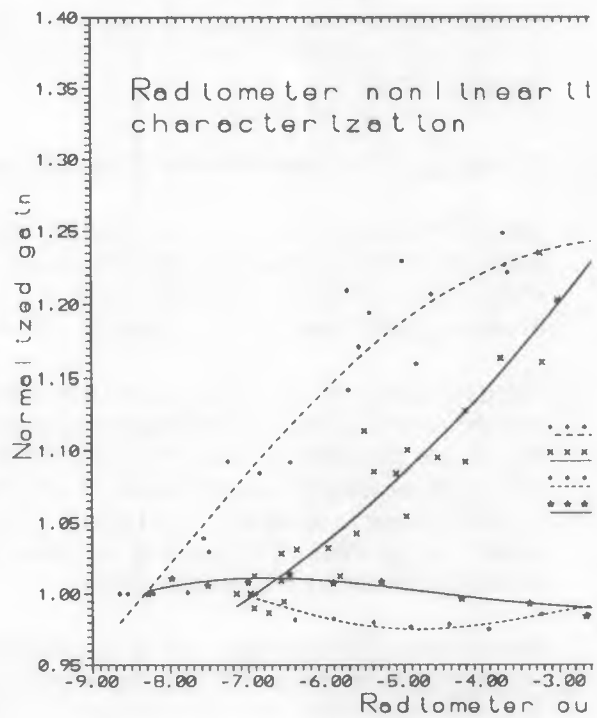

In principle it should be considered that the antenna receives radiation from different directions which include the main lobe and sidelobes. A convolution is performed between the antenna gain and the apparent temperature of the scenario, both terms depending on the direction Θ, Φ. Therefore the above relation could not apply to the antenna temperature when the convolution include a large range of directions and the brightness temperature of the atmosphere can not be considered constant within that range. For example, when the radiometer points at a given zenithal angle Θ the brightness temperature coming from directions $\Theta+\delta\Theta$ is bigger than brightness from elevation $\Theta-\delta\Theta$ thus giving an antenna temperature which should be associated to a higher angle when processing tipping curve. In order to quantify and eventually correct this effect a simulation has been performed by computing the antenna temperature as the convolution of a simulated atmospheric scenario (including the radiation from the ground surface) and different antenna patterns.

Results have been also computed by using the real antenna directivities described in Section I.1. The Figure I–5 shows the computed antenna temperature as a function of the elevation compared to the brightness temperature of the atmospheric scenario for different antenna dimensions. For a 20cm antenna diameter no significant differences can be observed between scenario and antenna temperatures. This is also confirmed when the actual antenna patterns are used, thus indicating that tipping curve data correction is not necessary in our experimental condition.

FIGURE I–5 Effect of the beam aperture on atmospheric scanning. The simulated antenna pattern, at 20 GHz, has $\tau = 0.2$ and an aperture illumination function of the form $(1 - r^2)^2$.